MASS TRANSFER WITH HOMOGENEOUS CHEMICAL REACTION AROUND SPHERICAL PARTICLES

by

WU-CHI CHEN

A dissertation submitted to the Graduate Faculty in Engineering in partial fulfillment of the requirements for the degree of Doctor of Philosophy,
The City University of New York.

1969

This manuscript has been read and accepted for the Graduate Faculty in Engineering in satisfaction of the dissertation requirement for the degree of Doctor of Philosophy.

5/12/69
date

Chairman of Examining Committee

May 13, 1969
date

Executive Officer

Robert A. Graff

Latif M. Jiji

Sherwood B. Menkes

Robert Pfeffer, Chairman

Supervisory Committee

THE CITY UNIVERSITY OF NEW YORK

ACKNOWLEDGEMENTS

The author is greatly indebted to Professor Robert Pfeffer for his continuous encouragement, guidance and advice during the progress of this research. Special thanks are extended to Professors A.E. Hamielec, Latif M. Jiji, Stanley Katz, and to Dr. Alan Peltzman for their valuable suggestions, and to Professors Alois X. Schmidt, Harvey L. List, Robert A. Graff, and Sherwood B. Menkes for their confidence and interest.

Acknowledgement is also due to the City College Computation Center for the use of its IBM computer. The technical assistance of Mr. John Bodnaruk and Mr. George DiIorio of the shop staff was especially helpful and is much appreciated. Heartfelt gratitude is expressed to the author's parents for their continuous encouragement.

The author also wishes to thank The City University of New York for supporting his graduate studies by means of a research assistantship.

TABLE OF CONTENTS

TABLES OF FIGURES

TABLE OF TABLES

NOMENCLATURE

The principal symbols are shown here. Symbols which have only a temporary significance have already been clearly defined in the text and are not included. Some symbols have more than one definition. All of these definitions are given here. The numbers in parenthesis which occasionally follow the definitions represent the equation number corresponding to the definition. The units are given in general forms as L (length, such as cm.), M (mass, such as gm.), and T (time, such as sec.)

Symbols	Definition	Units
a	radius of sphere	L
A_{2n-1}	coefficient in velocity profile, (IV-28)	dimensionless
A1	coefficient in diffusion equation for a two-sphere system, (IV-55)	"
B_{2n-1}	coefficient in velocity profile, (IV-28)	"
B1	coefficient in diffusion equation for a two-sphere system, (IV-55)	"
c	constant in bipolar coordinates system, (A-2)	L
C'_A	concentration of solute A, (IV-1)	ML^{-3}
C1	coefficient in diffusion equation for a two-sphere system, (IV-55)	dimensionless

Symbols	Definition	Units
C	concentration of solute, (IV-2)	dimensionless
C_A	concentration of solute A	"
C_B	concentration of reagent B	"
C_{2K}	perturbed concentration profile, (IV-120)	"
C_{oA}	zero order approximation of perturbed concentration of solute A	"
C_{oB}	zero order approximation of perturbed concentration profile of reagent B	"
$C_{i,j}$	concentration profile at mesh point (i,j)	"
C*	solute solubility at equilibrium	dimensionless ($M/M_{solution}$)
Co	bulk stream concentration of solute	"
C_{Ao}	solubility of solute A at equilibrium	ML^{-3}
C_{BM}	bulk stream concentration of reagent B	ML^{-3}
C	concentration driving force	dimensionless
d	center-to-origin distance in bipolar coordinates system (see Figure A-3)	L
$\mathscr{D}$	diffusivity	L^2T^{-1}
f(x)	function of x in velocity profiles expression, (IV-25)	dimensionless

Symbols	Definition	Units
M	constant defined by equation (IV-149)	dimensionless
N_{Gr}	particle Grashof number, $\frac{8a^3\rho^2 g_c a \Delta c}{\mu^2}$	"
N_{Re}	particle Reynolds number, $\frac{2a\,\rho_f\,U_\infty}{\mu}$	"
N_{Pe}	particle Peclet number, $\frac{2a\,U_\infty}{\mathfrak{D}}$	"
N_{Sc}	Schmidt number, $\frac{\nu}{\mathfrak{D}}$	"
N_{ScA}	Schmidt number for species A	"
N_{ScB}	Schmidt number for species B	"
N_{Sh_o}	overall Sherwood number, $\frac{2a\,K_o}{\mathfrak{D}\,\rho_f}$	"
$N_{Sh_o,R}$	overall Sherwood number with reaction	"
$N_{Sh_o,N}$	Overall Sherwood number without reaction	"
N_{Sh_ℓ}	local Sherwood number, $\frac{2r\,K_\ell}{\mathfrak{D}\,\rho_f}$	"
N_{ao}	overall mass flux, (V-1)	MT^{-1}
$N_{a\ell}$	local mass flux, (V-2)	MT^{-1}
q_1, q_2, q_3	orthogonal coordinates	dimensionless
r	spherical coordinate in radial direction	"
r_{sa}	surface average radius, (H-14)	L
$r_I(\theta)$	initial local radii	L

Symbols	Definition	Units
F	ratio of the mass transfer rate in the wake region to that in the front flow region, (IV-163)	dimensionless
F	ratio of the velocity terms in liquid drop study, (IV-126)	"
g (x)	function of x in velocity profiles expression, (IV-23)	"
h, h_i, h_2	constant greater than unity for non-uniform stepsize in numerical analysis, (IV-46), (IV-58), (IV-61)	"
h_1, h_2, h_3	metric coefficient of general orthogonal coordinates systems	"
K	ratio of velocity terms in liquid drop study, (IV-125)	"
k'''	reaction rate constant for first order homogeneous chemical reaction	T^{-1}
k_o	overall mass transfer coefficient in the continuous phase	LT^{-1}
k_ℓ	local mass transfer coefficient in the continuous phase	LT^{-1}
K	coefficient in reaction term in a two-sphere system, (IV-55)	dimensionless
$\ell_1 --- \ell_6$	coefficients for numerical analysis in single-sphere system an in multiparticle system, (IV-49)	"
L1, L2, L3, L55	coefficients for numerical analysis in a two-sphere system, (IV-62)	"

Symbols	Definition	Units
$r_F(\theta)$	final local radii	L
R_1, R_2	distance in a two-sphere system, (see Figure A-1)	L
U_∞	mean stream velocity or superficial velocity	LT^{-1}
$\underline{V}'$	velocity in vector notation, (IV-1)	LT^{-1}
$\underline{V}$	velocity in vector notation, (IV-2)	dimentionless
V_c	centerline velocity, (H-7)	LT^{-1}
V	volume of the sphere	L^3
V_x	velocity in angular (x) direction	dimentionless
V_y	velocity in radial (y) direction	"
V_ξ	velocity in angular (ξ) direction	"
V_η	velocity in radial (η) direction	"
$V_x^*, V_y^*, V_\xi^*, V_\eta^*$	velocity forms with O(1) in order of magnitude analysis	"
V_r	velocity in radial (r) direction	"
V_θ	velocity in angular (Θ) direction	"
ΔV_o	overall volume change	L^3
ΔV_ℓ	local volume change	L^3
W	function of void fraction, (IV-34a)	dimensionless
ΔW_o	overall weight loss	M

Symbols	Definition	Units
ΔW_ℓ	local weight loss	M
X_y (j)	function variable defined by equation (IV-61)	dimensionless
x	angular coordinate	"
y	radial coordinate	"
y'	stretched radial coordinate, (IV-52)	"
Δy_o	initial stepsize in y-direction	"
y*	stretched variable with O(1), (B-2, B-9)	"
Y_o	surface of the active sphere in a two-sphere system, (see Figures A-1, A-2, and A-3)	"
Z	cylindrical coordinate in flow direction	"

Greek Symbols

Symbols	Definition	Units
α	solute and reagent Schmidt number ratio, (IV-14)	dimensionless
β	reaction rate parameter, (IV-2)	"
γ	concentration ratio of reagent and solute, (IV-15)	"
δ	concentration boundary layer thickness	"
η	bipolar coordinate in radial direction, (A-4)	"

Symbols	Definition	Units
ϵ	void fraction	dimensionless
λ	function of void fraction, (IV-34)	"
μ	viscosity	$ML^{-1}T^{-1}$
ν	kinematic viscosity, $\nu = \frac{\mu}{\rho}$	L^2T^{-1}
ξ	bipolar coordinate in angular direction, (A-4)	dimensionless
ξ_A, ξ_B	combined variables for species A and B defined by equations (IV-74), (IV-75), (IV-100), (IV-101), (IV-127), (IV-128)	"
ξ_{AR}	assumed reaction zone, (IV-13)	"
$\Delta\xi_i$	angular stepsize in ξ-direction for numerical analysis	"
ϕ	enhancement factor	"
ψ	stream function	"
ψ_f	free stream function	"

Subscripts

Symbol	Definition
A	properties of species A
B	properties of species B
f	fluid properties
F	final properties
i	index in mesh net in angular direction
I	initial properties

Symbol	Definition
j	index in mesh net in radial direction
ℓ	local properties
N	without reaction
O	overall properties
R	with reaction
s	solid properties
x	in x-direction
y	in y-direction
ξ	in ξ-direction
η	in η-direction
∇	the gradient operator
∇^2	the Laplacian operator

ABSTRACT

Numerical solutions and perturbation solutions have been obtained to show the effects of homogeneous chemical reactions and particle-to-particle interaction in a two spheres system on the local and overall mass transfer rates from spherical particles. Experimental work has also been performed to verify some of the theoretical analyses. The research has concentrated on four major phases of study:

1. Mass transfer rates with first order homogeneous chemical reaction in single sphere systems and in multiparticle systems.
2. The effect of particle-to-particle interaction in a two sphere system on mass transfer rates with or without first order homogeneous chemical reactions.
3. Mass transfer rates with rapid, second order, irreversible chemical reaction around solid spheres, liquid drops and gas bubbles.
4. Experimental work verifying the effects of particle-to-particle interaction and rapid, second order chemical reaction on the mass transfer rates around single and two sphere systems.

General parameters combining the effect of the reaction rate constant and hydrodynamic behavior for the case of mass transfer around single solid spheres and in multiparticle systems with first order homogeneous chemical reaction have been obtained for both creeping flow and boundary layer flow fields to give a better understanding of whether the mass

transfer mechanism is either diffusion or reaction controlled.

The generalized parameter for the case of creeping flow was also used to correlate the mass transfer rates for two spheres placed in tandem parallel to the direction of flow with or without first order homogeneous chemical reaction. These results also indicated the effect of particle-to-particle interaction on mass transfer rates.

A boundary layer model has been used to predict the mass transfer rates around solid spheres, liquid drops and gas bubbles with a rapid, second order, irreversible homogeneous chemical reaction. A perturbation technique was used to obtain the solution for liquid drops. It was shown that the solutions to the solid sphere and gas bubble problems are the limiting cases of the liquid drop problem with the velocity or shear stress on the particle surface set equal to zero, respectively. The results are presented in terms of the enhancement factor.

The experimental work was performed to obtain data to show the effect of both particle-to-particle interaction on pure physical mass transfer in a two sphere system and of rapid second order chemical reaction on the local and overall mass transfer around single active spheres. These results agree reasonably well with theoretical predictions.

I. INTRODUCTION

Unit operations involving heat and mass transfer from gas bubbles, liquid drops or solid particles have been of considerable interest to chemical engineers for a long time. Of particular importance in the petroleum and chemical industries are processes which involve a chemical reaction or chemical reactions between a packed bed or a fluidized bed and a reagent in the continuous phase, such as catalysis, cracking, dissolution and sublimation of solids, absorption of gas bubbles or liquid drops, roasting of ores, etc. Since the concentration of the solute in the continuous phase will decrease due to the effect of the chemical reaction, the concentration gradients near the surface of the particle will tend to increase. Therefore, the resulting transfer rate will be greater than for pure physical mass transfer.

In practice, chemical reactions are usually accompanied by an enthalpy change. The problem then involves both simultaneous heat and mass transfer. The mass transfer mechanism, always involves the diffusion of the reagent from the continuous phase in the direction of the interface of the dispersed phase or vice versa. The chemical reaction can occur either at the surface of the solid particles as in catalysis, at a certain fixed distance from the interface where the reagent and solute meet as in a very rapid second order chemical reaction, or throughout the continuous phase as in the case of a slow homogeneous chemical reaction.

The reaction products diffuse back into the bulk of the continuous fluid and then are carried away by the flow of the fluid. To simplify the theoretical treatment of these problems the systems are usually assumed to be isothermal.

For the case of mass transfer with first order homogeneous chemical reaction, the hydrodynamic behavior around the dispersed phase is very important for low reaction rates, since an increase in fluid flow rate will remove solute from the region around the surface of the particle more quickly and cause an additional increase in mass transfer rate. This physical phenomenon can, of course, be directly verified from the solution of the governing diffusion equations. For extremely high reaction rates, the hydrodynamic behavior is not very important, because almost all of the solute reacts with the reagent in the fluid before it can diffuse away from the surface of the particle.

For the case of mass transfer with a very rapid second order reaction, the hydrodynamic effect and the physical properties of both the solute and the reagent are very important. Previous work in this area is usually presented in terms of the enhancement factor, i.e. the ratio of mass transfer with chemical reaction to that without chemical reaction. The available literature, however, for the most part, is based only on very simple geometries and flow patterns and the existing theories do not agree too well with one another. In addition, almost all of the theoretical

analyses are based on different mathematical models and assumptions so that the effect of the hydrodynamic behavior and physical properties of the systems on the mass transfer rate and enhancement factor is not well established.

The purpose of this investigation is to obtain both theoretical results and experimental data of the effect of hydrodynamic behavior, particle-to-particle interactions, homogeneous chemical reactions, and the physical properties of the chemical systems on both the local and overall mass transfer rate.

Very generalized parameters will be used to present the effect of hydrodynamic behavior and the properties of the systems on both the local and overall mass transfer rate with or without first order homogeneous chemical reactions. A mathematical model using a simplified flow pattern around gas bubbles, liquid drops or solid spheres will be developed to predict the mass transfer rates for a system with very rapid second order chemical reactions.

The effect of particle-to-particle interaction in a two-sphere system will be studied both experimentally and numerically for low Reynolds number flow for both physical mass transfer and mass transfer with a homogeneous chemical reaction. The theoretical and experimental studies will consider the two spheres to be placed in tandem in the direction of the flow; one sphere being active and the other inert.

II. LITERATURE REVIEW

The rate of mass transfer from particles to a fluid has been widely studied both theoretically and experimentally. These investigations include mass transfer from single particles as well as in multiparticle systems. The systems studied include solid or liquid particles as well as gas bubbles and both liquid and gaseous fluids. Theoretical studies have been mostly confined to studies of physical mass transfer rates from single particles to fluids which are flowing past them in Stokes' or in boundary layer flow. There are few theoretical studies on multiparticle systems because of the mathematical complexities involved with dealing with more than one particle. One of the major obstacles in doing theoretical studies in multiparticle systems is the difficulty of describing the hydrodynamic conditions around the spheres. Even for single sphere systems at high Reynolds numbers, the analytical solution of the complete Navier-Stokes equation is not feasible at present. This is because of the extreme non-linearity of the equations. Although numerical solutions have been recently attempted, the wake region becomes unstable at high values of Reynolds number. Obviously, the theoretical approach to forced convection mass transfer for both single and multiparticle systems would be simplified appreciably if accurate descriptions of the fluid flow field were available.

The description of the hydrodynamic behavior for flow around spherical particles which appears in the literature

is dependent on the range of the Reynolds numbers of interest. The Stokes' solution (78) gives the flow field around a single sphere for $N_{Re} \longrightarrow 0$. Oseen (58) and Proudman and Pearson (65) have extended the Stokes solution to a wider range of applicability of the Reynolds number. In the higher Reynolds number range solutions were obtained using finite-difference methods (31, 33, 37), Galerkin method (error-distribution method) (32, 34, 40), the Von Karman-Pohlhausen integral method (18) and perturbation methods (11). These techniques have all been shown to be successful, since the results obtained agree quite well with one another in the applicable range. However, it has been found (80) that the fluid velocity pattern around solid spheres become unstable as the Reynolds number increases above 500. These analytical or numerical results also agree reasonably well with available experimental data (79, 80). For the case of flow around gas bubbles it has also been shown that the potential flow solution gives a reasonably good description of the flow behavior.

1. Theoretical Studies of Heat and Mass Transfer Around Solid Spheres.

In order to obtain theoretical solutions to the problem of heat and mass transfer around solid spheres different approaches have been tried. These involve a number of different assumed mathematical models and the necessary techniques to solve the assumed mathematical models. The mathematical models include the assumed starting governing diffusion equations and boundary conditions and the assumed hydrodynamic behavior (velocity profiles). The mathematical methods used to solve the diffusion equations include both regular and singular perturbation techniques, combination or separation of variables, numerical techniques and integral methods.

The idea of the regular perturbation technique is to assume that the perturbed parameter is very small so that the original partial diffusion equation can be simplified into a new set of approximate equations. The final result involves a linear combination of all the solutions obtained from solving the simplified approximate equations. As the value of the perturbed parameter increases, the result obtained from the regular perturbation technique becomes unrealistic because of the basic assumption of using a small perturbed parameter for the analysis. The analysis, in general, always expresses the solution in terms of an assumed power series of the perturbed parameter. The assumed solution is then substituted back into the original diffusion equation and by collecting terms of equal order of the

perturbed parameter a set of simplified equations are obtained. Since the results are expressed in terms of the assumed power series of the perturbed parameter, the solution may blow up as the perturbed parameter becomes large. Unfortunately, there is no way to predict the range of the perturbed parameter within which the obtained solutions are applicable if the obtained solutions do not converge for all values of the perturbed parameter.

Singular perturbation techniques overcome some of the disadvantages of the regular perturbation technique. The idea is to apply stretched variables into the results obtained from the regular perturbation method. Upon assuming an appropriate form for the asymptotic expansion, outer and inner expansion terms can then be solved by matching principles or other techniques (11). However, by using the singular perturbation technique one is still unable to predict where the solutions of both the inner and outer expansions will break down. The success of singular perturbation technique strongly depends on the choice of stretched variables and assumed asymptotic forms. Both regular and singular perturbation technique have already been applied quite successfully to fluid mechanics problems (11).

Numerical solutions are obtained by converting the differential equation into finite-difference equations using either explicit or implicit methods. The utility of these methods depend not only on the stability and convergent speed but also on the stepsizes and difference forms. Both convergent speed and stepsizes should be

reasonable for practical use (high speed machine handling).

The idea of the integral method involves assuming an arbitrary form for the concentration (or temperature) profile satisfying as many boundary conditions as possible. The success of this method is very strongly dependent on the choice of the solution assumed.

For flow at high Peclet numbers, the thin concentration (or thermal) boundary layer approximation, neglecting diffusion terms in the angular direction is usually assumed as a reasonable model for transfer problems. This model was originally developed by Prandtl in dealing with fluid mechanics problems. The soundness of this technique must always be checked by an order of magnitude analysis.

The application of all of the methods to specific problems are discussed in the next sections.

a) $N_{Re} \ll 1$; single solid spheres; no reactions

In the creeping flow region, many analytical solutions have been presented to show that the local and overall Sherwood number is a function of Peclet number alone, i.e.

$$N_{Sh} = f(N_{Pe}) \qquad \text{(II-1)}$$

For small values of the Peclet number, the mass transfer rate expressed in terms of the Sherwood number can be expressed in terms of N_{Pe} as

$$N_{Sh} = 2 + A_1 N_{Pe} + A_2 N_{Pe}^2 + A_3 N_{Pe}^2 \ln N_{Pe} + \cdots \qquad \text{(II-2)}$$

For high values of Peclet number, the mass transfer rates, can be expressed in a more closed form as

$$N_{Sh} = B_1 N_{Pe}^{1/3} \qquad \text{(II-3)}$$

where the A_i's and B_1 in equations (II-2) and (II-3) are only functions of the angular argument of the spherical coordinate system and are dependent on the specific mathematical model chosen and the method of solution.

For $N_{Pe} < 1$, Kronig and Bruijsten (44) obtained a solution using a regular perturbation technique by expanding the temperature or concentration profile around the sphere in a simple power series of N_{Pe}. A point source solution was used as a basis. All boundary conditions were satisfied except the one at infinity when $\theta = 0$ (front stagnation line). Breiman (7) used the identical mathematical model as that used by Kronig and Bruijsten (44) but applied a Green's function to transform the diffusion equation into an integral equation and then solved the integral equation by iteration. Frisch (16) presented a similar solution for a single sphere falling in a stationary fluid. He also used N_{Pe} as the perturbation variable to represent the concentration field around the sphere. However, his results are questionable since he assumed an invalid boundary condition $C(r, 0) = C(r, \pi)$.

Illingworth (36) and Ogiwara (57) both used an Oseen-type approximation to solve the energy equation. They assumed that the fluid flows past the sphere in simple

harmonic motion about a mean velocity. Nielson (55) obtained a solution by solving the energy equation numerically by a relaxation procedure. His results expressed in terms of the coefficients in equation (II-2) was smaller than those presented by the other authors using the regular perturbation technique with N_{Pe} as the perturbation parameter.

Acrivos and Taylor (2) obtained a solution for the mass (or heat) transfer rate using the singular perturbation technique in the Peclet number range from 0 to 1. Their results were probably the most mathematically rigorous available for the low Peclet number region using a perturbation technique. Brenner (8) extended Acrivos and Taylor's (2) technique to solve the diffusion equation for Stokes' flow around a three-dimensional body of arbritary shape. For the special case of flow around a solid sphere, his results are in agreement with those given by Acrivos and Taylor (2).

For flow at very low Reynolds numbers under the condition that the Peclet number is very large and the "thin diffusional boundary layer" assumption can be made, the diffusion equation can be solved analytically as was done by Levich (47) and Friedlander (15). These solutions show that the overall Sherwood number is dependent on the Peclet number to the 1/3 power as given by equation (II-3).

Another solution covering the higher Peclet number range has been obtained by Yuge (84). He presented a perturbation method using successive power series approximations in terms of even powers of the spherical angle for the concentration profile. His technique reduces

the partial differential equation into an infinite number of ordinary differential equations. He then solved the lower order ordinary differential equations numerically. In general, the results obtained from his technique are only good for small values of the perturbed variable (spherical angle). Fortunately, however, he noted that the results for the expression of the concentration profile converges very rapidly with respect to the angular coordinate variable up to rear stagnation point. Therefore, only the first three out of the infinite set of ordinary differential equations had to be solved to obtain the results which were presented for Peclet numbers up to 10. However, his technique should be valid for the entire range of Peclet numbers because his analysis does not make any assumption regarding the magnitude of Peclet number. Yuge's results for $N_{Pe} > 10$ have been combined by Friedlander (15) with the Levich thin boundary layer solution of the diffusion equation at high Peclet number to obtain a correlation between the Sherwood number and the Peclet number for the entire Peclet number range.

In another paper, Friedlander (14), also presented a solution for the entire Peclet number range by using an assumed concentration profile and transforming the diffusion equation into integral form. However, he neglected diffusion in the angular direction which is not valid in the low Peclet number range.

Bowman et al. (6) extended Friedlander's (14) integral technique to the problem of transfer from both

gas bubbles and solid spheres. These workers noted that they were able to predict the mass transfer rate in agreement with experiment (82) up to Reynolds number of order of 10, despite the fact that they used velocity profiles which were applicable only for $N_{Re} < 1$. Boundary layer techniques have also been applied by Lochiel and Calderbank (50) for both Stokes' flow and high Reynolds number flow.

b) $N_{Re} > 1$; single solid spheres; no reaction

For the case of high Reynolds number flow, analytical solutions based both on the thin concentration boundary layer assumption and on integral methods of solution are presented. The results for both local and overall mass transfer rates are presented in the form of

$$N_{Sh} = C_1 N_{Sc}^{1/3} N_{Re}^{1/2} \qquad \text{(II-4)}$$

where C_1 is dependent on the mathematical model assumed and the method of solution. Analytical solutions based on the thin concentration boundary layer approximation cannot predict the constant C_1 for the overall mass (or heat) transfer rate since the velocity profile in the wake region in back of the sphere is unknown. Solutions to predict the mass transfer rates in the wake region have been presented using integral methods. However, it is difficult to say whether these predictions are meaningful.

The thin concentration boundary layer approach has been employed by Baird and Hamielec (5) and Lochiel and

Calderbank (50) to obtain analytical solutions for transfer from both gas bubbles and solid spheres. The latter authors used a velocity profile obtained by Milliken from an integral solution of the momentum boundary layer equations. Since this velocity profile can only be applied up to the boundary layer separation point, it is impossible to predict the mass transfer rate in the wake region. Lochiel and Calderbank, therefore, obtained overall mass transfer rates up to the flow separation point (approximately 108^{o} from the forward stagnation point) and then arbitrarily increased their result by 20% to account for mass transfer in the wake region.

Baird and Hamielec have suggested that there is "fresh fluid" entering the vortex region continuously along the line through the real stagnation point which would make the mass transfer rate in the wake region quite appreciable. However, the vortex region may contain very little "fresh fluid" but rather may be almost saturated with the solute being transferred. Thus, until the velocity profile in the wake region is established, it is very difficult to predict the mass transfer rate in the wake region. This difficulty has also been reported by Froessling (18), Aksel'rud (3), Linton and Sutherland (48), and Ruckenstein (69).

Garner and Keey (21) and Grafton (25) have presented results for the prediction of mass transfer rates in the wake region. Their methods involve the assumption of suitable polynomials to represent both the velocity

and concentration profiles together with a relationship between the hydrodynamic and concentration boundary layer thickness given by Levich (47). In the method presented by Grafton (25), a complete knowledge of the shape of the vortex region is required. The meaningfulness of these results is doubtful, even though the results agree quite well with the experimental work given by Garner and coworkers (19, 21, 22). The experimental work has been very strongly criticized because of the unknown effect of turbulence in their experiments (19, 22) and because the authors chose to use the unrealistic average velocity rather than the centerline velocity in calculating the particle Reynolds number.

Recently, Leclair and Hamielec (46) presented a numerical solution for mass transfer around a single sphere for the thin boundary layer concentration approximation at high Reynolds numbers using a velocity profile obtained from a numerical solution of the complete Navier-Stokes equations. Their results show that the maximum mass transfer rate occurs a few degrees away from the forward stagnation point. This unusual phenomenon has never been found by the experimental workers such as Peltzman and Pfeffer (61) and others.

More recently, Woo and Hamielec (83) presented a numerical solution for both single spheres and cylinders by solving the complete elliptic diffusion equation using finite-difference methods. Their results cover a very wide range of Reynolds and Peclet numbers, both ranging from 0 to 400. The velocity profiles used include

Stokes', Kawaguti's (40) (based on Galerkin's method) as well as those obtained from solving the Navier-Stokes equations by finite-difference techniques. This time the maximum mass transfer rate was always found to occur at the forward stagnation point.

c) Multiparticle systems; no reaction

Theoretical studies in this area are much fewer than those of single sphere systems, due to the complexity of description of the hydrodynamic behavior around the spheres. Pfeffer and Happel (64) presented an analytical study based on the Yuge perturbation technique using a cell model having a "free surface" (28) and the creeping motion equations to describe the velocity profiles around the spheres. Their solution does not assume thin boundary layers and does not neglect diffusion in the angular direction and therefore is applicable at very low Peclet numbers. These authors also determined the effect of heterogeneous chemical reaction on the surface of the particles on the mass transfer rate by simply changing the boundary condition on the spherical particle surface.

Pfeffer (63) also presented an analytical solution in which the "free surface model" was combined with the thin concentration boundary layer approximation for high Peclet numbers. This analytical result agrees very well with available experimental mass transfer data for fixed and fluidized beds at Peclet numbers higher than 70 and for Reynolds numbers up to 100 depending on the porosity of the multiparticle system. The reason why the analytical solution based on a velocity profile which neglects the

inertia terms in the Navier-Stokes equations gives good agreement with experimental data up to Reynolds numbers of 100 at $\epsilon = 0.4$ is due to the fact that as the particle assemblage becomes more concentrated the effect of boundary layer separation and wake flow tends to appear at higher and higher Reynolds numbers starting at a Reynolds number of about 1 for a single particle ($\epsilon = 1$) and going to a Reynolds number of about 100 for $\epsilon = 0.4$. This hypothesis has recently been verified by the work of Leclair and Hamielec (46) and Woo and Hamielec (83) who extended their computations for a mass transfer around a single sphere (see above) to multiparticle systems by employing a cell model similar to that used by Pfeffer (63). Using velocity profiles obtained by solving the Navier-Stokes equations for the fluid in a concentric spherical cell and assuming zero vorticity at the outer cell boundary, these authors have shown that as the void volume of the multiparticle decreases, the flow separation point moves closer and closer to the rear stagnation point, eventually disappearing altogether.

d) First order homogeneous reaction

The problem of adding a homogeneous chemical reaction in the continuous phase to the diffusion from a single solid sphere involves the addition of a source term to the diffusion equation. Johnson and Akehata (38) extended Yuge's perturbation method (84) and solved the problem with homogeneous first order chemical reaction at low Reynolds numbers. Rutland and Pfeffer (70) also presented the solution of mass transfer from a single sphere in

Stokes' flow with a homogeneous chemical reaction. Their results using a perturbation technique suggested by Kronig and Bruijston (44) agree very well with Johnson and Akehata's results. Recently, Johnson et al. (39) extended Pfeffer and Rutland's, and Johnson and Akehata's work to higher Reynolds numbers by using an approximate velocity profile obtained by applying Galerkin's method. They solved the governing diffusion equation with chemical reactions for flow around a single sphere numerically using the Crank-Nicolson implicit finite-difference method. The resulting local Sherwood numbers without chemical reaction were compared with the analytical solution given by Baird and Hamielec (5) using the thin boundary layer approximation. The numerical results were found to agree very well with the analytical solution. No solution, however, has been obtained for the single sphere with homogeneous chemical reaction using the approximate boundary layer solutions for the velocity profile.

In a recent paper, Goddard and Acrivos (23) presented a theoretical study of this problem using the thin boundary layer approximation for wedge type flows given by the Falkner-Skan equation. They presented solutions for the two limiting cases of very fast reactions and very slow reactions using a regular perturbation technique. However, their solutions were obtained only up to first order or second order approximation terms. As usual, when one obtains a regular perturbation solution, the applicable range of the perturbed parameter is unknown.

For the case of extremely fast reaction, their resulting solutions were of no practical use, since the solution approached its asymptotic value very rapidly. For the case of extremely slow reaction, their results are only of little interest to this problem because of the particular velocity profiles which they chose.

e) Rapid, irreversible, second-order chemical reaction

For the case of mass transfer with rapid, irreversible, second-order chemical reaction, many classical approaches have been presented including the application of film theory (30, 72), surface-renewal theory (42) and penetration theory (59, 74). Most of these models were applied using a simplified geometry because of the complexity of the diffusion mechanism. Even for the simplified geometry, specific assumptions (mathematical models) were usually made to solve the problem.

Boundary layer theory was applied to solve the rapid, irreversible, second-order chemical reaction problem by Litt and Friedlander (49) from a flat plate and the inside surface of a cylinder. Sherwood and Ryan (73) and Meyerink and Friedlander (54) later presented the same results assuming a general geometry of the particle surface. Their results which were obtained by neglecting the eddy diffusivity near the surface of the particles inside the reaction zone is not realistic for the case of a moderate concentration boundary layer thickness relative to the case of no reaction. Therefore, their results are good only for a very thin concentration boundary layer or

a concentrated reagent solution.

The problem dealing with an arbitrary shape of particle surface and simplified flow field over solid particles has been treated by Acrivos (1) using the thin diffusional boundary layer approximation. Later, Acrivos' technique was duplicated by Kitaura and Tanaka (43) for the case of flow around solid spheres. They used a velocity profile which, strictly speaking, applies only in the forward stagnation region. However, they obtained the same result as that presented by Acrivos (1).

2. Experimental Studies of Heat and Mass Transfer With and Without Homogeneous Chemical Reaction from Solid Spheres.

Experimental studies for forced convection mass transfer without chemical reactions are more readily available than analytical studies for both single sphere and multiparticle systems. Most of these investigations were conducted using an air stream or water as the continuous phase for physical mass transfer. Publications by Peltzman (60) and Peltzman and Pfeffer (61) give a very detailed review of this field. There is no experimental work with chemical reaction around single solid spheres. For the case of multiparticle systems such as packed beds on fluidized beds, the mass transfer studies with chemical reactions were mostly conducted under unknown hydrodynamic behavior (13). A review of these studies was given by Astarita (4). The results for pure physical mass transfer especially for a single-sphere system obtained by various investigators were usually correlated by assuming the additivity of natural and forced convection terms such as

$$N_{Sh} = N'_{Sh} + D_i N_{Sc}^{m_i} N_{Re}^{n_i} \qquad \text{(II-5)}$$

where D_i, m_i, and n_i, are constants and N'_{Sh} is a Sherwood number due to molecular diffusion and natural convection only (i.e. N_{Sh} at $N_{Re} = 0$). N'_{Sh} is usually expressed as

$$N_{Sh.}' = 2 + E\, N_{G_T}^{m_2} N_{Sc}^{n_2} \qquad \text{(II-6)}$$

where E, M_2 and N_2 are again constants.

The correlation of physical mass transfer rates in multiparticle systems are usually presented in terms of the Colburn "j" factor. The results presented by various investigators do not agree too well with one another, especially in fluidized bed systems.

For the case of mass transfer with homogeneous reaction, the results are usually correlated in terms of the enhancement factor. For a very rapid second order chemical reaction this is usually given in terms of

$$\phi = f\left(\frac{C_{BM}}{C_{Ao}}, \frac{N_{Sc_A}}{N_{Sc_B}}\right) \qquad \text{(II-7)}$$

and is assumed to be independent of the hydrodynamic behavior (Reynolds number), whereas for a first order homogeneous chemical reaction the enhancement factor depends strongly on the hydrodynamic behavior and is usually expressed as

$$\phi = f\left(N_{Re}, N_{Sc}, \beta\right) \qquad \text{(II-8)}$$

a) Single sphere systems without chemical reaction

For particle Reynolds numbers of 1000 or less, experimental data have been reported by Froessling (17), Garner and coworkers (19, 20, 21, 22), Linton and

Sutherland (48), Steinberger and Treybal (76), Rowe et al. (68), Keey and Glen (41), Yuge (85), Steel and Geankoplis (75), and others. Experimental verifications of the theoretical studies at low Reynolds and Peclet numbers have been limited, because of strong natural convection effects on mass (or heat) transfer data at low Reynolds number. The effects of natural convection at high Reynolds number have also been shown experimentally by Steinberger and Treybal (76), Garner and Suckling (22), and Garner and Keey (21). These authors note that even at particle Reynolds number as high as 750 natural convection effects are not entirely absent.

Froessling's work (17) which studied mass transfer from spheres of naphthalene, aniline, water and nitrobenzene into an air stream is probably the earliest. This work was criticized (68) since Froessling neglected natural convection effects and calculated the diffusivities from observed mass transfer rates at zero air velocity using the known theoretical relationship that the Sherwood number is equal to 2 at zero velocity.

Garner et al. (19, 20, 22) investigated forced convection mass transfer from benzoic acid spheres into water. Their mass transfer coefficient results were higher than those obtained by the majority of other workers in this field. Linton and Sutherland (48) believed that the screens used to obtain a uniform velocity profile in Garner and coworkers' work were placed too close to the test sphere. Thus, the turbulence effect may have caused abnormally high mass transfer rates. Another

study by Garner and Keey (21) for laminar flow in a circular tube used the average rather than the centerline velocity to correlate their results. It would have been more realistic to use the centerline velocity rather than the average velocity of the parabolic velocity profiles in the tube.

Steinberger and Treybal (76) also investigated forced convection mass transfer rates from benzoic-acid spheres into water over a very wide Reynolds number range. Their study was criticized not only in that the investigation was influenced by wall effects but also that it was difficult to choose a suitable correlation velocity under high wall effect conditions.

Rowe et al. (68) have presented experimental data for mass transfer from benzoic acid spheres to water and from naphthalene spheres into air. Analogous heat transfer studies have also been carried out by these authors. Their results were slightly higher than those presented by other investigators. Houghton (35) suggested that turbulence in the work of Rowe et al. was the reason for their high results. However, even the data obtained by Rowe et al. (68) under strictly laminar conditions for mass transfer to water were relatively higher than those obtained by others.

Studies of local mass transfer rates as well as overall mass transfer rates have appeared in the recent literature. Rhodes and Peebles (66), Garner and Stuckling (22) and Peltzman and Pfeffer (61) presented results in this area. Garner and Suckling measured the

local mass transfer rates using photgraphic methods and presented correlations for different regions over the sphere surface. Their results gave an idea as to what the distribution of the wake region is relative to the overall mass transfer. It is interesting to note that their results for the wake region were also correlated using the form of equation (II-5).

Rhodes and Peebles (66) presented overall and local mass transfer rate data for both single spheres and ordered arrays. For the case of single spheres they found that their results for the overall Sherwood number agree excellently with those of Garner et al. (19, 20, 21, 22). However, their local mass transfer rates results, especially in the wake region, were different than the patterns presented by Garner et al. (22) and later verified by Peltzman and Pfeffer (61).

Recently Peltzman and Pfeffer (61) studied the local and overall mass transfer rates from single spheres of benzoic acid and beta naphthol to water. They found that the benzoic acid spheres gave much higher Sherwood numbers than the beta naphthol spheres at the same value of the Peclet number. Attempts to explain the difference between the overall mass transfer coefficients found for the two systems on the basis of the effects of concentration driving force (flux), of natural convection and of Schmidt number were not successful so that these authors concluded that differences in the crystalline nature of the cast particles (grain droppings) might be the reason for the higher mass transfer rates

for the benzoic acid-water system.

Peltzman and Pfeffer found that the location of the minimum local mass transfer rate and the location of the hydrodynamic separation point were generally also the same. The coincidence of these two locations has also been observed in the intermediate Reynolds number range from 200 to 400 (19). Garner and Grafton (19) have suggested that at very high Reynolds number a small amount of stagnant fluid exists behind the flow separation point so that the minimum local mass transfer rates occur a few degrees behind the flow separation point.

b) multiparticle systems

Experimental studies in multiparticle systems concentrated mainly on obtaining mass transfer data for packed beds and fluidized beds (26, 27). Most of these data are correlated in terms of the Colburn "j" factor as a function of particle Reynolds numbers. However, the experimental investigations of particle-to-fluid mass transfer in packed beds showed that most of the correlations obtained by the individual investigators did not agree with each other. Investigations using fluidized beds showed an even greater disagreement between different studies. McConnachie and Thodos (53) investigated mass transfer rates using distended beds of spheres. They reported that the motion of the particles in fluidized beds did not appear to have a significant effect on mass transfer rates. They also noted that there was essentially no difference between the "j" factor vs. Reynolds number relationships for expanded

fixed beds formed by randomly dispersed solid spheres and those formed by holding the active spheres in position.

Some empirical correlations showed that the "j" factor vs. Reynolds numbers curve was a straight line with a negative slope of unity for low Reynolds numbers and low Schmidt numbers. This is in good agreement with the analytical solution (64) for low Reynolds numbers and Peclet numbers less than about 70. For low Reynolds numbers and high Peclet numbers (greater than 70) the slope of the "j" vs. Reynolds number curve has been found from the analytical solutions (63) to be -2/3 rather than -1. At high Reynolds number (above 100 at a void fraction of 0.4 for example) analytical solutions based on boundary layer theory predict the slope to change to -1/2. Thus, the analytical solutions predict a change in slope in the "j" factor vs. Reynolds numbers correlation from -1 to -2/3 to -1/2 depending on the values of the Schmidt number and Reynolds number. This tends to explain why a single correlation of "j" vs. N_{Re} as proposed by experimental correlations does not adequately represent all of the experimental data.

Recently, Rhodes and Peebles (66), and Peltzman and Pfeffer (61) experimentally investigated local and overall physical mass transfer rates from a single active sphere to the fluid flowing around it. The systems studied included a single test sphere with or without inert particles placed around it in simple arrays. Rhodes and Peebles found that the local transfer rate

was strongly dependent on the geometry of the array, the plane of the measurement around the sphere and the hydrodynamic conditions in the bed. They presented their results as local Sherwood numbers around the sphere but were not able to obtain a correlation. Peltzman and Pfeffer presented tneir results (of placing different geometrical configurations of inert spheres around a test sphere) as local and overall Sherwood numbers around the test sphere as a function of the Reynolds and Schmidt numbers. Peltzman and Pfeffer's study is of particular interest to this study, since the experimental part of this work has essentially applied their experimental technique and apparatus.

c) Mass transfer with homogeneous chemical reaction.

Up to the present time no experimental studies of mass transfer with chemical reaction from a single solid test sphere have been reported. Recently, Houghton (35) investigated the mass transfer rates with chemical reaction from carbon dioxide gas bubbles to monoethanolamine. Other investigations which have been concerned with chemical reactions have generally considered systems of simple geometry, such as in laminar liquid jets (56), falling films (67), films formed on a rotating cylinder or drum (10), plane interfaces, and stirred vessels (51, 52, 81) and the results are usually correlated in terms of the enhancement factor. Most of the experimental studies presented in fluidized beds and packed beds were conducted under unknown hydrodynamic conditions (13).

For the case of mass transfer with very rapid second order irreversible reaction, several experimental results have been presented. Friedlander et al. (49), (54) have studied diffusion of benzoic acid from a flat plate and from the inside wall of a benzoic acid cylinder into water containing NaOH. They found that their experimental results agreed very well with their theoretical studies even though the diffusion constant of NaOH in H_2O is not accurately known.

III. SCOPE OF THE RESEARCH

Present reactor design procedures are usually based upon empirical or semi-empirical techniques using pilot plant data and scale-up. The establishment of mathematical models and solution techniques to predict the mass (or heat) transfer rates including the effect of chemical reactions and particle-to-particle interactions should be very valuable in reactor designs. To verify the mathematical models and solution techniques and to be able to develop reasonable new models, it is also necessary to obtain pertinent experimental data.

With these ideas in mind, it was decided to study both theoretically and experimentally the effect of chemical reaction on both local and overall mass transfer rates around single spheres and in multiparticle systems. These studies would consist of four separate phases to include:

i) A numerical analysis of the effect of first order homogeneous chemical reaction on the local and overall mass transfer rates around single solid spheres and in multiparticle systems at low and high Reynolds numbers using velocity profiles obtained from Stokes' flow and from boundary layer theory. A more generalized parameter, combining both hydrodynamic effect and reaction effect, will be introduced here. The results of this phase of the study will be compared to any available solutions using different mathematical models and solution techniques.

ii) A numerical analysis of the effect of particle-to-particle interaction in a two sphere system on the local and overall mass transfer rates. The effects of first order

homogeneous chemical reaction on mass transfer rates would also be computed. This phase of the study would be performed in the Stokes' flow region where the flow field around two spheres is known and available. Since there are no mass or heat transfer solutions available for flow around two spheres, the mathematical model, solution techniques, and results will be presented as completely as possible for the case of

a) an active sphere placed in front of an inert sphere in the direction of flow.

b) an active sphere placed behind an inert sphere in the direction of flow.

iii) An analytical study of the effect of rapid, irreversible, second-order chemical reactions on the mass transfer rate around solid spheres, liquid drops and gas bubbles. A general mathematical model is to be established for all three cases. The effects of the physical properties of the solute and reagent and the effect of the flow field near the surface of the spherical particles on the enhancement factor will be emphasized. The results will also be compared with the available solutions using different mathematical models and solution techniques.

iv) Experimental measurements of local and overall mass transfer rates around solid single spheres and in two sphere systems. The enhancement factor for a rapid, irreversible, second-order chemical reaction on the local and overall mass transfer rates will be emphasized and compared with the results from the analytical analysis in this study, since there are no experimental data available using solid spheres. The effects of particle-to-particle interactions on mass transfer rate

using two spheres to simulate a very dilute multiparticle system will also be studied in order to get a qualitative comparison with the numerical results obtained in this study.

IV. THEORETICAL WORK

In the entire theoretical analysis of mass transfer problems in this study, several simplified assumptions are made. However, the mathematical models with these simplified assumptions are kept very close to the real physical systems so that the analysis results should be applicable to real physical situations such as those found in commercial packed and fluidized bed reactors. We assume steady state to exist in the system. In commercial systems a transient behavior may exist at the very beginning of the start-up; however, we assume that these transient states exist only within a very short period. Transient conditions are beyond the scope of present study. "Age distribution" behavior is not included in this study either. We also assume that the system is isothermal and the heat of dissolution or reaction is negligible. Therefore, we can reduce the real coupled simultaneous heat and mass transfer problems into pure mass transfer problems. This assumption also allows us to assume that the physical properties such as the density, viscosity and diffusivity of the systems are constant. Other assumptions are 1) The fluid is Newtonian and that the flow around spherical particles is axisymmetric. 2) The resistance to mass transfer is only in the continuous phase. 3) There is no transfer from the continuous phase into the dispersed phase. 4) Natural convection effects are negligible. 5) The Peclet number is large so that the thin concentration boundary layer approximation is applicable.

1. Governing Diffusion Equations

The basic diffusion equation with first order homogeneous chemical reaction at steady state is given in vector notation as:

$$\underline{V}' \cdot \nabla' C_A' = \mathcal{D} \nabla'^2 C_A' - k''' C_A' \qquad \text{(IV-1)}$$

Using the dimensionless variables

$$\begin{aligned} C &= \frac{C_A'}{C_{A0}} \\ \underline{V} &= \frac{\underline{V}'}{U_\infty} \\ N_{Re} &= \frac{2a U_\infty}{\mathcal{D}} \\ \beta &= \sqrt{\frac{k''' a^2}{\mathcal{D}}} \\ \nabla &= \nabla' a \\ \nabla^2 &= \nabla'^2 a^2 \end{aligned} \qquad \text{(IV-2)}$$

equation (IV-1) becomes

$$\nabla^2 C - \tfrac{1}{2} N_{Re} \underline{V} \cdot \nabla C - \beta^2 C = 0 \qquad \text{(IV-3)}$$

and in spherical coordinates with r = r'/a

$$\frac{1}{r^2}\frac{\partial}{\partial r}\left(r^2\frac{\partial C}{\partial r}\right)+\frac{1}{r^2\sin\theta}\frac{\partial}{\partial\theta}\left(\sin\theta\frac{\partial C}{\partial\theta}\right)$$
$$-\frac{1}{2}N_{Pe}\left(V_r\frac{\partial C}{\partial r}+\frac{V_\theta}{r}\frac{\partial C}{\partial\theta}\right)-\beta^2 C=0 \qquad \text{(IV-4)}$$

Equation (IV-4) is an elliptic partial differential equation and attempts to obtain numerical solutions of this equation in the high Peclet number range ($N_{Pe} > 100$) have failed because of the stability problems (38). It was noted in literature (12, 45) that these difficulties could only be overcome at the expense of using stepsizes which are too small to be practical.

If we apply the thin concentration boundary layer approximation for large peclet numbers ($N_{Pe} > 100$), however, and neglect diffusion in the angular direction, equation (IV-4) can be approximated by a parabolic partial differential equation given by

$$\frac{\partial^2 C}{\partial y^2}-\frac{1}{2}N_{Pe}\left(V_x\frac{\partial C}{\partial x}+V_y\frac{\partial C}{\partial y}\right)-\beta^2 C=0 \qquad \text{(IV-5)}$$

Verification of this equation by an order of magnitude analysis is given in Appendix B.

The boundary conditions to be used with equation (IV-5) are

$$\begin{aligned} C &= 1 && \text{at} && y=0 && ;\ \text{all } x \\ C &= 0 && \text{at} && y=\infty && ;\ \text{all } x \\ \frac{\partial C}{\partial x} &= 0 && \text{at} && x=0 && ;\ \text{all } y \end{aligned} \qquad \text{(IV-6)}$$

No difficulties are encountered in the numerical solution of the above equation. Since the Schmidt number for the mass transfer of solid in liquid systems is usually of the order of 10^3, equation (IV-5) is therefore applicable for particle Reynolds numbers greater than 0.1. Equation (IV-5) has been chosen as the starting governing equation in this study for the case of mass transfer with first order homogeneous chemical reactions in both the single sphere systems and the multi-particle systems.

For the case of mass transfer with first order homogeneous chemical reactions in a two sphere system such as one inert sphere placed either above or below one active sphere in the plane parallel to the flow direction, it is useful to use bipolar coordinates. Equation (IV-3) in bipolar coordinates becomes

$$\frac{(\cosh\eta-\cos\xi)^3}{\sin\xi}\left[\frac{\partial}{\partial\xi}\left(\frac{\sin\xi}{\cosh\eta-\cos\xi}\frac{\partial C}{\partial\xi}\right)+\frac{\partial}{\partial\eta}\left(\frac{\sin\xi}{\cosh\eta-\cos\xi}\frac{\partial C}{\partial\eta}\right)\right]$$

$$-\frac{1}{2}N_{Pe}\left(\frac{c}{a}\right)(\cosh\eta-\cos\xi)\left(V_\xi\frac{\partial C}{\partial\xi}+V_\eta\frac{\partial C}{\partial\eta}\right) \quad \text{(IV-7)}$$

$$-\left(\frac{c}{a}\right)^2\beta^2 C = 0$$

The details of the derivation of equation (IV-7) is given in Appendix A. Again, if we apply the thin concentration boundary layer approximation for large peclet numbers ($N_{Pe} \gg 1$) and neglect diffusion in the angular direction, equation (IV-7) can be approximated by a parabolic partial differential

equation given by

$$(\cosh\eta - \cos\xi)^2 \frac{\partial^2 C}{\partial \eta^2} - (\cosh\eta - \cos\xi)\frac{N_{Pe}}{2}\left(\frac{c}{a}\right)\cdot \left(V_\xi \frac{\partial C}{\partial \xi} + V_\eta \frac{\partial C}{\partial \eta}\right) - \left(\frac{c}{a}\right)^2 \beta^2 C = 0 \qquad \text{(IV-8)}$$

This equation is applicable as long as the concentration boundary layer in bipolar coordinates is very thin ($N_{Pe} \gg 1$) so that the diffusion term in the angular direction is negligible. Equation (IV-8) is the starting governing diffusion equation for the two sphere systems in this study.

An order of magnitude analysis verifying this equation for high Peclet numbers is also given in Appendix B.

The boundary conditions to be used with equation (IV-8) for the active sphere placed upstream of the inert sphere which locates at $Y_o > 0$ are

$$\begin{aligned} C &= 1 \quad \text{at} \quad \eta = \gamma_o \quad ; \text{ all } \xi \\ C &= 0 \quad \text{at} \quad \eta = 0 \quad ; \quad \xi = 0 \\ \frac{\partial C}{\partial \xi} &= 0 \quad \text{at} \quad \xi = 0 \quad ; \text{ all } \eta \end{aligned} \qquad \text{(IV-9)}$$

Similarly, the boundary conditions to be used with equation (IV-8) for the active sphere placed downstream of the inert sphere which locates at $Y_o < 0$ are

$$\begin{aligned} C &= 1 \quad \text{at} \quad \eta = \gamma_o \quad ; \text{ all } \xi \\ C &= 0 \quad \text{at} \quad \eta = -\gamma_o \quad ; \quad \xi = \pi \\ \frac{\partial C}{\partial \xi} &= 0 \quad \text{at} \quad \xi = \pi \quad ; \text{ all } \eta \end{aligned} \qquad \text{(IV-10)}$$

For the case of mass transfer from spherical particles into a continuous phase with a rapid second order irreversible chemical reaction occurring in the continuous phase, we assume that the reaction always takes place at a certain fixed distance very near the surface of the spherical particles. Although a spherical shape will be assumed here for the dispersed phase particle, the solutions presented here may readily be generalized to particles with an arbitrary surface geometry. Consider a fluid containing the reagent, species B, flowing past a spherical particle containing the other reagent, species A, which will be referred to as the solute. The rate of reaction of solute A and reagent B is assumed to be a very rapid second order irreversible reaction occurring according to the stoichiometric equation

$$aA + bB \longrightarrow \text{Product} \qquad \text{(IV-11)}$$

Since the reaction between A and B is assumed instantaneous the diffusion equation with a source term (reaction term) is not applicable to this situation. Rather it is assumed that the reaction takes place in a zone of infinitesimal thickness at a certain distance ξ_{AR} away from the surface of the discontinuous phase where ξ_{AR} is, in general, dependent on the spherical angle θ. Thus the governing equations for the diffusion of both species A and B are the same as those for the case of pure physical mass transfer with no chemical reaction being present.

We again assume that the Peclet number is large or that the diffusional boundary layer is very thin relative to the radius of the spherical particle, i.e. $y \ll 1$ so that the

governing equation becomes:

$$\frac{\partial^2 C}{\partial y^2} - \frac{1}{2} N_{Pe} \left(V_x \frac{\partial C}{\partial x} + V_y \frac{\partial C}{\partial y} \right) = 0 \qquad \text{(IV-12)}$$

This equation can be obtained directly from equation (IV-5) with $K''' = 0$ or $\beta = 0$.

For the problem of diffusion with chemical reaction which we are interested in here, the thin diffusional boundary layer approximation will be even more realistic than for physical mass transfer since the chemical reaction will tend to reduce the thickness of the boundary layer. Thus we choose equation (IV-12) as the governing equation for the diffusion of both species A and B. This will result in very little error as long as the continuous phase is a liquid such that $N_{Sc} \gg 1$.

The boundary conditions are such that at the surface of the dispersed phase (or particle surface) the dimensionless concentration of the solute $C_A = 1$ and at the reaction zone, ξ_{AR}, the concentration of both the solute and the reagent $C_A = C_B = 0$. Very far away from the particle surface the dimensionless concentration of species B, $C_B = 1$. The last boundary condition is obtained from the stoichiometry of the chemical reaction. Thus at ξ_{AR} the net molar flux of species A and B must be equal to zero or

$$\left.\frac{\partial C_A}{\partial y}\right|_{y \text{ at } \xi_{AR}} = -\frac{a}{b} \frac{N_{Sc_A}}{N_{Sc_B}} \frac{C_{BM}}{C_{A0}} \left.\frac{\partial C_B}{\partial y}\right|_{y \text{ at } \xi_{AR}} \qquad \text{(IV-13)}$$

If we let

$$\alpha = \frac{N_{Sc_A}}{N_{Sc_B}} \quad ; \; \alpha > 0 \qquad \text{(IV-14)}$$

and

$$\gamma = \frac{a}{b} \frac{C_{BM}}{C_{Ao}} \quad ; \quad \gamma > 0 \tag{IV-15}$$

then the last boundary condition, equation (IV-13), reduces to

$$\left.\frac{\partial C_A}{\partial y}\right|_{y \text{ at } \xi_{AR}} = -\alpha\gamma \left.\frac{\partial C_B}{\partial \xi}\right|_{y \text{ at } \xi_{AR}} \tag{IV-16}$$

where α and γ are known parameters for any particular problem.

Once the concentration profile in the fluid is known the local Sherwood number around the surface of the sphere can be obtained from the relation

$$N_{Sh_\ell} = -2 \left.\frac{\partial C}{\partial y}\right|_{y=0} \tag{IV-17}$$

and the overall Sherwood number from

$$N_{Sh_o} = \int_0^\pi -\left.\frac{\partial C}{\partial y}\right|_{y=0} \sin x \, dx \tag{IV-18}$$

The enhancement factor ϕ, defined as the ratio of the overall Sherwood number with chemical reaction to the Sherwood number without any chemical reaction can be obtained from

$$\phi = \frac{N_{Sho,R}}{N_{Sho,N}} \tag{IV-19}$$

2. Hydrodynamic Behavior

Since we are assuming the solute in the continuous phase to have a Schmidt number much greater than unity, the concentration boundary layer is much thinner than the hydrodynamic boundary layer and the diffusion of the solute into the continuous phase takes place only in a very thin layer of the fluid near the surface of the spherical particles. Therefore, it should be possible to represent the velocity profile of the continuous phase by a linearized relationship in the distance variable normal to the surface of the sphere. If the tangential (or flow direction) velocity, V_x, can be considered to be an analytical function with respect to y, we can expand V_x in a Taylor series around the surface of the dispersed phase, i.e., y = 0, such that

$$V_x = (V_x)_{y=0} + \left(\frac{\partial V_x}{\partial y}\right)_{y=0} y + \left(\frac{\partial^2 V_x}{\partial y^2}\right)_{y=0} \frac{y^2}{2!} + \cdots \qquad \text{(IV-20)}$$

Since we are assuming a thin diffusional boundary layer, only the first two terms in the right hand side of equation (IV-20) are important.

The continuity equation for the continuous fluid in spherical coordinates is given as

$$\frac{1}{r^2}\frac{\partial}{\partial r}(r^2 V_r) + \frac{1}{r^2 \sin\theta}\frac{\partial}{\partial \theta}(V_\theta \sin\theta) = 0 \qquad \text{(IV-21)}$$

Very close to the surface of the sphere, equation (IV-21) can be approximated by

$$\frac{\partial V_y}{\partial y} + \frac{1}{\sin x}\frac{\partial}{\partial x}(V_x \sin x) = 0 \qquad \text{(IV-22)}$$

Thus as soon as V_x is specified, the corresponding V_y can be easily obtained by solving equation (IV-22). The integration constant is equal to zero because of the boundary condition which specifies that the continuous fluid will not penetrate into the dispersed phase.

We now examine more closely the form that equations (IV-20) and (IV-22) take for V_x and V_y for three cases of interest i) solid particles, ii) gas bubbles and iii) liquid drops.

i) For the case of mass transfer from a solid particle such as a benzoic acid sphere slowly dissolving into a continuous liquid phase the tangential velocity on the surface of the sphere can be assumed negligible, i.e. $(V_x)_{y=0} = 0$. Therefore, equation (IV-20) reduces to

$$V_x = \left(\frac{\partial V_x}{\partial y}\right)_{y=0} y = g(x)\, y \qquad \text{(IV-23)}$$

where g(x) is proportional to the shear stress at the surface of the particle. The corresponding V_y is given by equation (IV-22) as

$$V_y = -\frac{y^2}{2 \sin x} \frac{d}{dx} [\, g(x) \sin x \,] \qquad \text{(IV-24)}$$

ii) For the case of mass transfer from gas bubbles dissolving into a continuous liquid phase, the interfacial velocity $(V_x)_{y=0} \neq 0$. However if the density and viscosity of the gas are small as compared to those of the continuous liquid phase then the tangential stress at the surface of the bubble can be assumed negligible. Thus equation (IV-20) can be approximated by

$$V_x = (V_x)_{y=0} = f(x) \qquad \text{(IV-25)}$$

The corresponding V_y is given by

$$V_y = -\frac{y}{\sin x}\frac{d}{dx}\left[f(x)\sin x\right] \qquad \text{(IV-26)}$$

iii) For the case of mass transfer of a solute from liquid drops into a second immiscible continuous liquid phase, neither the first nor the second term in equation (IV-20) can be assumed to be negligible and in general:

$$V_x = f(x) + g(x)\,y \qquad \text{(IV-27)}$$

If we assume that both f(x) and g(x) are odd functions of x and set

$$f(x) = \sum_{n=1} A_{2n-1} x^{2n-1}$$

$$g(x) = \sum_{n=1} B_{2n-1} x^{2n-1} \qquad \text{(IV-28)}$$

equation (IV-27) becomes

$$V_x = \sum_{n=1} \left(A_{2n-1} + B_{2n-1}\,y\right) x^{2n-1} \qquad \text{(IV-29)}$$

and the corresponding V_y is

$$V_y = -\frac{1}{\sin x}\frac{\partial}{\partial x}\left[\int_0^y V_x \sin x \, dy\right]$$

$$= -\frac{1}{\sin x}\frac{\partial}{\partial x}\left[\sum_{n=1}\left\{\left(A_{2n-1}y + \tfrac{1}{2}B_{2n-1}y^2\right)\cdot \sin x \cdot x^{2n-1}\right\}\right] \qquad \text{(IV-30)}$$

Since

$$\sin x = \sum_{m=1} \frac{1}{(2m-1)!}(-1)^{m-1} x^{2m-1}$$

equation (IV-30) can be written as

$$V_y = -\frac{\sum_{n=1} \left[\left(A_{2n-1} \chi + \frac{1}{2} B_{2n-1} \chi^2 \right) \left\{ \sum_{m=1} \frac{(-1)^{m-1}}{(2m-1)!} (2m+2n-2) X^{2m+2n-\frac{5}{2}} \right\} \right]}{\sum_{m=1} \frac{1}{(2m-1)!} (-1)^{m-1} X^{2m-2}} \qquad \text{(IV-31)}$$

For the case of mass transfer with a very rapid second order irreversible chemical reaction, analytical solutions have been obtained using a generalized model for all three types of particles, i.e., solid spheres, liquid drops and gas bubbles. For the case of mass transfer with first order homogeneous chemical reaction, numerical solutions have been obtained around solid spheres specifying the function g(x) for the particular Reynolds number range of interest.

Velocity profiles for the fluid in creeping flow around single spheres can be derived from the Stokes' stream function which is given as:

$$\psi = \frac{1}{2} U_\infty r^2 \sin\theta \left[\frac{1}{2} \left(\frac{a}{r} \right)^3 - \frac{3}{2} \left(\frac{a}{r} \right) + 1 \right] \qquad \text{(IV-32a)}$$

Applying the thin boundary layer approximation, equation (IV-32a) reduces to

$$\psi \cong -\frac{3}{4} U_\infty y^2 \sin^2 X \qquad \text{(IV-32b)}$$

Using equation (IV-32b) the velocity profiles in the form of equations (IV-23) and (IV-24) are given by

$$V_x = \frac{3}{2} \chi \sin X \qquad \text{(IV-33a)}$$

$$V_y = -\frac{3}{2} \chi^2 \cos X \qquad \text{(IV-33b)}$$

For the case of multiparticle systems, the hydrodynamic behavior in creeping flow around spherical particles has been idealized by Happel (28) using the free surface model as

$$\psi = -\frac{U_\infty \sin^2\theta}{2W}\left[(2+3\lambda^5)r^2 + \frac{a^3}{r} - (3+2\lambda^5)ar - \frac{\lambda^5 r^4}{a^2}\right] \qquad \text{(IV-34a)}$$

where λ and W depend only on the porosity of the multiparticle system and U_∞ is the superficial velocity. Again applying the thin boundary layer approximation, the stream function reduces to

$$\psi \cong -\frac{U_\infty \sin^2 X}{2W}\left[3(1-\lambda^5)y^2\right] \qquad \text{(IV-34b)}$$

and the corresponding velocity profiles in the form of equations (IV-23) and (IV-24) becomes

$$V_x = \frac{3(1-\lambda^5)}{W} y \sin X \qquad \text{(IV-35)}$$

$$V_y = -\frac{3(1-\lambda^5)}{W} y^2 \cos X \qquad \text{(IV-36)}$$

Note that as λ approaches zero, the porosity of the multiparticle system approaches unity ($\varepsilon \to 1$) and the parameter W approaches 2 and equations (IV-35) and (IV-36) reduce to equations (IV-33a) and (IV-33b) respectively when the porosity is unity.

Velocity profiles around a single sphere at high Reynolds numbers can be approximated up to the flow separation point by using boundary layer theory. The tangential velocity

profile is given by Lochiel and Calderbank (50) using the Karman-Pohlhausen integral method as

$$V_x = \sqrt{\frac{3}{10} N_{Re}}\; y \left[\frac{\sin^{12.5} x}{\int_0^x \sin^{9.5}\theta \, d\theta} \right]^{1/2} \qquad \text{(IV-37)}$$

The corresponding radial velocity profile using equation (IV-22) is given by

$$V_y = \sqrt{\frac{3}{160} N_{Re}}\; y^2 \frac{14.5 \sin^{5.25} x \cos x \int_0^x \sin^{9.5}\theta \, d\theta - \sin^{15.75} x}{\left(\int_0^x \sin^{9.5}\theta \, d\theta \right)^{1.5}} \qquad \text{(IV-38)}$$

Since these velocity profiles are based on boundary layer theory they are good only up to the boundary layer separation point, approximately 108° or 1.885 radians from the forward stagnation point.

For a two sphere system, the velocity profile developed in a viscous fluid at rest at infinity by two equal solid spheres moving with small constant velocities parallel to their line of centers has been presented by Stimson and Jeffery (77) using bipolar coordinates as

$$\psi(\xi,\eta) = (\cosh\eta - \cos\xi)^{1/2} \sum_{n=1} U_n(\eta)\, V_n(\xi) \qquad \text{(IV-39)}$$

where

$V_n(\xi) = P_{n-1}(\cos\xi) - P_{n+1}(\cos\xi)$; P : Legendre function

$V_n(\xi) = P_{n-1}(\cos\xi) - P_{n+1}(\cos\xi)$; P : Legendre function

$$U_n(\eta) = A_n \cosh\left(n-\tfrac{1}{2}\right)\eta + C_n \cosh\left(n+\tfrac{3}{2}\right)\eta$$

$$A_n = -(2n+3)\,K\, \frac{2(1-e^{-(2n+1)\alpha}) + (2n+1)(e^{2\alpha}-1)}{\cdots} \qquad \text{(IV-40)}$$

$$C_n = (2n-1)\,K\, \frac{2(1-e^{-(2n+1)\alpha}) + (2n+1)(1-e^{-2\alpha})}{2\sinh(2n+1)\alpha + (2n+1)\sinh 2\alpha}$$

$$K = \frac{c^2 U_\infty n(n+1)}{\sqrt{2}\,(2n-1)(2n+1)(2n+3)}$$

$\alpha = |Y_0|$: surface of the sphere ; $\alpha > 0$

Equation (IV-39) can be readily transformed to the corresponding problem in which the spheres are fixed and the fluid streams past them with a constant velocity. By superimposing a constant velocity equal to $-U_\infty$ at infinity, the actual stream function that we are interested in, is therefore given as

$$\psi = \frac{1}{2}c^2 \frac{\sin\xi}{(\cosh\eta - \cos\xi)^2} + (\cosh\eta - \cos\xi)^{-3/2} \sum_{n=1} U_n(\eta) V_n(\xi) \quad \text{(IV-41)}$$

It should be noted that this velocity profile is valid only in creeping flow.

The expressions for the velocity profile in terms of the derivatives of the stream function in general orthogonal coordinates have been given by Goldstein (24) as

$$V_{\theta_1} = h_2 h_3 \frac{\partial \psi}{\partial \theta_2}$$

$$V_{\theta_2} = -h_3 h_1 \frac{\partial \psi}{\partial \theta_1} \quad \text{(IV-42)}$$

where h_1, h_2 and h_3 are metric coefficients and θ_1 and θ_2 are general orthogonal coordinates.

These corresponding velocities have been derived in Appendix C and are given as

$$V_\xi = -\frac{\sin\xi \sinh\eta}{(\cosh\eta - \cos\xi)} + \frac{\sin\xi}{c^2} \cdot$$

$$\left[-1.5(\cosh\eta - \cos\xi)^{-0.5} \cdot \sinh\eta \cdot \left(\sum_{n=1} U_n(\eta) \frac{V_n(\xi)}{\sin^2\xi}\right)\right. \quad \text{(IV-43)}$$

$$\left. + (\cosh\eta - \cos\xi)^{0.5} \left(\sum_{n=1} \frac{dU_n(\eta)}{d\eta} \frac{V_n(\xi)}{\sin^2\xi}\right)\right]$$

$$V_\eta = \frac{1-\cosh\eta\cos\xi}{(\cosh\eta-\cos\xi)} - \frac{1}{C^2}\left[-1.5\,(\cosh\eta-\cos\xi)^{-0.5}\cdot\right.$$

$$\sin^2\xi\left(\sum_{n=1} U_n(\eta)\,\frac{V_n(\xi)}{\sin^2\xi}\right) \qquad \text{(IV-44)}$$

$$\left.+(\cosh\eta-\cos\xi)^{0.5}\left(\sum_{n=1} U_n(\eta)\,\frac{1}{\sin^2\xi}\,\frac{dV_n(\xi)}{d\xi}\right)\right]$$

Note that equations (IV-43) and (IV-44) should reduce to equations (IV-32) and (IV-33) respectively when the two spheres are very far apart and the diffusional boundary layer is very thin.

3. Solutions of the Governing Diffusion Equations.

For cases of mass transfer with first order homogeneous chemical reaction for single sphere systems, two sphere systems axially located in the flow direction and multiparticle systems, numerical solutions are obtained using finite-difference techniques. In this study, the Crank-Nicolson implicit finite-difference method is applied to solve these diffusion equations. The procedure involved substituting the derivatives in the angular direction by a straight forward finite-difference approximation. The radial derivatives are given by the average values over two succeeding angular increments with the average weighting factor taken as 0.5. The resulting finite-difference equation consists of a set of simultaneous algebraic equations which are solved using Peaceman and Rachford's method (9).

For the case of mass transfer from spherical particles consisting of either solid spheres, liquid drops or gas bubbles into a continuous phase with a rapid second order irreversible chemical reaction occurring in the continuous phase, we apply a generalized model and solve the diffusion equations with appropriate boundary conditions analytically by the method of combination of variables. Simplified hydrodynamic flow patterns are used in this part of study. Although the calculations are made assuming spherical particles, the results, presented in terms of the enhancement factor, should be good for any arbitrary shape surface of the dispersed particles, as long as the assumptions

made are applicable to the system of interest.

A. First Order Homogeneous Chemical Reactions around Single Sphere and Multiparticle Systems.

The following finite-difference forms are used for the differential terms:

$$C = \frac{1}{2}\left(C_{i+1,j} + C_{i,j}\right)$$

$$\frac{\partial C}{\partial X} = \frac{C_{i+1,j} - C_{i,j}}{\Delta X}$$

$$\frac{\partial C}{\partial y} = \frac{1}{2}\left[\frac{C_{i+1,j+1} - C_{i+1,j-1}}{y_{j+1} - y_{j-1}} + \frac{C_{i,j+1} - C_{i,j-1}}{y_{j+1} - y_{j-1}}\right] \qquad \text{(IV-45)}$$

$$\frac{\partial^2 C}{\partial y^2} = \frac{1}{2}\left[\frac{2\,C_{i+1,j+1}}{(y_{j+1}-y_j)(y_{j+1}-y_{j-1})} - \frac{2\,C_{i+1,j}}{(y_{j+1}-y_j)(y_j - y_{j-1})}\right.$$

$$+ \frac{2\,C_{i+1,j-1}}{(y_j - y_{j-1})(y_{j+1}-y_{j-1})} + \frac{2C_{i,j+1}}{(y_{j+1}-y_j)(y_{j+1}-y_{j-1})}$$

$$\left. - \frac{2\,C_{i,j}}{(y_{j+1}-y_j)(y_j - y_{j-1})} + \frac{2\,C_{i,j-1}}{(y_j - y_{j-1})(y_{j+1}-y_{j-1})}\right]$$

where

i = index in x-direction (angular)

j = index in y-direction (radial)

The stepsize used in the angular direction was taken as uniform but the stepsize in the radial direction was increased as y increased according to the relation

$$y_j = \Delta y_0 \frac{h^j - 1}{h - 1} \quad ; \quad j = 0, 1, 2 \cdots \qquad \text{(IV-46)}$$

and

$$y_{j+1} - y_j = \Delta y_0 \cdot h^j \qquad \text{(IV-47)}$$

where Y_o is the initial stepsize and h is an arbitrary constant greater than 1. This is done since the concentration profile very far away from the surface of the spheres is much less important than that very close to the surface of the sphere.

Equations (IV-5), (IV-45), and (IV-47) give

$$\begin{aligned} & C_{i+1,j-1}(\ell_3+\ell_5) + C_{i+1,j}(-\ell_2-\ell_4-\ell_6) \\ & \quad + C_{i+1,j+1}(\ell_1-\ell_5) + C^*_{i,j-1}(\ell_3+\ell_5) \\ & \quad + C^*_{i,j}(-\ell_2+\ell_4-\ell_6) + C^*_{i,j+1}(\ell_1-\ell_5) = 0 \end{aligned} \qquad \text{(IV-48)}$$

where the C*'s are known values and

$$\begin{aligned} \ell_1 &= 1/[(\Delta y_0)^2 h^{2j-1}(h+1)] \\ \ell_2 &= 1/[(\Delta y_0)^2 h^{2j-1}] \\ \ell_3 &= 1/[(\Delta y_0)^2 h^{2j-2}(h+1)] \\ \ell_4 &= N_{Re} V_x/(2\Delta x) \\ \ell_5 &= N_{Re} V_y/[4\Delta y_0 h^{j-1}(h+1)] \\ \ell_6 &= \beta^2/2 \end{aligned} \qquad \text{(IV-49)}$$

This resulting difference equation, equation (IV-48), represents a set of simultaneous algebraic equations which can be solved by matrix inversion at each angular increment. However, in this part of study these sets of simultaneous algebraic equations were solved by using Peaceman and Rachford's method. It is noted (9) that Peaceman and Rachford's method will not create too much round-off error in high speed machine calculations. Details of Peaceman and Rachford's method are given in Appendix D. The concentration profiles at the first two angular steps, however, were obtained by using ordinary relaxation methods which automatically take care of the boundary conditions along the forward stagnation line (θ = zero).

Boundary conditions are obtained from equation (IV-6) as

$$\begin{aligned} C_{i,0} &= 1 \quad ; \quad \text{all } i \\ C_{i,M} &= 0 \quad ; \quad \text{all } i \\ C_{0,j} &= C_{1,j} \quad ; \quad \text{all } j \end{aligned} \tag{IV-50}$$

where M is the index representing the position on the outside surface of the concentration boundary layer. Although M is a constant, it can be increased in the process of the computation to conform to the actual thickness of the concentration boundary layer.

For the case of mass transfer and homogeneous chemical reaction from solid spheres, it is interesting

to note that we are able to generate a characteristic parameter containing both hydrodynamic and reaction rate parameters. For example, if we combine equations (IV-5) with the flow velocity profile, equations (IV-23) and (IV-24), we obtain

$$\frac{\partial^2 C}{\partial y^2} - \frac{N_{Pe}}{2}\left[g(x)\, y \frac{\partial C}{\partial X} - \frac{y^2}{2\sin x}\frac{d}{dx}\{g(x)\sin x\}\frac{\partial C}{\partial y}\right] - \beta^2 C = 0 \quad \text{(IV-51)}$$

If we let

$$y' = \beta y \quad ; \quad \beta \neq 0 \qquad \text{(IV-52)}$$

equation (IV-51) becomes

$$\frac{\partial^2 C}{\partial y'^2} - \frac{N_{Pe}}{2\beta^3}\left[g(x)\, y' \frac{\partial C}{\partial X} - \frac{y'^2}{2\sin x}\frac{d}{dx}\{g(x)\sin x\}\frac{\partial C}{\partial y'}\right] - C = 0 \qquad \text{(IV-53)}$$

Equation (IV-53) indicates that the constant N_{Pe}/β^3 should be treated as a single parameter. For the case of high Reynolds number boundary layer flow, the function g(x) already contains the parameter $(N_{Re})^{\frac{1}{2}}$. In that case, we simply use $N_{Pe}\, N_{Re}^{1/2}/\beta^3$ as the characteristic single parameter for the numerical solutions.

The same finite-difference technique which we applied to equation (IV-5) is also applicable to equation (IV-53) with the boundary conditions as

$$\begin{aligned} C &= 1 \quad \text{at} \quad y' = 0 \quad ; \text{ all } X \\ C &= 0 \quad \text{at} \quad y' = \infty \quad ; \text{ all } X \\ \frac{\partial C}{\partial X} &= 0 \quad \text{at} \quad x = 0 \quad ; \text{ all } y' \end{aligned} \qquad \text{(IV-54)}$$

Computer programs solving equations (IV-5), (IV-6), (IV-53), and (IV-54) with velocity profiles described by equations (IV-32) and (IV-33), (IV-35) and (IV-36), and (IV-37) and (IV-38) are given in Appendix J.

B. Mass Transfer with First Order Homogeneous Chemical Reaction around a Two-Sphere System.

Upon setting

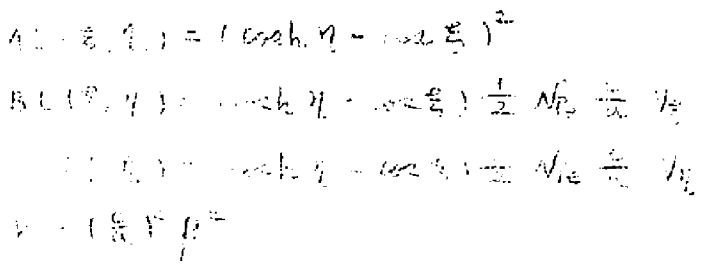

(IV-55)

equation (IV-8) becomes

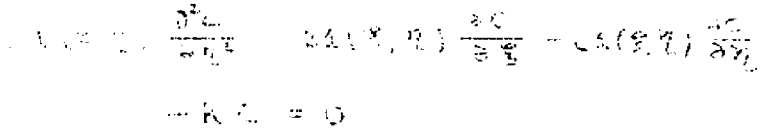

(IV-56)

The numerical techniques to solve this equation with appropriate boundary conditions are similar to those in section A. However, because of the use of bipolar coordinates in this analysis, the optimum stepsizes and step numbers in the numerical solutions are not necessarily the same as those chosen for spherical coordinates as given in section A. The stepsizes and step numbers are chosen here so that the region very near the surface of the particles is given more weight in the analysis.

The finite-difference forms for the differential terms are similar to those given in equation (IV-45) and are

$$C = \frac{1}{2}\left(C_{i+1,j} + C_{i,j}\right)$$

$$\frac{\partial C}{\partial \xi} = \frac{C_{i+1,j} - C_{i,j}}{\Delta \xi_i}$$

$$\frac{\partial C}{\partial \eta} = \frac{1}{2}\left[\frac{C_{i+1,j+1} - C_{i+1,j-1}}{\eta_{j+1} - \eta_{j-1}} + \frac{C_{i,j+1} - C_{i,j-1}}{\eta_{j+1} - \eta_{j-1}}\right] \qquad \text{(IV-57)}$$

$$\frac{\partial^2 C}{\partial \eta^2} = \frac{1}{2}\left[\frac{2\,C_{i+1,j+1}}{(\eta_{j+1}-\eta_j)(\eta_{j+1}-\eta_{j-1})} - \frac{2\,C_{i+1,j}}{(\eta_j-\eta_{j-1})(\eta_{j+1}-\eta_j)}\right.$$
$$+\frac{2\,C_{i+1,j-1}}{(\eta_j-\eta_{j-1})(\eta_{j+1}-\eta_{j-1})} + \frac{2\,C_{i,j+1}}{(\eta_{j+1}-\eta_j)(\eta_{j+1}-\eta_{j-1})}$$
$$\left. - \frac{2\,C_{i,j}}{(\eta_j-\eta_{j-1})(\eta_{j+1}-\eta_j)} + \frac{2\,C_{i,j-1}}{(\eta_j-\eta_{j-1})(\eta_{j+1}-\eta_{j-1})}\right]$$

where

i = index in ξ-direction

j = index in η-direction

The stepsize used in angular direction was taken as

$$\xi_i = \Delta\xi_0 \frac{h_1^i - 1}{h_1 - 1}\,; \quad i = 0, 1, 2 \cdots \qquad \text{(IV-58)}$$

and

$$\Delta\xi_i = \xi_{i+1} - \xi_i = \Delta\xi_0\, h_1^i \qquad \text{(IV-59)}$$

where $\Delta\xi_0$ is the initial stepsize in the angular (ξ) direction and h_1 is an arbitrary constant greater than 1. This is done to conform to the behavior of the bipolar coordinates and to decrease the necessary iteration times

in the relaxation process for the concentration profiles in the first two angular increments. By comparing the corresponding angles, ξ and θ , on the surface of the sphere of interest (upper one $Y_o > 0$, or lower one, $Y_o < 0$) between the bipolar coordinates and spherical coordinates we will find that ξ is approximately equal to θ when the two spheres are very far apart whereas is quite different from when two spheres become closer to each other. The corrcsponding values of ξ and θ are given in tabular form in Appendix F for convenience in comparing the bipolar coordinates to spherical coordinates.

The stepsize in the radial direction (η -direction) was taken as

$$\eta_j = \gamma_o \cdot \cos [X_y(j)] \qquad \text{(IV-60)}$$

where Y_o is the η coordinate of the two-sphere system on the surface of the particular sphere ($Y_o > 0$ for upper sphere and $Y_o < 0$ for lower sphere) of interest. We also set

$$X_y(j) = \Delta X_{yo} \frac{h_2^j - 1}{h_2 - 1} \quad ; j = 0, 1, 2 \cdots \qquad \text{(IV-61)}$$

where ΔX_{yo} is the initial stepsize variable for equation (IV-61) and h_2 is an arbitrary constant greater than 1. Because of the fact that we are also interested in the concentration profiles in the region where ξ is around π , especially when the active sphere is behind the inert sphere or the two spheres are close to each other,

the mesh net that was used in this part of the study covers the whole range of space, i.e., from $-Y_o$ to Y_o. The mesh net that was used is symmetric with respect to $\eta = 0$ in the η-direction. Several different choices have been tried for the mess net description in the η-direction and we found that equation (IV-60) is the most convenient.

If we let

$$
\begin{aligned}
L1 &= 1/[(\eta_{j+1} - \eta_j)(\eta_{j+1} - \eta_{j-1})] \\
L2 &= 1/[(\eta_{j+1} - \eta_j)(\eta_j - \eta_{j-1})] \\
L3 &= 1/[(\eta_j - \eta_{j-1})(\eta_{j+1} - \eta_{j-1})] \\
L55 &= 1/(\eta_{j+1} - \eta_{j-1})
\end{aligned}
\tag{IV-62}
$$

equations (IV-56) and (IV-57) gives

$$
\begin{aligned}
&A1\,(L1 \cdot C_{i+1,j+1} - L2 \cdot C_{i+1,j} + L3 \cdot C_{i+1,j-1} \\
&\quad + L1 \cdot C_{i,j+1} - L2 \cdot C_{i,j} + L3 \cdot C_{i,j-1}) \\
&- B1 \cdot \frac{1}{\Delta\xi_i}\,(C_{i+1,j} - C_{i,j}) \\
&- C1 \cdot \tfrac{1}{2} \cdot L55\,(C_{i+1,j+1} - C_{i+1,j-1} + C_{i,j+1} - C_{i,j-1}) \\
&- K \cdot \tfrac{1}{2}\,(C_{i+1,j} + C_{i,j}) = 0
\end{aligned}
\tag{IV-63}
$$

or

$$
\begin{aligned}
&C_{i+1,j-1}\left(A1\cdot L3+\tfrac{1}{2}C1\cdot L55\right)\\
&\quad+C_{i+1,j}\left(A1\cdot L2-\frac{1}{\Delta\xi_i}B1-\frac{K}{2}\right)\\
&\quad+C_{i+1,j+1}\left(A1\cdot L1-\tfrac{1}{2}C1\cdot L55\right)\\
&=C^{*}_{i,j-1}\left(-A1\cdot L3-\tfrac{1}{2}C1\cdot L55\right)\\
&\quad+C^{*}_{i,j}\left(A1\cdot L2-\frac{1}{\Delta\xi_i}B1+\frac{K}{2}\right)\\
&\quad+C^{*}_{i,j+1}\left(-A1\cdot L1+\tfrac{1}{2}C1\cdot L55\right)
\end{aligned}
\qquad \text{(IV-64)}
$$

where the C*'s are known values from proceeding computations.

Equation (IV-64), the resulting diffusion equation in finite-difference form, gives a set of simultaneous algebraic equations which is then solved by Peaceman and Rachford's method. The concentration profiles at the first two angular steps, as in section A, are obtained by using a relaxation method. The boundary conditions coupled with equation (IV-64) are obtained from equations (IV-9) and (IV-10) as

$$
\begin{aligned}
C_{i,0} &= 1 && ;\ \text{all } i\\
C_{i,M} &= 0 && ;\ \text{all } i\\
C_{0,j} &= C_{1,j} && ;\ \text{all } j
\end{aligned}
\qquad \text{(IV-65)}
$$

where M is the index for the position on the outside surface of the concentration boundary layer. As mentioned before, M should be increased or decreased in the computation to conform to the thickness of the con-

centration boundary layer in the coordinate system used in this part of the study.

For this particular system (two-sphere system) it is very difficult to reduce the diffusion equation, equation (IV-8) into the more simplified form of equation (IV-53) due to the complexity of velocity profiles. However, we will correlate the numerical results of this study in terms of N_{Pe}/β^3 for consistency.

As soon as the concentration profiles are known in bipolar coordinates, the mass transfer rate in terms of the Sherwood number is given as

$$N_{Sh_2} = -2\left.\frac{\partial C}{\partial y}\right|_{y=0} = -2\left[\left.\frac{\partial C}{\partial \eta}\right|_{\eta=\gamma_o}\left.\frac{\partial \eta}{\partial y}\right|_{y=0} + \left.\frac{\partial C}{\partial \xi}\right|_{\xi}\left.\frac{\partial \xi}{\partial y}\right|_{y=0}\right] \quad \text{(IV-66)}$$

Details of this expression are given in Appendix E for both cases of Y_o greater than zero and Y_o less than zero.

Computer programs solving equations (IV-8), (IV-9), and (IV-10) with velocity profiles described by equations (IV-43) and (IV-44) are given in Appendix J.

C. Rapid Second Order Chemical Reaction Around Solid Spheres, Liquid Drops and Gas Bubbles.

a) Enhancement Factor for Flow Past a Solid Dispersed Phase

Substituting equations (IV-23) and (IV-24) into equation (IV-12) give the diffusion equations for species A and B as follows:

$$\frac{\partial^2 C_A}{\partial y^2} - \frac{N_{Pe_A}}{2}\left[g(x)\,y\,\frac{\partial C_A}{\partial x} - \frac{y^2}{2\sin x}\frac{d}{dx}\{g(x)\sin x\}\frac{\partial C_A}{\partial y}\right] = 0 \quad \text{(IV-67)}$$

$$\frac{\partial^2 C_B}{\partial y^2} - \frac{N_{Pe_B}}{2}\left[g(x)\, y \frac{\partial C_B}{\partial x} - \frac{y^2}{2\sin x}\frac{d}{dx}\{g(x)\sin x\}\frac{\partial C_B}{\partial y}\right] = 0 \qquad \text{(IV-68)}$$

We now define new variables y', dx'_A, dx'_B as

$$y' = y\,[g(x)\sin x]^{1/2} \qquad \text{(IV-69)}$$

$$dx'_A = \frac{2\,[g(x)\sin x]^{3/2}}{N_{Pe_A}\, g(x)}\, dx \qquad \text{(IV-70)}$$

$$dx'_B = \frac{2\,[g(x)\sin x]^{3/2}}{N_{Pe_B}\, g(x)}\, dx \qquad \text{(IV-71)}$$

Substituting these variables into equations (IV-67) and (IV-68), we obtain

$$\frac{\partial^2 C_A}{\partial y'^2} - y'\frac{\partial C_A}{\partial x'_A} = 0 \qquad \text{(IV-72)}$$

$$\frac{\partial^2 C_B}{\partial y'^2} - y'\frac{\partial C_B}{\partial x'_B} = 0 \qquad \text{(IV-73)}$$

If we set

$$\xi_A = \frac{y'}{(9x'_A)^{1/3}} \qquad \text{(IV-74)}$$

$$\xi_B = \frac{y'}{(9x'_B)^{1/3}} \qquad \text{(IV-75)}$$

and also note that

$$\xi_B = \left(\frac{N_{Sc_B}}{N_{Sc_A}}\right)^{1/3} \xi_A = \alpha^{-1/3}\xi_A \qquad \text{(IV-76)}$$

Equations (IV-72) and (IV-73) become

$$\frac{\partial^2 C_A}{\partial \xi_A^2} + 3\xi_A^2 \frac{\partial C_A}{\partial \xi_A} = 0 \qquad \text{(IV-77)}$$

$$\frac{\partial^2 C_B}{\partial \xi_B^2} + 3\xi_B^2 \frac{\partial C_B}{\partial \xi_B} = 0 \qquad \text{(IV-78)}$$

Using the appropriate boundary conditions discussed earlier in Section 1 and assuming that the reaction takes place at $\xi_A = \xi_{AR}$, the solution of equations (IV-77) and (IV-78) give the concentration profiles of species A and B as

$$C_A = 1 - \frac{\int_0^{\xi_A} e^{-\beta^3}\, d\beta}{\int_0^{\xi_{AR}} e^{-\beta^3}\, d\beta} \quad ; \quad 0 < \xi_A < \xi_{AR} \qquad \text{(IV-79)}$$

and

$$C_B = \frac{\int_{\xi_{AR}\alpha^{-1/3}}^{\xi_A \alpha^{-1/3}} e^{-\beta^3}\, d\beta}{\int_{\xi_{AR}\alpha^{-1/3}}^{\infty} e^{-\beta^3}\, d\beta} \quad ; \quad \xi_{AR} < \xi_A < \infty \qquad \text{(IV-80)}$$

Substituting these solutions into the stoichiometric condition given by equation (IV-16) yields:

$$\alpha^{2/3}\gamma = e^{-\xi_{AR}^3\left(1-\frac{1}{\alpha}\right)} \frac{\Gamma\left(\frac{4}{3}\right) - \int_0^{\xi_{AR}\alpha^{-1/3}} e^{-\beta^3}\, d\beta}{\int_0^{\xi_{AR}} e^{-\beta^3}\, d\beta} \qquad \text{(IV-81)}$$

Since α and γ are constants for a given chemical system, equation (IV-81) can be used to compute the position ξ_{AR} at which the chemical reaction occurs in the continuous phase.

The local and overall (up to x radians) Sherwood number with chemical reaction present can readily be written down as

$$N_{sh\ell,R} = -2\left.\frac{\partial C}{\partial y}\right|_{y=0}$$

$$= \frac{2}{\int_0^{\xi_{AR}} e^{-\beta^3}\,d\beta}\ \frac{[g(x)\sin x]^{1/2}}{(9X_A')^{1/3}} \qquad \text{(IV-82)}$$

$$N_{sho,R} = \int_0^X -\left.\frac{\partial C}{\partial y}\right|_{y=0} \sin x\ dX$$

$$= \frac{1}{\int_0^{\xi_{AR}} e^{-\beta^3}\,d\beta}\ \int_0^X \frac{[g(x)\sin x]^{1/2}}{(9X_A')^{1/3}} \sin x\ dX \qquad \text{(IV-83)}$$

The corresponding Sherwood numbers without chemical reaction in the system are

$$N_{sh\ell,N} = \lim_{\xi_{AR}\to\infty} N_{sh\ell,R} = \frac{2}{\int_0^{\infty} e^{-\beta^3}\,d\beta}\ \frac{[g(x)\sin x]^{1/2}}{(9X_A')^{1/3}} \qquad \text{(IV-84)}$$

$$N_{sho,N} = \lim_{\xi_{AR}\to\infty} N_{sho,R} = \frac{2}{\int_0^{\infty} e^{-\beta^3}\,d\beta}\int_0^X \frac{[g(x)\sin x]^{1/2}}{(9X_A')^{1/3}} \sin x\,dX \qquad \text{(IV-85)}$$

It is clear from the above results that the enhancement factor ϕ will be the same with respect to either the local or the overall mass transfer rate and is simply given as

$$\phi = \frac{\Gamma(\frac{4}{3})}{\int_0^{\xi_{AR}} e^{-\beta^3}\,d\beta} \qquad \text{(IV-86)}$$

Equation (IV-86) together with equation (IV-81) can be used to obtain the relation between the parameters α and γ and enhancement factor ϕ.

Special cases:

i) The Schmidt numbers of species A and B are equal or $\alpha = 1$.

Equation (IV-81) gives

$$\int_0^{\xi_{AR}} e^{-\beta^3} d\beta = \frac{\Gamma(\frac{4}{3})}{1+\gamma} \qquad \text{(IV-87)}$$

Therefore, equation (IV-86) becomes

$$\phi = 1 + \gamma \qquad \text{(IV-88)}$$

ii) $\xi_{AR} \longrightarrow 0 \quad ; \quad \alpha \neq 1$

Since

$$e^{-\xi_{AR}^3(1-\frac{1}{\alpha})} = 1 - \xi_{AR}^3(1-\frac{1}{\alpha}) + \cdots \qquad \text{(IV-89)}$$

and

$$\int_0^{\xi_{AR}} e^{-\beta^3} d\beta = \xi_{AR} - \frac{1}{4}\xi_{AR}^4 + \cdots \qquad \text{(IV-90)}$$

equation (IV-81) gives

$$\alpha^{1/3}\gamma \simeq \frac{\Gamma(\frac{4}{3})}{\xi_{AR}} \qquad \text{(IV-91)}$$

as $\xi_{AR} \longrightarrow 0$. Therefore, equations (IV-86), (IV-90), and

(IV-91) give

$$\phi = \alpha^{3/2} \gamma \qquad \text{(IV-92)}$$

b) Enhancement Factor for Flow Past Gas Bubbles

Following the same procedure as for the solid spheres we substitute equations (IV-25) and (IV-26) into equation (IV-12) to give the diffusion equations for species A and B as:

$$\frac{\partial^2 C_A}{\partial y^2} - \frac{N_{Pe_A}}{2}\left[f(x) \frac{\partial C_A}{\partial x} - \frac{y}{\sin x} \frac{d}{dx}\{f(x) \sin x\} \frac{\partial C_A}{\partial y} \right] = 0 \qquad \text{(IV-93)}$$

$$\frac{\partial^2 C_B}{\partial y^2} - \frac{N_{Pe_B}}{2}\left[f(x) \frac{\partial C_B}{\partial x} - \frac{y}{\sin x} \frac{d}{dx}\{f(x) \sin x\} \frac{\partial C_B}{\partial y} \right] = 0 \qquad \text{(IV-94)}$$

The new variables y', dx_A' and dx_B' are now defined as

$$y' = y\, f(x) \sin x \qquad \text{(IV-95)}$$

$$dX_A' = \frac{2\,[f(x) \sin x]^2}{N_{Pe_A}\, f(x)} \qquad \text{(IV-96)}$$

$$dX_B' = \frac{2\,[f(x) \sin x]^2}{N_{Pe_B}\, f(x)} \qquad \text{(IV-97)}$$

and the resulting diffusion equations are

$$\frac{\partial^2 C_A}{\partial y'^2} - \frac{\partial C_A}{\partial X_A'} = 0 \qquad \text{(IV-98)}$$

$$\frac{\partial^2 C_B}{\partial y'^2} - \frac{\partial C_B}{\partial X_B'} = 0 \qquad \text{(IV-99)}$$

We now set

$$\xi_A = \frac{y'}{2X_A'^{1/2}} \tag{IV-100}$$

$$\xi_B = \frac{y'}{2X_B'^{1/2}} \tag{IV-101}$$

and note that

$$\xi_B = \left(\frac{N_{Sc\,B}}{N_{Sc\,A}}\right)^{1/2} \xi_A = \alpha^{-1/2}\,\xi_A \tag{IV-102}$$

Equations (IV-98) and (IV-99) become

$$\frac{d^2C_A}{d\xi_A^2} + 2\xi_A \frac{dC_A}{d\xi_A} = 0 \tag{IV-103}$$

$$\frac{d^2C_B}{d\xi_B^2} + 2\xi_B \frac{dC_B}{d\xi_B} = 0 \tag{IV-104}$$

Again, assuming that the reaction takes place at $\xi_A = \xi_{AR}$ the solution of equations (IV-103) and (IV-104) are

$$C_A = 1 - \frac{\int_0^{\xi_A} e^{-\beta^2}\,d\beta}{\int_0^{\xi_{AR}} e^{-\beta^2}\,d\beta} \quad ; \quad 0 < \xi_A < \xi_{AR} \tag{IV-105}$$

$$C_B = \frac{\int_{\xi_{AR}\alpha^{-1/2}}^{\xi_A\alpha^{-1/2}} e^{-\beta^2}\,d\beta}{\int_{\xi_{AR}\alpha^{-1/2}}^{\infty} e^{-\beta^2}\,d\beta} \quad ; \quad \xi_{AR} < \xi_A < \infty \tag{IV-106}$$

Equations (IV-105), (IV-106) and (IV-16) give

$$\alpha^{1/2}\gamma = e^{-\xi_{AR}^2(1-\frac{1}{\alpha})}\,\frac{\frac{\sqrt{\pi}}{2} - \int_0^{\xi_{AR}\alpha^{-1/2}} e^{-\beta^2}\,d\beta}{\int_0^{\xi_{AR}} e^{-\beta^2}\,d\beta} \tag{IV-107}$$

For this case the local Sherwood number and the overall Sherwood number (up to x radians) are

$$N_{Sh_{\ell},R} = \frac{1}{\int_0^{\xi_{AR}} e^{-\beta^2} d\beta} \frac{f(x) \sin x}{X_A'^{1/2}} \qquad \text{(IV-108)}$$

$$N_{Sh_{o},R} = \frac{1}{\int_0^{\xi_{AR}} e^{-\beta^2} d\beta} \int_0^{X} \frac{f(x) \sin^2 x}{2 X_A'^{1/2}} dX \qquad \text{(IV-109)}$$

For mass transfer without chemical reaction

$$N_{Sh_{\ell},N} = \lim_{\xi_{AR}\to\infty} N_{Sh_{\ell},R} = \frac{1}{\int_0^{\infty} e^{-\beta^2} d\beta} \frac{f(x) \sin x}{X_A'^{1/2}} \qquad \text{(IV-110)}$$

$$N_{Sh_{o},N} = \lim_{\xi_{AR}\to\infty} N_{Sh_{o},R} = \frac{1}{\int_0^{\infty} e^{-\beta^2} d\beta} \int_0^{X} \frac{f(x) \sin^2 x}{2 X_A'^{1/2}} dX \qquad \text{(IV-111)}$$

So that the enhancement factor ϕ is given as

$$\phi = \frac{\sqrt{\pi}}{2\int_0^{\xi_{AR}} e^{-\beta^2} d\beta} \qquad \text{(IV-112)}$$

Special cases:

i) $\alpha = 1$

Equation (IV-107) gives

$$\gamma = \frac{\sqrt{\pi}}{2\int_0^{\xi_{AR}} e^{-\beta^2} d\beta} - 1 \qquad \text{(IV-113)}$$

so that

$$\int_0^{\xi_{AR}} e^{-\beta^2}\, d\beta = \frac{\sqrt{\pi}}{2(1+\gamma)} \qquad \text{(IV-114)}$$

Equations (IV-112) and (IV-114) give

$$\phi = 1 + \gamma \qquad \text{(IV-115)}$$

which is exactly the same result as obtained for the case of flow around a solid sphere.

ii) $\xi_{AR} \rightarrow 0 \quad ; \alpha \neq 1$

Since

$$e^{-\xi_{AR}^2(1-\frac{1}{\alpha})} = 1 - \xi_{AR}^2\left(1-\frac{1}{\alpha}\right) + \cdots \qquad \text{(IV-116)}$$

and

$$\int_0^{\xi_{AR}} e^{-\beta^2}\, d\beta = \xi_{AR} - \frac{1}{3}\xi_{AR}^3 + \cdots \qquad \text{(IV-117)}$$

equation (IV-107) gives

$$\xi_{AR} \doteq \frac{\sqrt{\pi}}{2\alpha^{1/2}\gamma} \qquad \text{(IV-118)}$$

as $\xi_{AR} \rightarrow 0$. Equations (IV-117), (IV-118), and (IV-112) give

$$\phi = \alpha^{1/2}\gamma \qquad \text{(IV-119)}$$

C. Enhancement Factor for Flow Past Liquid Drops

We have already shown that for both flow past solid spheres and for flow around a gas bubble that the local and overall enhancement factor are the same. With this idea in mind we assume an even power series solution in x for the concentration profile in the continuous phase similar to that suggested by Yuge (84) such as:

$$C = C_0(y) + C_2(y)x^2 + C_4(y)x^4 + \cdots = \sum_{k=0}^{\infty} C_{2k}(y)x^{2k} \qquad \text{(IV-120)}$$

where the coefficients C_{2k}'s are functions of y alone. Substituting equation (IV-120) into the diffusion equation, equation (IV-12), together with equation (IV-29) and (IV-31) for the velocity profile components V_x and V_y we obtain

$$\sum_{k=0}^{\infty} C_{2k}''(y)x^{2k} - \frac{N_{Pe}}{2}\left[\left\{\sum_{n=1}^{\infty}(A_{2n-1}+B_{2n-1}y)x^{2n-1}\right\}\cdot\left\{\sum_{k=1}^{\infty}C_{2k}(y)\cdot 2k\,x^{2k-1}\right\}\right. \qquad \text{(IV-121)}$$

$$\left. - \frac{\sum_{n=1}^{\infty}(A_{2n-1}y + \frac{1}{2}B_{2n-1}y^2)\cdot\left\{\sum_{m=1}^{\infty}\frac{(-1)^{m-1}}{(2m-1)!}(2m+2n-2)\,x^{2m+2n-4}\right\}}{\sum_{m=1}^{\infty}\frac{(-1)^{m-1}}{(2m-1)!}x^{2m-2}}\cdot\sum_{k=0}^{\infty}C_{2k}'(y)x^{2k}\right] = 0$$

Taking x^0 terms, the Oth order approximation of equation (IV-121) can be written as

$$\frac{d^2C_0(y)}{dy^2} + \frac{N_{Pe}}{2}(2A_1y + B_1y^2)\frac{dC_0(y)}{dy} = 0 \qquad \text{(IV-122)}$$

This equation which holds for both species A and B can be solved to obtain the concentration profiles of species A and B, respectively. However, because we consider only x^0 terms in equation (IV-121) the concentration profiles

obtained from equation (IV-122) represent the profiles of species A and B along the front stagnation line. Since we have shown that the local and overall enhancement factor are the same for the system, the concentration profiles obtained from equation (IV-122), however, can be used to obtain the enhancement factor. We now proceed to obtain the solutions of equation (IV-122) for both species A and B using the assumed boundary conditions.

Set

$$\xi_A = \gamma A_1^{1/2} \left[\left(\frac{N_{Pe_A}}{2} \right)^{1/2} + \left(\frac{B_1}{A_1^{3/2}} \frac{N_{Pe_A}}{6} \right)^{1/3} \right] \qquad \text{(IV-123)}$$

$$\xi_B = \gamma A_1^{1/2} \left[\left(\frac{N_{Pe_B}}{2} \right)^{1/2} + \left(\frac{B_1}{A_1^{3/2}} \frac{N_{Pe_B}}{6} \right)^{1/3} \right] \qquad \text{(IV-124)}$$

and

$$\frac{B_1}{A_1^{3/2}} = K \qquad \text{(IV-125)}$$

$$\left(\frac{K}{3} \right)^{1/3} \left(\frac{2}{N_{Pe_A}} \right)^{1/6} = F \qquad \text{(IV-126)}$$

so that

$$\xi_A = \gamma A_1^{1/2} \left(\frac{N_{Pe_A}}{2} \right)^{1/2} (1+F) \qquad \text{(IV-127)}$$

$$\xi_B = \frac{\alpha^{-1/2} (1+\alpha^{1/6} F)}{1+F} \xi_A \qquad \text{(IV-128)}$$

Since A_1 represents the slip velocity of the liquid drop and B_1 the shearing stress at the surface of the liquid drop (both at the forward stagnation point) the parameter K

can be determined from the hydrodynamics of the system. For the special case of flow around a solid sphere K would approach infinity and for the special case of potential flow around a gas bubble K would approach zero.

Using equations (IV-127) and (IV-128), the diffusion equation, equation (IV-122) for both species A and B becomes

$$\frac{d^2 C_{oA}}{d\xi_A^2} + \left[\frac{2\xi_A}{(1+F)^2} + \frac{3\xi_A^2}{(1+\frac{1}{F})^3} \right] \frac{dC_{oA}}{d\xi_A} = 0 \qquad \text{(IV-129)}$$

$$\frac{d^2 C_{oB}}{d\xi_B^2} + \left[\frac{2\xi_B}{(1+\alpha^{-1/2}F)^2} + \frac{3\xi_B^2}{(1+\alpha^{-1/2}F)^3} \right] \frac{dC_{oB}}{d\xi_B} = 0 \qquad \text{(IV-130)}$$

and

$$\xi_B = \xi_A \frac{\alpha^{-1/2} + \alpha^{-1/3} F}{1+F} \qquad \text{(IV-131)}$$

The boundary conditions are

$$C_{oA}(\xi_A) = 1 \qquad \text{at } \xi_A = 0$$

$$C_{oB}(\xi_B) = 1 \qquad \text{at } \xi_B = \infty \qquad \text{(IV-132)}$$

$$C_{oA}(\xi_A) = C_{oB}(\xi_B) = 0 \quad \text{at } \xi_A = \xi_{AR} \text{ or } \xi_B = \xi_{AR} \frac{\alpha^{-1/2} + \alpha^{-1/3} F}{1+F}$$

The solutions to equations (IV-129), (IV-130), and (IV-132) are

$$C_{oA} = 1 - \frac{\int_0^{\xi_A} e^{-\left[\frac{\beta^2}{(1+F)^2} + \frac{\beta^3}{(1+\frac{1}{F})^3}\right]} d\beta}{\int_0^{\xi_{AR}} e^{-\left[\frac{\beta^2}{(1+F)^2} + \frac{\beta^3}{(1+\frac{1}{F})^3}\right]} d\beta} \qquad \text{(IV-133)}$$

$$C_{oB} = \frac{\int_{\xi_{AR}\frac{1+\alpha^{1/6}F}{\alpha^{1/2}(1+F)}}^{\xi_A \frac{1+\alpha^{1/6}F}{\alpha^{1/2}(1+F)}} e^{-\left[\frac{\beta^2}{(1+\alpha^{1/6}F)^2} + \frac{\beta^3}{(1+\frac{1}{\alpha^{1/2}F})^3}\right]} d\beta}{\int_{\xi_{AR}\frac{1+\alpha^{1/6}F}{\alpha^{1/2}(1+F)}}^{\infty} e^{-\left[\frac{\beta^2}{(1+\alpha^{1/6}F)^2} + \frac{\beta^3}{(1+\frac{1}{\alpha^{1/2}F})^3}\right]} d\beta} \qquad \text{(IV-134)}$$

Since

$$\left.\frac{\partial C_{oA}}{\partial y}\right|_{y \text{ at } \xi_{AR}} = -\alpha\gamma \left.\frac{\partial C_{oB}}{\partial y}\right|_{y \text{ at } \xi_{AR}} \qquad \text{(IV-135)}$$

we obtain

$$\alpha^{1/2}\gamma \frac{1+\alpha^{1/6}F}{1+F} = e^{-(1-\frac{1}{\alpha})\left[\frac{\xi_{AR}^2}{(1+F)^2} + \frac{\xi_{AR}^3}{(1+\frac{1}{F})^3}\right]} \frac{M_1 - \int_0^{\xi_{AR}\frac{1+\alpha^{1/6}F}{\alpha^{1/2}(1+F)}} e^{-\left[\frac{\beta^2}{(1+\alpha^{1/6}F)^2} + \frac{\beta^3}{(1+\frac{1}{\alpha^{1/2}F})^3}\right]} d\beta}{\int_0^{\xi_{AR}} e^{-\left[\frac{\beta^2}{(1+F)^2} + \frac{\beta^3}{(1+\frac{1}{F})^3}\right]} d\beta} \qquad \text{(IV-136)}$$

where

$$M_1 = \int_0^{\infty} e^{-\left[\frac{\beta^2}{(1+\alpha^{1/6}F)^2} + \frac{\beta^3}{(1+\frac{1}{\alpha^{1/2}F})^3}\right]} d\beta \qquad \text{(IV-137)}$$

The enhancement factor ϕ becomes

$$\phi = \frac{\int_0^{\infty} e^{-\left[\frac{\beta^2}{(1+F)^2} + \frac{\beta^3}{(1+\frac{1}{F})^3}\right]} d\beta}{\int_0^{\xi_{AR}} e^{-\left[\frac{\beta^2}{(1+F)^2} + \frac{\beta^3}{(1+\frac{1}{F})^3}\right]} d\beta} \qquad \text{(IV-138)}$$

For the special cases of $F = \infty$ (flow past solid spheres) equation (IV-138) reduces to equation (IV-86) and for $F = 0$ (flow past gas bubbles) equation (IV-138) reduces to equation (IV-122).

Special cases:

i) $\alpha = 1$

Equation (IV-136) becomes

$$\gamma = \frac{M}{\int_0^{\xi_{AR}} e^{-\left[\frac{\beta^2}{(1+F)^2} + \frac{\beta^3}{(1+\frac{1}{F})^3}\right]} d\beta} - 1 \qquad \text{(IV-139)}$$

or

$$\int_0^{\xi_{AR}} e^{-\left[\frac{\beta^2}{(1+F)^2} + \frac{\beta^3}{(1+\frac{1}{F})^3}\right]} d\beta = \frac{M}{1+\gamma} \qquad \text{(IV-140)}$$

Substituting equation (IV-140) into equation (IV-130), we obtain

$$\phi = 1 + \gamma \qquad \text{(IV-141)}$$

ii) $\xi_{AR} \longrightarrow 0 \quad ; \quad \alpha \neq 1$

Since

$$e^{-(1-\frac{1}{\alpha})\left[\frac{\xi_{AR}^2}{(1+F)^2} + \frac{\xi_{AR}^3}{(1+\frac{1}{F})^3}\right]} \simeq 1 \qquad \text{(IV-142)}$$

and

$$\int_0^{\xi_{AR}\frac{1+\alpha^{1/2}F}{\alpha^{1/2}(1+F)}} e^{-\left[\frac{\beta^2}{(1+\alpha^{1/2}F)^2} + \frac{\beta^3}{(1+\frac{1}{\alpha^{1/2}F})^3}\right]} d\beta \simeq 0 \qquad \text{(IV-143)}$$

as $\xi_{AR} \longrightarrow 0$, equation (IV-137) becomes

$$\int_0^{\xi_{AR}} e^{-\left[\frac{\beta^2}{(1+F)^2} + \frac{\beta^3}{(1+\frac{1}{F})^3}\right]} d\beta = M\alpha^{1/2}\gamma^{-1}\frac{1+F}{1+\alpha^{1/2}F} \qquad \text{(IV-144)}$$

and the enhancement factor becomes

$$\phi = \alpha^{1/2}\gamma \frac{1+\alpha^{1/6}F}{1+F} \cdot \frac{\int_0^\infty e^{-\left[\frac{\beta^2}{(1+F)^2} + \frac{\beta^3}{(1+\frac{1}{F})^3}\right]} d\beta}{\int_0^\infty e^{-\left[\frac{\beta^2}{(1+\alpha^{1/6}F)^2} + \frac{\beta^3}{(1+\frac{1}{\alpha^{1/6}F})^3}\right]} d\beta} \qquad \text{(IV-145)}$$

For $\alpha \doteq 1$, equation (IV-145) can be approximately written as

$$\phi \doteq \alpha^{1/2}\gamma \frac{1+\alpha^{1/6}F}{1+F} \qquad \text{(IV-146)}$$

or

$$\phi = \gamma\left[\alpha^{1/2}\left(\frac{1}{1+F}\right) + \alpha^{2/3}\left(\frac{1}{1+\frac{1}{F}}\right)\right] \qquad \text{(IV-147)}$$

iii) $F = 1$, equation (IV-137) becomes

$$\frac{1}{2}\alpha^{1/2}\gamma(1+\alpha^{1/6}) = e^{-(1-\frac{1}{\alpha})\left[\frac{\beta_{AR}^2}{4} + \frac{\beta_{AR}^3}{8}\right]} \frac{M - \int_0^{\beta_{AR}\frac{1+\alpha^{1/6}}{2\alpha^{1/6}}} e^{-\left[\frac{\beta^2}{(1+\alpha^{1/6})^2} + \frac{\beta^3}{(1+\frac{1}{\alpha^{1/6}})^3}\right]} d\beta}{\int_0^{\beta_{AR}} e^{-\left[\frac{\beta^2}{4} + \frac{\beta^3}{8}\right]} d\beta} \qquad \text{(IV-148)}$$

where

$$M = \int_0^\infty e^{-\left[\frac{\beta^2}{(1+\alpha^{1/6})^2} + \frac{\beta^3}{(1+\frac{1}{\alpha^{1/6}})^3}\right]} d\beta \qquad \text{(IV-149)}$$

and the enhancement factor, ϕ , is given by

$$\phi = \frac{\int_0^\infty e^{-\left[\frac{\beta^2}{4} + \frac{\beta^3}{8}\right]} d\beta}{\int_0^{\beta_{AR}} e^{-\left[\frac{\beta^2}{4} + \frac{\beta^3}{8}\right]} d\beta} \qquad \text{(IV-150)}$$

d) Enhancement Factor Around a Spherical Particle Immersed in a Stagnant Fluid.

We consider here the special case of diffusion and very fast reaction in a stagnant fluid. Spherical coordinates are used for consistency with the previous analyses. Equation (IV-4) gives the diffusion equation for species A and B in a stagnat fluid as

$$\frac{\partial}{\partial r}\left(r^2 \frac{\partial C_A}{\partial r}\right) = 0 \qquad \text{(IV-151)}$$

$$\frac{\partial}{\partial r}\left(r^2 \frac{\partial C_B}{\partial r}\right) = 0 \qquad \text{(IV-152)}$$

Equations (IV-151) and (IV-152) are solved with the boundary conditions

$$\begin{aligned} C_A &= 1 && \text{at } r = 1 \\ C_B &= 1 && \text{at } r = \infty \\ C_A &= C_B = 0 && \text{at } r = 1 + \xi_{AR} \end{aligned} \qquad \text{(IV-153)}$$

The solutions to equations (IV-151), (IV-152) and (IV-153) are

$$C_A = \frac{1+\xi_{AR}}{\xi_{AR}} \frac{1}{r} - \frac{1}{\xi_{AR}} \qquad \text{(IV-154)}$$

$$C_B = -(1+\xi_{AR}) \frac{1}{r} + 1 \qquad \text{(IV-155)}$$

Equations (IV-154), (IV-155), and (IV-16) give

$$\xi_{AR} = \frac{1}{\alpha \gamma} \qquad \text{(IV-156)}$$

The local and overall Sherwood numbers are given as

$$N_{Sh_{l,R}} = \frac{2(1+\xi_{AR})}{\xi_{AR}} \qquad \text{(IV-157)}$$

$$N_{Sh_{o,R}} = \frac{1+\xi_{AR}}{\xi_{AR}} \int_0^X \sin X \, dX \qquad \text{(IV-158)}$$

The enhancement factor, therefore, for both the local and overall mass transfer rate is

$$\phi = \frac{1+\xi_{AR}}{\xi_{AR}} \qquad \text{(IV-159)}$$

Substituting equation (IV-156) into equation (IV-159), we obtain

$$\phi = 1 + \alpha\gamma \qquad \text{(IV-160)}$$

Special cases:

i) $\alpha = 1$

Equation (IV-160) becomes

$$\phi = 1 + \gamma \qquad \text{(IV-161)}$$

ii) $\xi_{AR} \longrightarrow 0 \quad ; \quad \alpha \neq 1$

Equation (IV-159) gives

$$\phi \doteq \frac{1}{\xi_{AR}} = \alpha\gamma \qquad \text{(IV-162)}$$

The results given by equations (IV-160), (IV-161) and (IV-162) are, of course, identical to those obtained by applying "film theory" as originally developed by Hatta (30).

4. Results and Discussion

A. First-Order Homogeneous Chemicals Around Single Spheres and Multiparticle Systems.

Various angular and radial stepsizes have been used to test the convergence of the computations to be certain that the numerical solutions are of sufficient accuracy. The results presented here were obtained using a constant angular stepsize of 1.5 degrees, an initial radial stepsize of 5×10^{-5} and a value of $h = 1.3$. The number of the steps in the radial direction varied from 30 to 90 depending on the hydrodynamic behavior and reaction rate parameter. The larger the Reynolds number and reaction rate parameter, the thinner the diffusional boundary layer and the less the number of steps that were required in the radial direction for the solution of equations (IV-5) and (IV-6).

For the case of creeping flow around the sphere, the number of radial steps must be readjusted in the region near the rear stagnation point unless the reaction rate parameter is very large. The reason for this is that at large values of x ($x > 2.8$) the fluid is almost saturated with solute and the concentration boundary layer thickness is much larger than that near the forward stagnation point. However, the contribution to the overall mass transfer rate in this region is less than 2% at very low reaction rate such as $\beta \leq 1$. Since equations (IV-32), (IV-33), (IV-35), and (IV-36) describe the hydrodynamic behavior around the entire sphere, the computations are

performed over the entire range of x = 0 to x = π and equation (IV-18) is used to obtain the overall Sherwood number.

For $N_{Re} \gg 1$, equations (IV-37) and (IV-38) describe the hydrodynamic behavior only up to the flow separation point and solutions to equation (IV-5) or (IV-53) can only be obtained up to this point which is assumed to be 108^{o} or 1.885 radians from the forward stagnation point in the Reynolds number range of interest. Therefore, the overall Sherwood number cannot be obtained from equation (IV-18) but is instead estimated by the relation

$$Nsh_o = (1+F)\int_0^{1.885} -\frac{\partial C}{\partial \eta}\Big|_{\eta=0} \sin x \, dx \qquad \text{(IV-163)}$$

Here F is a weighting factor and is defined as the ratio of the mass transfer rate in the wake region to that in the forward flow region. For the case of pure physical mass transfer (β = 0) Lochiel and Calderbank (50) have assumed that the mass transfer occurring in the wake region amounts to 20% (F = 0.2) of the frontal transfer which is in good agreement with experiment. However, as the reaction rate parameter β approaches infinity, the local Sherwood number will become constant over the entire surface of the sphere so that the ratio of the contribution to mass transfer in the wake region to that in the forward flow region becomes

$$F = \frac{\int_{1.885}^{3.1416} \sin x \, dx}{\int_0^{1.885} \sin x \, dx} = 0.528 \qquad \text{(IV-164)}$$

and amounts to 52.8%.

Figures 1 - 4 show the effects of the reaction rate parameter β and the hydrodynamic conditions on the local mass transfer rate both at $N_{Re} \ll 1$ and $N_{Re} \gg 1$. These figures show that the higher the reaction rate parameter is, the less important the hydrodynamic effect. The reason for this is that at high reaction rates the solute from the solid sphere reacts with the reagent in the continuous phase before it has a change to diffuse further into the fluid. In this special case of high reaction rate, the volume to surface ratio of the reaction phase (thickness of the concentration boundary layer) is very small and all of the solute leaving the solid sphere reacts with the reagent in the continuous phase within a very thin concentration boundary layer. Furthermore, at very high reaction rate the thickness of the thin concentration boundary layer becomes uniform all around the surface of the sphere and the local Sherwood number becomes essentially constant. Mathematically speaking, if the last term due to reaction in equation (IV-5) is much greater than the second and third terms due to convection, equation (IV-5) can be approximated by

$$\frac{\partial^2 C}{\partial y^2} - \beta^2 C = 0 \qquad \text{(IV-165)}$$

According to this equation, both the local and the overall Sherwood numbers are given by

$$N_{Sh_o} = N_{Sh_\ell} = 2 \qquad \text{(IV-166)}$$

Fig. 1: Effect of low reaction rates and hydrodynamic behavior at $N_{Re} \ll 1$ on the local mass transfer around single solid spheres

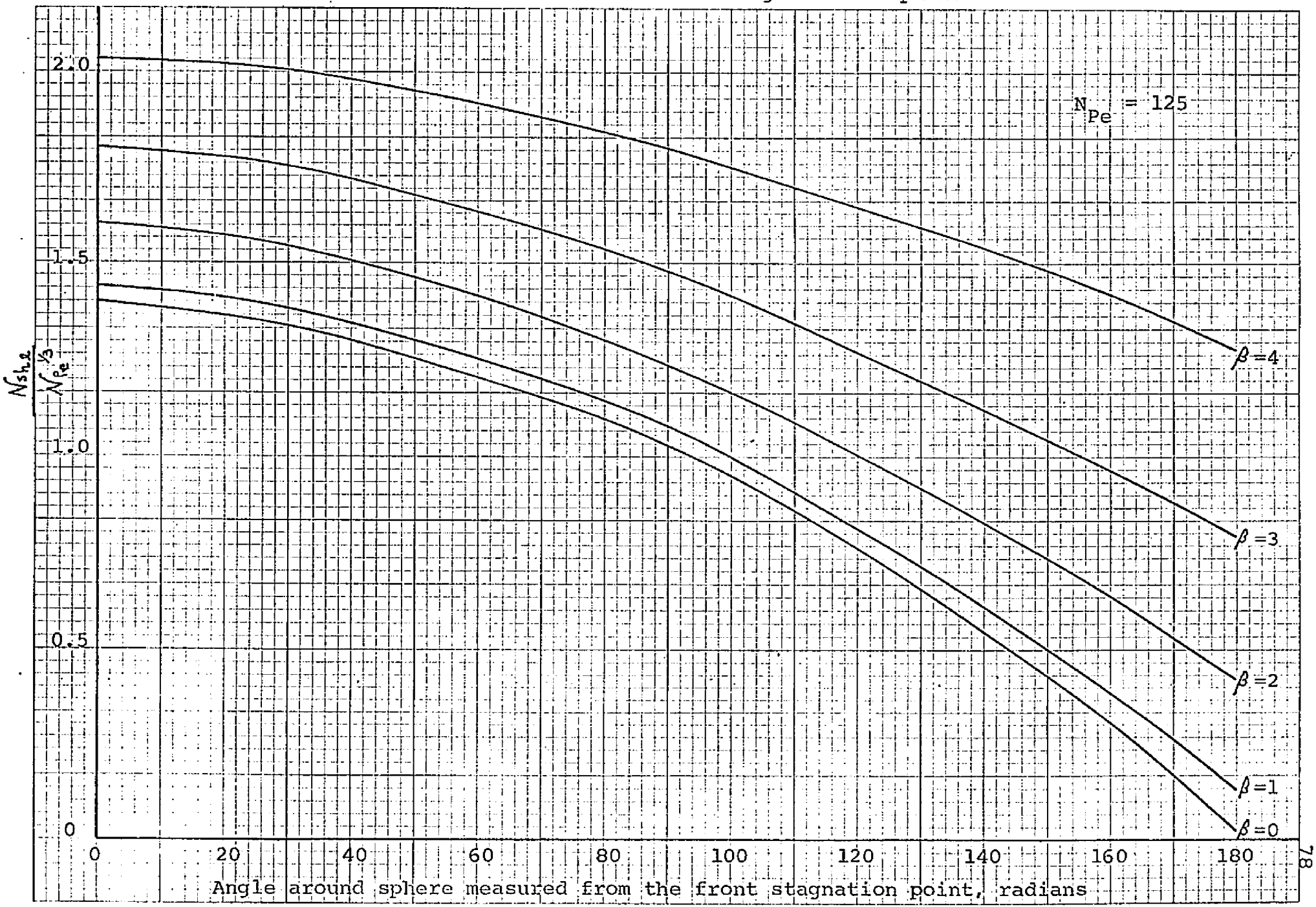

Fig. 2: Effect of high reaction rates and hydrodynamic behavior at $N_{Re} \ll 1$ on the local mass transfer around single solid spheres

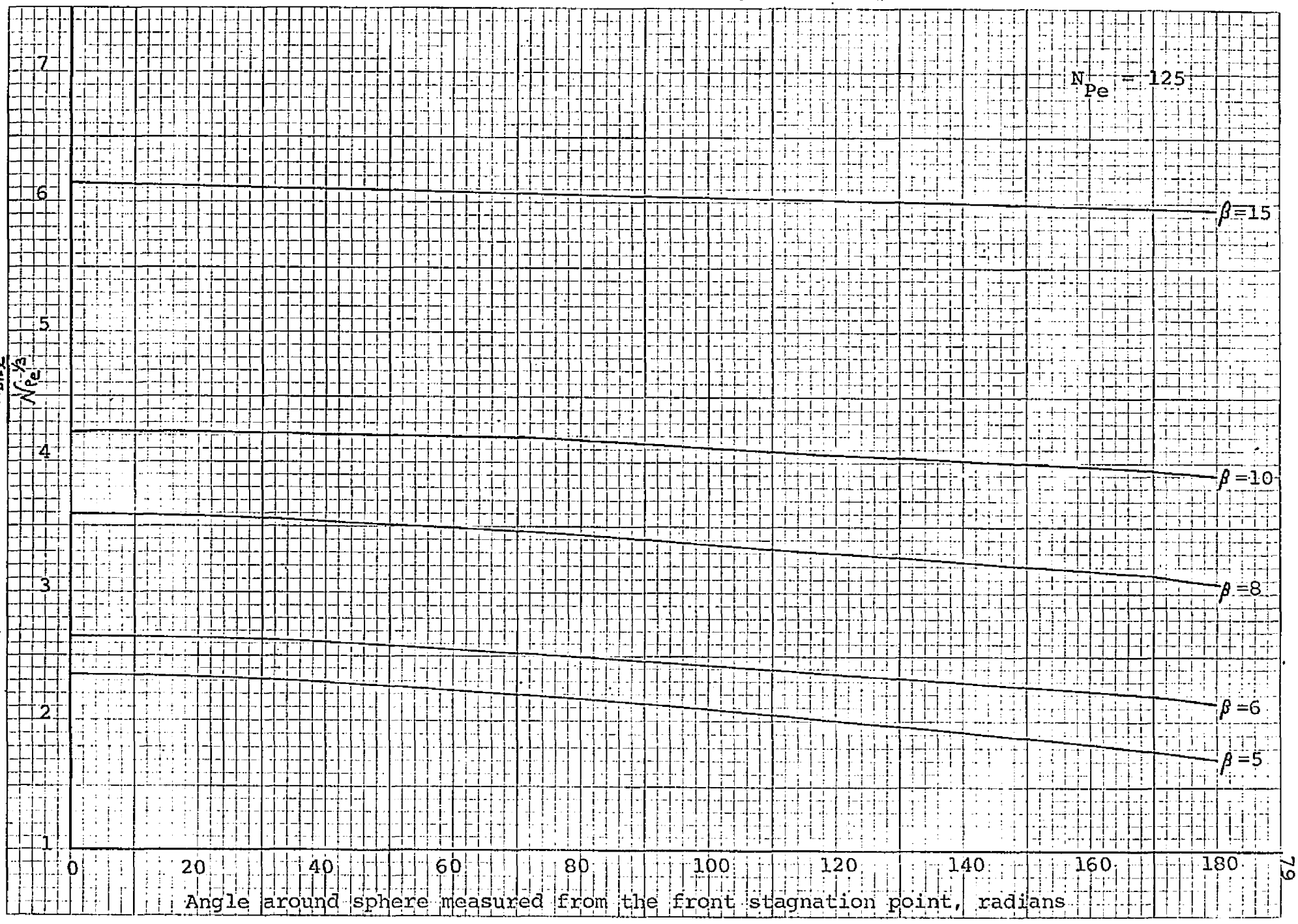

Fig.3: Effect of low reaction rates and hydrodynamic behavior at $N_{Re} \gg 1$ on local mass transfer around single solid spheres

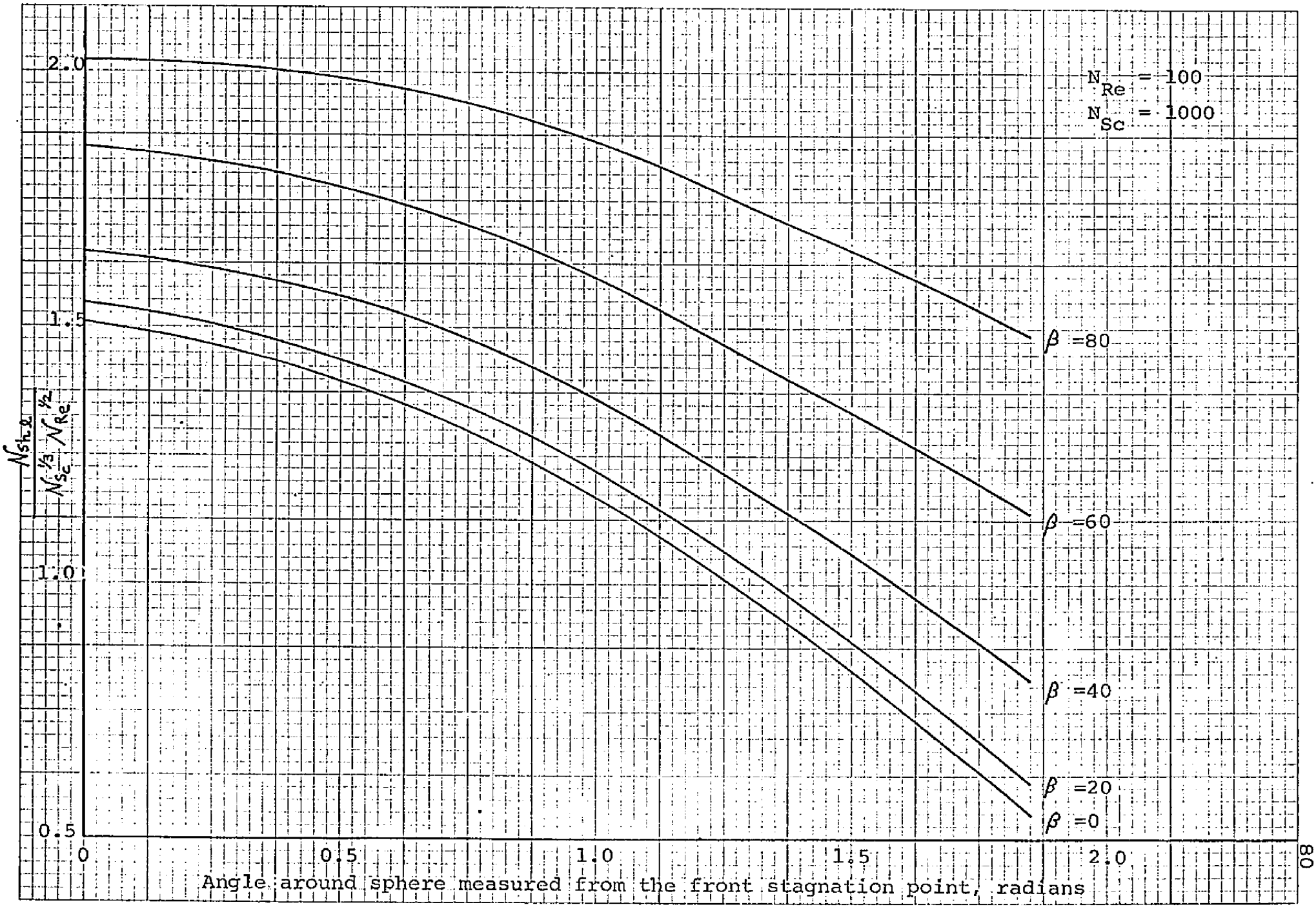

Fig. 4: Effect of high reaction rates and hydrodynamic behavior at $N_{Re} \gg 1$ on local mass transfer around single solid spheres

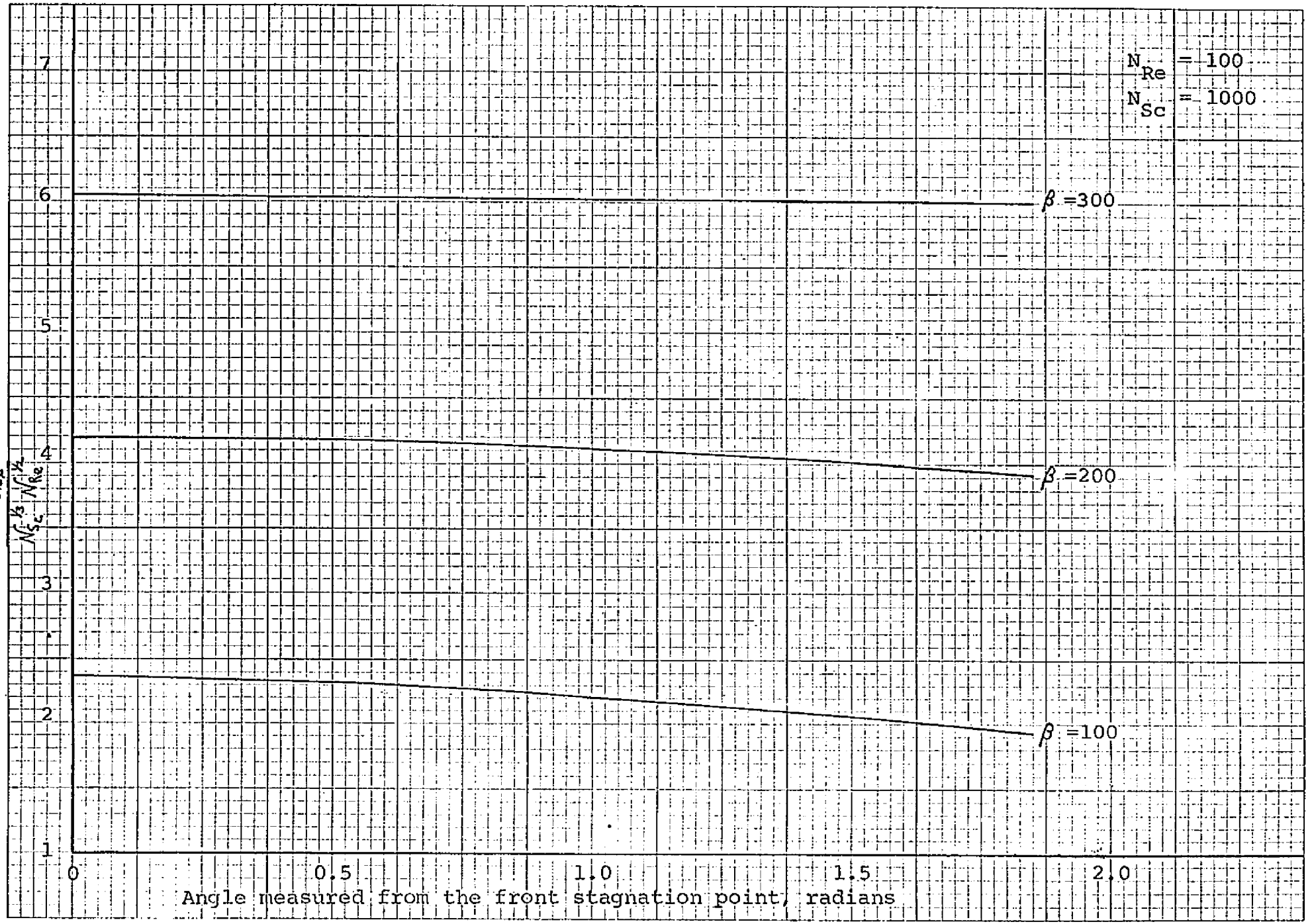

Figures 5 and 6 show the generalized correlation for the overall mass transfer rate and at the forward stagnation point with first order chemical reaction from solid spheres at $N_{Re} \ll 1$. These results were computed directly from equations (IV-32), (IV-33), and (IV-53) and depend only on the single parameter $Pe^{1/3}/\beta$. As a comparison the results of Johnson and Akehata (38) and Rutland and Pfeffer (70) for $N_{Pe} = 100$ are also presented in Figure 5 and are found to be in good agreement with the correlation.

The generalized correlation can also be applied directly to multiparticle systems by replacing the Peclet number by a pseudo Peclet number defined as

$$N_{Pe}' = \varphi(\epsilon)\, N_{Pe} \qquad \text{(IV-167)}$$

where $\varphi(\epsilon)$ is simply a function of the porosity of the multiparticle system. The quantity $\varphi(\epsilon)$ is obtained simply by comparing the stream functions for the single sphere and the multiparticle systems (Equations (IV-32b) and (IV-34b) respectively) and is given by

$$\varphi(\epsilon) = \frac{2(1-\lambda^5)}{W} = \frac{2\left[1-(1-\varepsilon)^{5/3}\right]}{2-3(1-\varepsilon)^{8/3}+3(1-\varepsilon)^{5/3}-2(1-\varepsilon)^2} \qquad \text{(IV-168)}$$

Figure 7 shows the correlation of the overall Sherwood number versus the pseudo Peclet number using β as parameter for multiparticle systems. For the case of physical mass transfer only ($\beta = 0$), the numerical result presented here agrees very well with the analytical result presented

Fig. 5: Generalized correlation for the overall mass transfer rate with first order homogeneous chemical reaction from single solid spheres at $N_{Re} \ll 1$

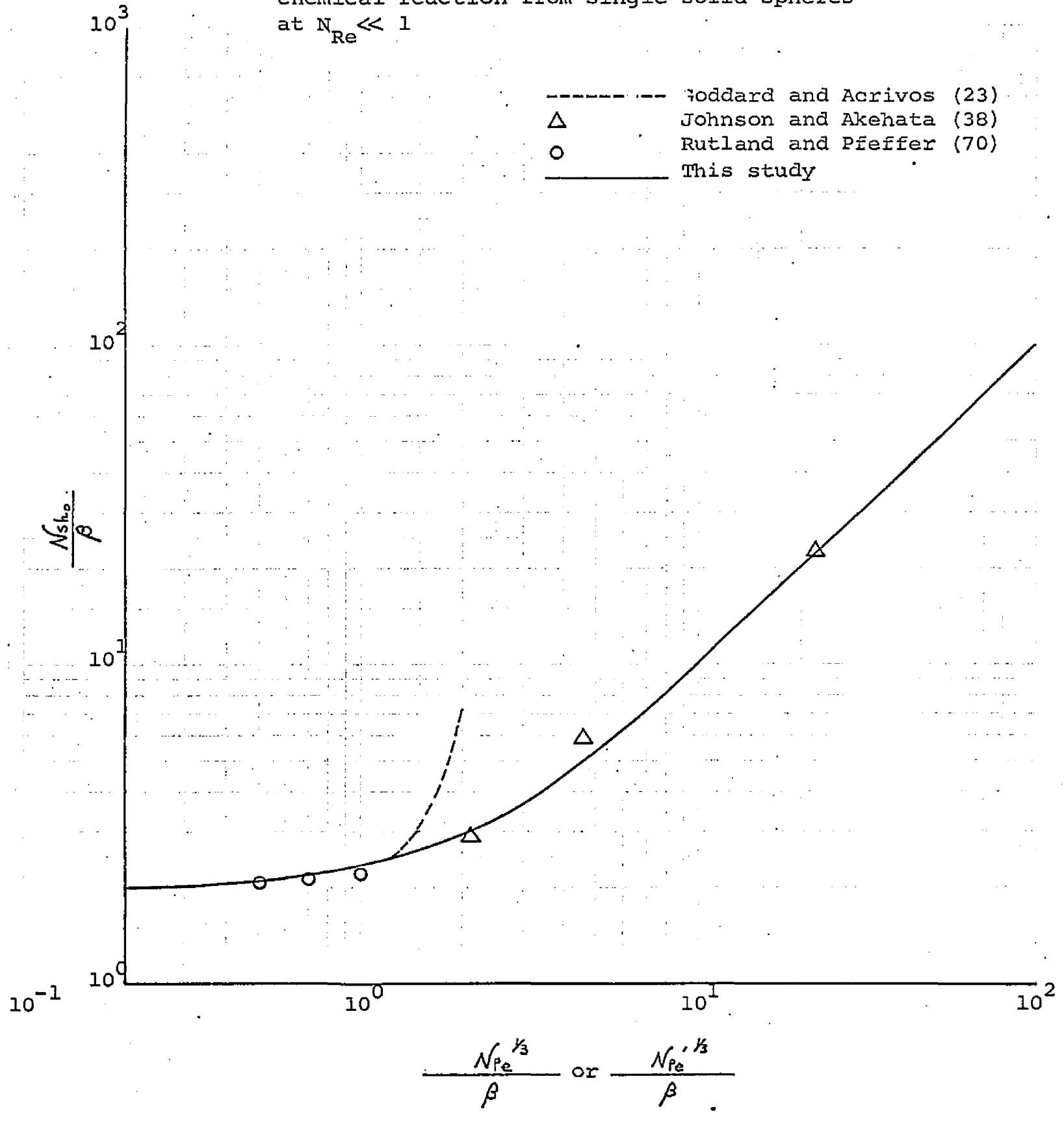

Fig. 6: Generalized correlation for the local mass transfer rate at the front stagnation point with first order homogeneous chemical reaction from single solid spheres at $Re \ll 1$

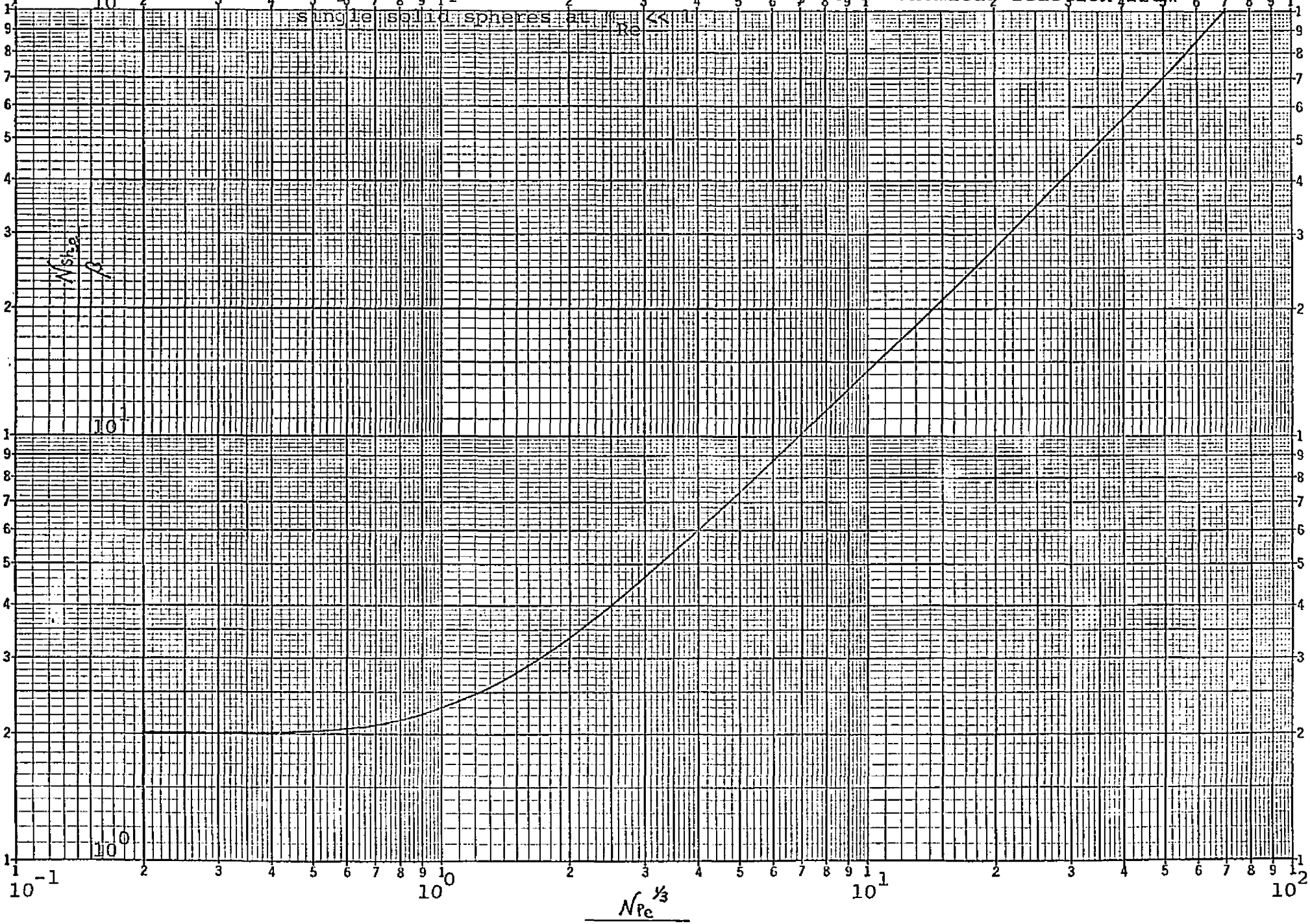

Fig. 7: Overall Sherwood number with first order homogeneous chemical reaction from a single solid sphere in multiparticle systems at $N_{Re} \ll 1$

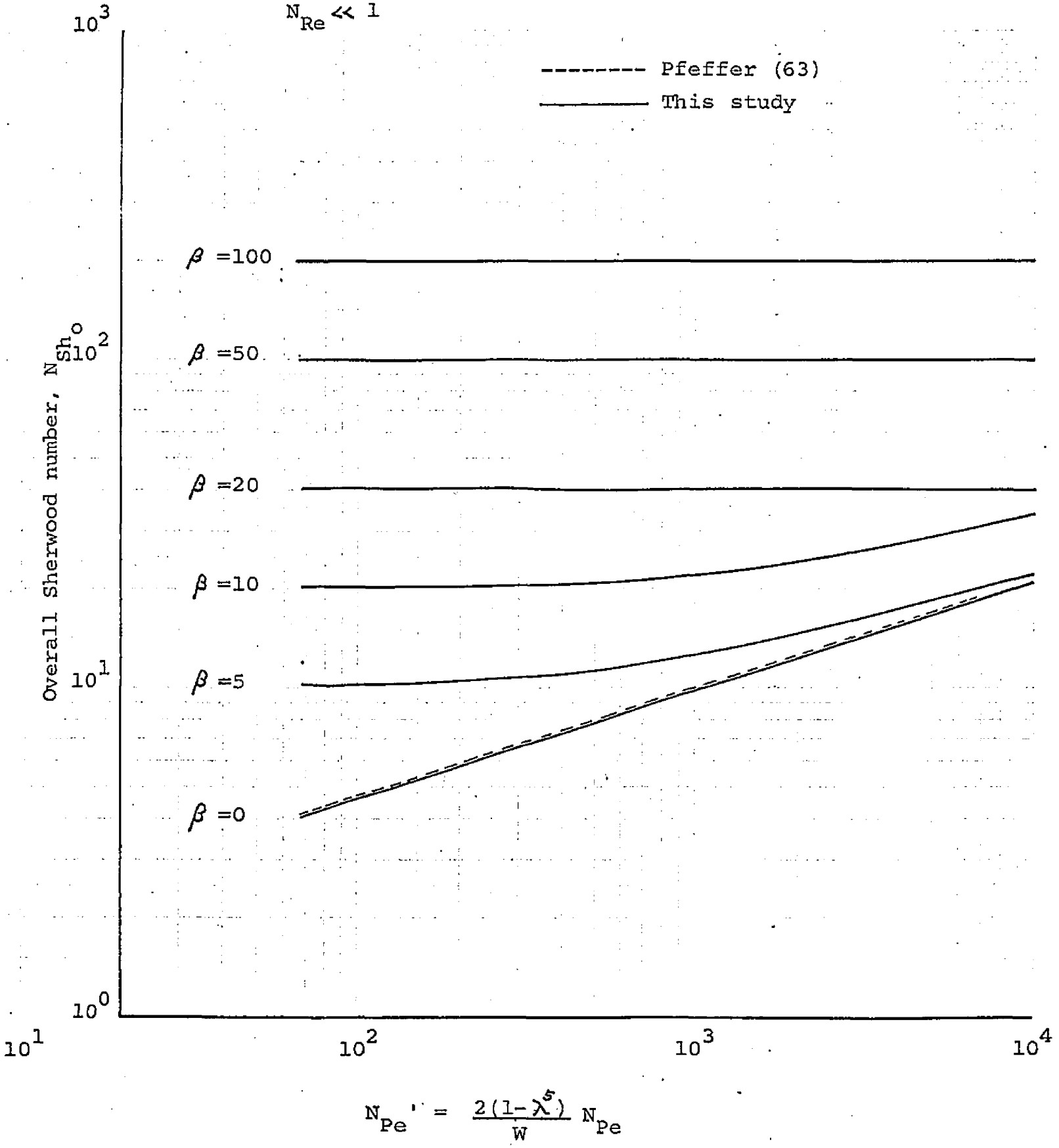

by Pfeffer (63). Unfortunately there are no available experimental data for the case of chemical reaction in multiparticle systems to compare with the results presented here.

Figures 8 and 9 present the generalized correlation for the overall mass transfer rate and at the forward stagnation point with first order homogeneous chemical reaction from solid spheres for $N_{Re} \gg 1$ in terms of the single parameter $N_{Re}^{1/2} N_{Sc}^{1/3} / \beta$. This parameter is also a direct result of equation (IV-53) since both g(x) in equations (IV-37) and (IV-38) depend on $N_{Re}^{1/2}$. The correlation for the overall Sherwood number was obtained by assuming that at very low reaction rates ($N_{Re}^{1/2} N_{Sc}^{1/3} / \beta \geq 10$) the wake region contributes 20% of the mass transfer as compared to that contributed by the forward flow region, i.e., F = 0.2 in equation (IV-163), and that at very high reaction rates ($N_{Re}^{1/2} N_{Sc}^{1/3} / \beta \leq 1$) the wake region contributes 52.8% of the mass transfer as compared to that contributed by the forward flow region (F = 0.528). Thus at very low reaction rates the correlation is adequately represented by

$$\frac{N_{Sh_o}}{\beta} = 0.84 \frac{N_{Sc}^{1/3} N_{Re}^{1/2}}{\beta} \qquad \text{(IV-169)}$$

and at very high reaction rates the correlation is given by

$$\frac{N_{Sh_o}}{\beta} = 2 \qquad \text{(IV-170)}$$

Fig. 8: Generalized correlation for the overall mass transfer rate with first order homogeneous chemical reaction from single solid spheres at $N_{Re} \gg 1$

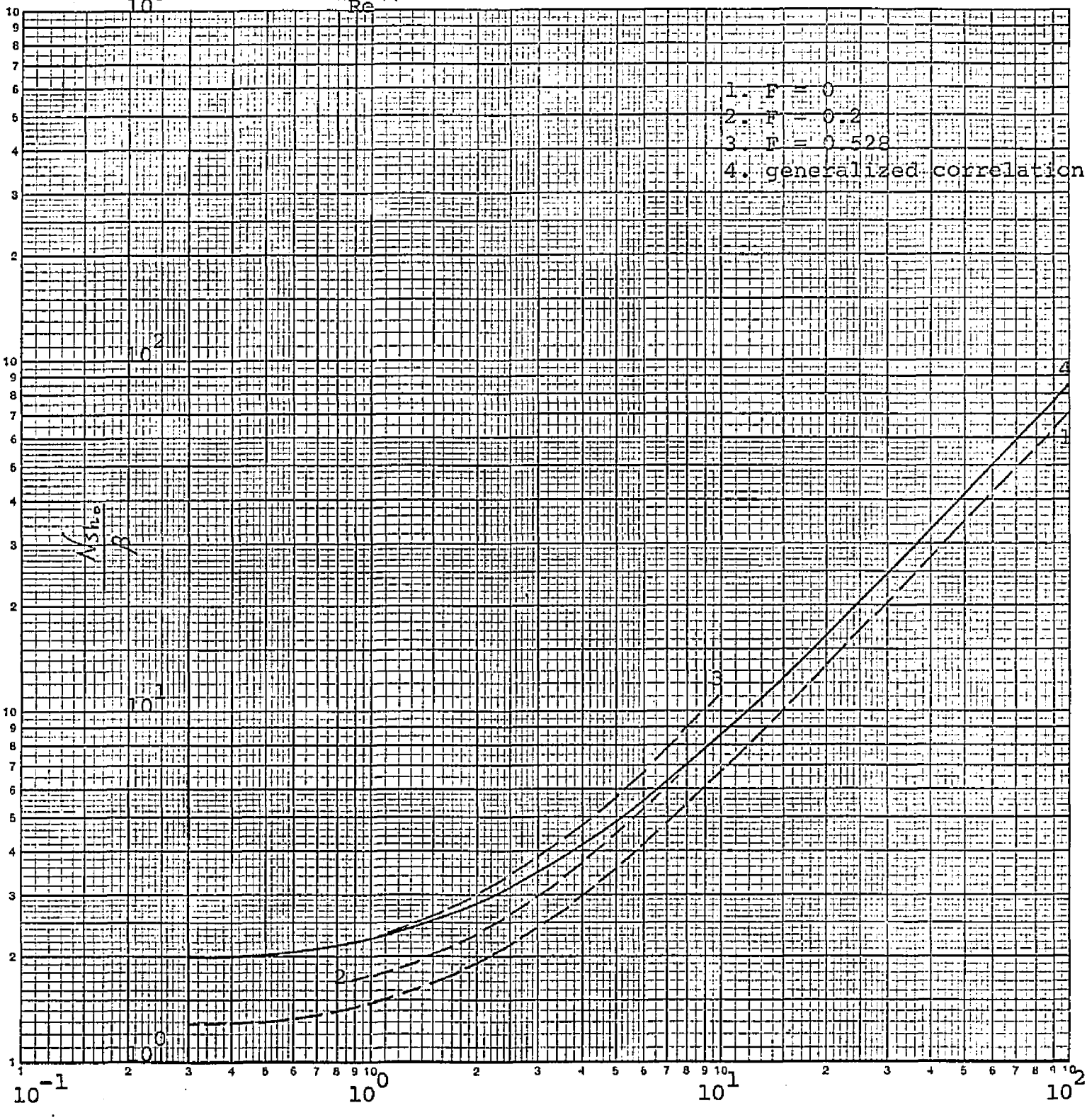

Fig. 9: Generalized correlation for the local mass transfer at the front stagnation point with first order homogeneous chemical reaction from single solid spheres at $N_{Pr} \geq 1$.

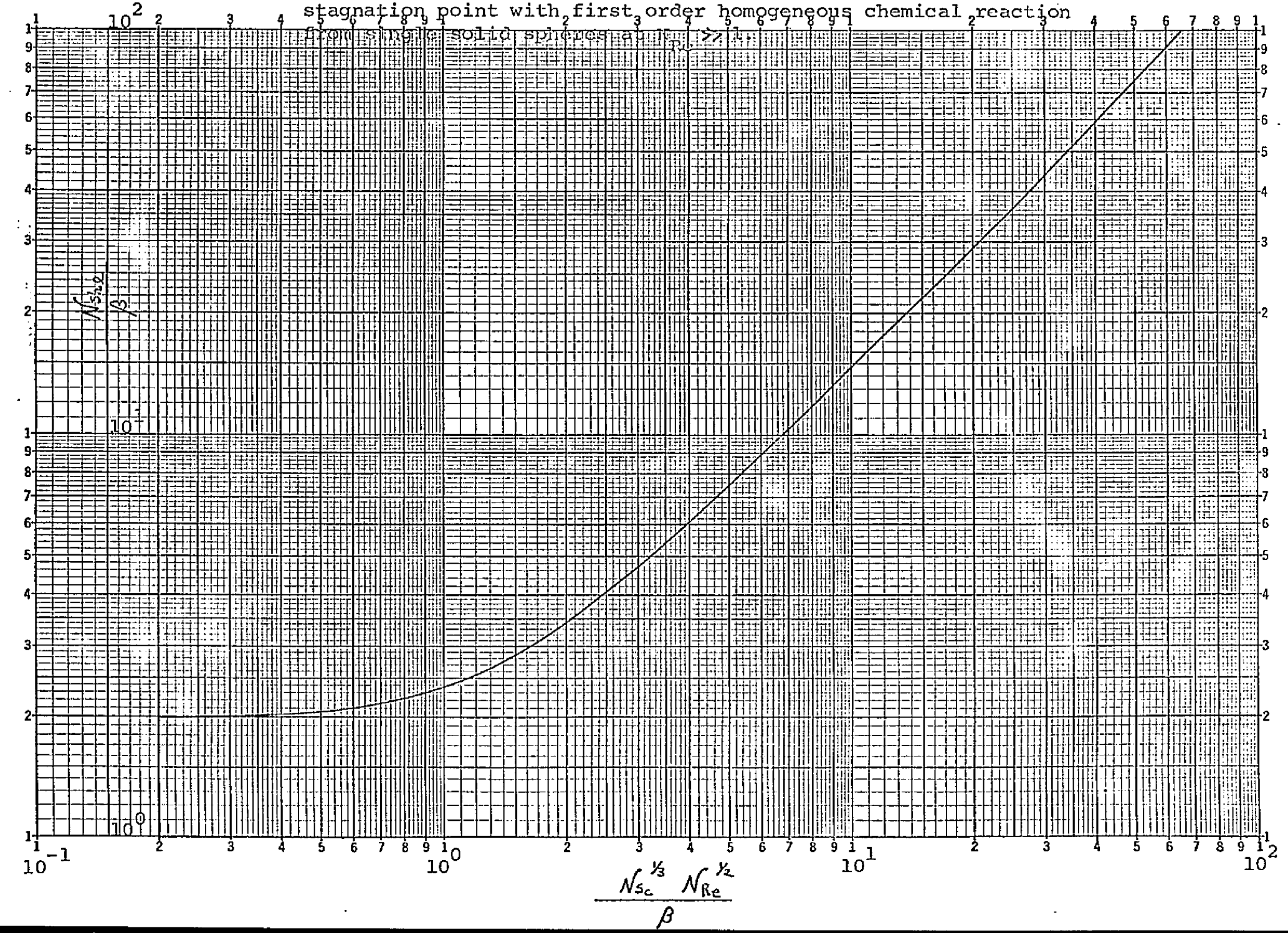

For intermediate reaction rate ($1 < N_{Re}^{1/2} N_{Sc}^{1/3} / \beta < 10$) the correlation can be estimated by fairing in a curve between these two lower and upper bounds. Curve 1 in Figure 8 shows the contribution to the overall mass transfer rate up to the separation point as obtained directly from the numerical solutions of equations (IV-53), (IV-37), and (IV-38) with F = 0. Curve 2 represents equation (IV-163) with F = 0.2 and curve 3 represents equation (IV-163) with F = 0.528. The generalized correlation is given by the solid line faired in between curves 2 and 3 and should give accurate estimates of the overall mass transfer rate for a very wide range of the reaction rate parameter β and the Reynolds and Schmidt numbers as long as the thin boundary layer approximation holds true.

The enhancement factor ϕ, defined as the ratio of the overall Sherwood number with chemical reaction to the Sherwood number without any chemical reaction, for single sphere systems at $N_{Re} \ll 1$ and $N_{Re} \gg 1$ is shown in Figures 10 and 11, respectively. For low Reynolds number flow, the enhancement factor is correlated with $N_{Pe}^{1/3}$ with β as a parameter. Figure 10 shows that approaches unity as $N_{Pe}^{1/3}$ increases to infinity. Since the thin boundary layer approximation is used throughout the entire study the results presented here are good for $N_{Pe} > 100$. At high values of the reaction rate parameter and Peclet number less than 1000, Figure 10 shows that $\log \phi$ versus $\log N_{Pe}^{1/3}$ is a straight line with slope -1 and intercept 2 which corresponds to the equation

Fig. 10: Enhancement factor for mass transfer with first order homogeneous chemical reaction from single solid spheres at $N_{Re} \ll 1$

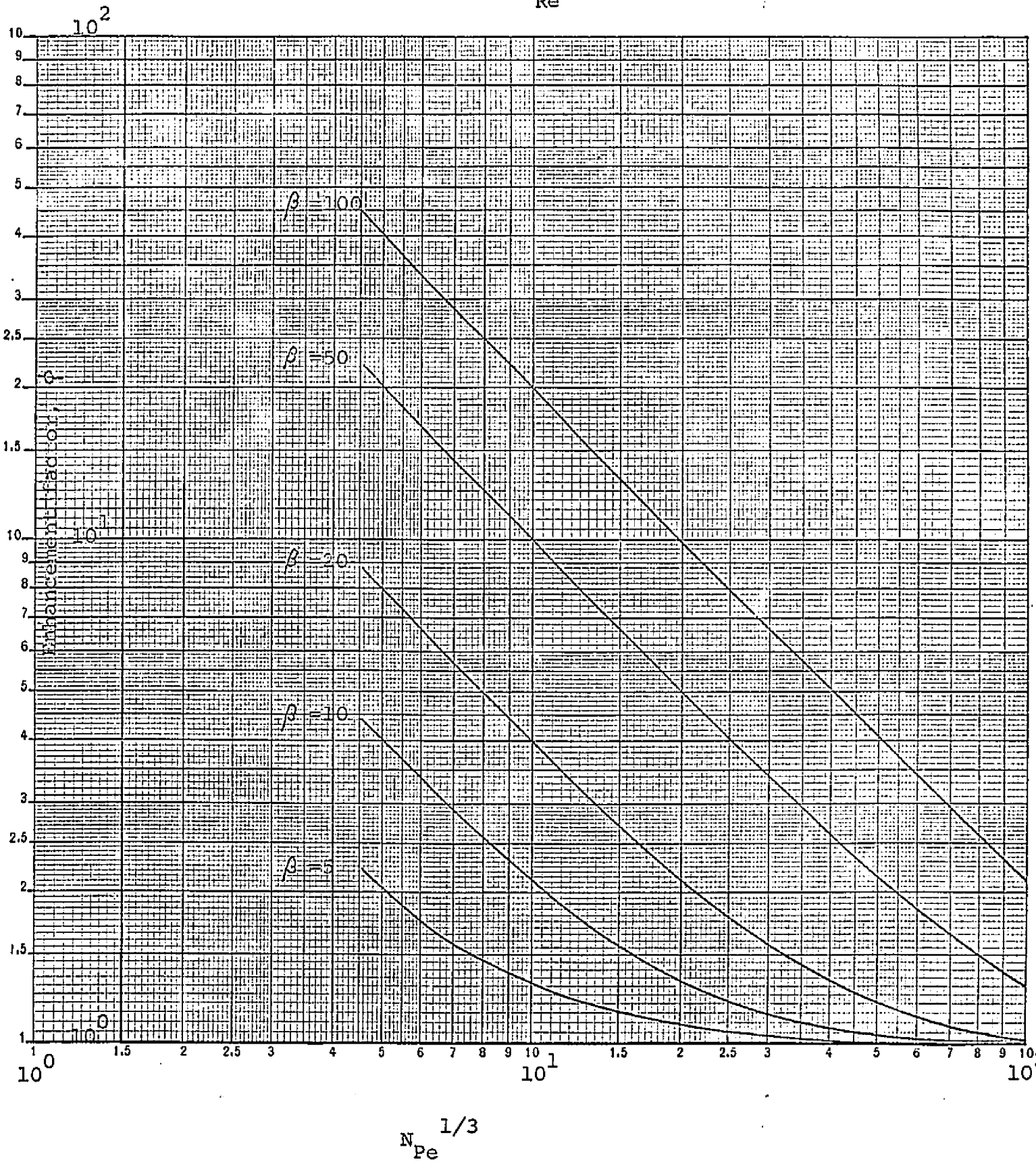

Fig. 11: Enhancement factor for mass transfer with first order homogeneous chemical reaction from single solid spheres at $N_{Re} \gg 1$

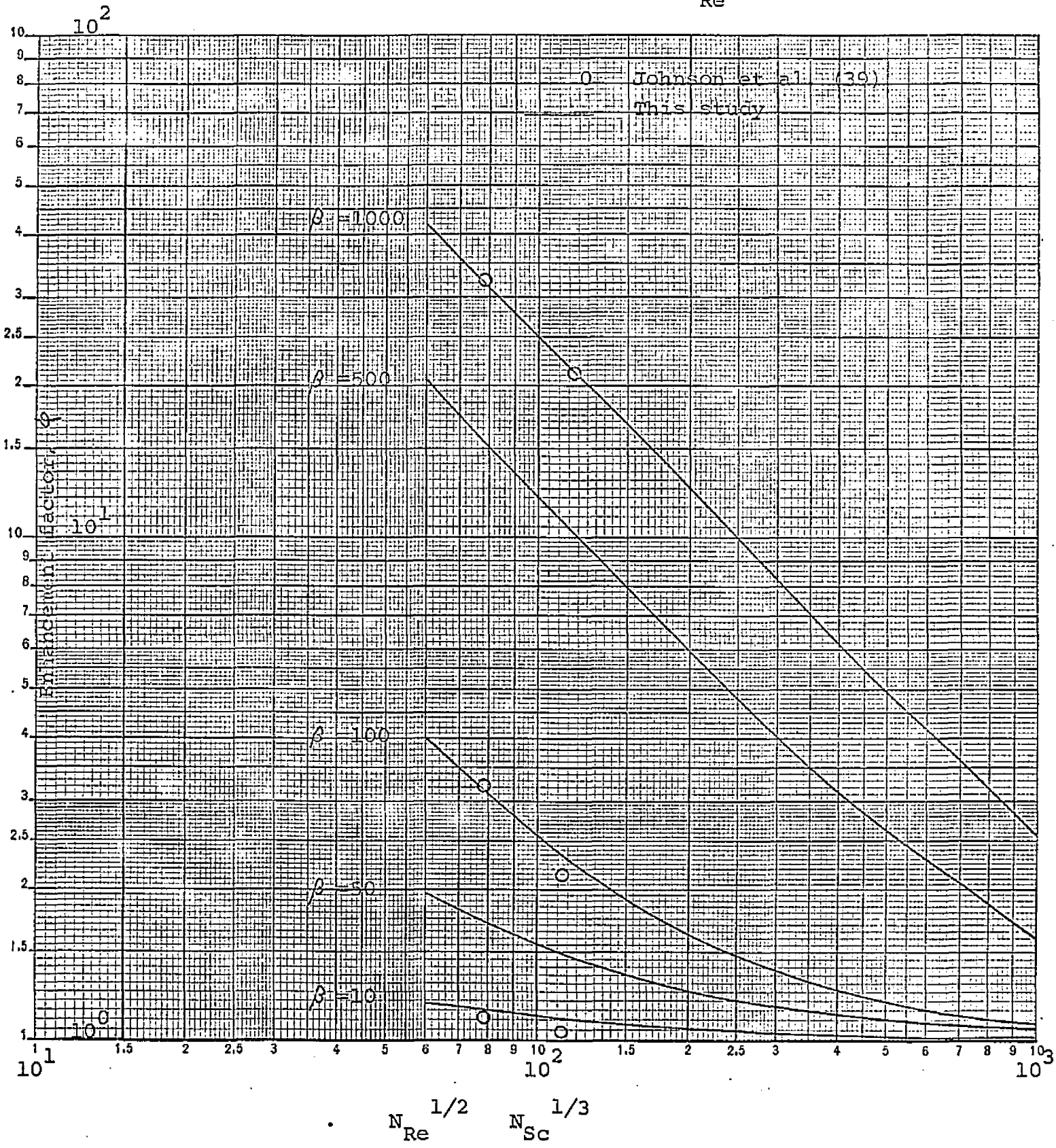

$$\phi \cong \frac{2\beta}{N_{Pe}^{1/3}} \qquad \text{(IV-171)}$$

At lower values of β or very high Peclet numbers this relation no longer applies and the straight lines become curves as seen in the figure.

Figure 11 shows the enhancement factor for mass transfer with first order homogeneous chemical reaction from solid spheres at $N_{Re} \gg 1$ using the correlation ϕ versus $N_{Re}^{1/2} N_{Sc}^{1/3}$ with β as a parameter. The results presented by Johnson, Hamielec and Houghton (39) are compared with this study for values of β= 10, 100, and 1000. Although the value of N_{Sc} was not given in reference (39) the points were calculated assuming N_{Sc} = 500. The agreement between these two studies is quite reasonable. As can be seen from Figure 9, the effects of both the parameters $N_{Re}^{1/2} N_{Sc}^{1/3}$ and β on the enhancement factor are quite similar to those found at low Reynolds numbers (Figure 10).

The analytical results presented by Goddard and Acrivos (23) for the limiting cases of very fast or very slow first order reaction in wedge type flows obeying the Falkner-Skan equation cannot be directly compared with the results obtained here because of the difference in geometry. However, an approximate comparisons was made for the case of very rapid reaction and is shown in Figure 5. A more detailed discussion of this comparison appears in Appendix F.

The numerical solutions presented here agree very well

with available analytical results with the added advantage that the generalized correlations can be used over a wide range of the reaction rate and hydrodynamic variables. The extension of the results to multiparticle systems based on the creeping flow equations and the free surface cell model should also prove valuable since it has already been shown in reference (63) that at low porosities, the multiparticle results for physical mass transfer agree with experimental data for Reynolds numbers as high as 100 because of wake suppression caused by neighboring particles. Of course, additional experimental data to verify the correlations presented here would be very helpful; to obtain useful data, however, the reaction rate parameter must be chosen between 10 and 100 for high Reynolds numbers and between 1 and 10 for low Reynolds numbers.

B. First Order Homogeneous Chemical Reaction Around Two Equal Spheres Placed One Behind the Other in the Direction of Flow.

As was discussed in section A, for the single sphere and multiparticle systems, various angular and radial stepsized have been used to test the convergence of the computations to be certain that the numerical solutions are of sufficient accuracy. The results which will be presented here were obtained using a constant number of steps in the angular direction and a variable number of steps in the radial direction. The number of the steps in the angular direction was chosen as 100. The stepsize in the angular direction was varied depending

on the center-to-center distance between the two spheres (h_1 was taken between 1.005 and 1.01 in equation (IV-58)). The maximum number of steps in the radial direction was chosen as 80. The stepsize in the radial direction was varied so that the profile near the surface of the active sphere is emphasized (h_2 was taken between 1.01 and 1.05 in equation (IV-61)).

In general, as Y_o approaches zero, i.e., the center-to-center distance between the two spheres decreases, the rate of physical transfer in the region $\xi \doteq \pi$ is dominated by molecular diffusion rather than by convection. In this region the fluid is practically saturated with solute when the two spheres are very close to each other. Therefore, we need to have a description of the concentration profile in the entire range between $-Y_o$ and $+Y_o$.

For the case of the active sphere placed in front of the inert sphere in the direction of flow ($Y_o > 0$) the initial number of steps was always taken as 35. As the computation progressed in the angular reaction, the number of steps was increased as necessary up to 80.

For the case of active spheres placed behind the inert sphere in the direction of flow ($Y_o < 0$), the initial step number was set depending on the center-to-center distance between the two spheres (value of Y_o). As the bipolar angle decreases from π to 0, the corresponding spherical angle changes from 0 (front stagnation point) to π (rear stagnation point), the number of steps should decrease because of the difference in the corresponding value of ξ in bipolar coordinates and the value of θ in

spherical coordinates in the region around $\xi = 0$. At ξ around zero, a small change $\Delta\eta$ in bipolar coordinates gives a very large change in Δr in spherical coordinates. This is the reason for decreasing the number of steps in the computation as ξ decreases to zero.

The computer programs were written so that the number of steps would be automatically increased or decreased depending on the assumed outer concentration boundary layer thickness. The computation results from the previous value of ξ take care of this requirement.

If the two spheres are too close to each other, however, the assumed governing diffusion equation will not be valid. This is clearly seen from the order of magnitude analysis given in Appendix B, i.e., the concentration boundary layer thickness always depends on N_{Pe}, β and the center-to-center distance between the two spheres. Since we have assumed here that the concentration thickness is very thin so that $y/Y_o \ll 1$, the analysis becomes invalid when the concentration boundary layer becomes thick since the diffusion terms in the angular direction are no longer negligible. In this case the appropriate diffusion equation should be of the elliptic form instead of the parabolic form used here.

In order to test the validity of the computations for the two-sphere systems the results for the single sphere with no chemical reaction ($\beta = 0$) which has already been computed using spherical coordinates in Section A were compared with the results obtained using the

program for solving the diffusion equation in bipolar coordinates with the Stimson and Jeffrey velocity profile at large values of $\pm Y_o$. Figure 12 presents the results obtained for $Y_o = \pm 4$ which is equivalent to a center-to-center distance of 27.5. As expected these curves are practically identical to that obtained for the single sphere.

Figures 13 and 14 show the effects of particle-to-particle interaction on the local mass transfer rate. As Y_o approaches zero, the local mass transfer rate in the region around $\xi \doteq \pi$, i.e., rear stagnation point (for $Y_o > 0$) or the front stagnation point (for $Y_o < 0$) is negligible. For $Y_o > 0$, the local mass transfer rate at the front stagnation point appears to be the same at a given value of N_{Pe} independent of the center-to-center distance between spheres. For $Y_o < 0$, the local mass transfer rate at the front stagnation point decreases as the two spheres get closer and closer. The maximum local mass transfer rates appear at an angle away from the front stagnation point depending on the center-to-center distance between the spheres. This phenomenon has been obtained experimentally by Peltzman and Pfeffer (61) and others, even though they performed their experiments at relatively higher Reynolds numbers than those which apply to this analysis.

The effect of the concentration boundary layer thickness are shown in Figures 15 and 16 by comparing results from $N_{Pe} = 1000$ and $N_{Pe} = 125$. The thicker the concentration boundary layer thickness, the stronger the effect of

Fig. 12: Comparison of two sphere results at Y_o=+4 and single sphere results for β = 0 and N_{Re} = 1000

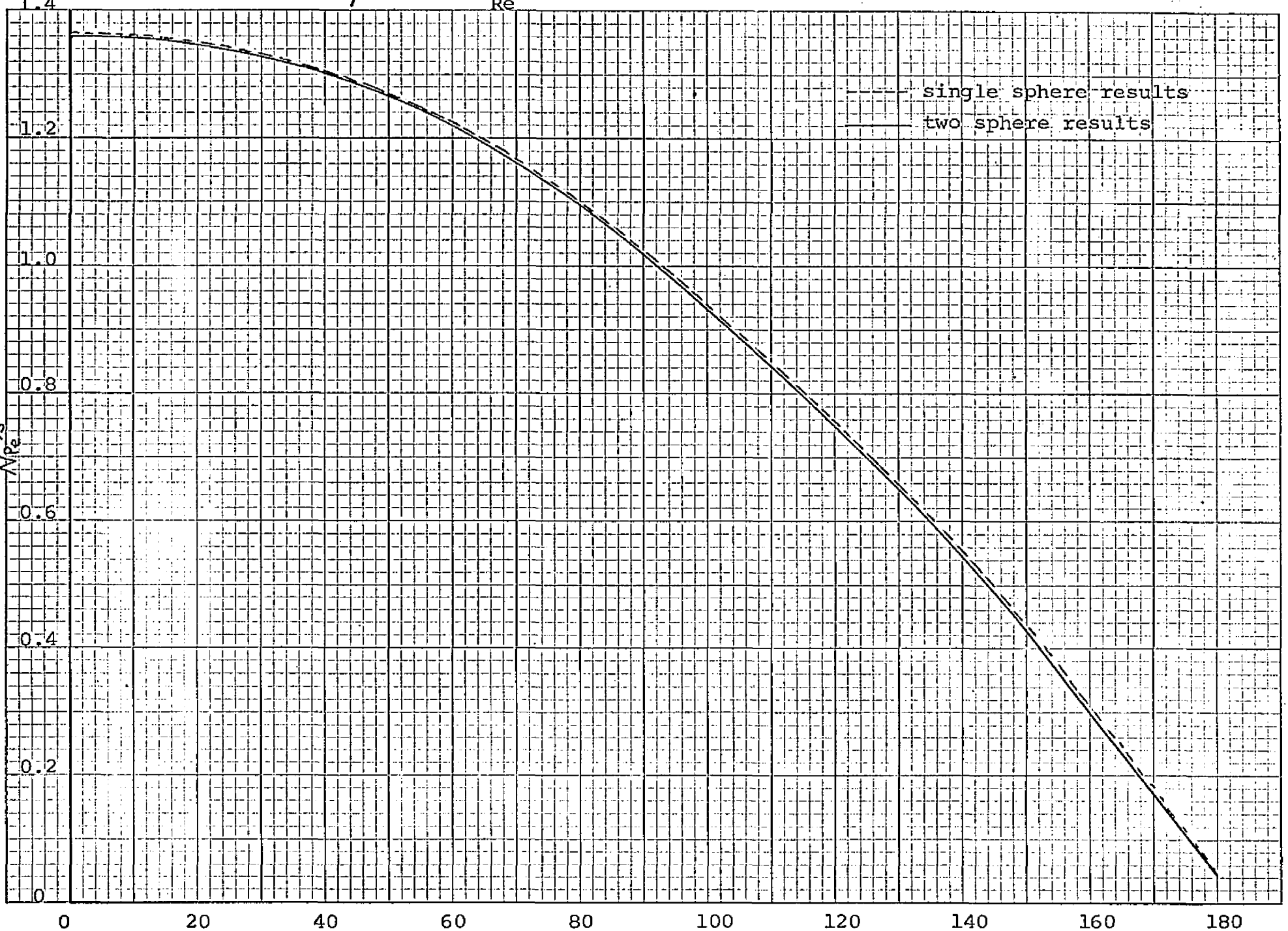

Fig. 13: Effect of particle-to-particle interaction on the local mass transfer rate for the case of an active sphere placed in front of an inert sphere in a two-sphere system ($Y_o > 0$)

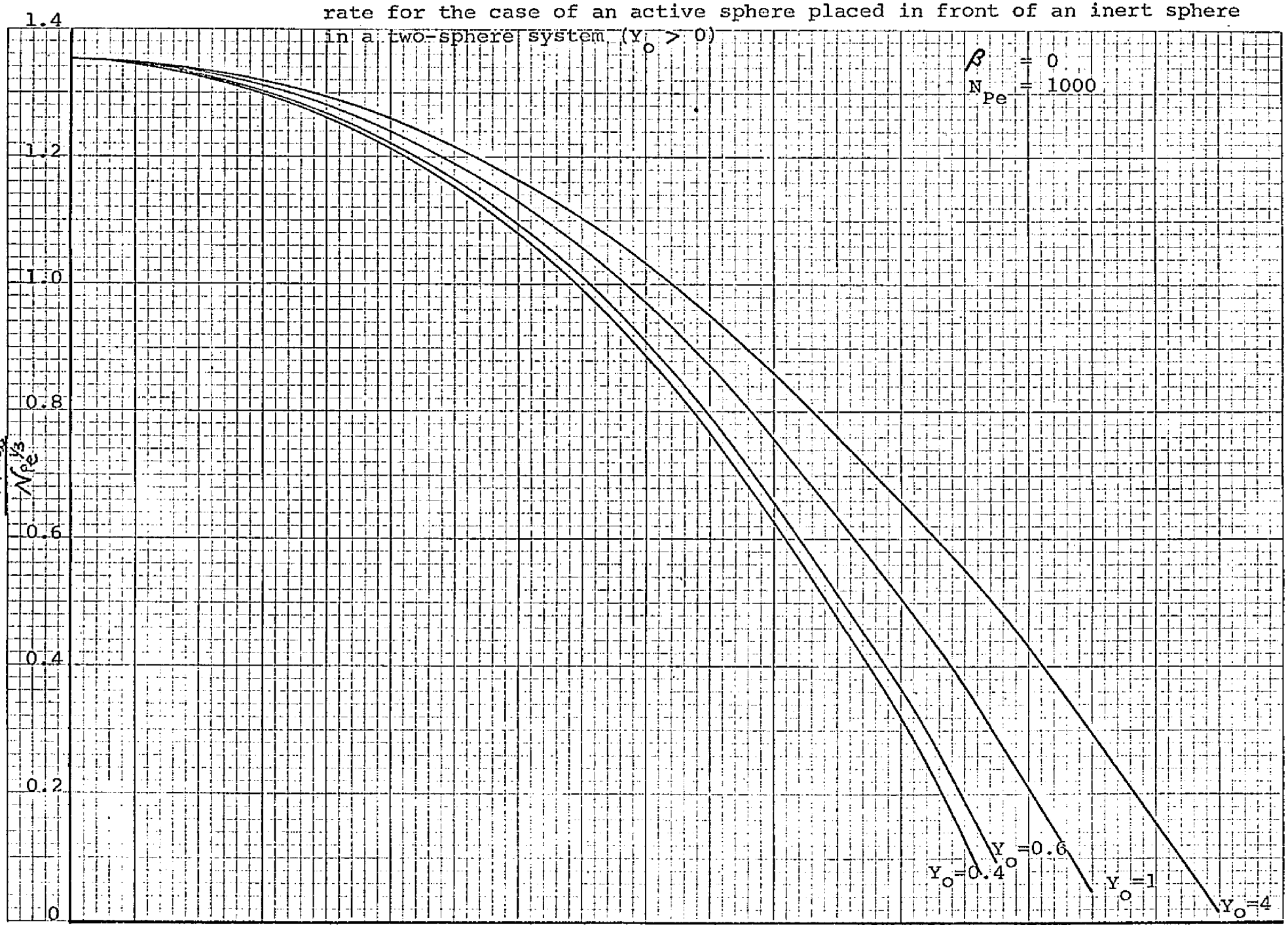

Fig. 14: Effect of particle-to-particle interaction on the local mass transfer rate for the case of an active sphere placed behind an inert sphere in a two-sphere system ($Y_o < 0$)

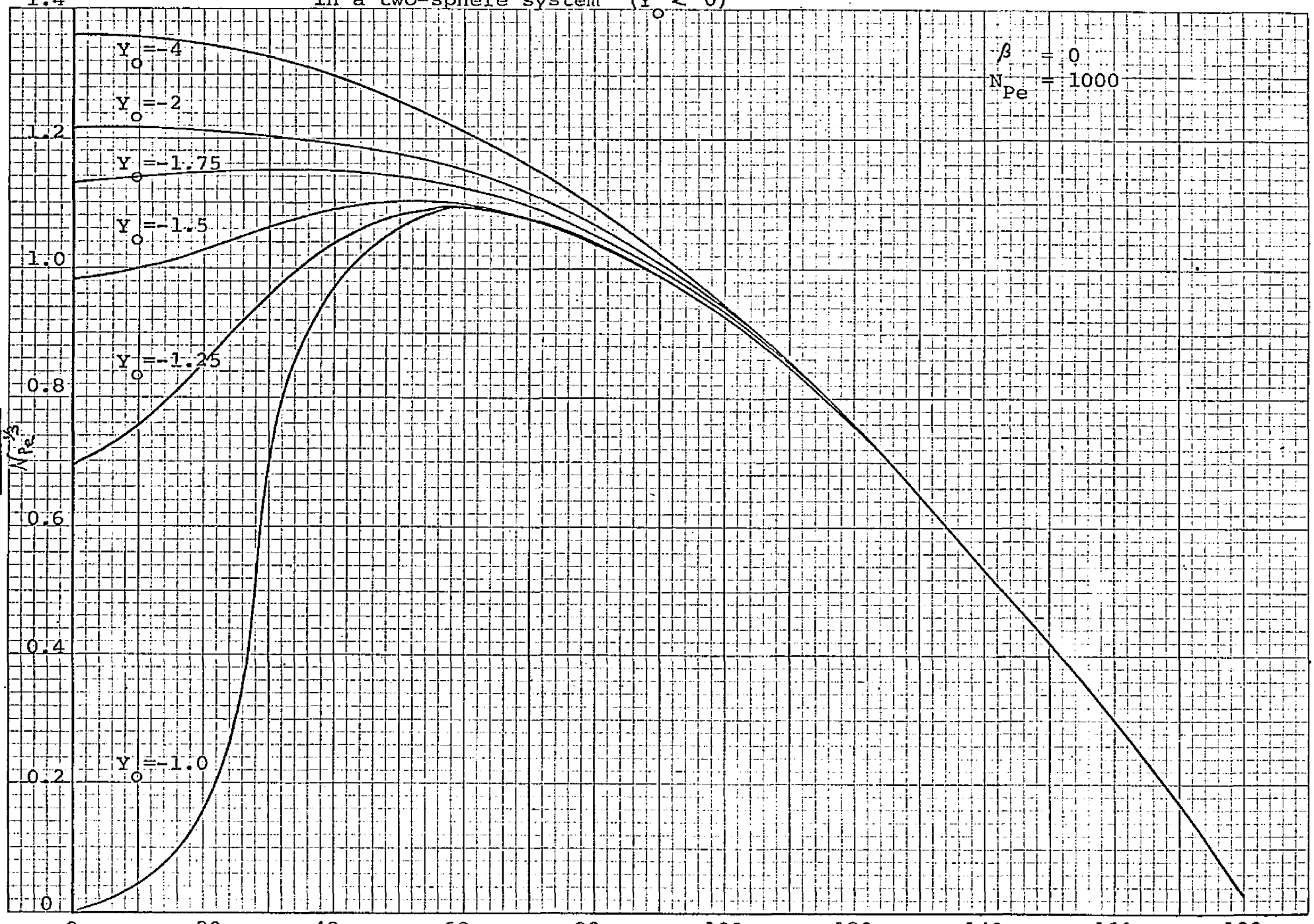

Fig. 15: Effect of Peclet number on the local mass transfer rate for the case of an active sphere placed in front of an inert sphere in a two-sphere system ($Y_o = +1$)

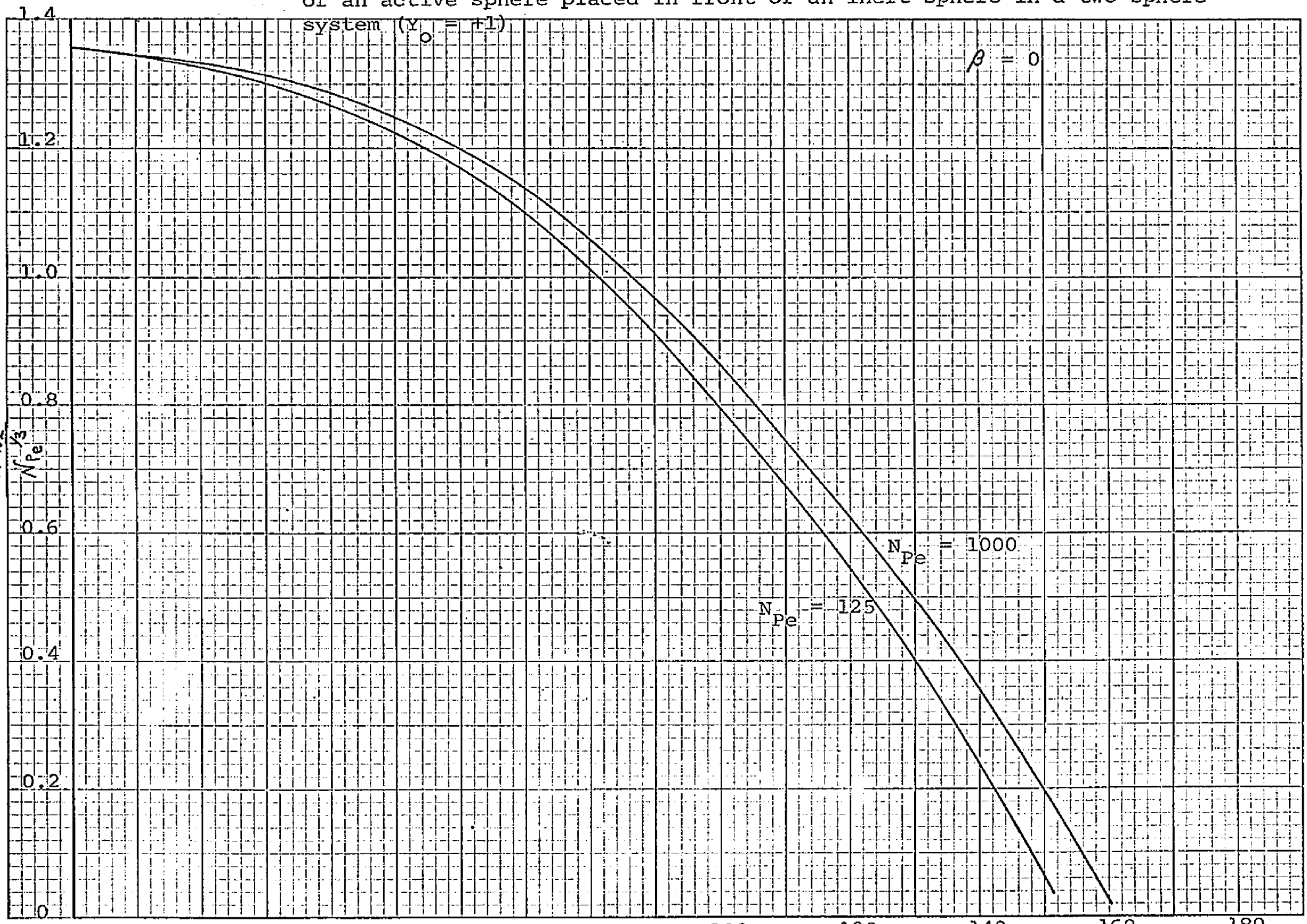

Fig. 16: Effect of Peclet number on the local mass transfer rate for the case of an active sphere placed behind an inert sphere in a two-sphere system ($Y_o = -2$)

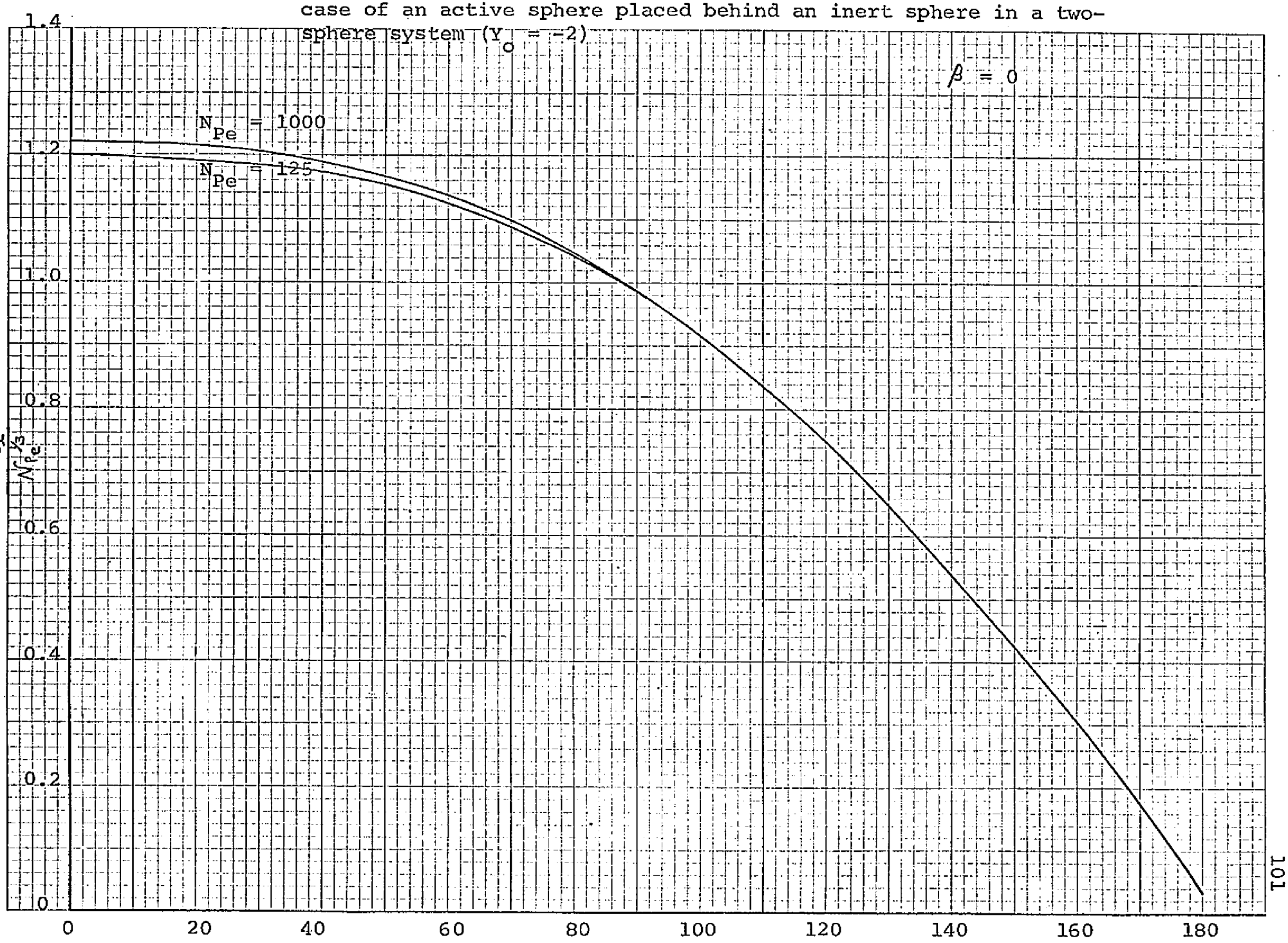

particle-to-particle interactions on mass transfer rates.

Figures 17, 18, 19, and 20 show the effect of Y_o or the center-to-center distance L/D on the overall mass transfer rate around an active sphere for both cases of $Y_o > 0$ and $Y_o < 0$ for Peclet numbers of 125 and 1000. Figures 17 and 18 show that at $Y_o \gg 0$ or $Y_o \ll 0$, i.e., two spheres which are very far apart, the mass transfer rate approaches that of a single sphere. This is quite obvious and does not need any further explanation. When the two spheres are placed closer and closer to each other, the overall mass transfer rate decreases because of the effect of particle-to-particle interaction on the hydrodynamic flow pattern. This same phenomena has been observed for the drag around two spherical particles; for two spheres touching the drag on each sphere is 55% lower than the drag on one sphere present alone. The resulting pure physical mass transfer rate is therefore very strongly dependent on the hydrodynamic flow pattern around the spheres as was also mentioned for the single sphere system discussed in the previous section.

It is interesting to note that at the same absolute value of Y_o, the resulting overall mass transfer rates are quite close to each other despite the fact that local mass transfer rates patterns are quite different from each other. The reason for this is that the contribution to the overall mass transfer rate is dominated by the local mass transfer rates from $\theta = 25^\circ$ to $\theta = 165^\circ$ and in this region the mass transfer profiles are similar.

A study of the plot of N_{Sh_o} versus Y_o at a Peclet number of 1000 shows that the Sherwood numbers appear to

Fig. 17: Effect of particle-to-particle distance, L/D, on the overall mass transfer rate for the case of an active sphere placed in front of an inert sphere in a two-sphere system ($Y_{\infty} > 0$)

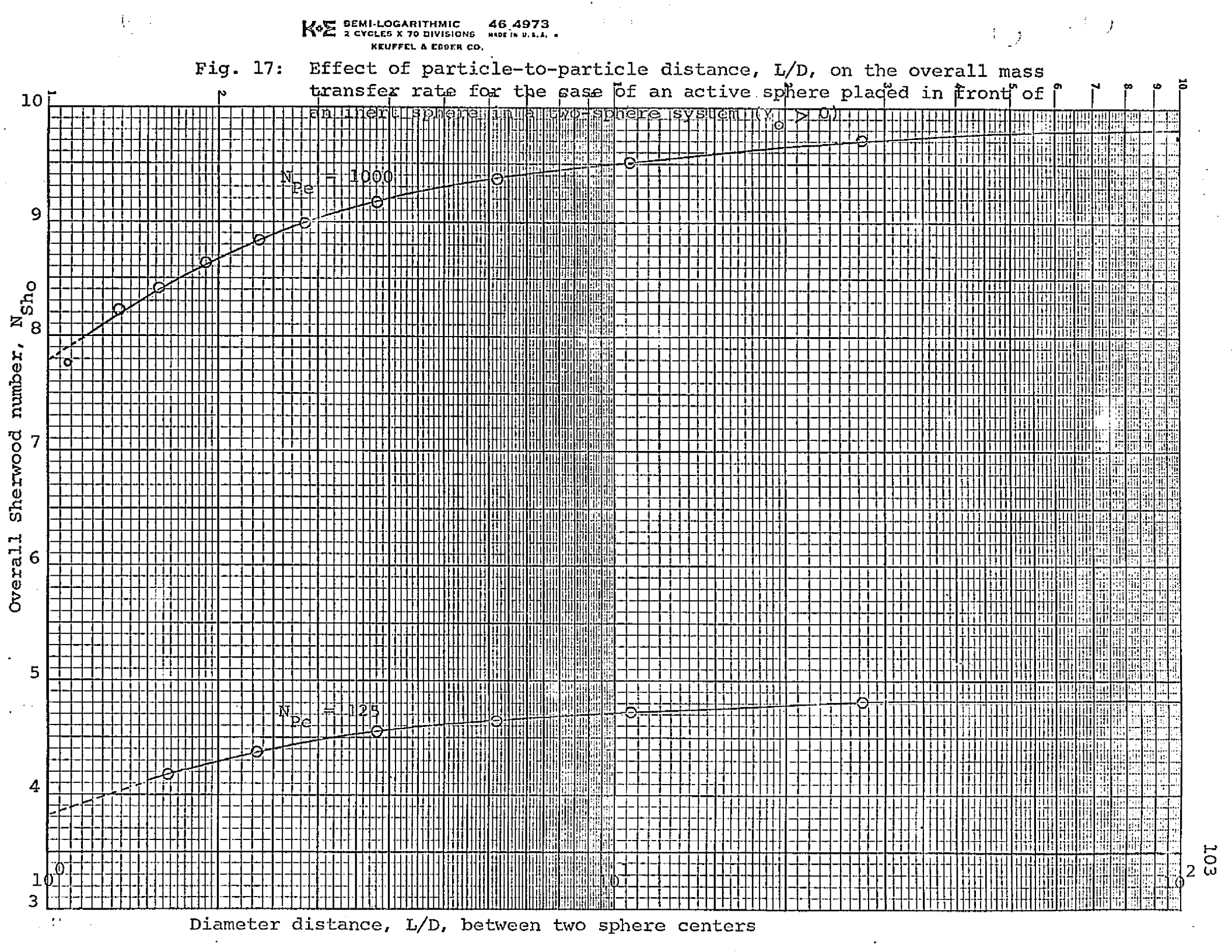

Fig. 18: Effect of particle-to-particle distance, L/D, on the overall mass transfer rate for the case of an active sphere placed behind an inert sphere in a two-sphere system (Y, Z, 0)

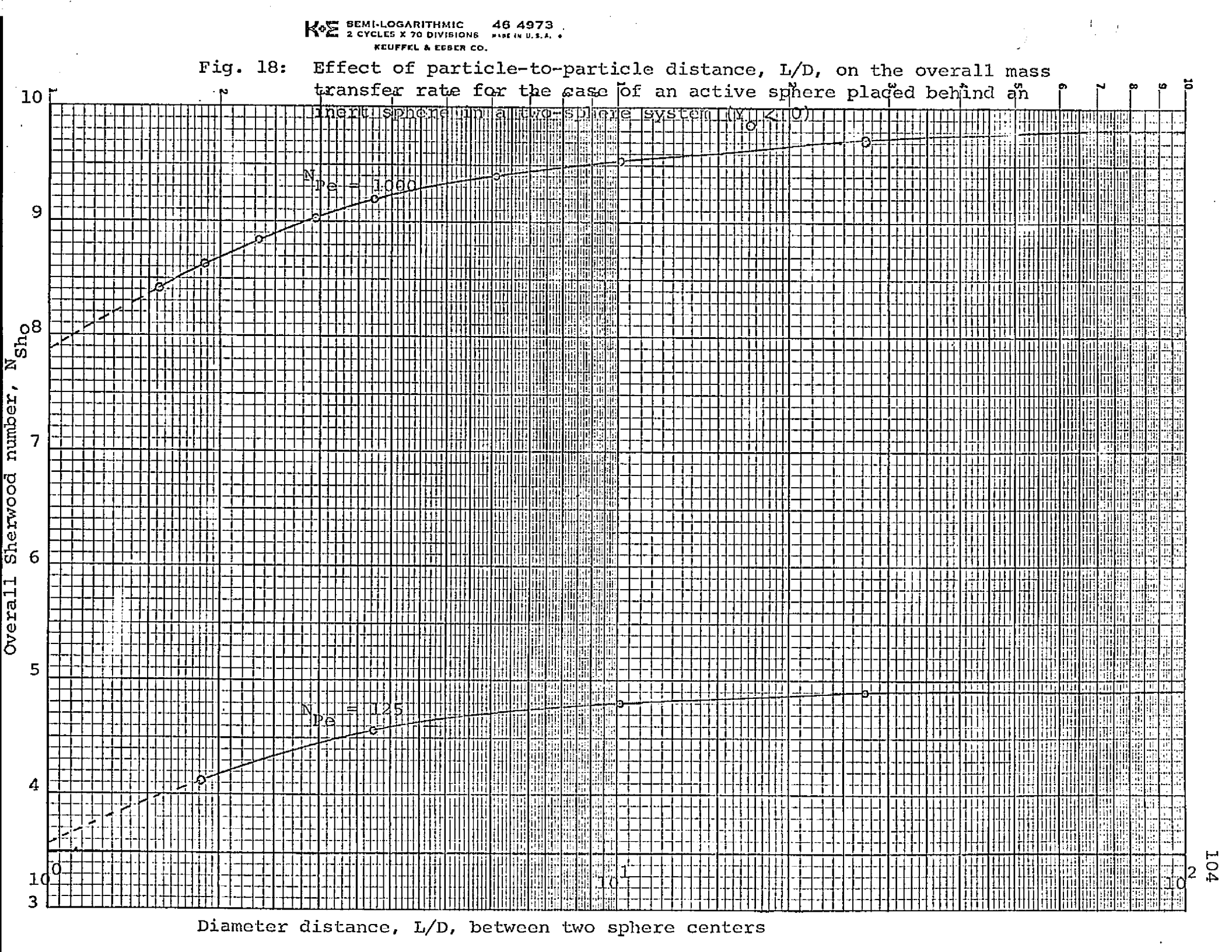

Fig. 19: Effect of particle-to-particle distance, Y_o, on the overall mass transfer rate for the case of an active sphere placed in front of an inert sphere in a two-sphere system ($Y_o > 0$)

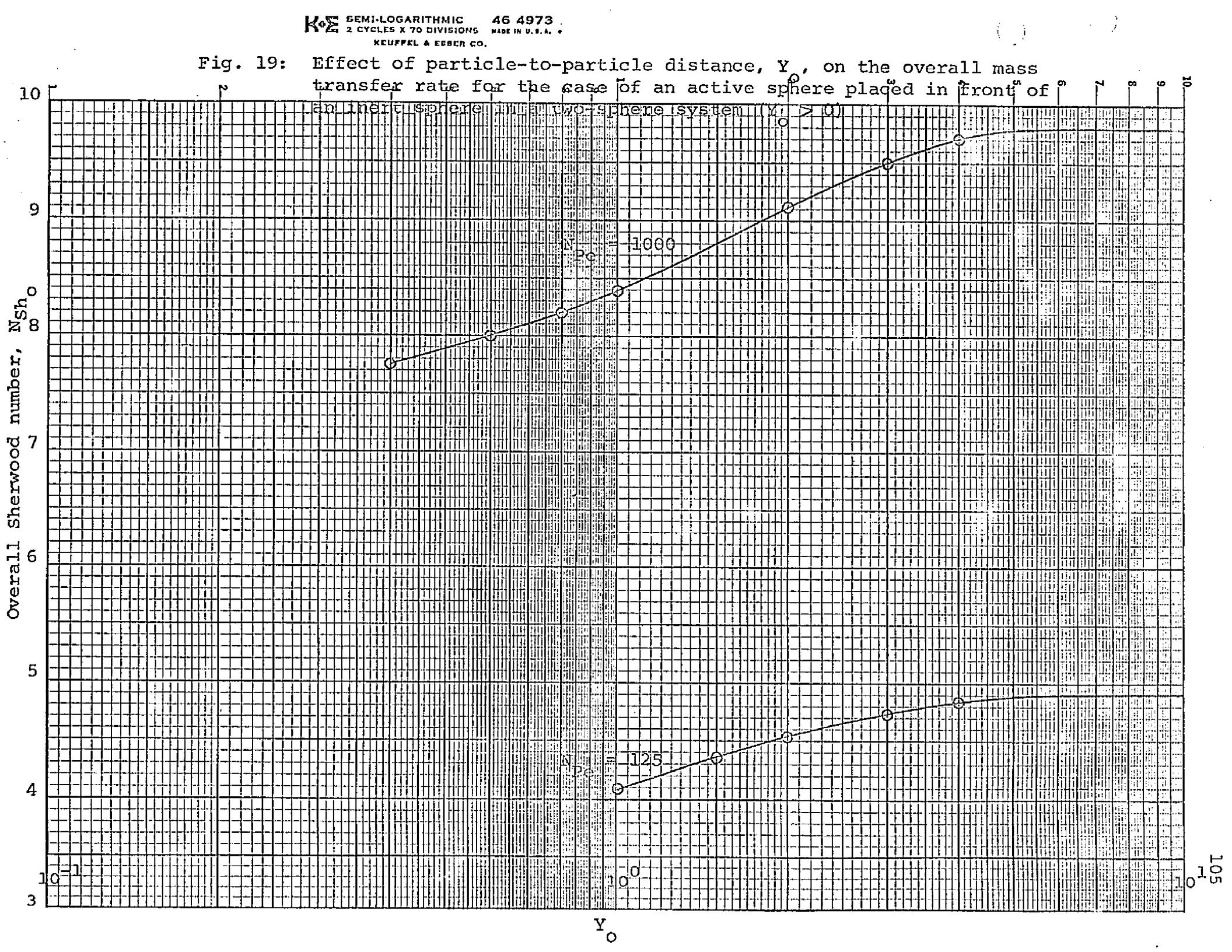

Fig. 20: Effect of particle-to-particle distance, Y_o, on the overall mass transfer rate for the case of an active sphere placed behind an inert sphere in a cylinder system ($N_{Pe_o} < 10$)

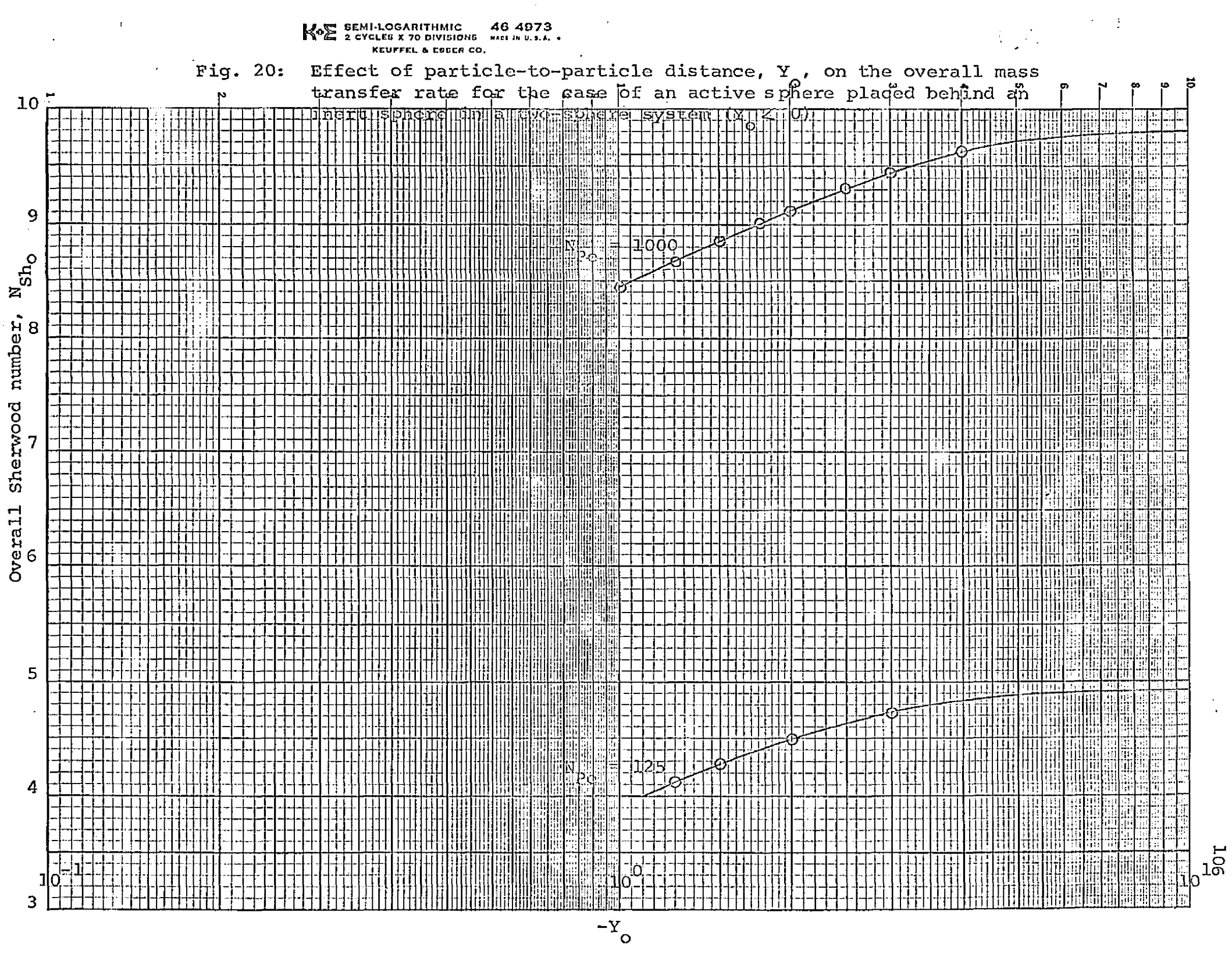

approach an asymptotic value at both very large and very small values of Y_o. This behavior is quite logical since at large values of Y_o, N_{Sh_o} approaches its value for a single sphere and at very small values of Y_o the Sherwood number will approach its minimum value for the case of two spheres touching.

Figure 19 shows an inflection point between the asymptotic minimum value of N_{Sh_o} (at $Y_o = 0$) and the maximum value of N_{Sh_o} (at $Y_o = \infty$). The figures also indicate that at different values of N_{Pe} the mass transfer rate obtained using the thin boundary layer approximation is strongly affected by the Peclet number and particle-to-particle interaction. However, it appears that the data can be correlated according to

$$N_{Sh_o} = A\, N_{Pe}^{1/3} \qquad \text{(IV-172)}$$

when the N_{Pe} is large, where the constant A is strongly dependent on the center-to-center distance between the two spheres. It is clear that A decreases as the two spheres get closer and closer to one another.

The effects of homogeneous first-order chemical reaction on the local mass transfer rates are shown in Figures 21, 22, 23, and 24. For the case of the active sphere placed behind an inert sphere in the direction of flow, the local mass transfer rate pattern is similar to that of the single sphere around $\theta = \pi$. Around $\theta = 0$, the local mass transfer rate is dependent of both the particle-to-particle interaction and reaction rate term.

Fig. 21: Effect of first order homogeneous chemical reaction on the local mass transfer rate for the case of an active sphere placed behind an inert sphere at $N_{Pe} = 1000$ and $Y_o = -2$

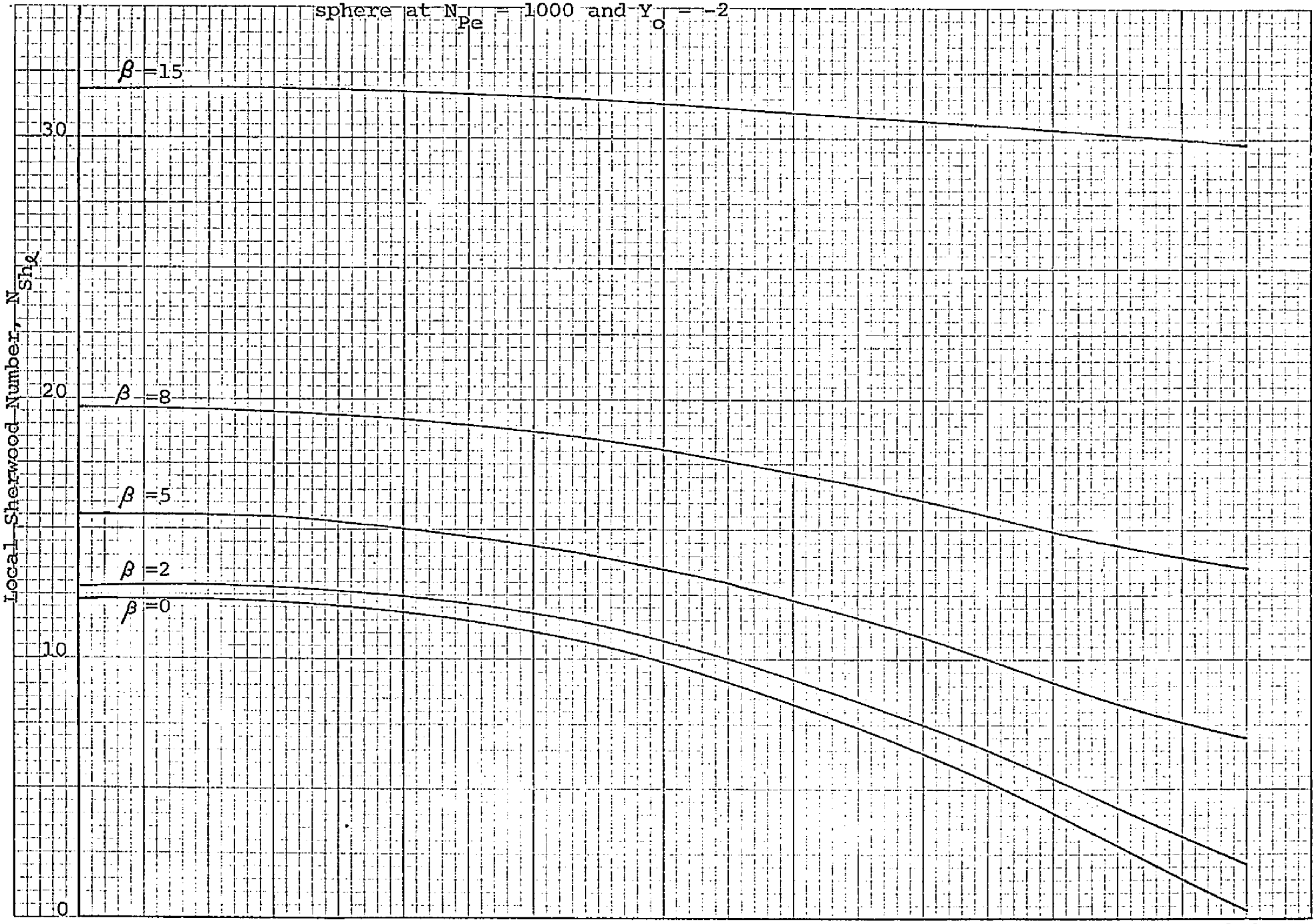

Fig. 22: Effect of first order homogeneous chemical reaction on the local mass transfer rate for the case of an active sphere placed behind an inert sphere at $N_{Pe} = 1000$ and $Y_o = -1.25$

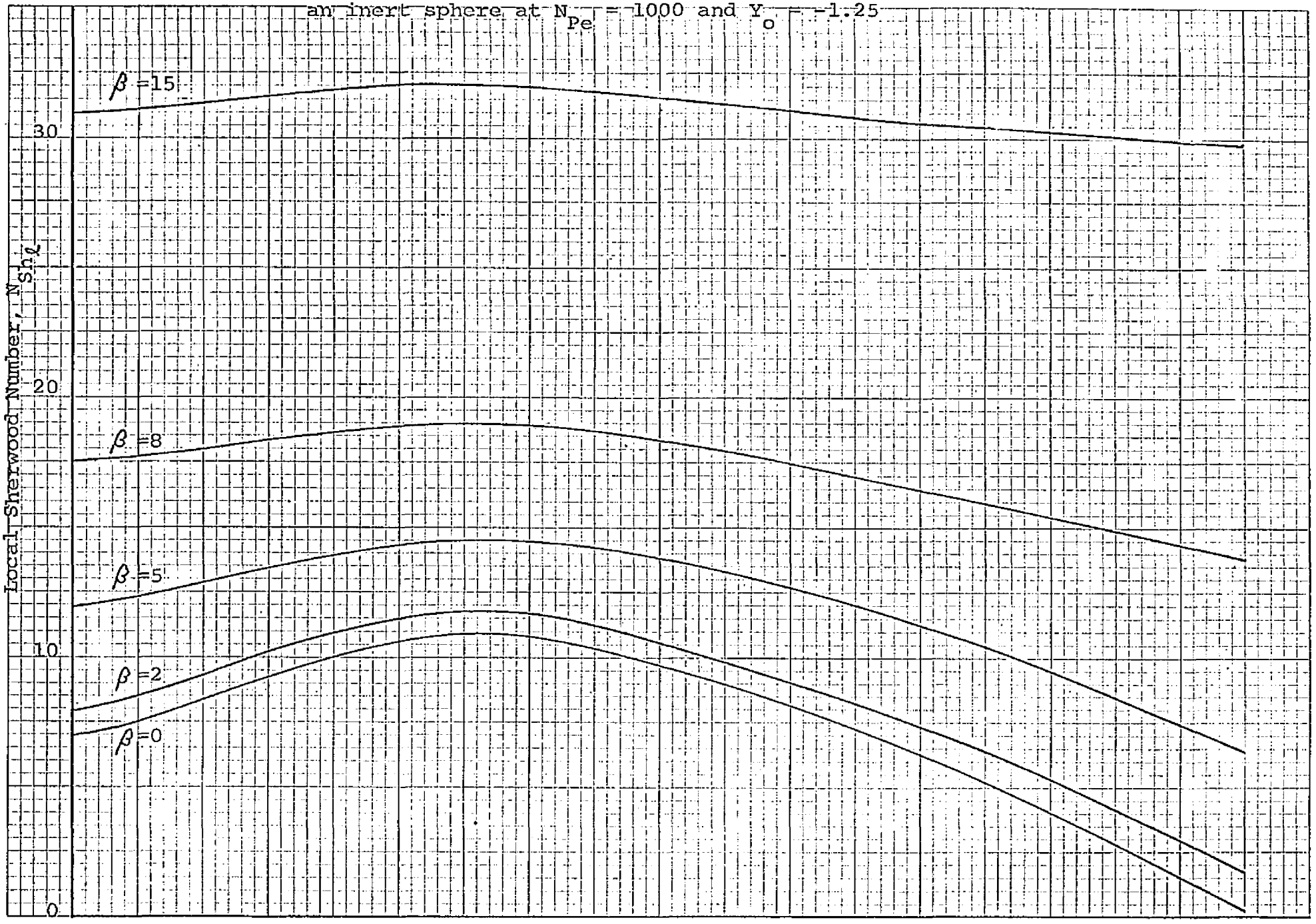

Fig. 23: Effect of first order homogeneous chemical reaction on the local mass transfer rate for the case of an active sphere placed in front of an inert sphere at $N_{Pe} = 1000$ and $Y_o = 2$

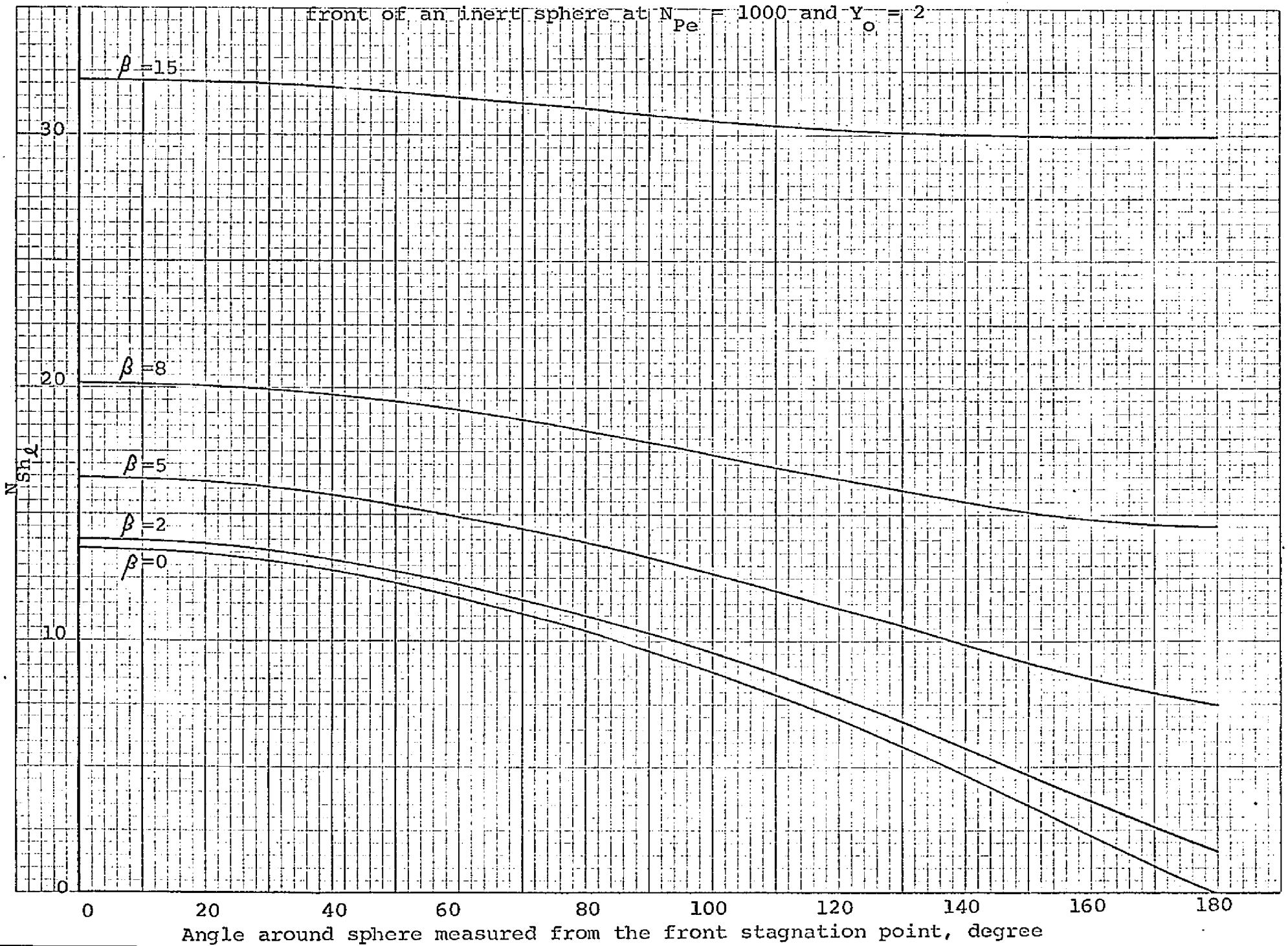

Fig. 24: Effect of first order homogeneous chemical reaction on the local mass transfer rate for the case of an active sphere placed in front of an inert sphere at $N_{Pe} = 1000$ and $Y_o = 1$

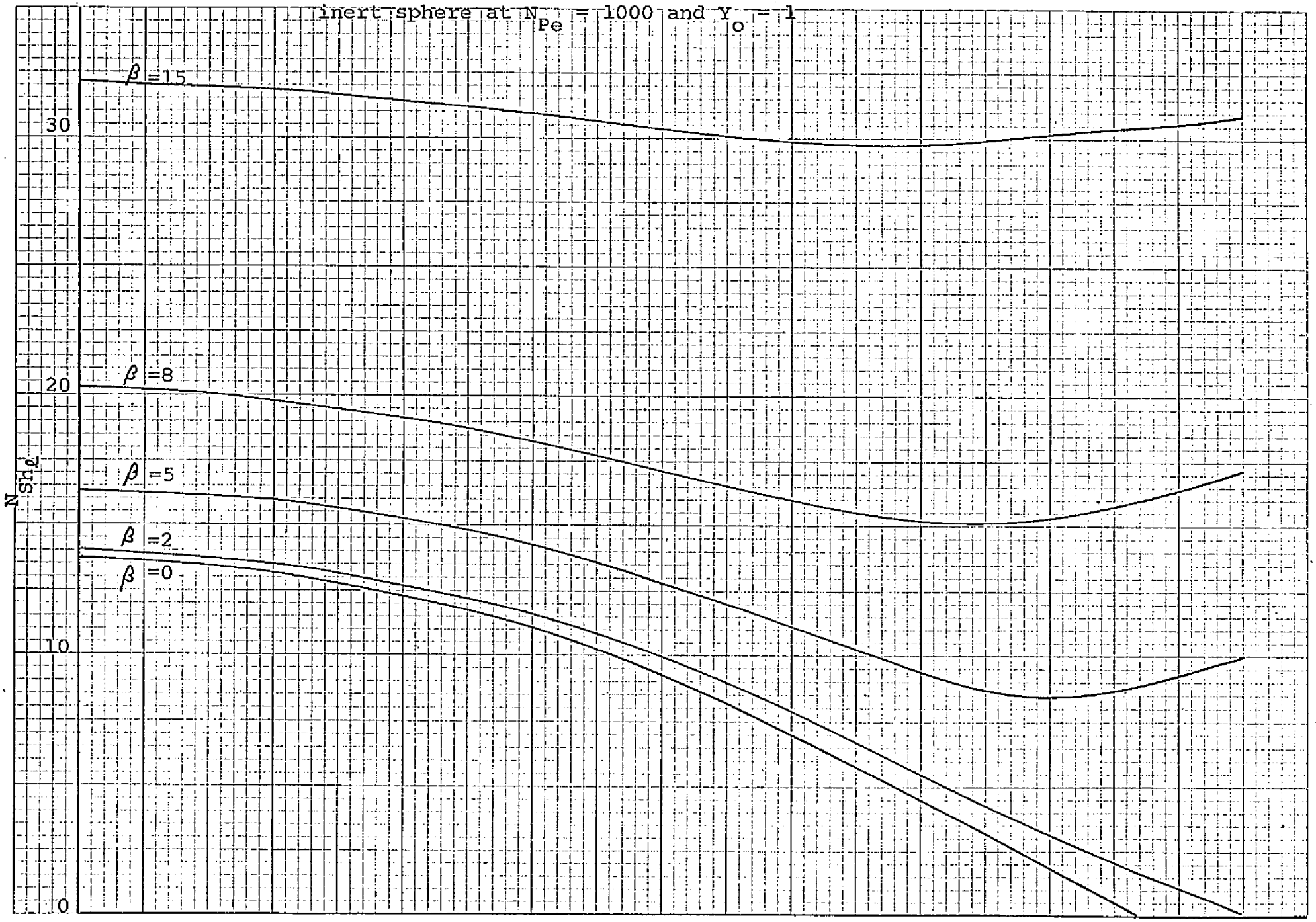

As was discussed in previous paragraphs for the local mass transfer rates without chemical reaction, there is a maximum transfer rate at an angle away from the front stagnation point depending on the center-to-center distance between the two spheres. Figures 21 and 22 show that the local mass transfer rates tend to flatten out with angle as reaction rate increases. As with the single sphere, the reason for this is explained by the fact that the reaction term dominates the convection terms.

For the case of the active sphere placed in front of the inert sphere in the direction of flow, Figures 23 and 24 show the effect of the reaction term on local mass transfer rate. When the two spheres are far from each other, the local mass transfer profile resembles the single-sphere pattern with the minimum transfer rate at the rear stagnation point.

However, when the two spheres are brought closer to one another this minimum transfer rate shifts from the rear stagnation point for $\beta = 0$ to an angle away from the rear stagnation point for larger β values. This local mass transfer pattern can be explained both mathematically and physically.

The governing diffusion equation for this case is given by

$$(\cosh\eta - \cos\xi)^2 \frac{\partial^2 C}{\partial \eta^2} - \frac{N_{Re}}{2}\left(\frac{c}{a}\right)(\cosh\eta - \cos\xi)\left(V_\xi \frac{\partial C}{\partial \xi} + V_\eta \frac{\partial C}{\partial \eta}\right) - \left(\frac{c}{a}\right)^2 \beta^2 C = 0 \qquad \text{(IV-173)}$$

As V_ξ and V_η approach zero around the rear stagnation region, the mass transfer process will tend to behave like

mass transfer with first-order homogeneous chemical reaction into a stagnant fluid. The local gradient in the η direction is related to the value $\partial^2 C/\partial^2\eta$. The larger the value of $\partial^2 C/\partial^2\eta$ the greater the concentration gradient in the η - direction. For $Y_o > 0$, $\partial C/\partial\xi$, $\partial C/\partial\eta$, and V_ξ are always positive whereas V_η changes from a positive value at the front stagnation point to a negative value at the rear stagnation point. Somewhere around $\xi = \pi$, there is a point which gives a minimum value of $\partial^2 C/\partial^2\eta$. This corresponds to $\partial N_{Sh_\ell}/\partial\theta = 0$ and is the minimum local mass transfer point.

The physical interpretation of this phenomena involves the interplay of the convective and reaction terms in the mass transfer rate from the sphere. When the two spheres are very close together there is very little convection in the region behind the sphere: i.e., very little saturated fluid is brought in from the flow. Hence the Sherwood number is governed only by the diffusion and reaction terms. It has already been shown that the solution of the diffusion equation without convection present will give a higher Sherwood number than the corresponding solution of the diffusion equation with convection present when one is near the rear stagnation point. Since the reaction term will always tend to increase the Sherwood number this would explain why it is possible to obtain a larger Sherwood number at the rear of the sphere.

Another comparison plotting N_{Sh_ℓ}/β vs. angle with $\beta = 8$ and $Pe = 1000$ for different values of Y_o is given in Figure 25. For the case of mass transfer with chemical reaction from a sphere to an infinite stagnant fluid, the

Fig.25: Effect of particle-to-particle interaction on the local mass transfer rate at $N_{Pe} = 1000$ and $\beta = 8$

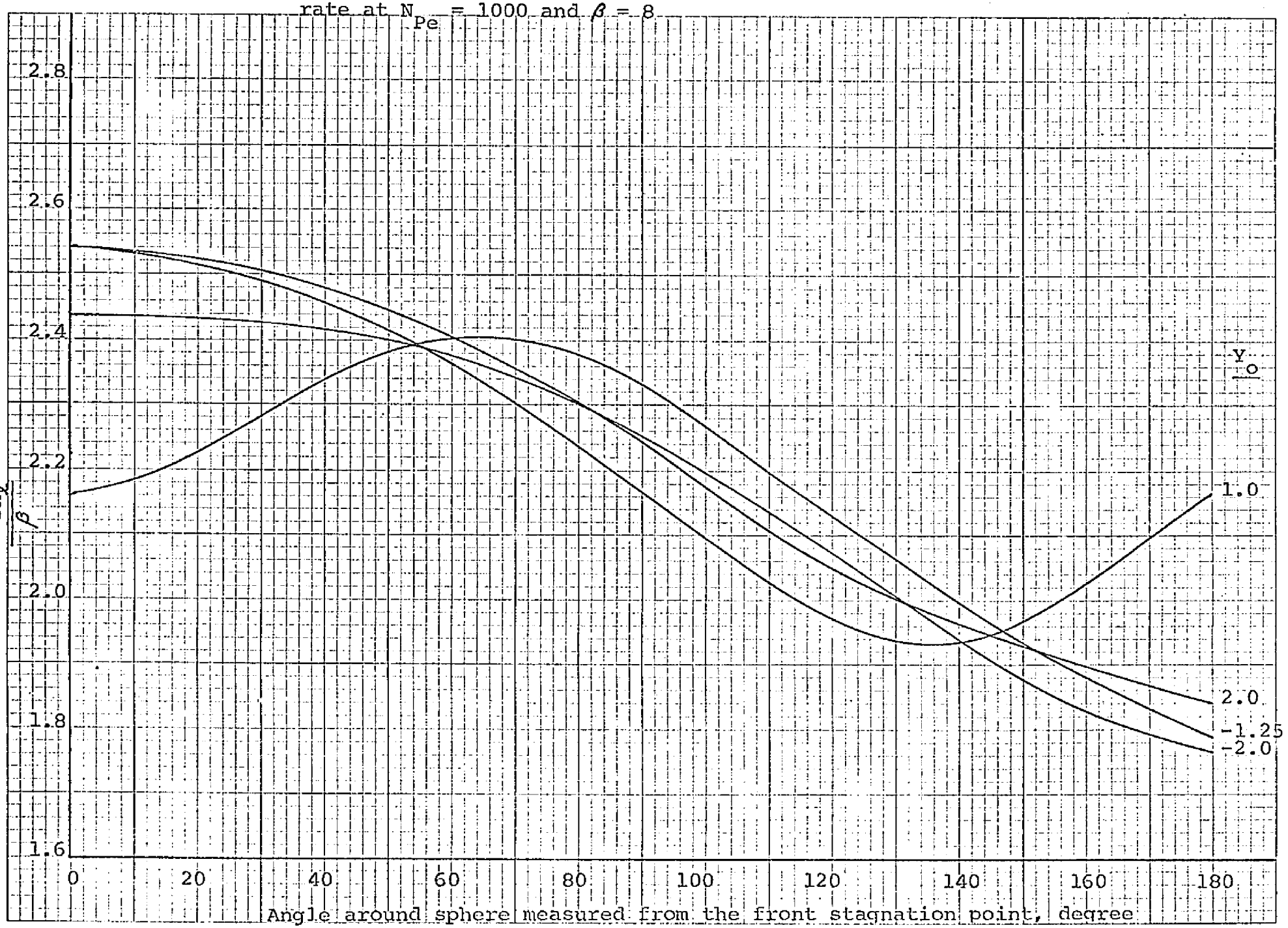

overall and local mass transfer rates are both equal to $2 + 2\beta$. The difference in local mass transfer rates is obviously due to different hydrodynamic patterns around the active sphere.

Generalized relations between N_{Sh_o}/β, $N_{Pe}^{1/3}/\beta$ and Y_o are given in Figures 26 and 27. As Y_o approaches $+\infty$ or $-\infty$, the mass transfer rate behavior becomes equivalent to that of the single-sphere system. As β increases the reaction term reduces the effect of forced convection mass transfer mechanism and as $N_{Pe}^{1/3}/\beta \longrightarrow 0$, $N_{Sh_o}/\beta \longrightarrow 2$.

C. Rapid Second Order Chemical Reaction Around Solid Spheres, Liquid Drops and Gas Bubbles.

Figures 28, 29, and 30 which are calculated from equations (IV-81), (IV-107), and (IV-136) respectively show the effect of the bulk concentration ratio of the reagent and solute, $\frac{a}{b}\frac{C_{BM}}{C_{AO}} = \gamma$, on the concentration boundary thickness of the solute around solid spheres, liquid drops and gas bubbles with the ratio of diffusivities of the solute and reagent, $N_{Sh_A}/N_{Sh_B} = \alpha$, as a parameter. These figures show that at fixed C_{AO}, the larger the concentration of the reagent C_B, the thinner the concentration boundary layer of the solute, ξ_{AR}. The effects of the diffusivity ratio, α, on the solute concentration boundary layer thickness are also shown by these figures, i.e., the larger the value of α, the thinner the solute concentration boundary layer thickness. For example, at fixed N_{Sc_B}, the larger the value of N_{Sc_A}, the thinner the solute concentration boundary layer, whereas, at fixed N_{Sc_A}, the larger the value of N_{Sc_B}, the thicker the solute concentration boundary layer. Of course, the thinner the solute concentration

Fig. 26: Generalized correlation for the overall mass transfer rate with first order homogeneous chemical reaction from an active sphere placed in front of an inert sphere ($Y_o > 0$)

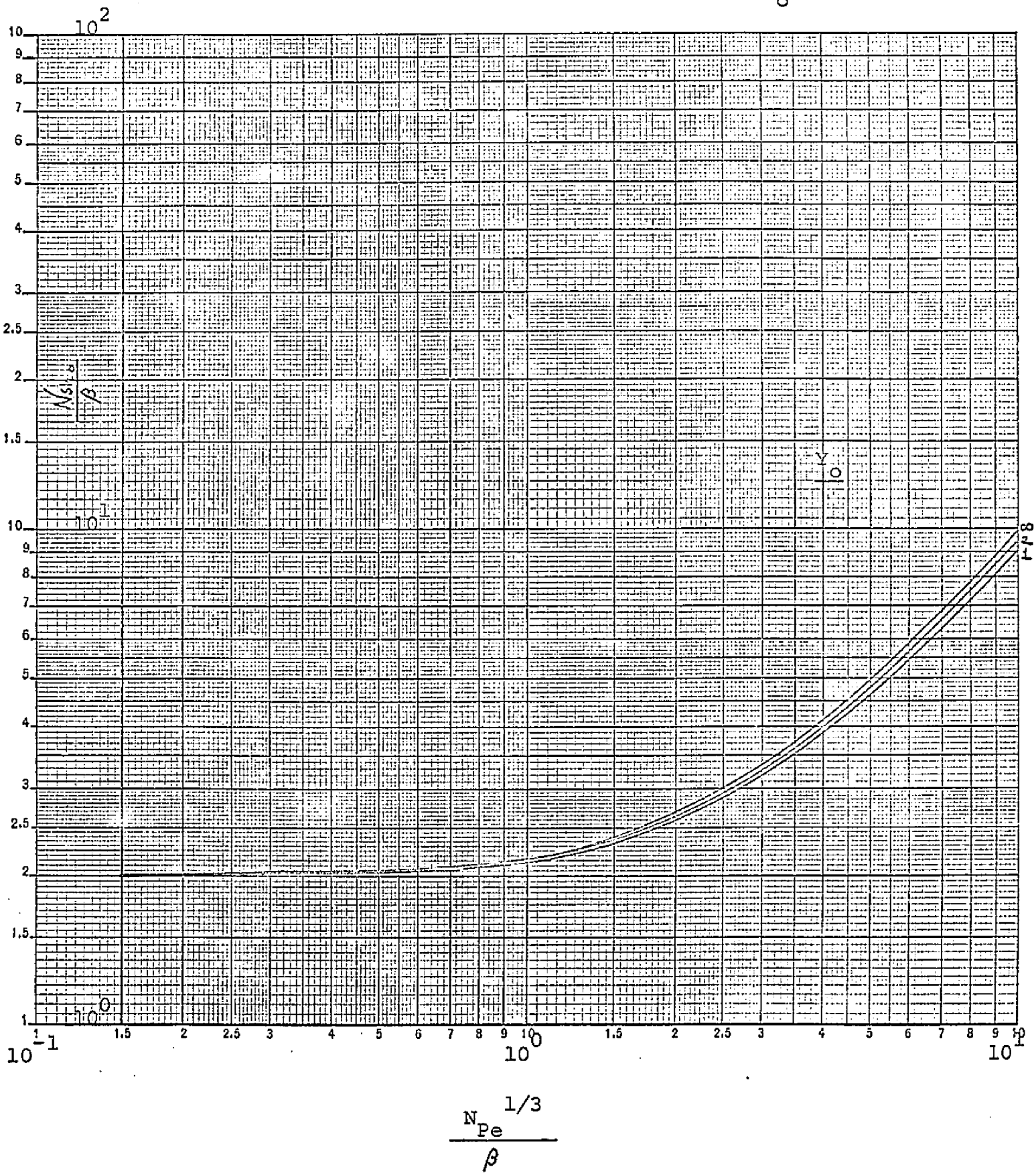

Fig. 27: Generalized correlation for the overall mass transfer rate first order homogeneous chemical reaction from an active sphere placed behind an inert sphere ($Y_o < 0$)

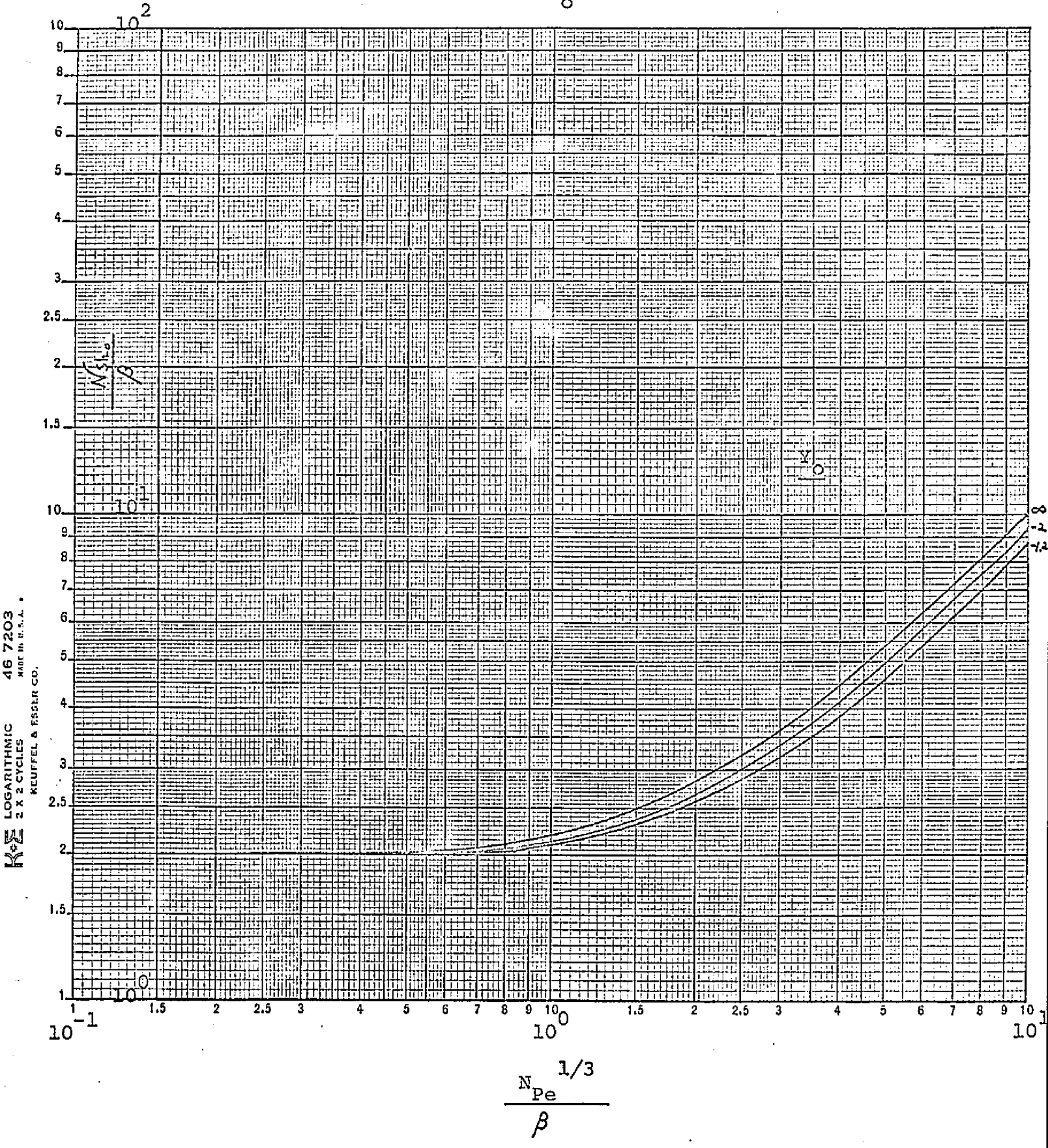

Fig. 28: Effect of bulk stream concentration ratio, γ, and Schmidt number ratio, α, on the concentration boundary layer thickness, ξ_{AR}, for mass transfer from a solid sphere

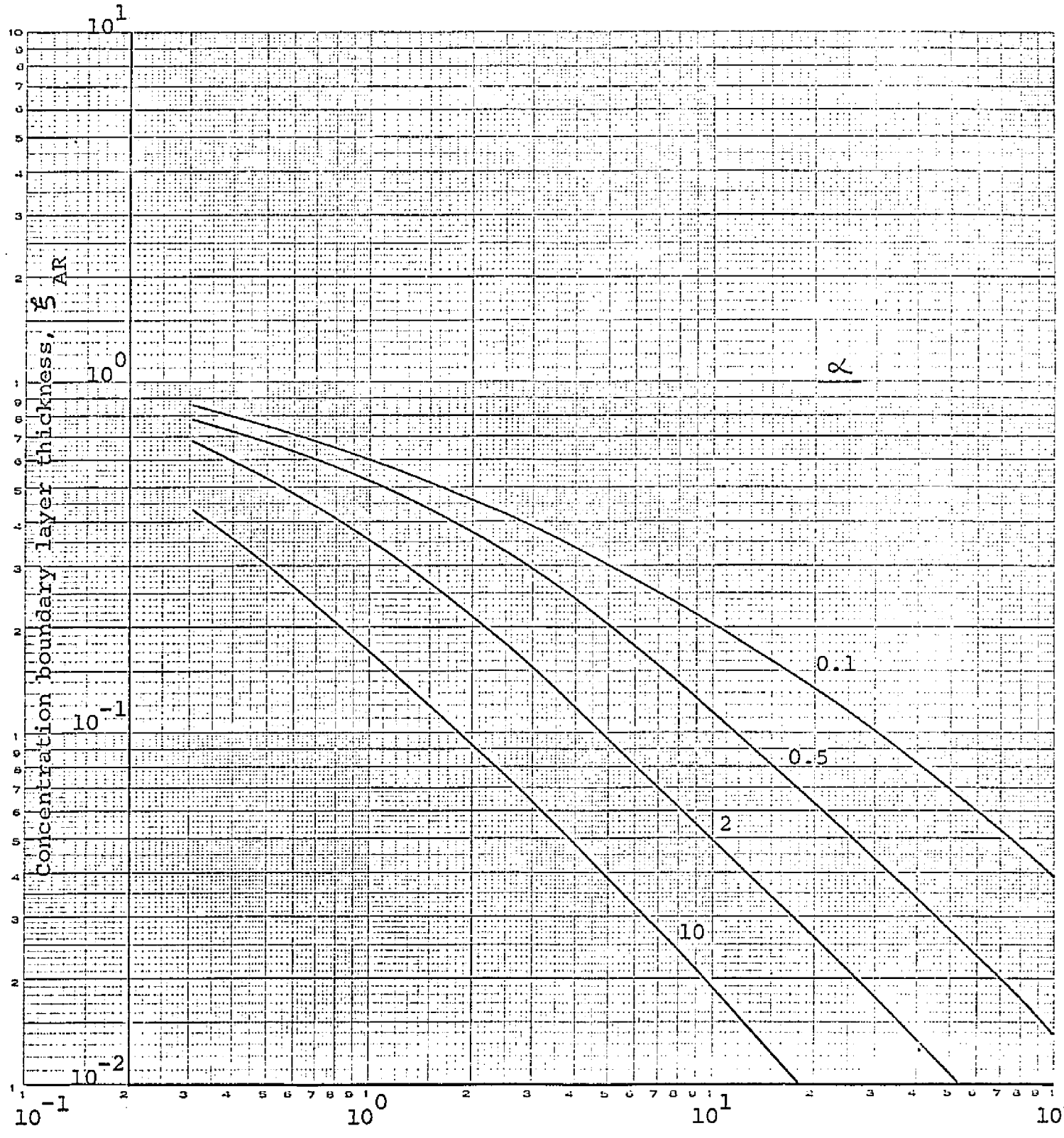

Fig. 29: Effect of bulk stream concentration ratio, γ, and Schmidt number ratio, α, on the concentratrion boundary layer thickness, ξ_{AR}, for mass transfer from a liquid drop ($F = 1$)

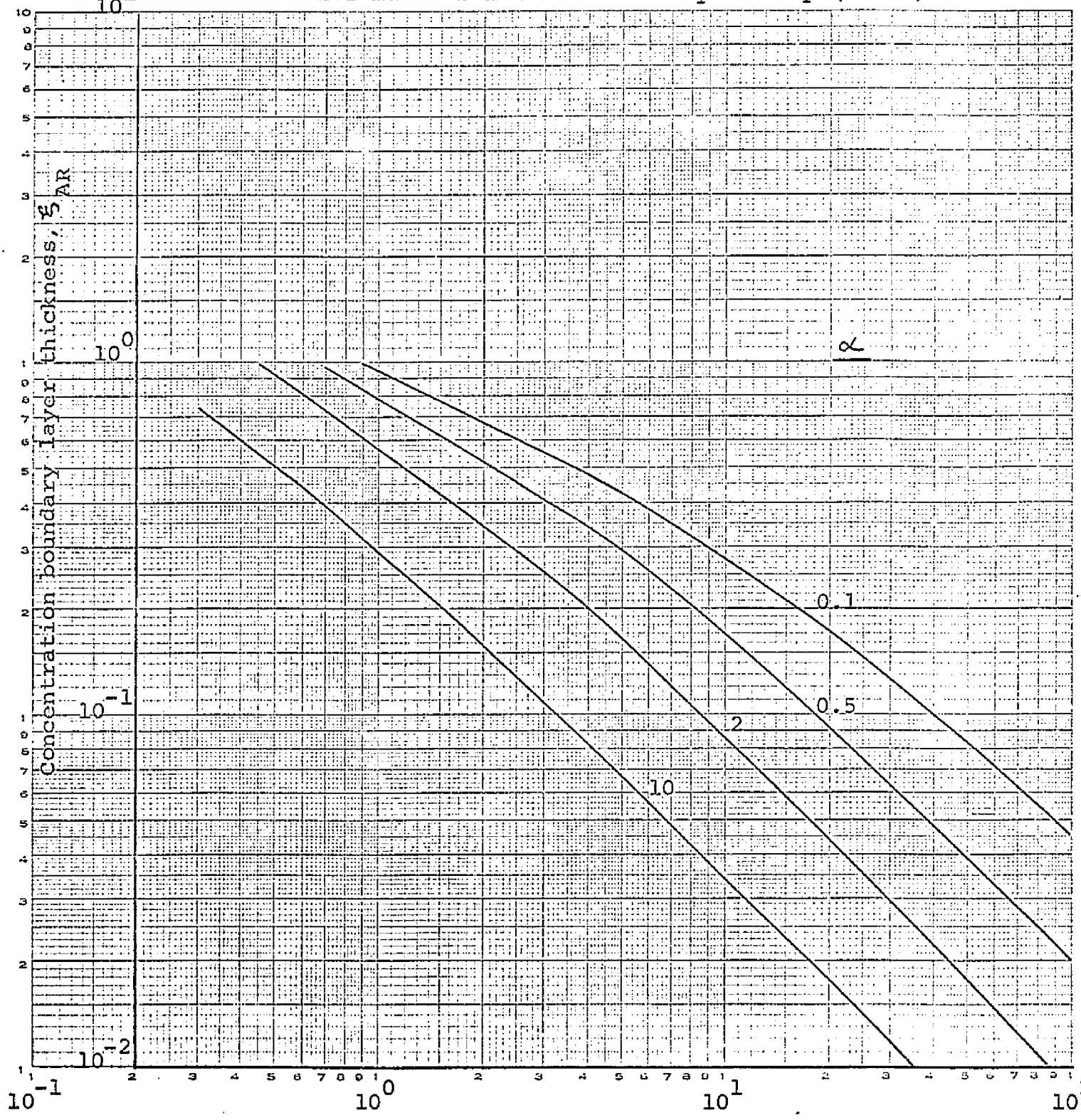

Fig. 30: Effect of bulk stream concentration ratio, γ, and Schmidt number ratio, α, on the concentration boundary layer thickness, ξ_{AR}, for mass transfer from a gas bubble

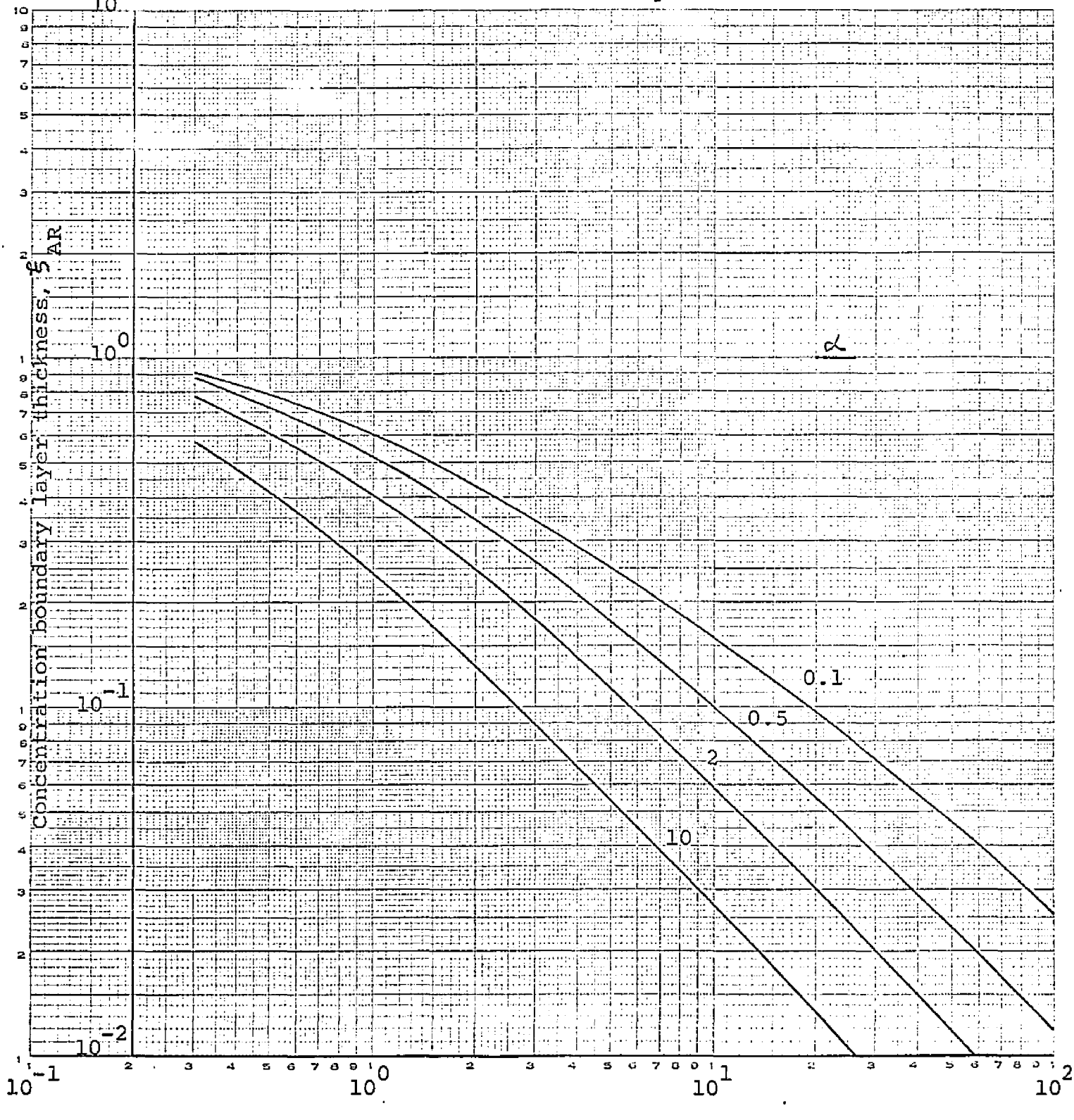

boundary layer, the smaller the resistance for the solute diffusing into the continuous phase and the larger the mass transfer rates and the larger the corresponding enhancement factor. These figures give a qualitative idea of the effect of α and γ on mass transfer rates.

Since ξ_{AR} is a function of spherical angle x and radial distance from the surface of the sphere y, it is interesting to know what the corresponding values of x and y are at a fixed value of ξ_{AR}. If we recall equations (IV-74) and (IV-100) for the definition of ξ_{AR} for the cases of solid spheres and gas bubbles respectively, we note that ξ_{AR} is given in general form as

$$\xi_{AR} = \frac{F(y)}{G(x)} \qquad \text{(IV-174)}$$

where F and G are increasing functions of y and x. At fixed ξ_{AR}, as x, the spherical angle increases, or G(x) increases and thus corresponding values of y or F(y) also increase. This gives the physical picture that the larger the spherical angle, the thicker the solute boundary layer thickness.

Figures 31, 32, and 33 give the mass transfer rates in terms of the enhancement factor, ϕ , as a function of $\alpha^n\gamma$ using α as a parameter for the cases of solid spheres, liquid drops (special case F = 1) and gas bubbles. Here n is an asymptotic value such that $\phi = \alpha^n\gamma$ as $\xi_{AR} \longrightarrow 0$. These figures are calculated directly from equations (IV-81), (IV-86), (IV-148), (IV-150), (IV-107), and (IV-112). The effect of the values of α and γ on the mass transfer rates

Fig. 31: Effect of bulk stream concentration ratio, γ, and Schmidt number ratio, α, on the enhancement factor, ϕ, for mass transfer from solid sphere

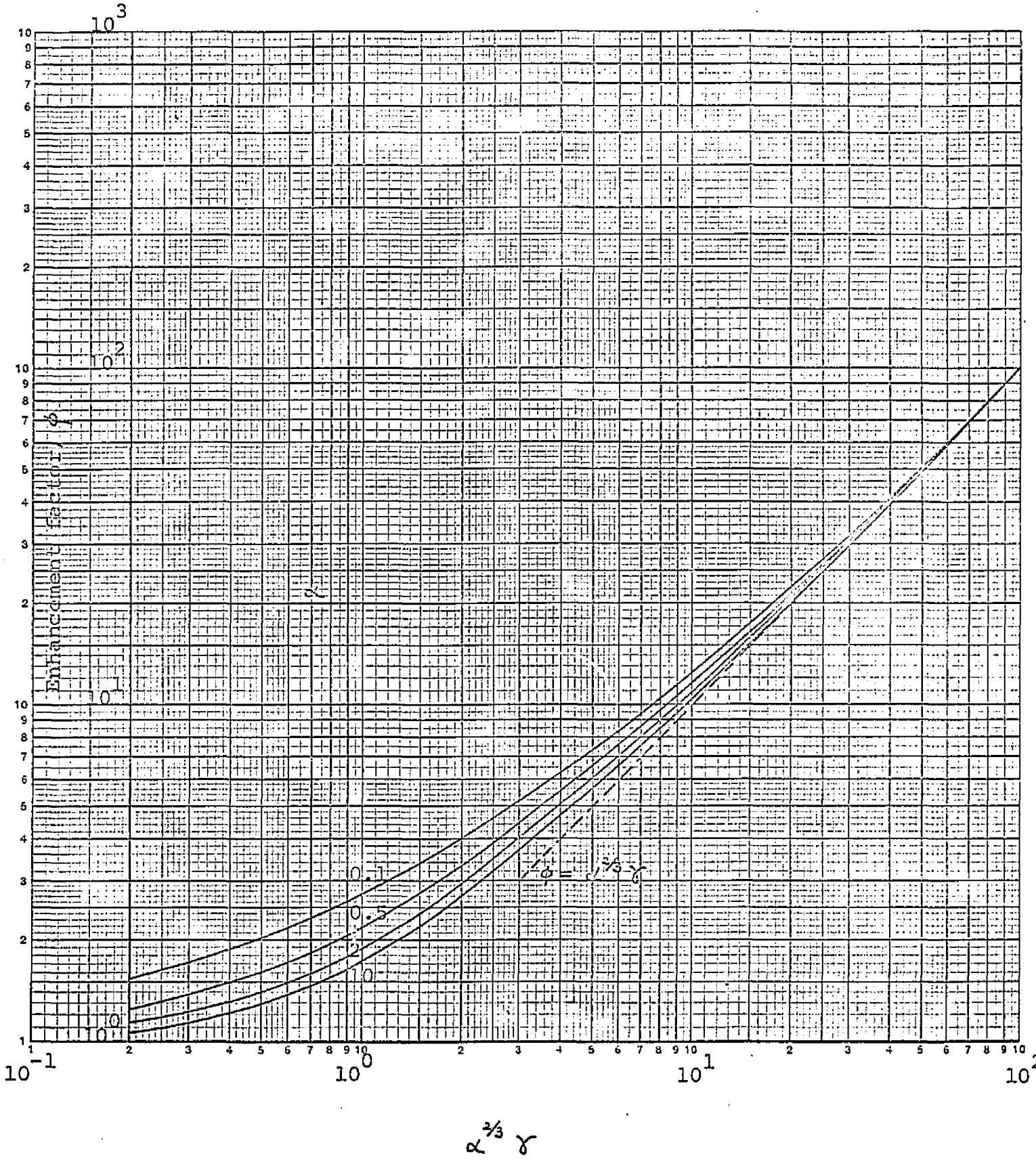

Fig. 32: Effect of bulk stream concentration ratio, γ, and Schmidt number ratio, α, on the enhancement factor, ϕ, for mass transfer from a liquid drop (F = 1)

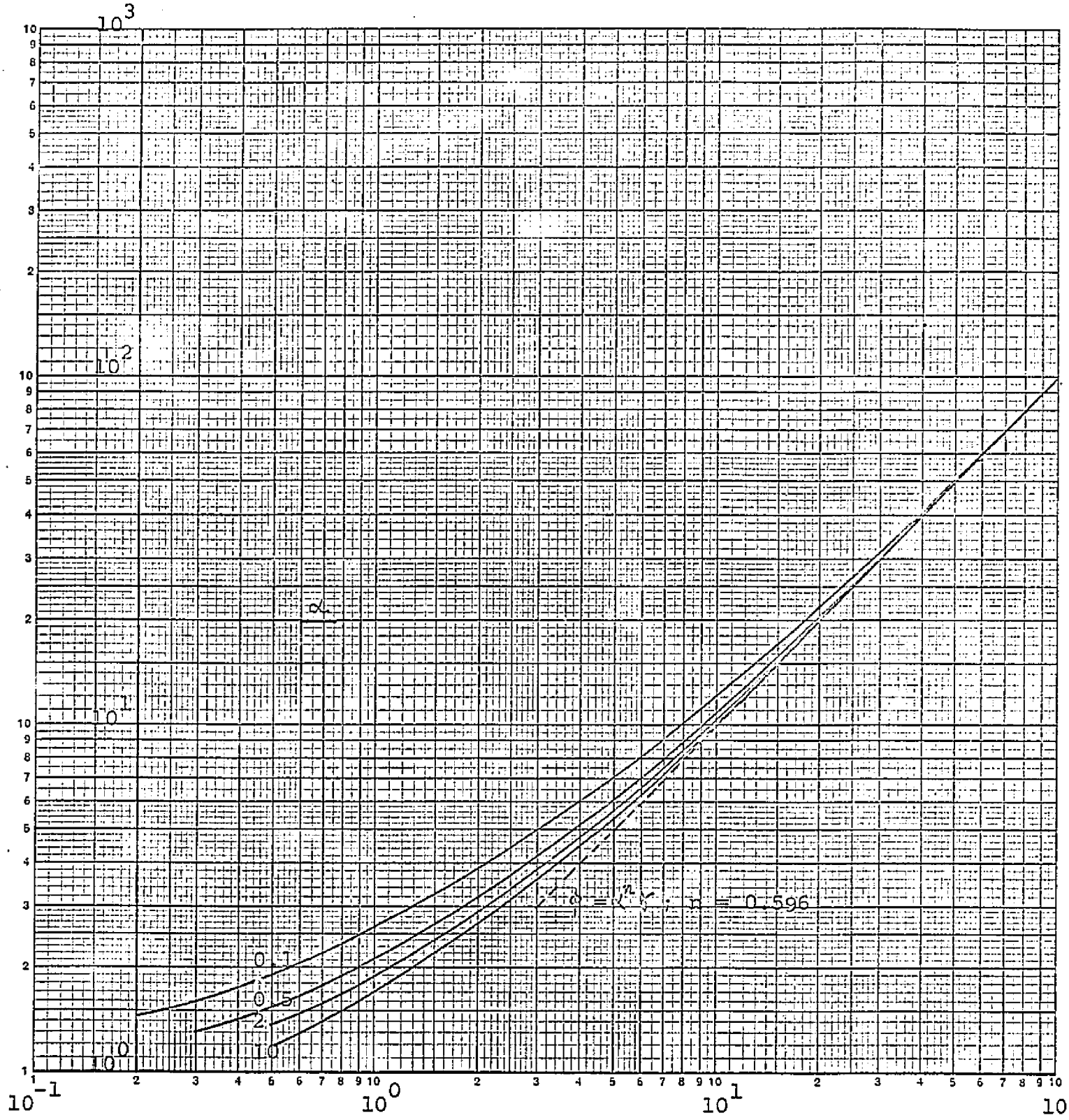

Fig. 33: Effect of bulk stream concentration ratio, γ, and Schmidt number ratio, α, on the enhancement factor, ϕ, for mass transfer from a gas bubble

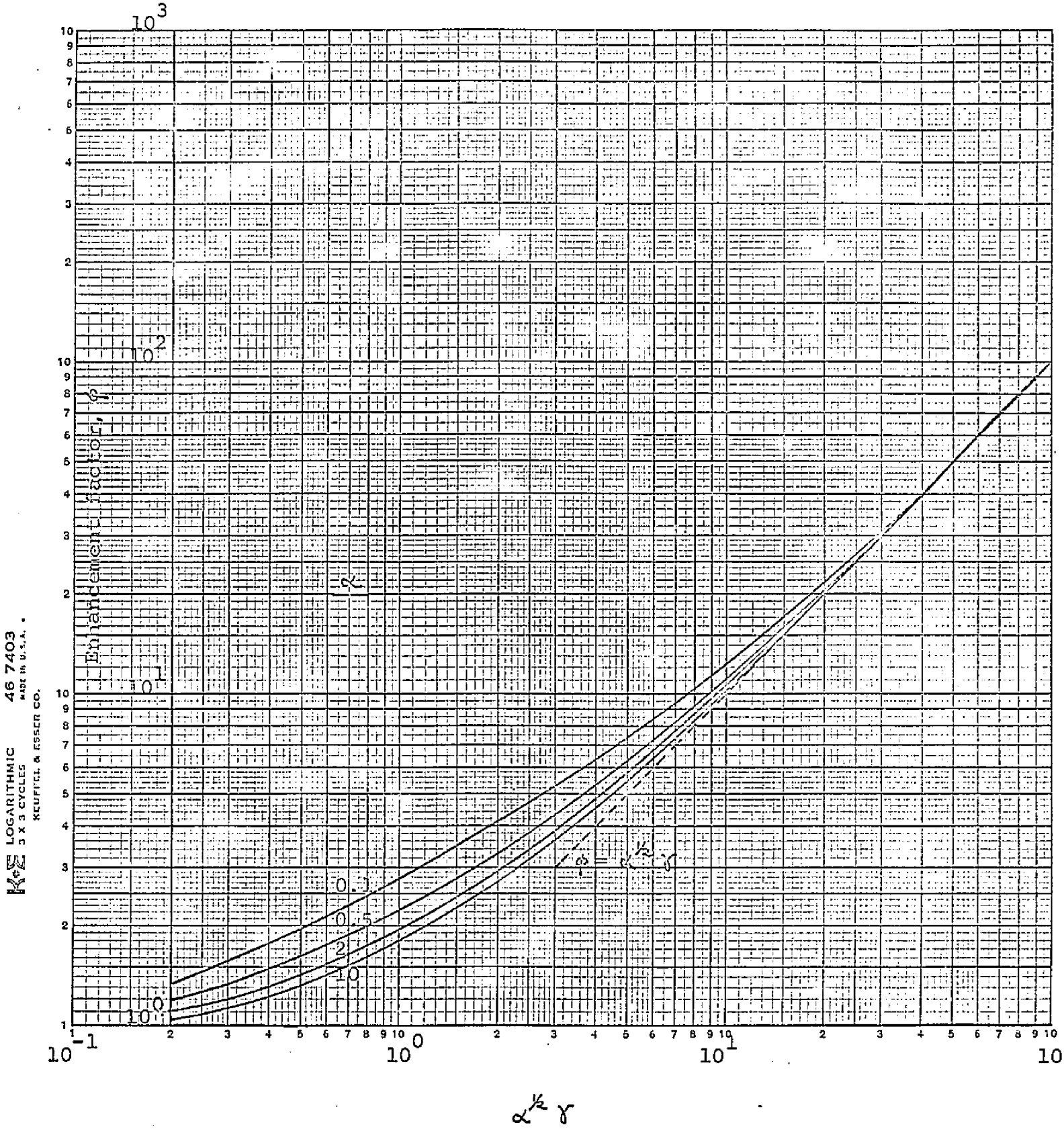

described in the previous paragraphs are clearly shown by these figures. The figures also show that the enhancement factor approaches an asymptotic line $\phi = \alpha^n \gamma$ and the variables α and γ can be combined together as a single variable. These asymptotic lines are those given by equations (IV-92), (IV-145), and (IV-119) for the case of $\xi_{AR} \rightarrow 0$. It is interesting to note that at large values of α, smaller values of $\alpha^n \gamma$ are required to reach the asymptotic line for the case of a very concentrated reagent solution.

Figure 34 shows ϕ/γ vs. α for the case of $\phi \longrightarrow \infty$ (or $\xi_{AR} \longrightarrow 0$). Four cases of different flow field patterns (velocity profiles) are shown here. These curves are obtained from equations (IV-145) and (IV-162). The slope of ϕ/γ vs. α in this figure is given, in general, as n. For the case of mass transfer into a stagnant fluid, n = 1. For the case of mass transfer from a solid sphere into a fluid flowing past it, n =2/3. For the case of mass transfer from a gas bubble into a liquid flowing past it, n = ½. For the case of mass transfer from a liquid drop into another immiscible fluid flowing past it, n is, in general, a function of F and is also somewhat dependent on α. However, for $\alpha \geq 1$, n is a function of only F and as shown in the figure, n is approximately equal to 0.596 for F = 1. In fact, for liquid drops, the value of n varies from ½ for F = 0 (special case of gas bubbles) to 2/3 for F = ∞ (special case of solid spheres).

It is interesting to note that this study covers the range from n = ½ to n =2/3. However, there is a gap between

Fig. 34: Comparison of enhancement factor, ϕ, for liquid flow around solid spheres, liquid drops and gas bubbles as $\xi_{AR} \rightarrow 0$

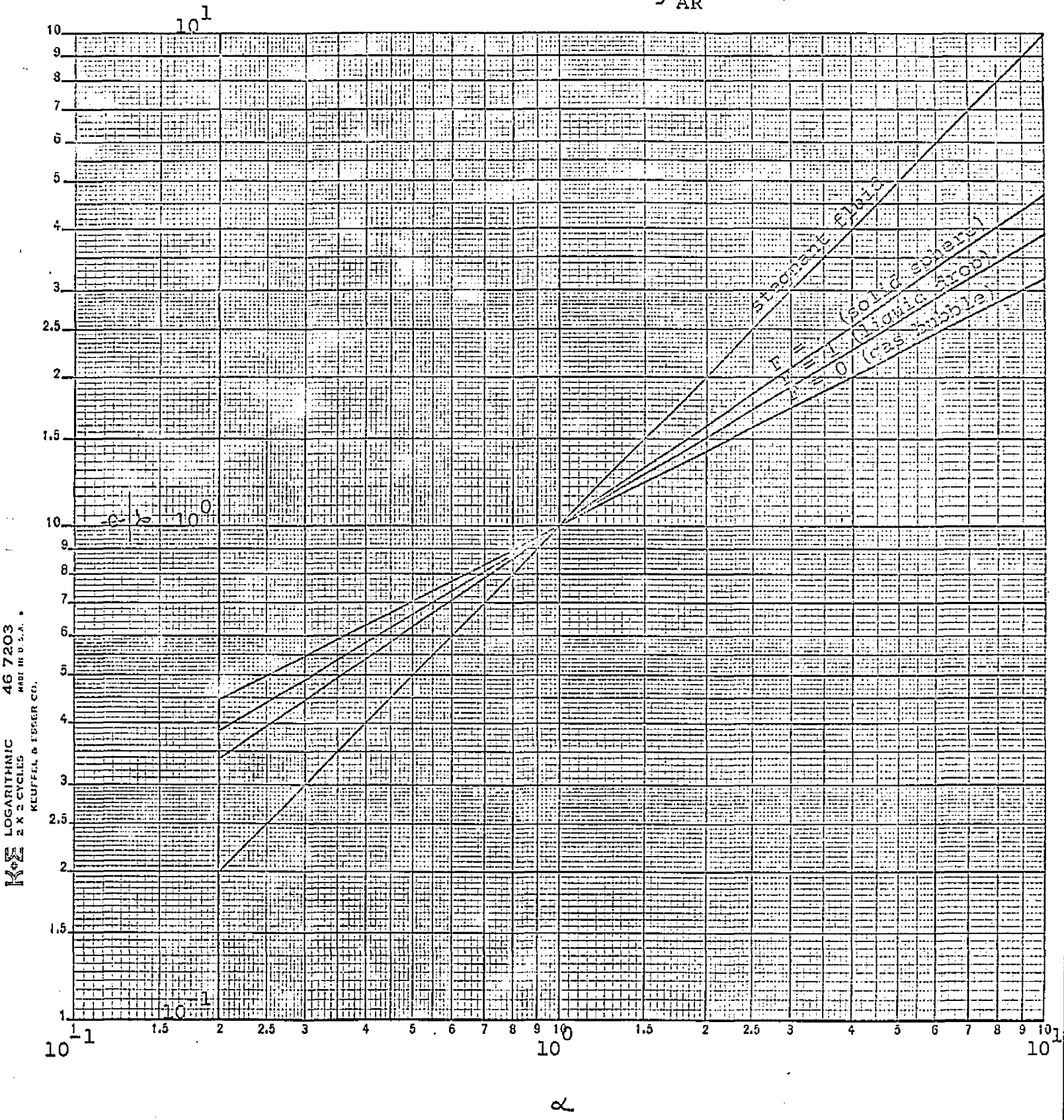

n = 2/3 and n = 1; i.e., flow past a solid sphere and no flow at all.

The effect of diffusion controlled reactions on mass transfer rates proposed by Sherwood and Pigford (72) based on film theory is given as

$$\phi = 1 + \alpha \gamma \qquad \text{(IV-175)}$$

which is exactly identical with one of the specific models in this study, i.e., the case of a stagnat fluid.

Peaceman (59) presented an equation for the reaction factor based on penetration theory as

$$\phi = 1 + \alpha^{1/2} \gamma \qquad \text{(IV-176)}$$

which agrees very well (for high enhancement factors) with the model in this study for the special case of gas bubbles. A comparison with Peaceman's equation of the enhancement factor, ϕ vs. bulk concentration γ with diffusivity ratio α as parameter is shown in Figure 35 for $\alpha = 4$. For the case of $\alpha = 1$, equation (IV-176) and equation (IV-115) are identical.

Sherwood and Ryan (73) and Meyerink and Friedlander (54) presented an equation for the enhancement factor as

$$\phi = (1 + \alpha\gamma)\alpha^{-p} \qquad \text{(IV-177)}$$

where p is obtained from the pure physical mass transfer correlation without chemical reaction

Fig. 35: Comparison of results of the gas bubble model with previous studies

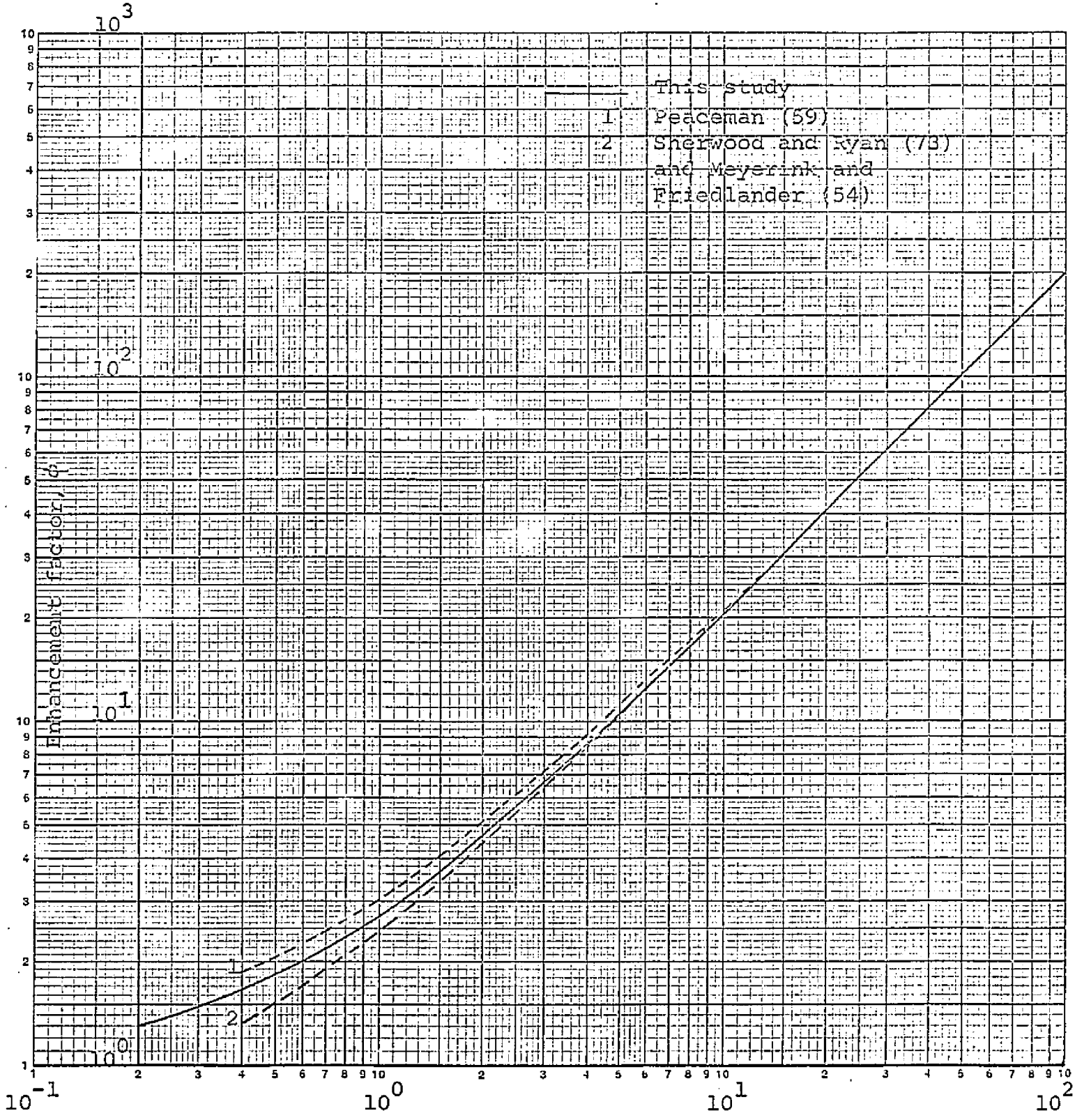

$$N_{Sh} = m N_{Sc}^{p} N_{Re}^{q} \qquad \text{(IV-178)}$$

For the case of mass transfer around solid spheres, p = 1/3, and equation (IV-177) agrees very well with equation (IV-92) for the case of high enhancement factor. For the case of mass transfer around gas bubbles, p = ½, and equation (IV-177) agrees very well for the case of high enhancement factor with equation (IV-119).

A comparison of the enhancement factor based on equation (IV-177) with p = ½ with our result, equation (IV-112), is also shown in Figure 35 for $\alpha = 4$.

A comparison of the enhancement factor of equation (IV-177) with p = 1/3 with the proposed model in this study, equation (IV-86), is shown in Figure 36. One should note that equation (IV-177) is not valid for $\gamma < \frac{\alpha^{4}-1}{\alpha}$, since ϕ will be less than unity for this case.

The Kishinevsky model (42) using a surface renewal mechanism with eddy diffusion rather than molecular diffusion controlling the transfer at the interface gave

$$\phi = 1 + \gamma \qquad \text{(IV-179)}$$

This model did not consider the effect of diffusion of both solute and reagent in the system. Therefore, we can say that this model is only valid for the special case of $\alpha = 1$ in this study for the rapid, irreversible second order chemical reaction.

Fig. 36: Comparison of results of the solid sphere model with previous studies

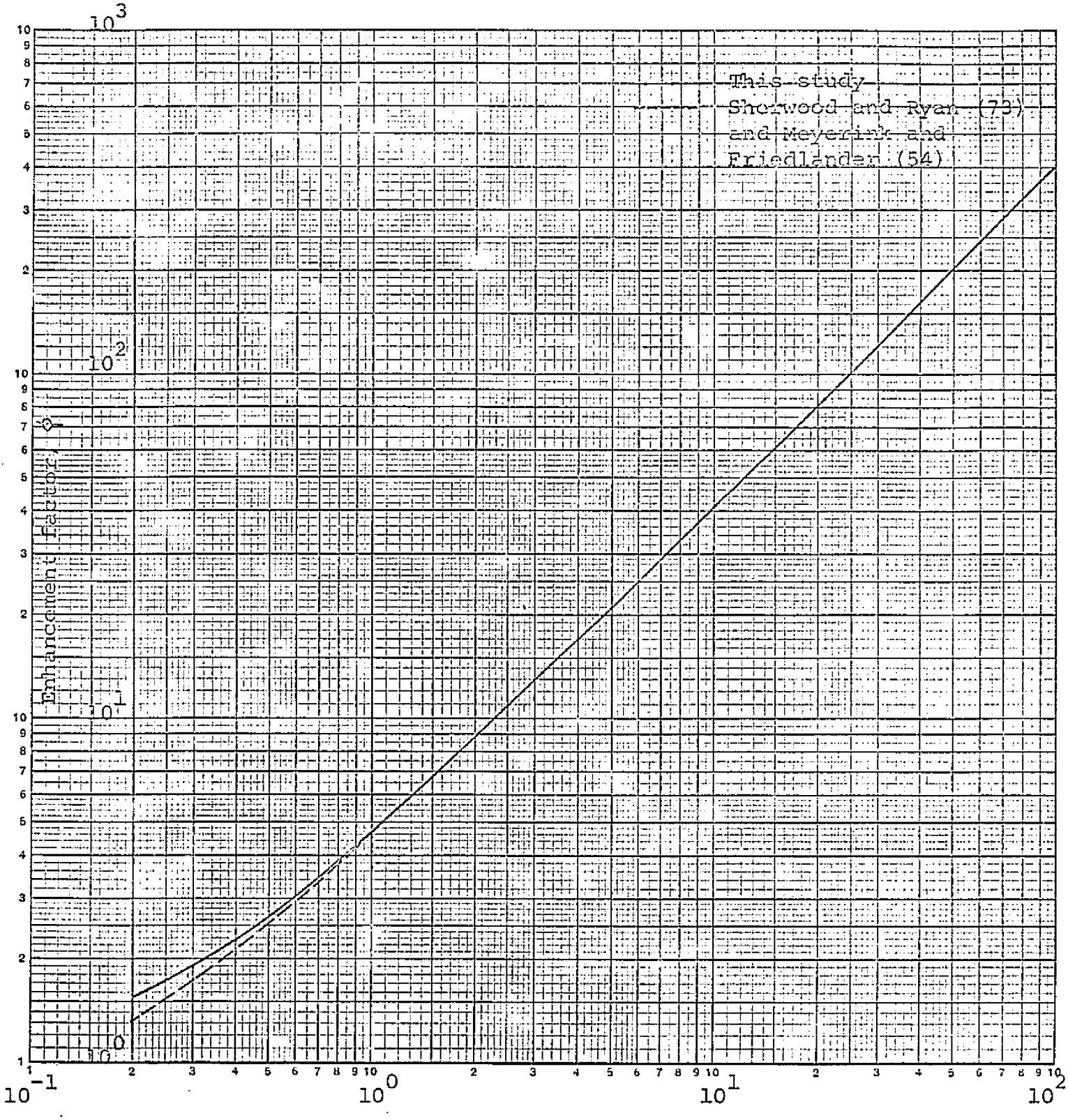

It is interesting to note that all of the equations presented by the different investigators are identical with the models presented here for the special case of $\alpha = 1$. For values of α other than unity, the models presented in previous studies can always be fit by the models presented in this study once the description of hydrodynamic behavior very near the surface of the interface of the continuous and discontinuous phases is known. A comparison of these different models with this study are given in Figure 37. For the case of $\alpha = 1$, all of these models and these presented in this study agree very well. However, as departs from unity, the results differ from one another.

In conclusion, the entire development of the reaction factor presented here agrees very well with previous studies in the literature with the added advantage that this study systematically considers the flow cases for very rapid moving interfaces (gas bubbles) to moderate moving interface (liquid drops) to rigid interface (solid spheres) and finally to the case of no flow at all (stagnant fluid). The results presented here are based on mass transfer rates across spherical particles. However, it is clear that these results can be applied to any two dimensional flow surface. Thus, the results should be valid not only for mass transfer from single spheres but also around multiparticle systems such as fluidized beds or packed beds as well as non-spherical interfaces as long as the flow pattern near the thin boundary layer around the interface is known.

Fig. 37: General comparison among different models of mass transfer with rapid second order reaction

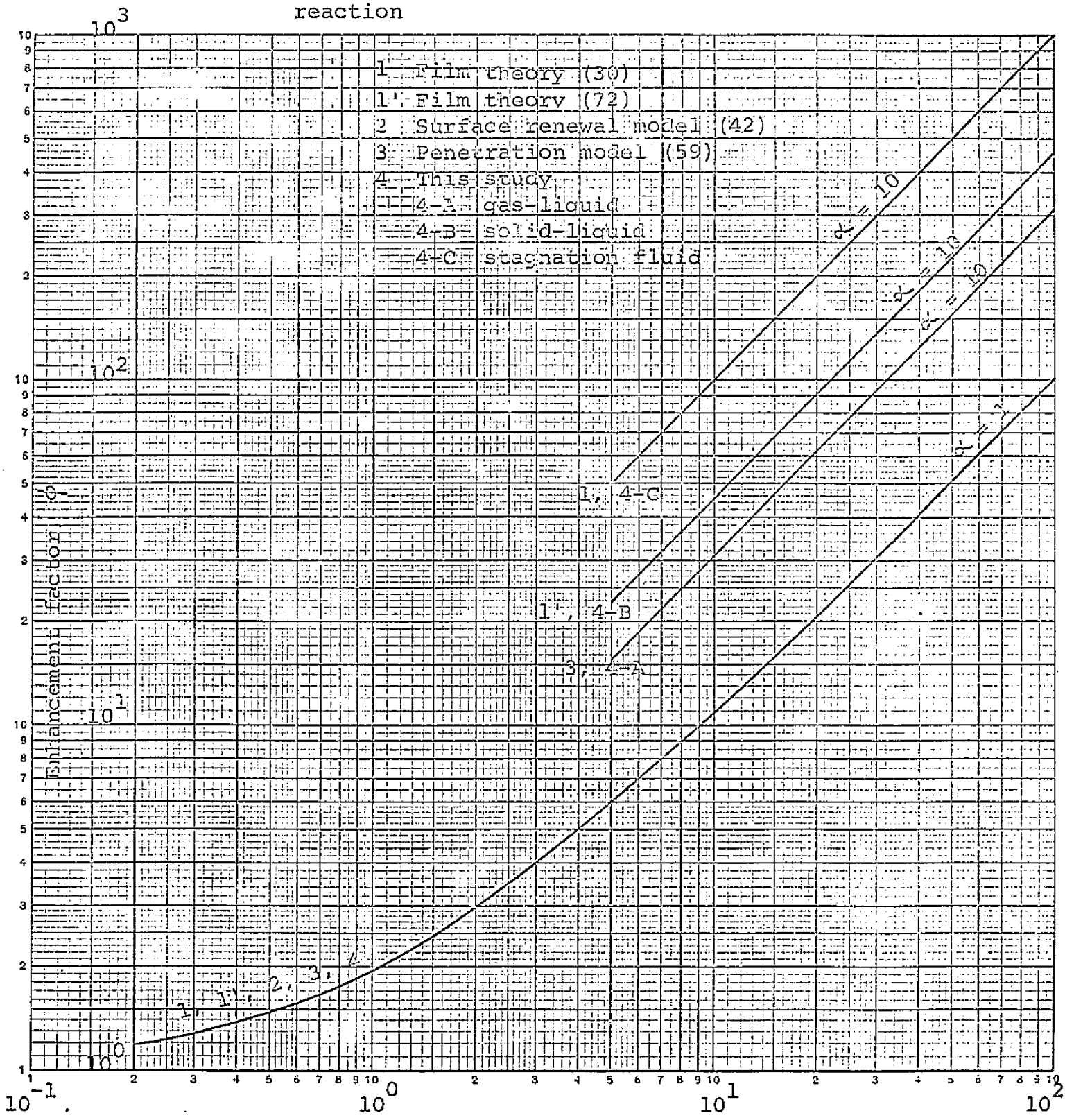

V. EXPERIMENTAL

1. Chemical Systems

No experimental work has been reported on both local and overall mass transfer rates with chemical reactions from single solid spheres. Recently, the effect of particle-to-particle interaction without chemical reaction using a small number of particles to simulate a multiparticle system such as packed or fluidized beds has been presented experimentally. To fully evaluate the mathematical models developed in this study, it is necessary to obtain some experimental data. Therefore, experiments were performed using either a single sphere or a two sphere system both with and without chemical reaction present.

The chemical system to be used in the experiments should be such that the effect of the reaction rate can be easily detected. Also this effect should be high enough to give a good comparison with the theoretical analysis in this study. The kinetics of the reaction system should be available or at least should be able to be determined so that complicated auxiliary kinetic studies should not be necessary. Of course, the system chosen should not corrode or otherwise react with the apparatus.

After a careful survey of the literature and a few preliminary experiments, it was decided that the system of Benzoic acid—dilute NaOH solution was to be used for this study. Some investigation of benzoic acid—dilute NaOH solution have been presented for mass transfer studies in agitated vessels (51,52)

and in flow over flat plate and inside of cylinders (54) but not for flow around single solid spheres or a small number of spheres. This reaction system chosen is a very rapid, irreversible, second order chemical reaction. The reaction can be assumed to occur instantaneously as soon as solute (benzoic acid) and reagent (NaOH) meet each other.

2. Apparatus and Operating Procedures

An apparatus suitable for this study was available in the Chemical Engineering Department of the City College of The City University of New York. The apparatus consisted of copper tubing, aluminum ball valves and overhead drum, a cast iron pump, stainless steel rotameters, and a 15.5 foot horizontal lucite water tunnel. In order to use the dilute NaOH solution, the aluminum ball valves were replaced by cast steel valves and the aluminum drum was replaced by a 50 gallon polyethylene tank. A Nikon model 6C optical comparator fitted with stage, micrometers, and a circular screen was used to obtain the local and overall mass transfer rates around the active sphere. In order to measure the mass transfer rate for the case of an inert sphere placed in back of an active sphere (in the flow direction), a ½ inch lucite sphere was drilled out so that the lucite sphere could be attached to the supporting rod of the active sphere. A completely detailed description of the apparatus and experimental operating procedures can be found in the thesis of Peltzman (60).

The overall rate of mass transfer from the surface of the particle to the flowing fluid can be determined from either the weight loss of the sphere or from measuring the change in volume of the sphere if the density is known. Similarly, the local rate of mass transfer from the sphere can be obtained from a local change in volume, which, in turn, is dependent on the local radium diminution. For small changes in radius, that is, small $\Delta r/r$ ratios, the assumption that the diminution varies linearly with time can be made. The overall or local

rate of mass transfer is related to the overall or local mass transfer coefficient as shown by equations (V-1) and (V-2).

$$N_{ao} = \frac{\Delta W_o}{\Delta t} = \frac{\Delta V_o \cdot \rho_s}{\Delta t} = k_o A_o (C^* - C_o) \qquad \text{(V-1)}$$

$$N_{al} = \frac{\Delta W_l}{\Delta t} = \frac{\Delta V_l \cdot \rho_s}{\Delta t} = k_l A_l (C^* - C_o) \qquad \text{(V-2)}$$

Thus, by measuring the initial and final radius profile over a known interval of mass transfer time Δt, the local or overall mass transfer coefficient can be computed, for a known concentration gradient $(C^* - C_o)$ from an integrated overall or local volume change. The size of the local volume element, V_l was chosen as a 20-degrees sector in the plane of measurement around the sphere.

The overall or local mass transfer coefficient is conveniently expressed in terms of the dimensionless Sherwood number as

$$N_{sh_o} = \frac{2 r_{sar} k_o}{\mathscr{D} \rho_f} \qquad \text{(V-3)}$$

and

$$N_{sh_l} = \frac{2 r_l k_l}{\mathscr{D} \rho_f} \qquad \text{(V-4)}$$

In the experiments performed in this study the bulk fluid had a negligible concentration of the dissolving solute. Thus, the concentration gradient $(C^* - C_o)$ was simply C^*, the equilibrium solubility of the active sphere material in water at the

temperature of each run. The diffusion coefficient, $\mathcal{D}$, as well as the equilibrium solubility, C*, for benzoic acid were determined as functions of run temperature from data available in the literature (60,62,76). These data in the temperature range of interest are given in Appendix I.

3. Results and Discussion

The primary interest of the experimental investigation was to study of the effect of particle-to-particle interaction for two spheres placed one behind the other in the direction of flow and the effect of very rapid chemical reaction on the mass transfer rate. Nevertheless, experiments were performed to obtain the mass transfer rate around a single sphere without chemical reaction in order to establish the reliability of the experimental techniques by comparing the results obtained in the present study with the results of Peltzman and Pfeffer. The single sphere results were also used as a basis for obtaining the enhancement factor correlation for the case of mass transfer with chemical reaction.

To observe the effect of particle-to-particle interaction for the two sphere system eight different configurations of active particle and inert particle arrangements were performed (i.e. series I - VIII). To observe the effects of the hydrodynamic flow patterns on rate of mass transfer with chemical reaction systems, three different configurations of active particle and inert particle were performed (i.e. Series I, II, VI). These configurations are shown in Figure 38. The particle Reynolds number was calculated using the surface average sphere diameter and the average centerline fluid velocity in the tube. A more detailed description of the data analysis is found in Appendix H

A. Pure physical mass transfer (no chemical reaction present)

i) Single spheres

The local mass transfer rate around a single sphere,

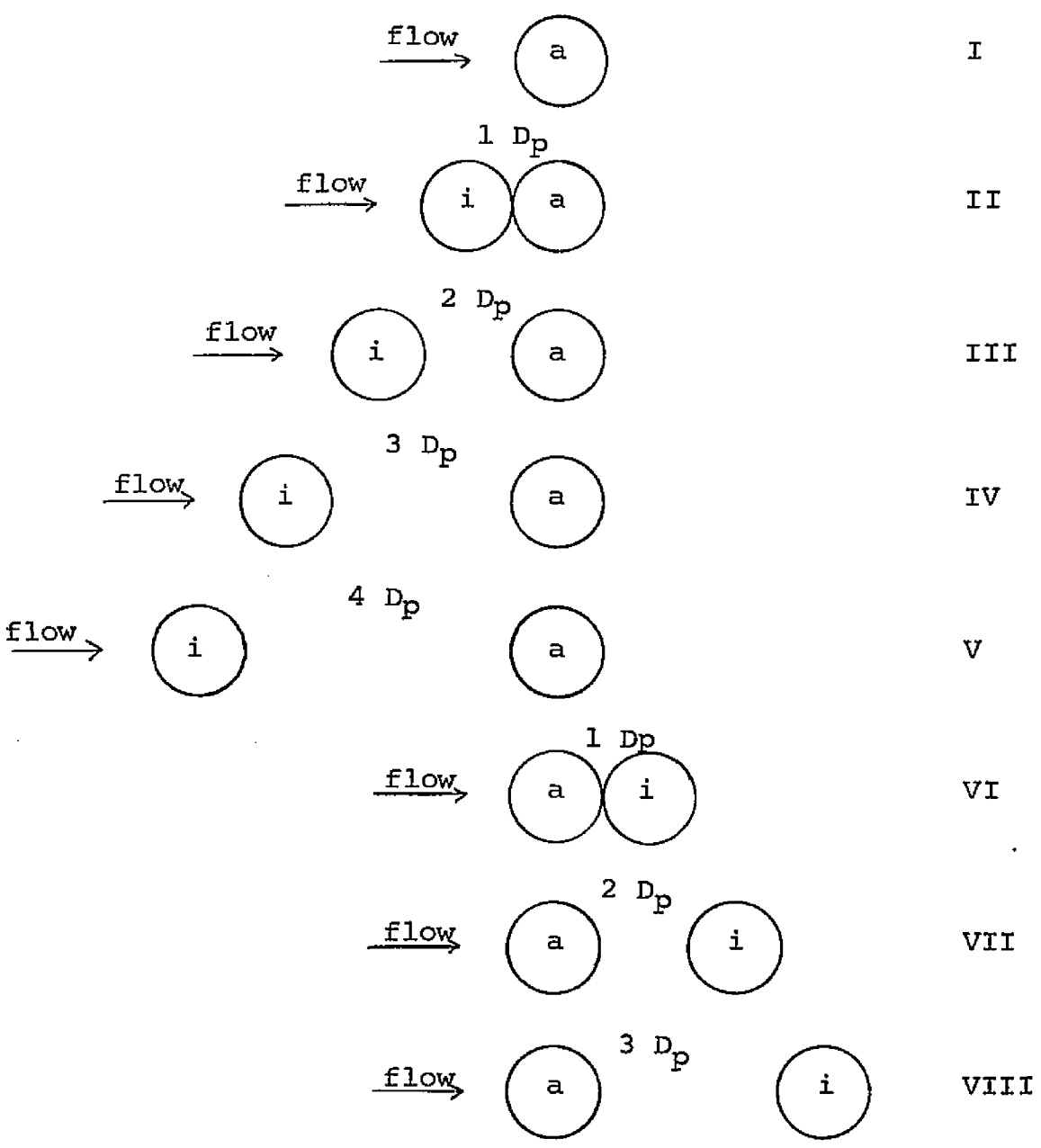

Fig. 38: Experimental configurations

plotted as the local Sherwood number vs. angle (θ) measured from the forward stagnation point on the surface of the sphere using the particle Reynolds number as aparameter are shown in Figure 39. These results agree very well with those presented by Peltzman and Pfeffer (61) and other investigators. The local mass transfer rates are known to decrease from a maximum at the front stagnation point to a minimum at a position corresponding to the ring of separation of the hydrodynamic boundary layer. Behind the flow separation point, there is a wake region of the flow and the local mass transfer rates increase to a second maximum at the rear stagnation point.

The overall mass transfer rates were calculated both directly from the overall weight loss of the test sphere and by numerical integration of the local mass transfer rates over the surface of the sphere. The agreement between these two values was always found to be within 15% and the average difference between N_{Sh_o} calculated by both methods was 4.73% (See Appendix K). The overall mass transfer rates presented here were based on overall weight loss. The comparison of these results with those presented by Peltzman and Pfeffer and other investigators are shown in Figures 40 and 41. Although the results reported here were somewhat lower than those of Peltzman and Pfeffer it is evident from the figures that the agreement with the earlier reported mass transfer data is within experimental error.

ii) Two spheres

Typical local mass transfer profiles obtained for series II through VIII are shown in figures 42 through 48 as N_{Sh_L} vs. the angle θ measured from the forward stagnation point with particle

Fig. 39: Local mass transfer rate around single spheres (Series I), without chemical reaction ($\gamma = 0$)

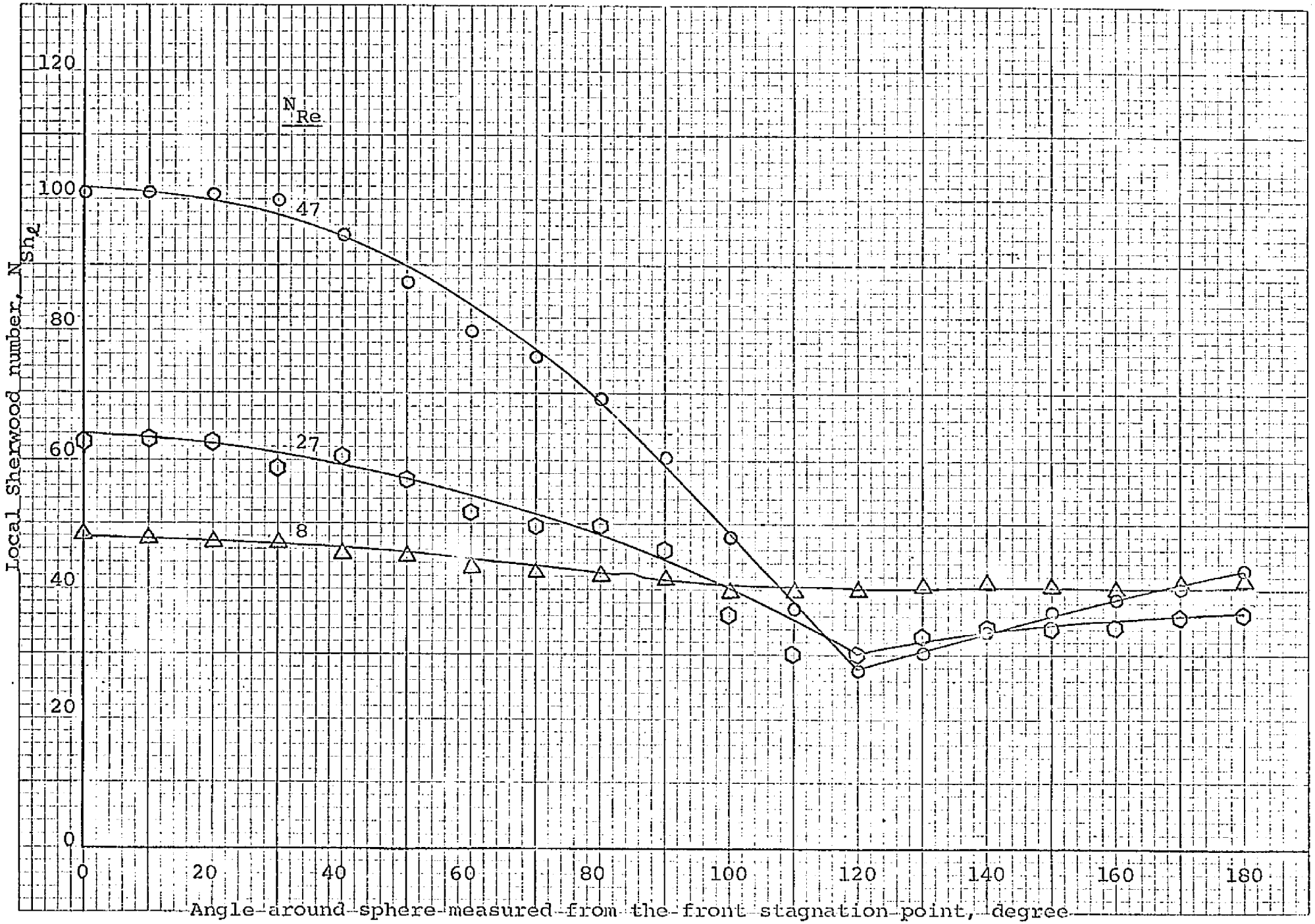

Fig. 40: Overall mass transfer rate around single spheres (series I) without chemical reaction ($\gamma = 0$), N_{Sh_o} vs. $N_{Sc}^{1/3} N_{Pe}^{1/2}$

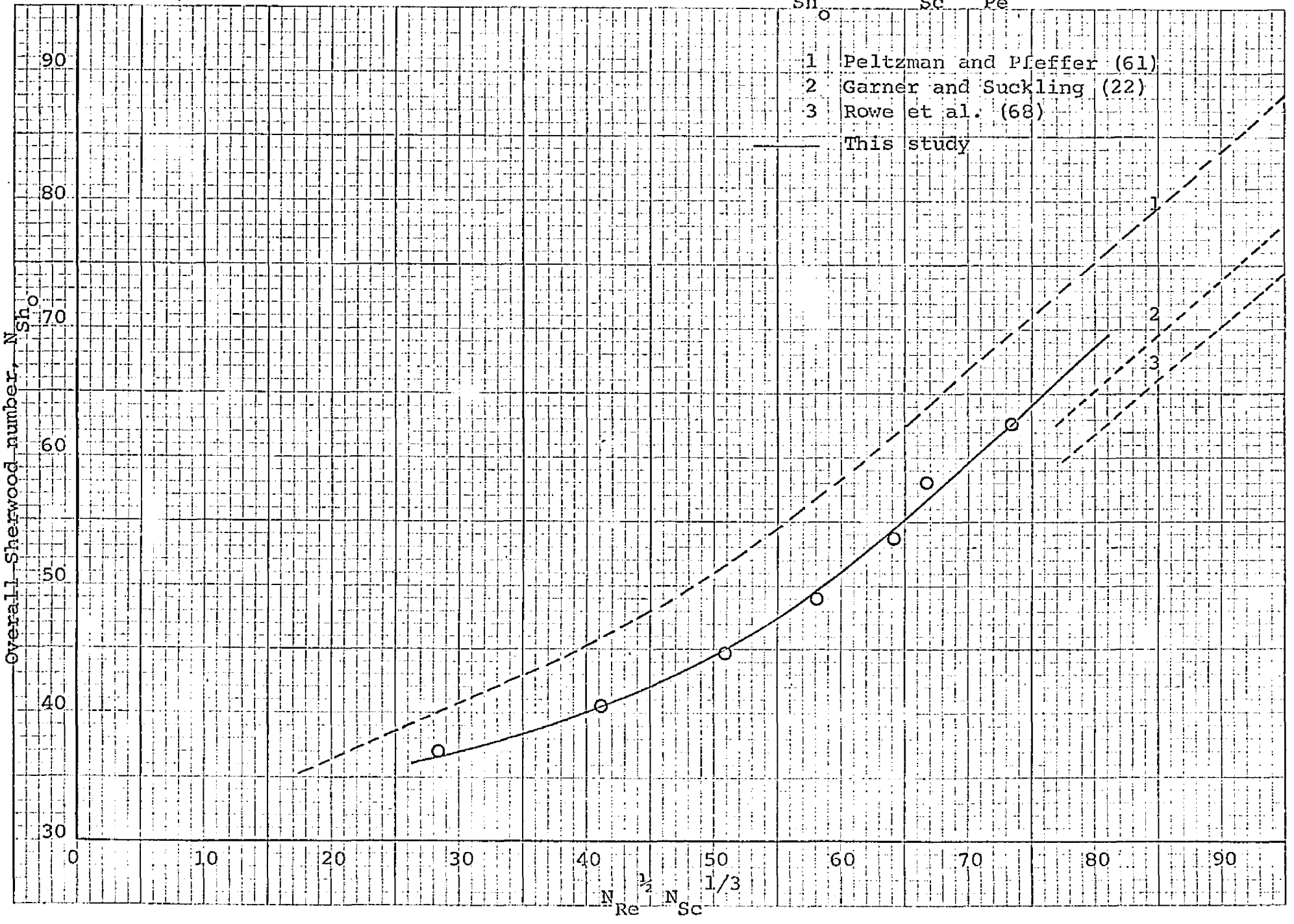

Fig. 41: Overall mass transfer around single spheres (series I) without chemical reaction ($\gamma = 0$), N_{Sh_o} vs. $N_{Pe}^{1/3}$

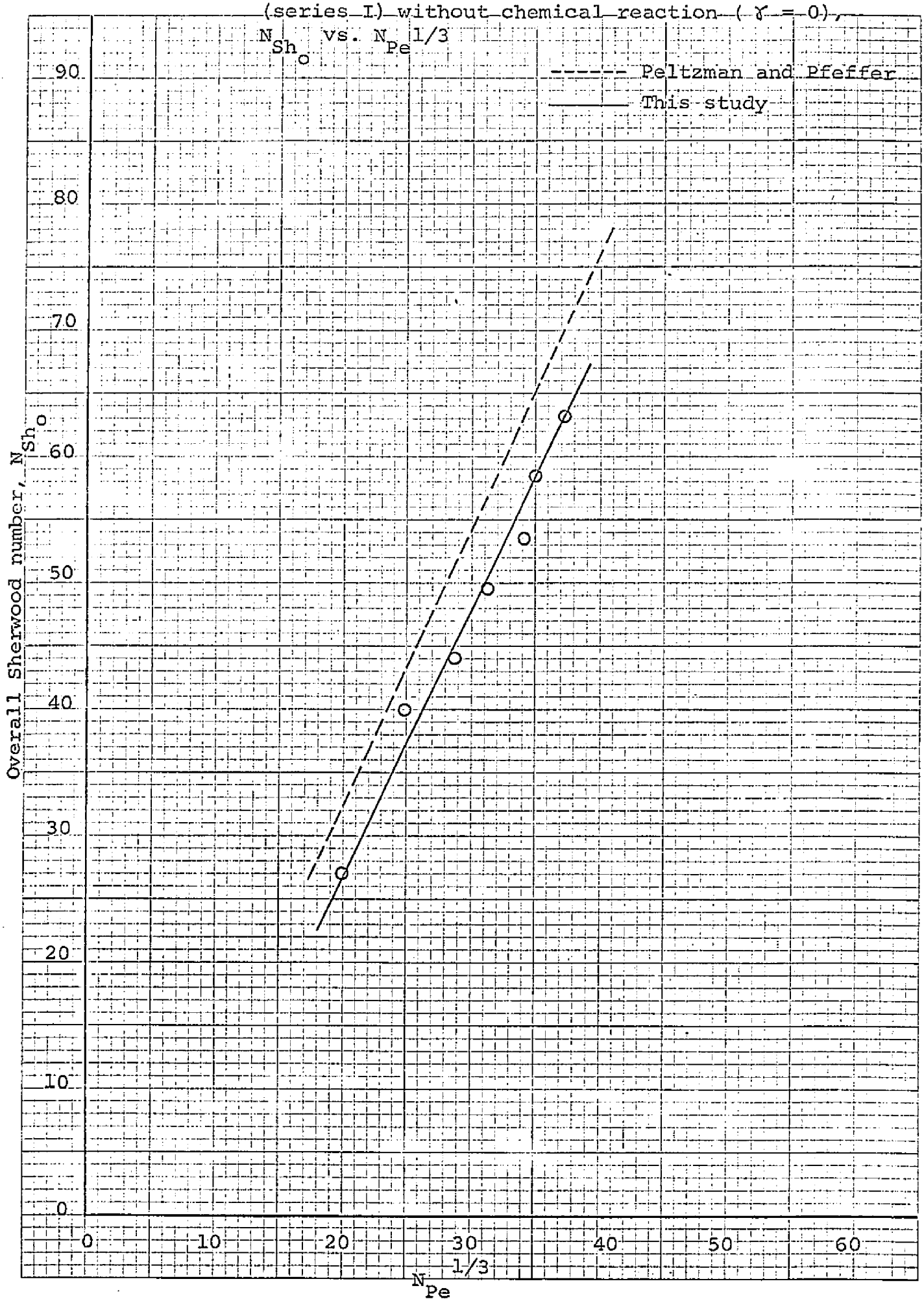

Fig. 42: Local mass transfer rate for series II, without chemical reaction ($\gamma = 0$)

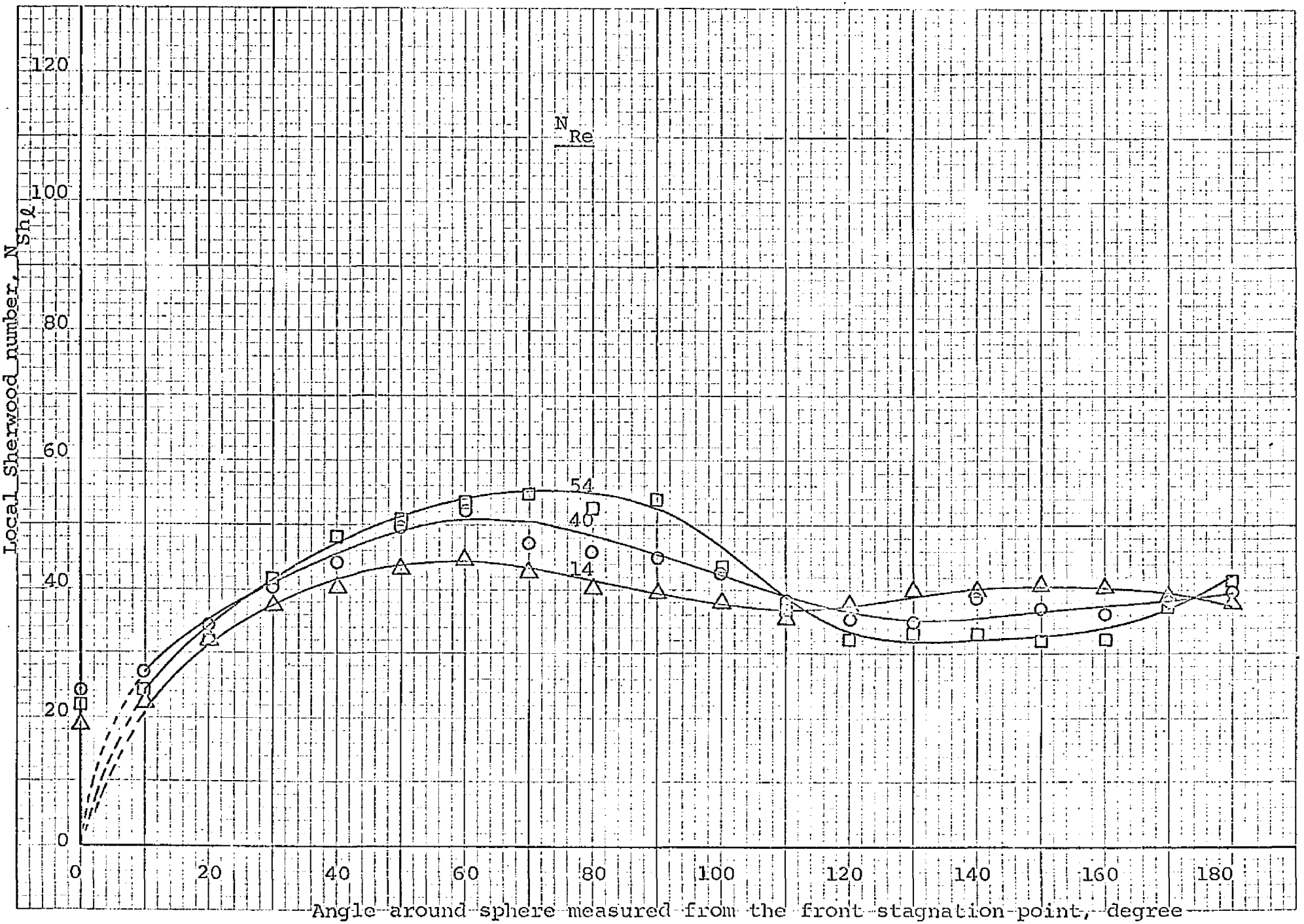

Fig. 43: Local mass transfer rate for series III, without chemical reaction ($\gamma = 0$)

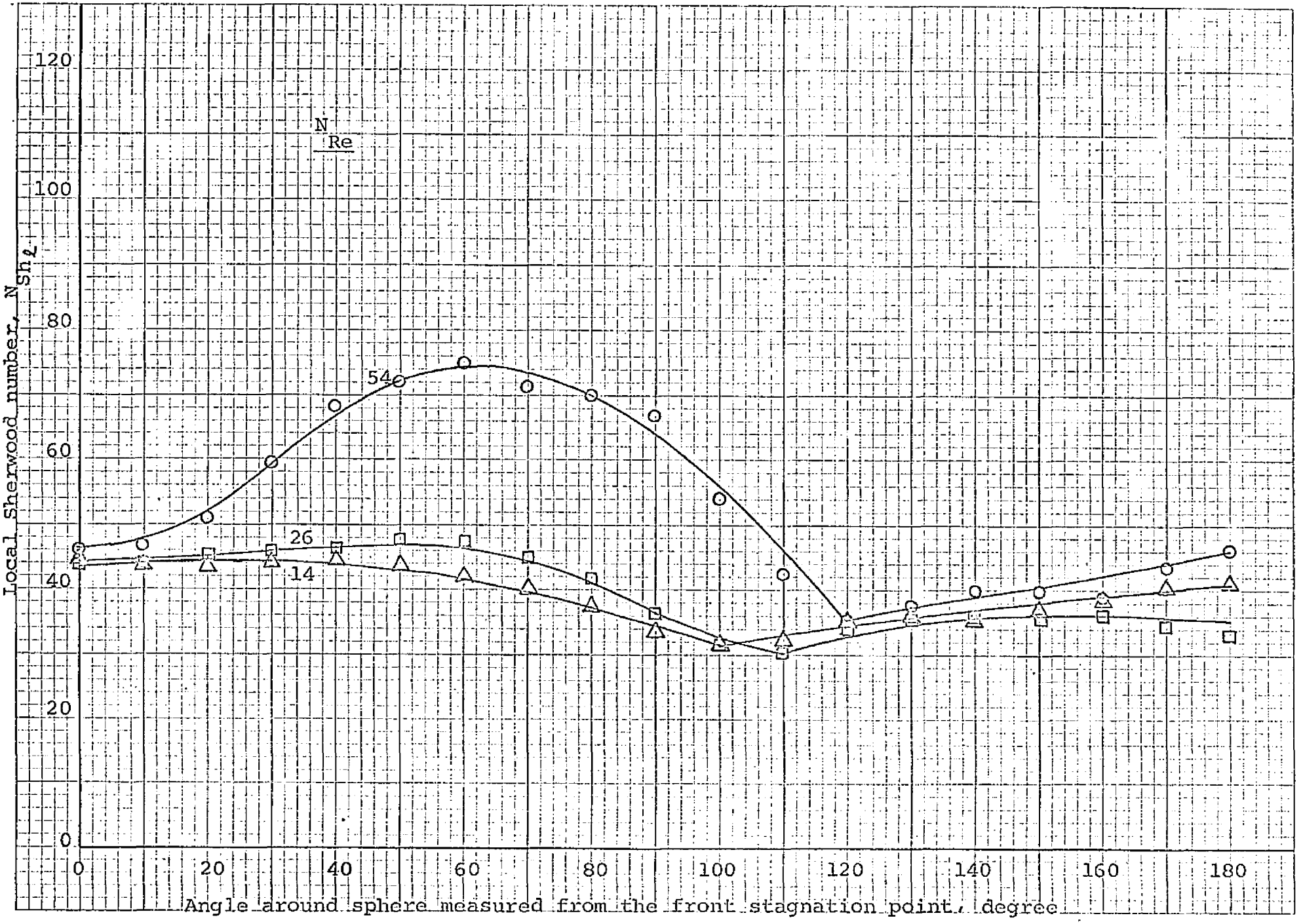

Fig. 44: Local mass transfer rate for series IV, without chemical reaction ($\gamma = 0$)

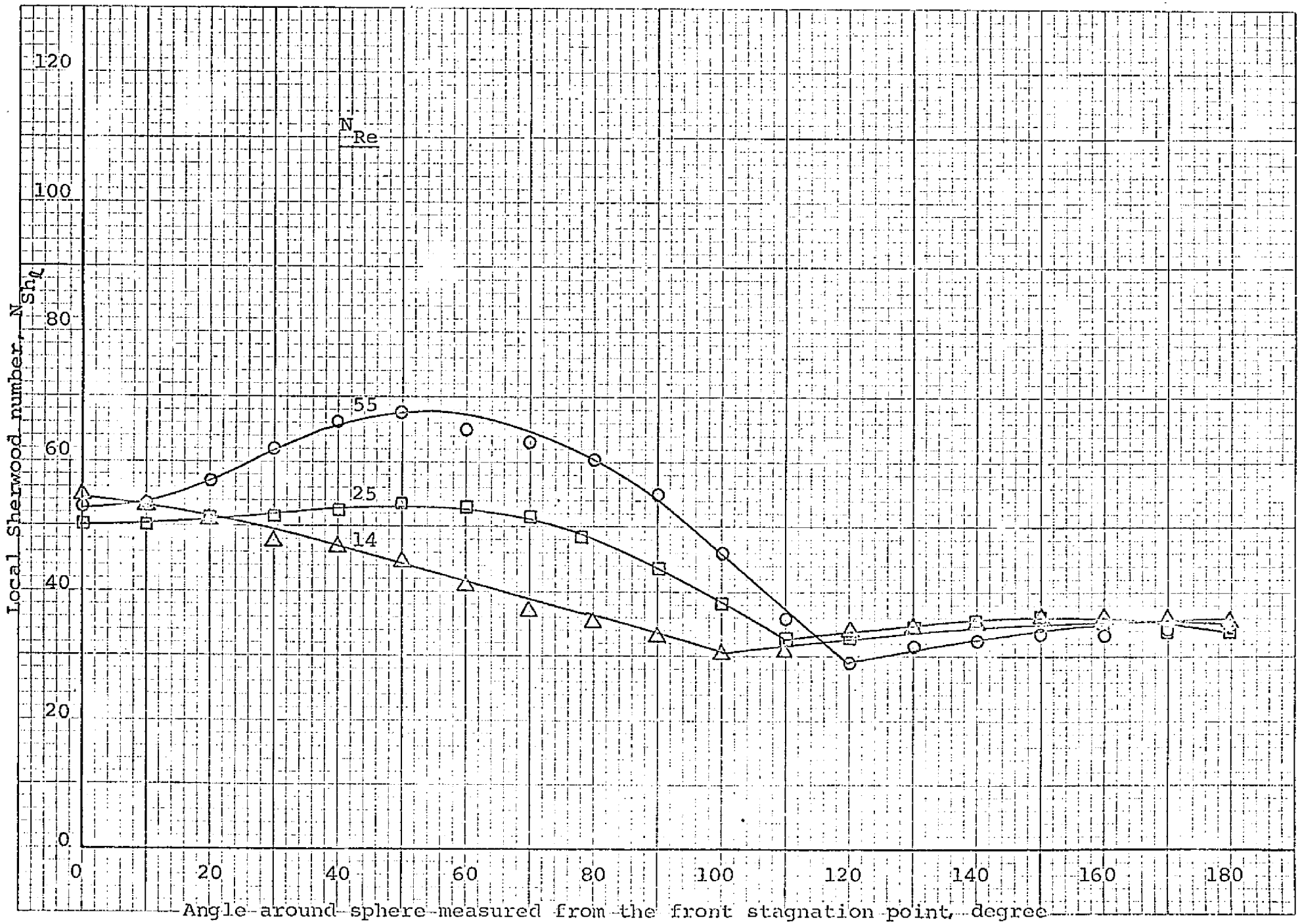

Fig. 45: Local mass transfer rate for series V, without chemical reaction ($\gamma = 0$)

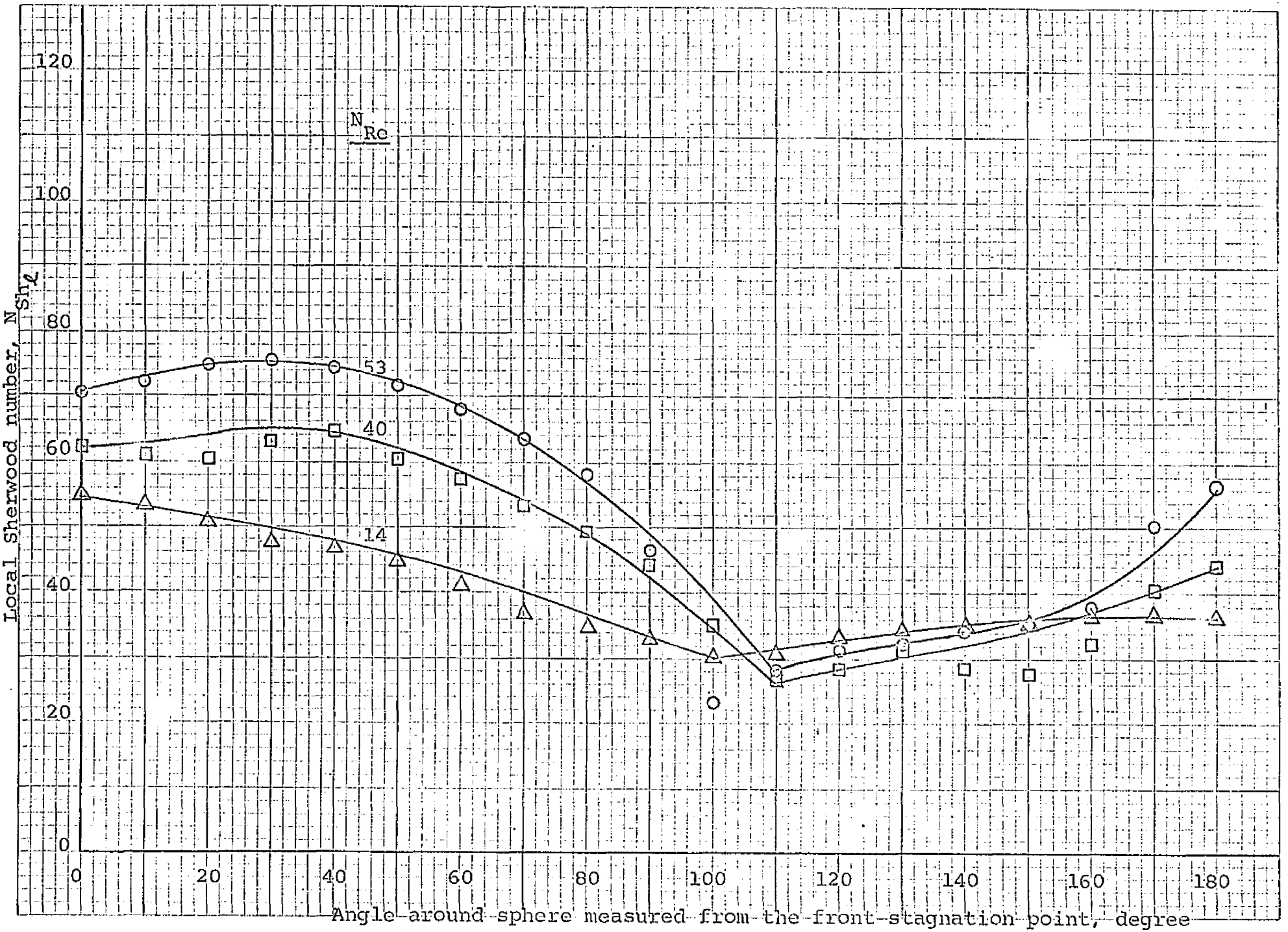

Fig. 46: Local mass transfer rate for series VI, without chemical reaction ($\gamma = 0$)

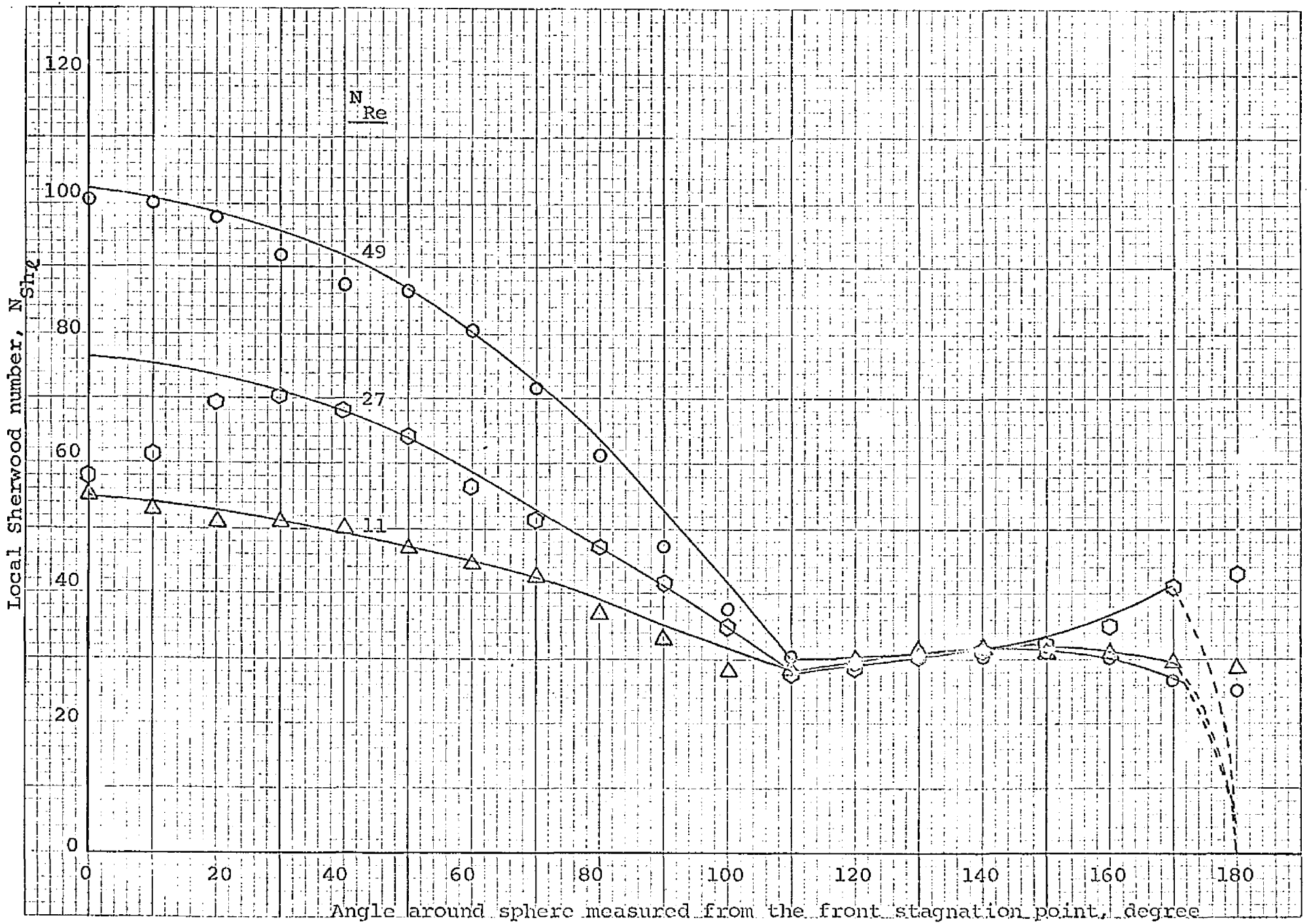

Fig. 47: Local mass transfer rate for Series VII, without chemical reaction ($\gamma = 0$)

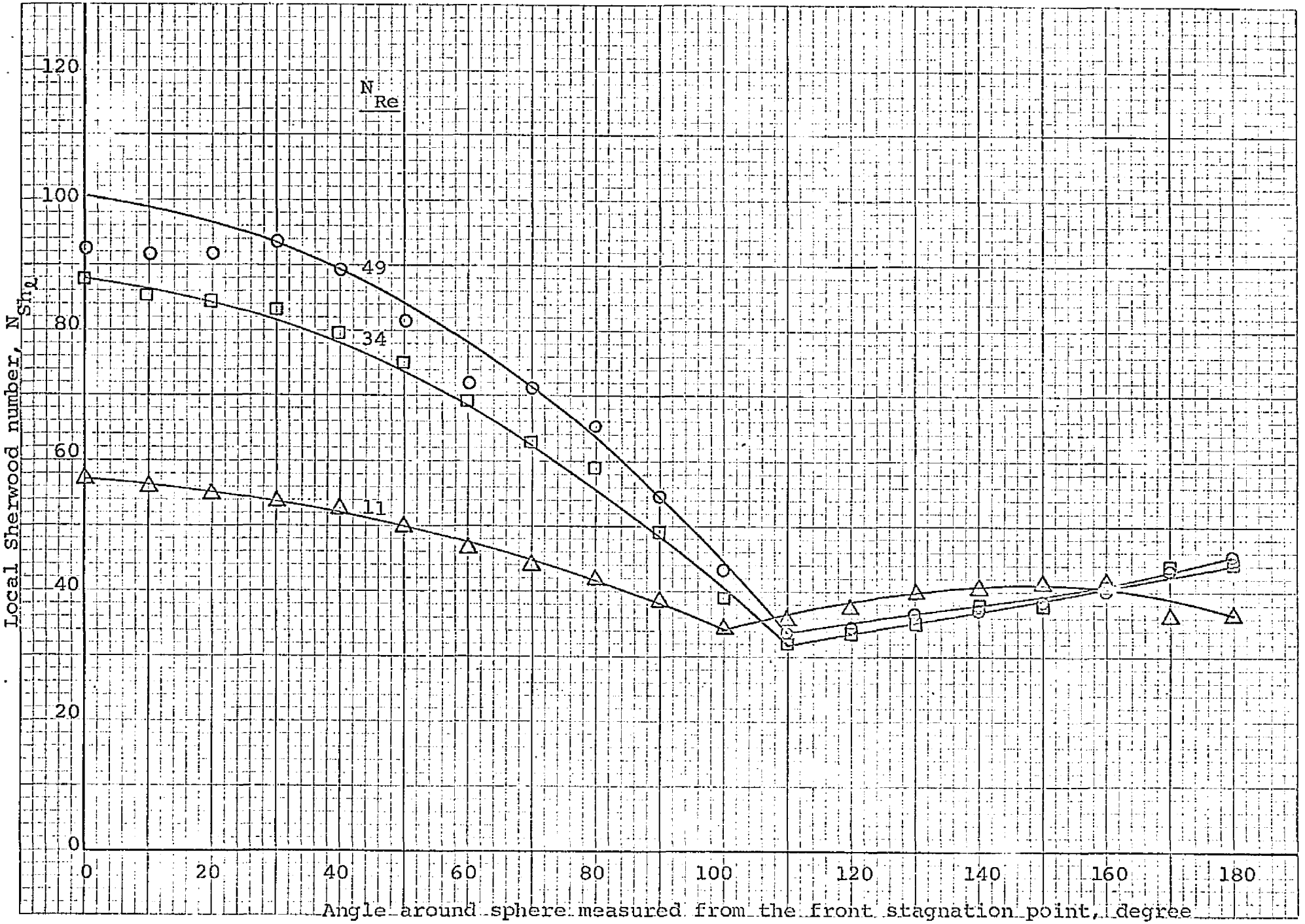

Fig. 48: Local mass transfer rate for Series VIII, without chemical reaction ($\gamma = 0$)

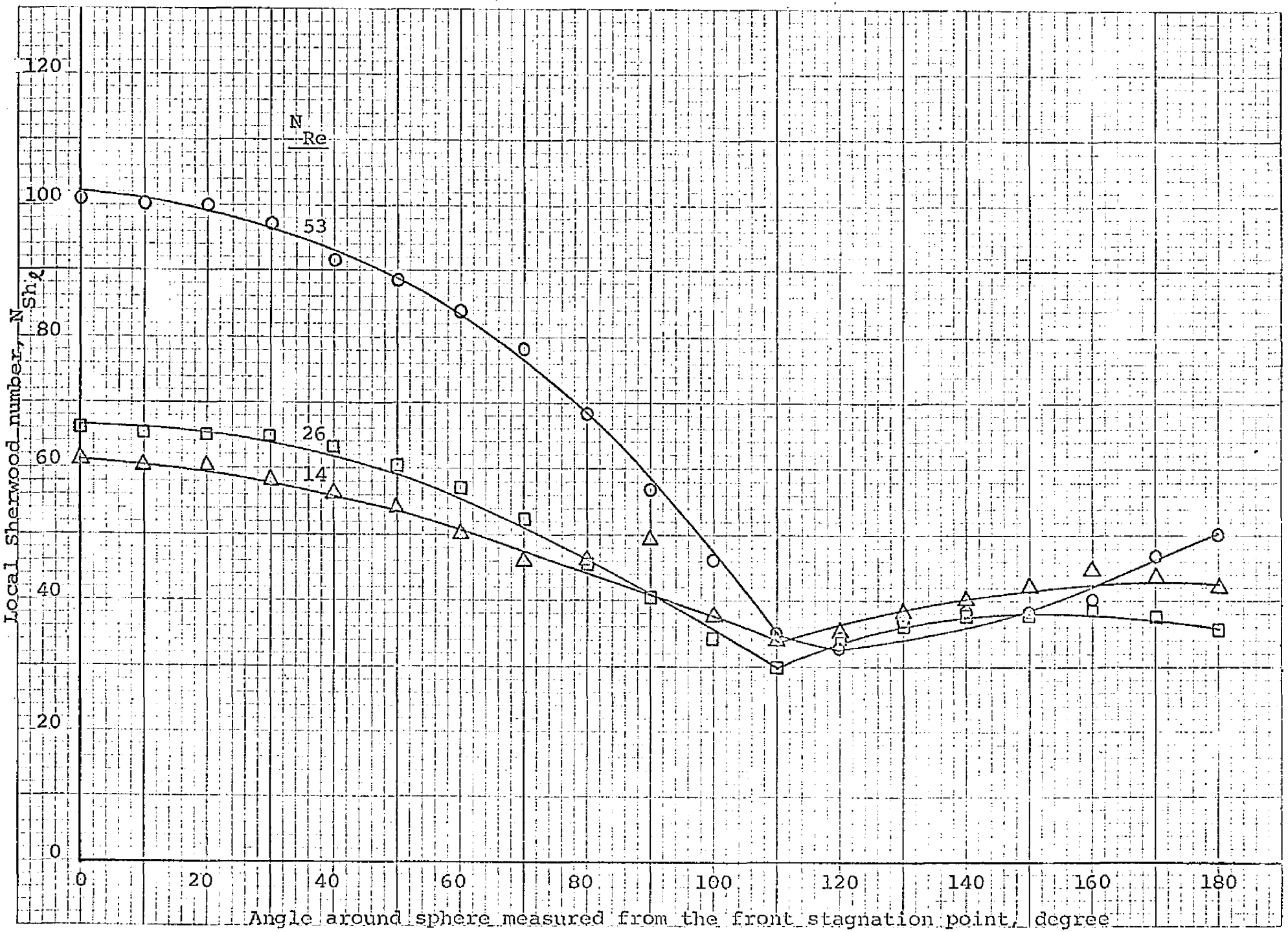

Reynolds number as a parameter. From the local mass transfer rates shown in these figures the following observations were made.

For the active sphere placed behind the inert one as in series II through V, the effects of particle-to-particle interaction on local mass transfer rate are quite obvious. When two spheres are very close to each other, a minimum transfer rate at the front stagnation point is found. The transfer rate then increases due to the exposure to the flow of fluid (forced convection term) and then decreases to a minimum again at the location of the separation ring. In the wake area the transfer rate again increases up to the rear stagnation point.

At Reynolds numbers large enough to cause a flow separation around the rear stagnation point, there are always two maximum transfer rates. The first one appears in the forward flow region and the second one appears in the wake flow region. As the particle Reynolds number decreases at fixed particle-to-particle distance between spheres these two maximum point locations shift closer to the front stagnation point. At fixed Reynolds number, as the distance between the two particles increase, the location of the first maximum point shifts closer to the front stagnation point but the location of second maximum point shifts closer to the rear stagnation point. Similar experimental data for series II and III have been presented by Peltzman and Pfeffer but they were not able to observe some of these phenomena. A qualitative comparison of local mass transfer rates for series I, II, III, IV and V at a particle Reynolds number of about 50 is shown in Figure 49.

Fig. 49: Comparison of local mass transfer profiles, Series I, II, III, IV, and V at N_{Re} = 50, without chemical reaction (γ = 0)

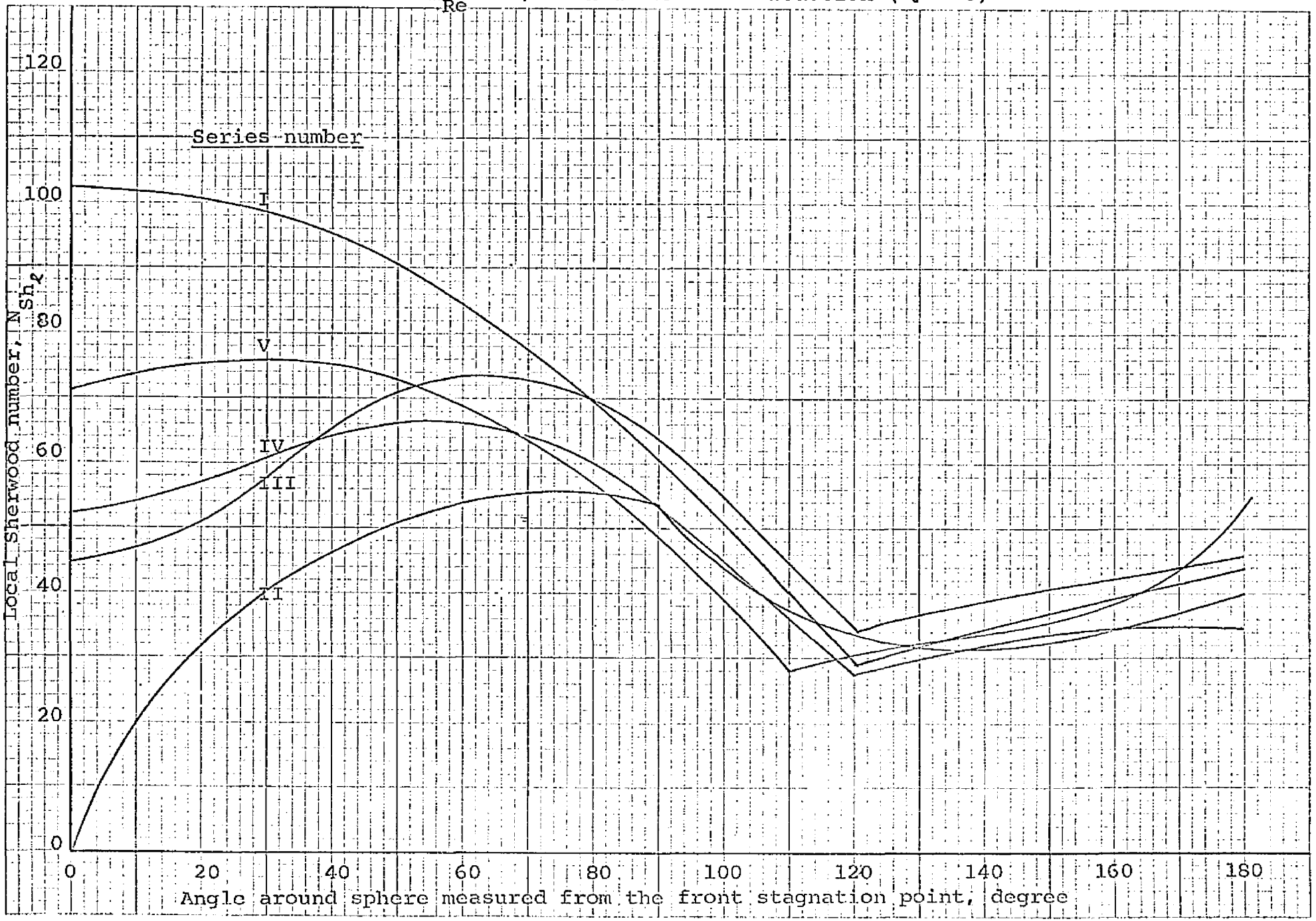

Around the rear stagnation point, the local mass transfer rates (for the inert sphere in front of the active sphere) behaves like that of a single sphere. Around the front stagnation point the mass transfer rate behaves similarly to that predicted in the numerical analysis of this study.

For the active sphere placed in front of the inert one as in series VI, VII and VIII, a maximum transfer rate at the front stagnation point was always found. The transfer rate then decreases to a minimum at the location of the separation ring; the mass transfer behavior essentially follows that of the single sphere. In the wake region the transfer rate increases up to another maximum point. The location of this second maximum point is strongly dependent on the particle-to-particle distance between two spheres and the Reynolds number. For the case of the two spheres touching one another, as in series VI, the maximum transfer rate is obtained at the rear stagnation point. Therefore, the second maximum point is always located somewhere in the wake region near the rear stagnation point.

As the separation between the two spheres increases the spheres have a smaller effect upon one another. For two spheres one or two particle diameters apart as in series VII or VIII, the second maximum transfer rate appears at the rear stagnation point for high Reynolds number flow. For low Reynolds number flow the transfer rate at the rear stagnation point is another minimum point and therefore the second maximum point is again located somewhere near the rear stagnation point in the wake region. The presence of the inert sphere also shifts the location of the flow separation point further away from the rear stagnation point.

A qualitative comparison of local mass transfer rates for series I, VI, VII and VIII at a particle Reynolds number of about 50 is shown in Figure 50. In the region around the front stagnation point the local transfer rate (with the inert sphere behind the active sphere) behaves like that around a single sphere. When the two spheres are far apart results similar to that for the single sphere are found over the entire surface of the active sphere. This qualitative comparison of the experimental data agrees with the predicted results given in the numerical analysis of the two sphere system presented earlier in this study.

A comparison of the overall mass transfer rates for series II through V with series I is shown in Figure 51 plotting N_{Sh_o} vs. $N_{Sc}^{1/3}N_{Re}^{1/2}$. This figure shows that at low Reynolds number the inert particle has a small effect on the overall mass transfer process. Similar results have been presented by Peltzman and Pfeffer. Figure (52) shows the effect of the spacing between the two spheres at two different values of the parameter $N_{Re}^{1/2}N_{Sc}^{1/3}$. This figure can only be qualitatively compared to the numerical results obtained for the creeping flow region given in Figure 14. Nevertheless, the behavior of the Sherwood number is quite similar.

A comparison of the overall mass transfer rates for series VI through VIII with series I is shown in Figure 53. These results are somewhat peculiar in that the overall Sherwood number does not follow a definite trend as the sphere spacing is increased from two spheres touching to two spheres separated by two particle diameters as was the case for the active sphere placed behind the inert sphere. Figure 54 shows

Fig. 50: Comparison of local mass transfer profiles, series I, VI, VII, and VIII at N_{Re} = 50, without chemical reaction ($\gamma = 0$)

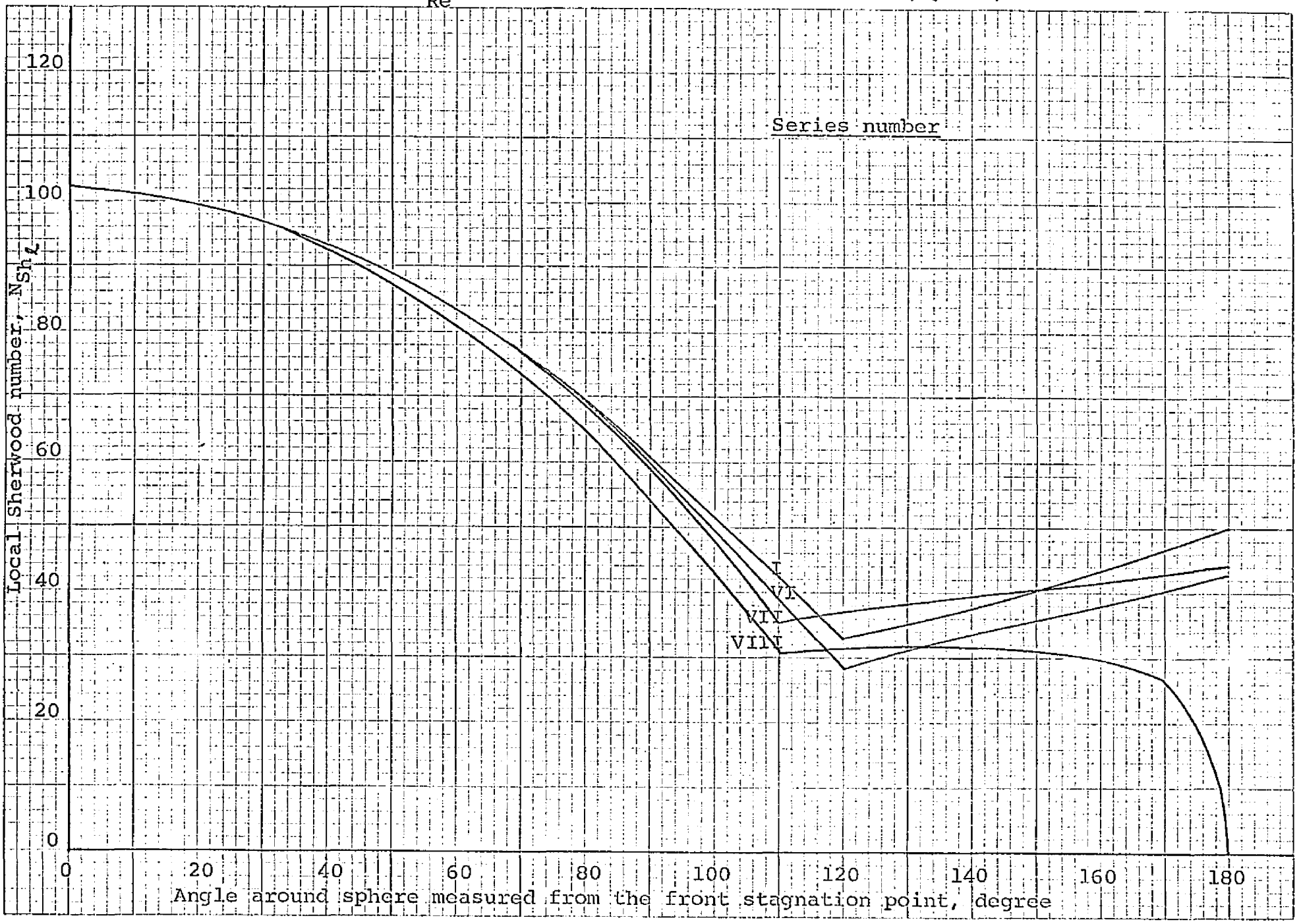

Fig. 51: Comparison of overall mass transfer rate, series I, II, III, IV, and V, without chemical reaction ($\gamma = 0$)

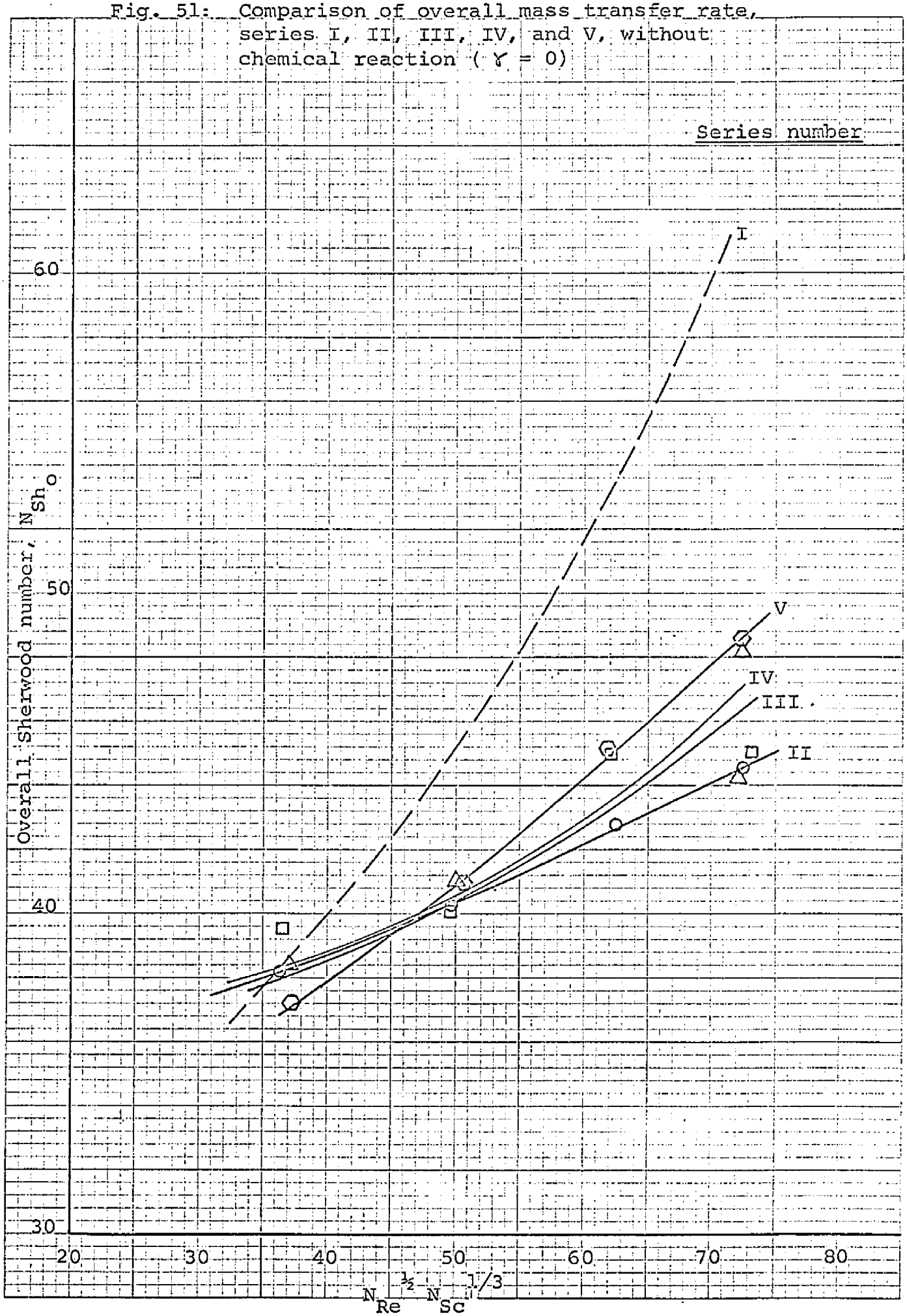

Fig. 52: Effect of particle-to-particle spacing on the overall mass transfer rate around an active sphere placed behind an inert sphere ($Y_o < 0$)

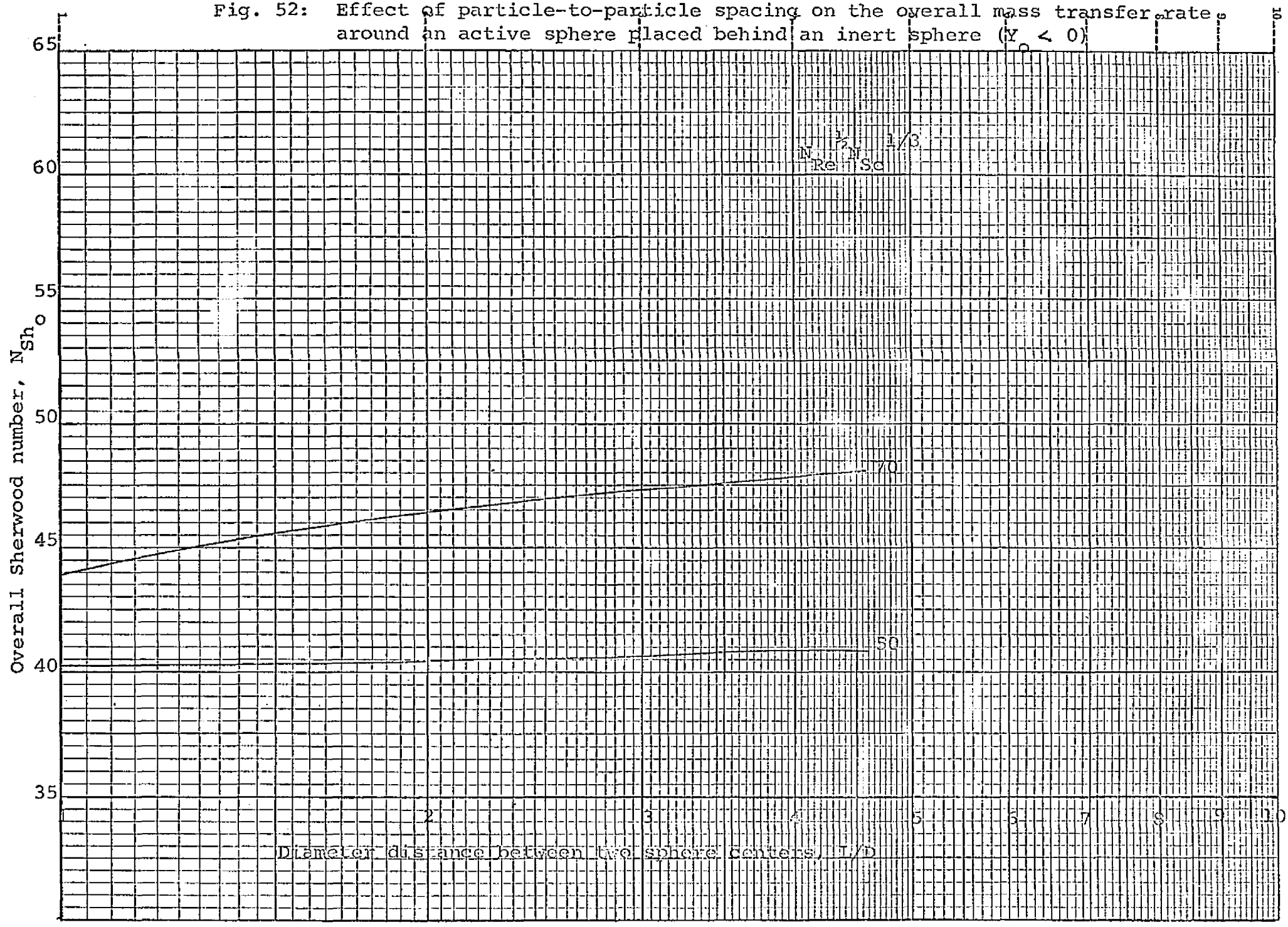

Fig. 53: Comparison of overall mass transfer rate, series I, VI, VII, and VIII, without chemical reaction ($\gamma = 0$)

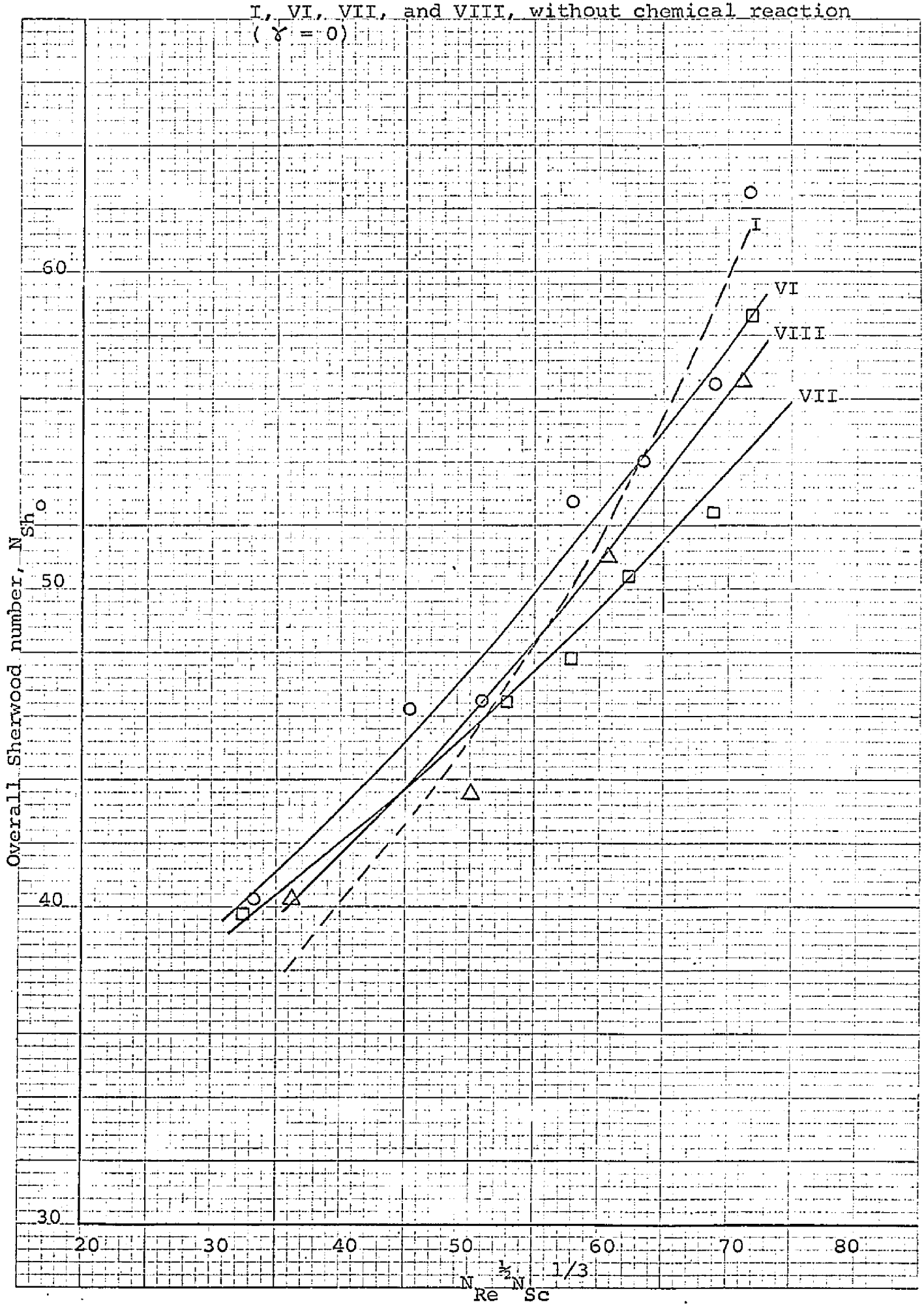

Fig. 54: Effect of particle-to-particle spacing on the overall mass transfer around an active sphere placed in front of an inert sphere ($Y_0 > 0$)

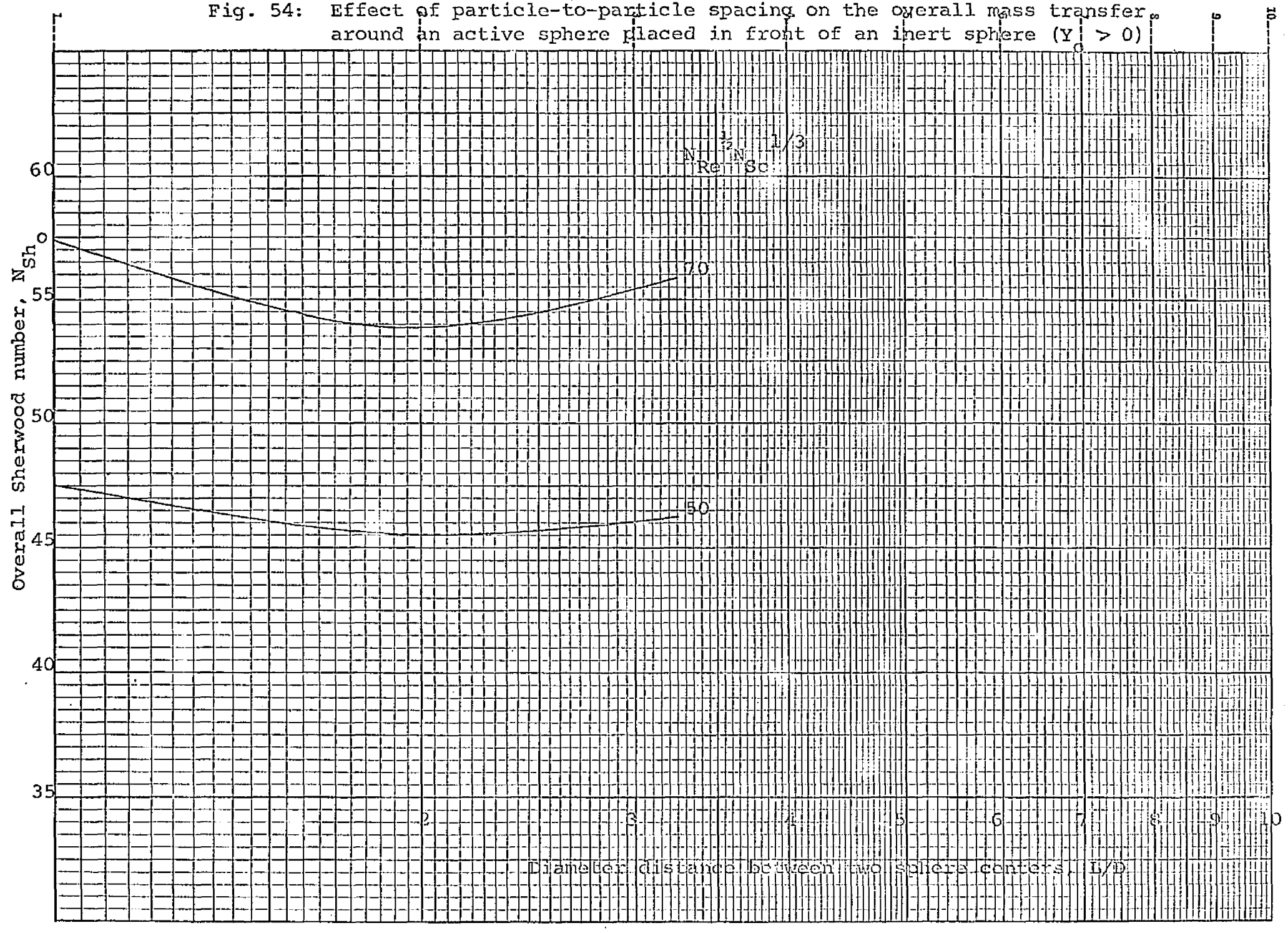

the unusual effect of particle spacing on the Sherwood number for two different values of the parameter $N_{Re}^{\frac{1}{2}} N_{Sc}^{1/3}$. The fact that these curves do not agree even qualitatively with the numerical results obtained for the creeping flow region can not be presently explained.

B. Mass transfer with rapid chemical reaction

The local mass transfer rates around a single sphere, plotted as the local Sherwood number vs. angle (θ) measured from the forward stagnation point on the surface of the sphere using particle Reynolds number as a parameter are shown in Figures 55, 56 and 57 for different values of the concentration ratio of reagent to solute γ. The ratio of the Schmidt number of the solute to that of the reagent, α, was kept constant in all of the experiments at a value of 3.2. As in the case of mass transfer without chemical reaction, these local mass transfer rates decrease from a maximum at the front stagnation point to a minimum at a position somewhere in the wake region. The local transfer rates then increase to a second maximum at the rear stagnation point. At low Reynolds number, this second maximum point shifts closer to the rear stagnation point (as in the case of mass transfer without reaction) and finally to the rear stagnation point itself. A study of these figures indicates that the minimum transfer rates for the concentration rates used in this study were located somewhere around 150° measured from forward stagnation point. This result is quite different for pure physical mass transfer where the minimum mass transfer points were found around 110-120 drgrees from the front stagnation point. Since there are no previous data of this kind presented in the literature, no comparison

Fig. 55: Local mass transfer rate around single spheres (series I), with chemical reaction (γ = 3.22)

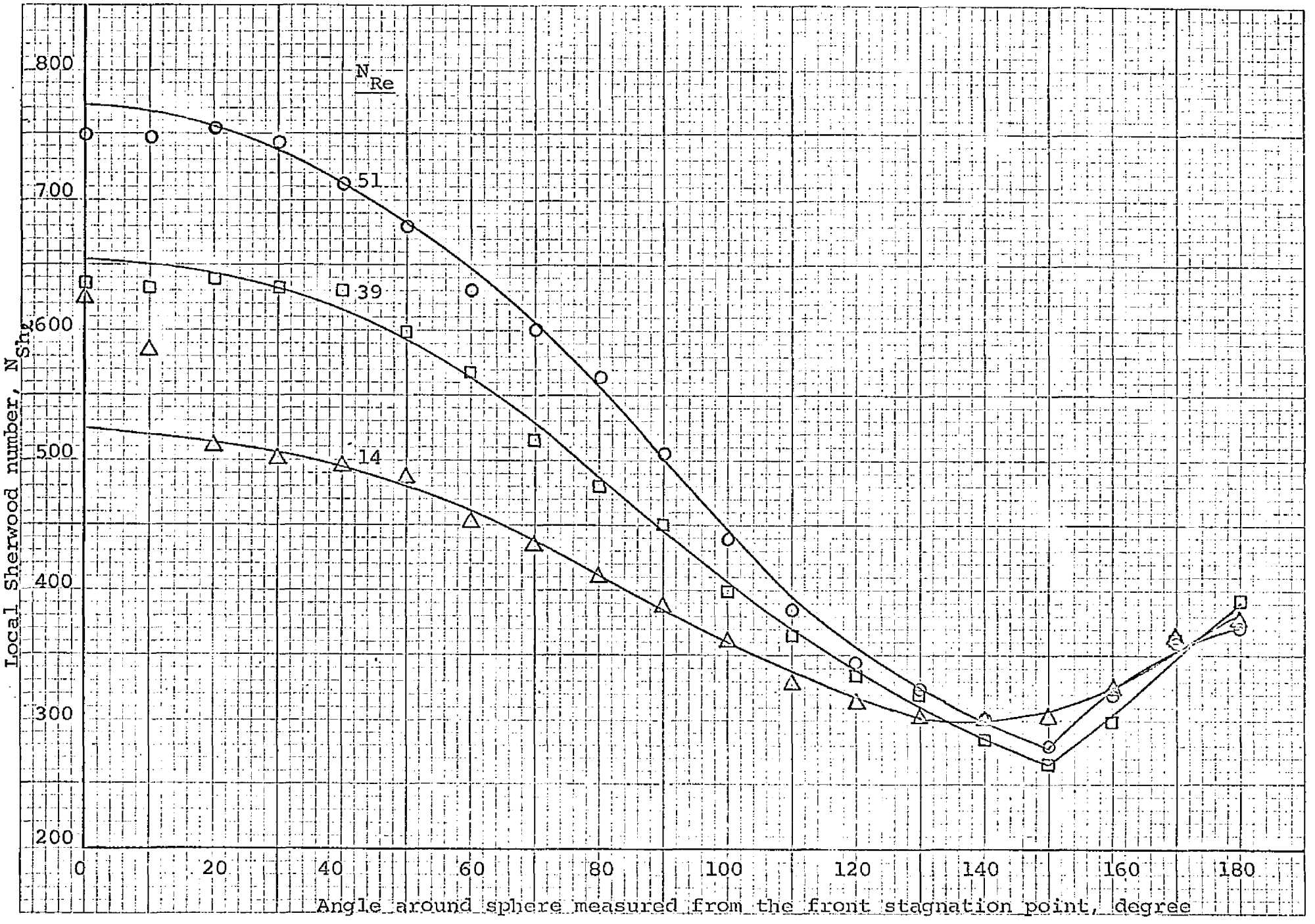

Fig. 56: Local mass transfer rate around single spheres (Series I) with chemical reaction, $\gamma = 2.43$

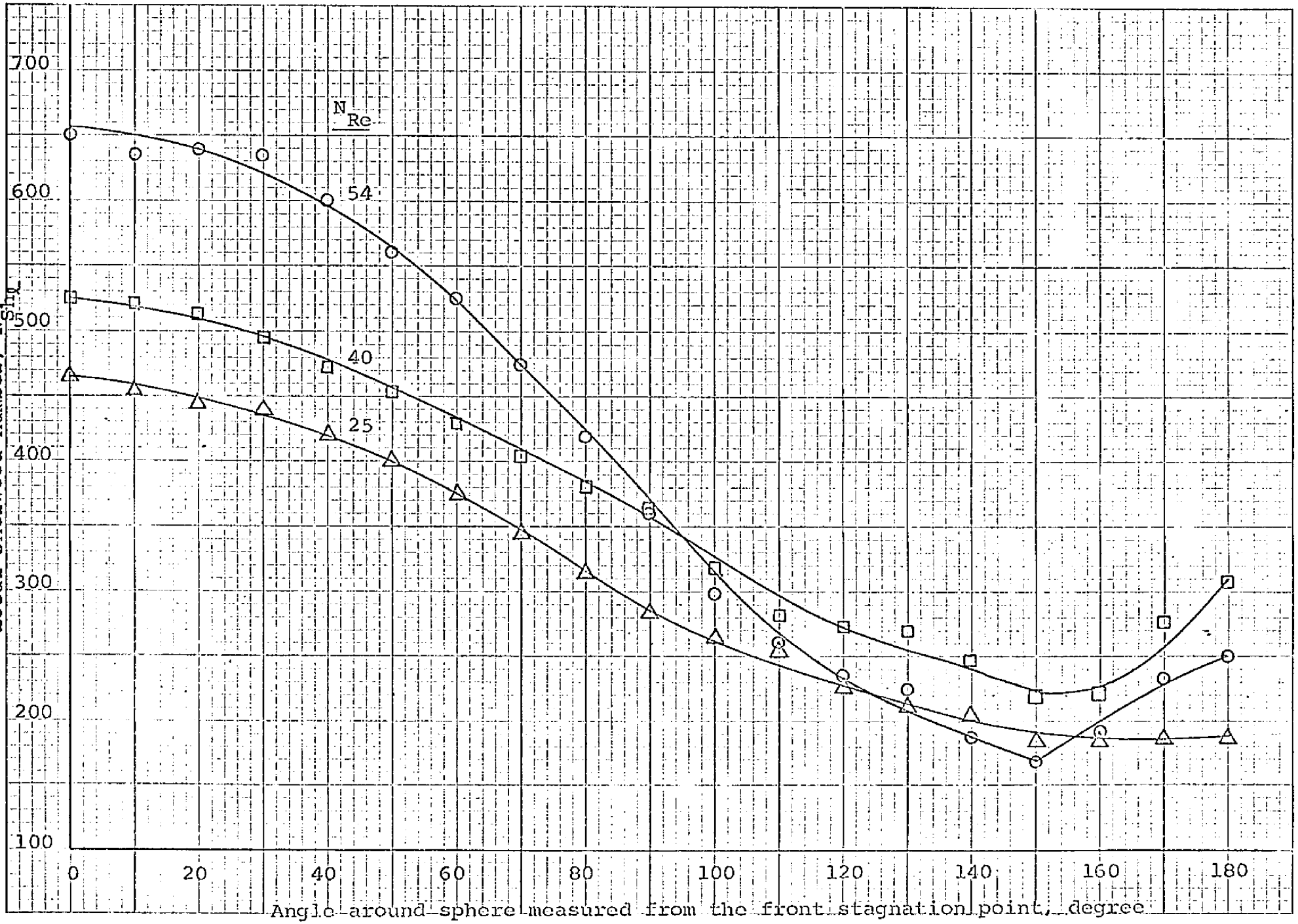

Fig. 57: Local mass transfer rate around single spheres (series I) with chemical reaction, $\gamma = 1.53$

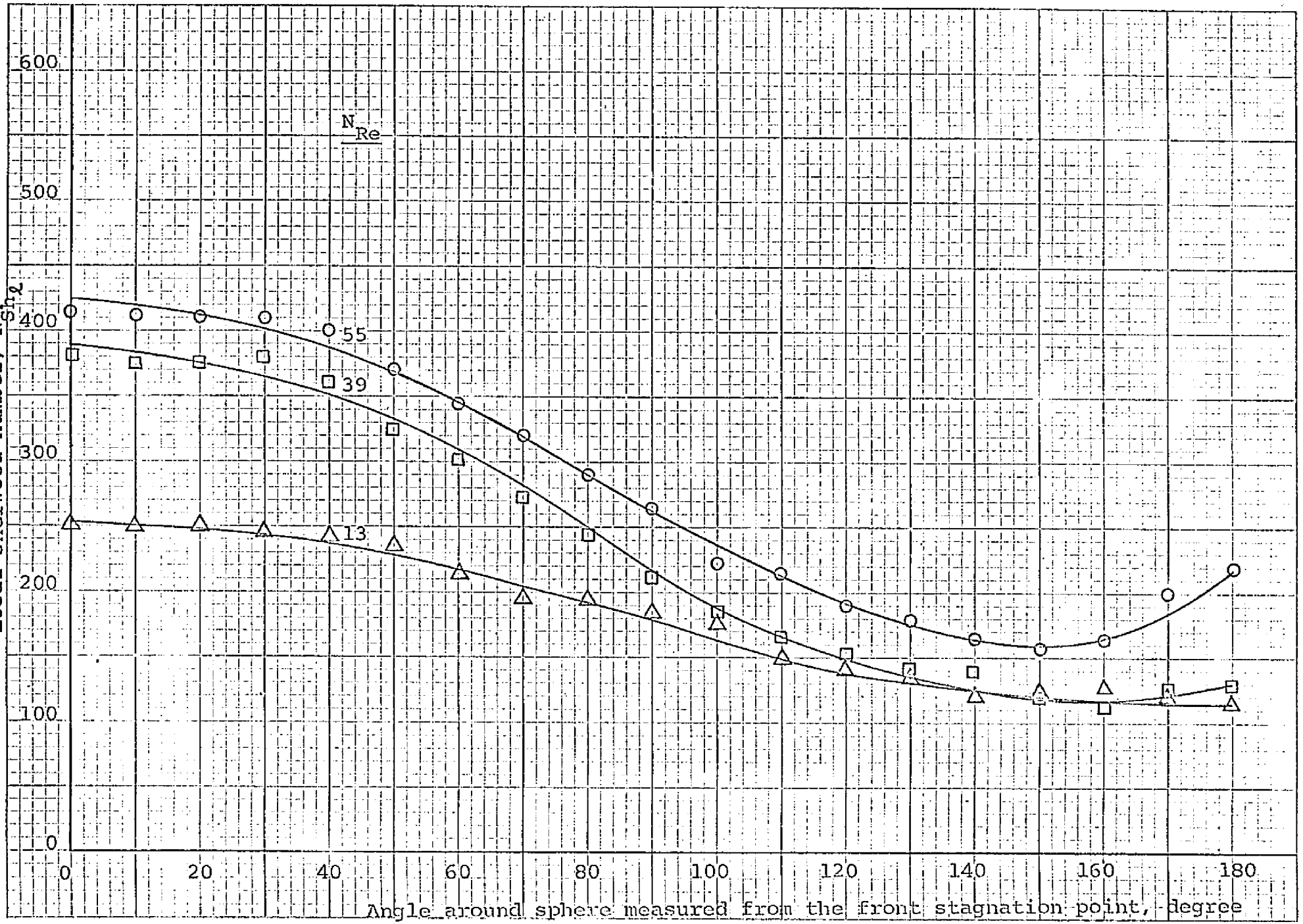

can be made with these results.

In order to explain their experimental results (with no reaction) of the location of minimum local mass transfer rate around a single solid sphere, Garner and Grafton (19) have suggested that a small amount of stagnant fluid exists behind the flow separation point so that the minimum local mass transfer rates occur a few degrees behind the flow separation point. This stagnant fluid hypothesis can reasonably explain the shift in the location of the minimum transfer rate for the case of mass transfer with reaction. The transfer rate decreases from the front stagnation point to the flow separation point and into the stagnant fluid region. Right after that stagnant fluid region, the concentration of the reagent (NaOH) is relatively small so that until some additional reagent diffuses into the reaction zone the local transfer rate will continue to decrease to a further extent and the location of the minimum transfer rate will move closer to the rear stagnation point.

With this explanation, we can predict that for a chemical system having a ratio of Schmidt number of solute to that of reagent much less than unity, the location of the minimum transfer rate will shift even closer to the rear stagnation point whereas for a system with the ratio of Schmidt number of solute to that of reagent much larger than unity, the location of minimum transfer rate will shift closer to the flow separation point. Furthermore, at fixed ratio of Schmidt numbers, the more concentrated the bulk stream reagent concentration is, the closer the location of the minimum transfer rate to the flow separation point.

The local mass transfer rates for two cases of the two

sphere system (series II and VI) for different reagent and solution concentration ratio are shown in Figures 58, 59, 60 and 61. These local mass transfer rates are qualitatively similar to those without chemical reaction. The only difference is the location of the minimum transfer rate somewhat beyond the flow separation point. The explanation for this shift in the location of the minimum mass transfer rate is the same as that discussed above for the single sphere system.

The overall mass transfer rates plotted as $N_{Sh_{o,R}}$ vs. $N_{Re}^{1/2}N_{Sc}^{1/3}$ using reagent to solute concentration ratio, γ, as the parameter for series I, II and VI are shown in Figure 62. This figure confirms the expected result that the mass transfer rate is an increasing function of reagent concentration and that the higher the concentration of the reagent, the higher the mass transfer rate. The effects of particle-to-particle interaction in the two sphere system and Reynolds number on the mass transfer rates are similar to that for the case of no reaction.

The overall mass transfer rates plotted as $N_{Sh_{o,R}}$ vs. γ using $N_{Re}^{1/2}N_{Sc}^{1/3}$ as the parameter for the cases of series I (single sphere) and series II and VI (two spheres) are shown in Figure 63. A linear relationship between N_{Sh_o} and γ is obtained. The slope of log $N_{Sh_{o,R}}$ vs. log γ is unity. This was predicted in the analytical part of this study.

The same overall mass transfer rates for series I, II and VI and different reagent and solute concentration ratio plotted in terms of enhancement factor ϕ vs. particle Reynolds number is shown in Figure 64. A study of this figure shows that the enhancement factor can be assumed to be independent

Fig. 58: Local mass transfer rater for series II, with chemical reaction
(= 3.23)

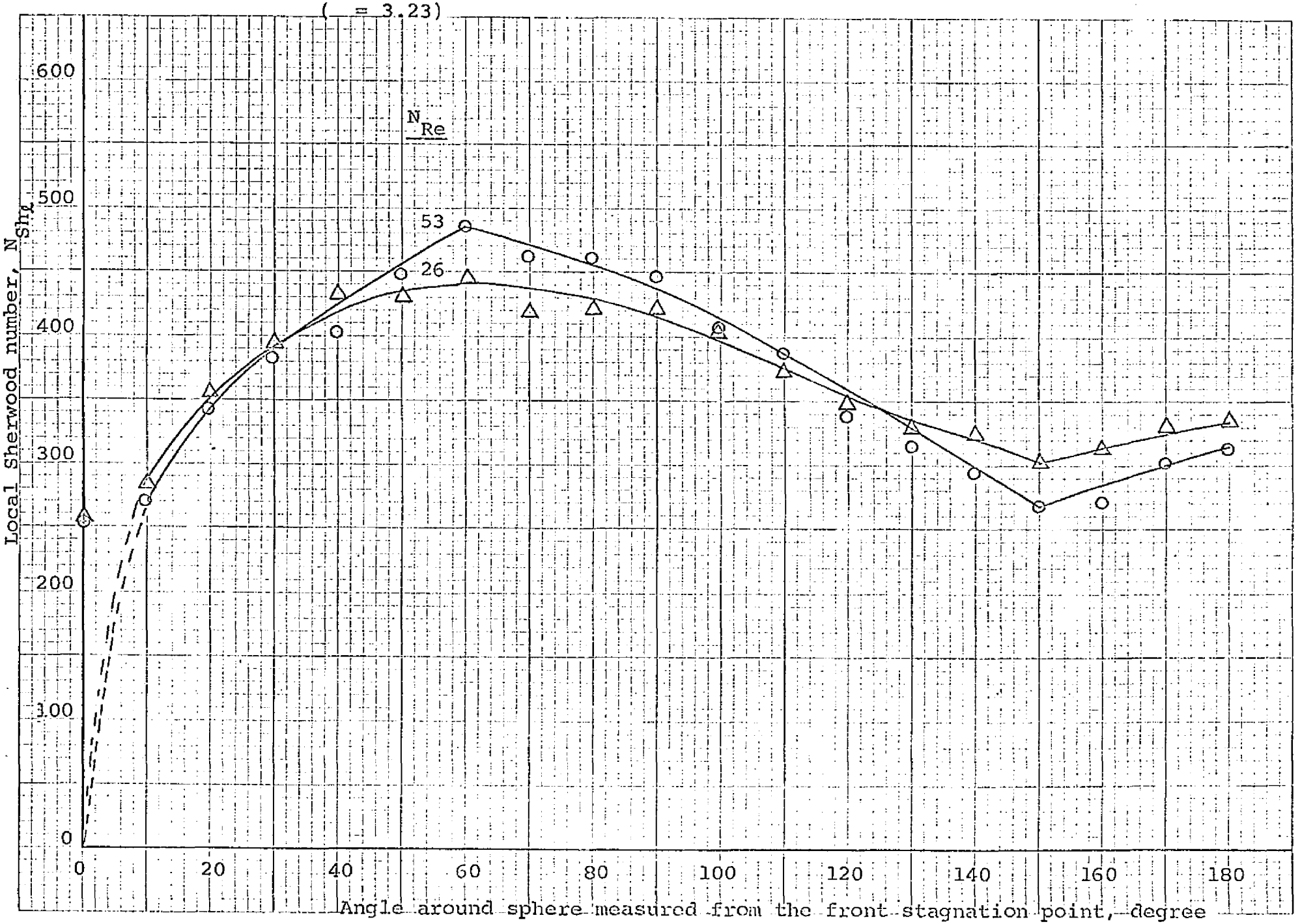

Fig. 59: Local mass transfer rate for series II, with chemical reaction, $\gamma = 1.52$

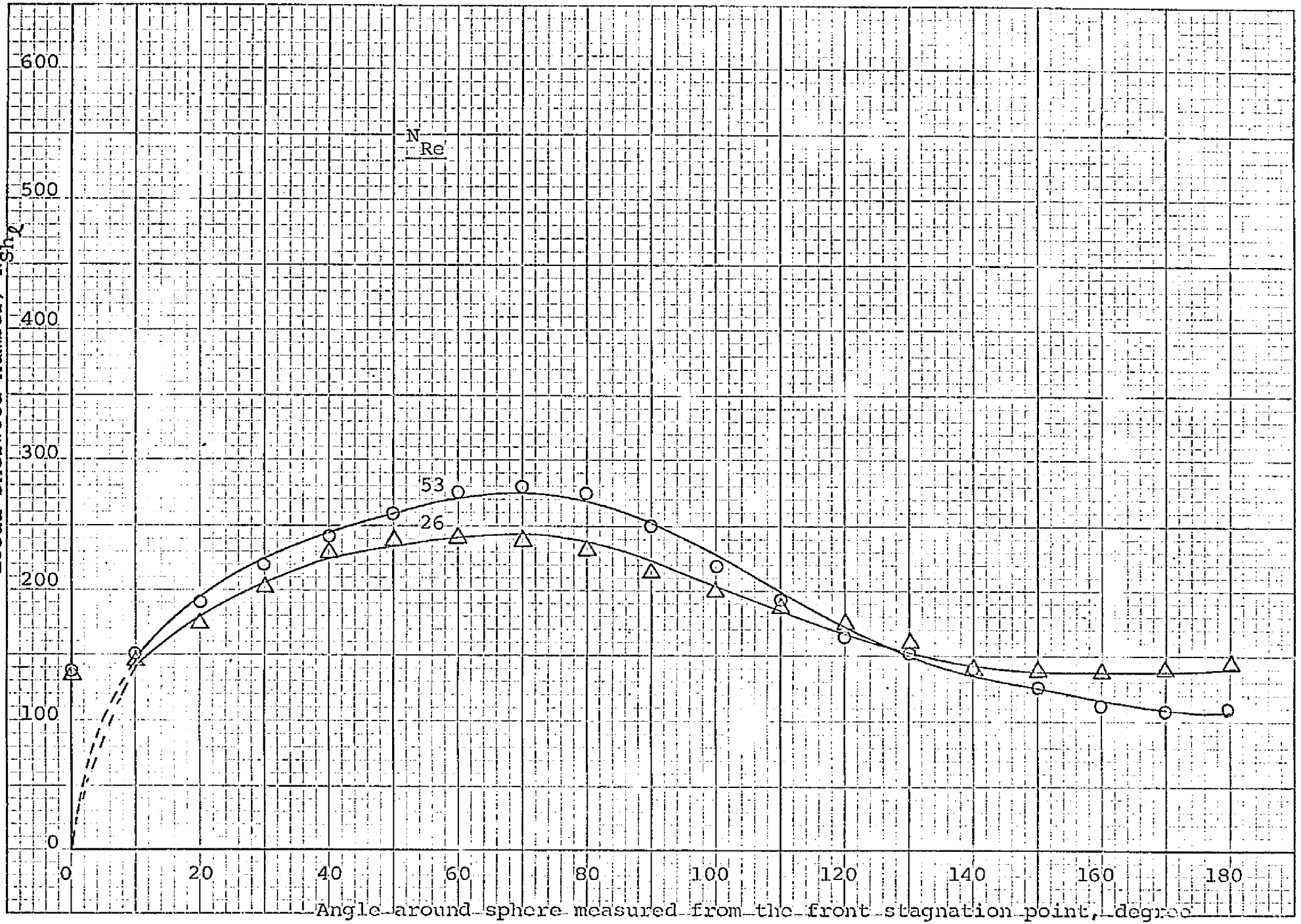

Fig. 60: Local mass transfer rate for series VI, with chemical reaction, $\gamma = 3.23$

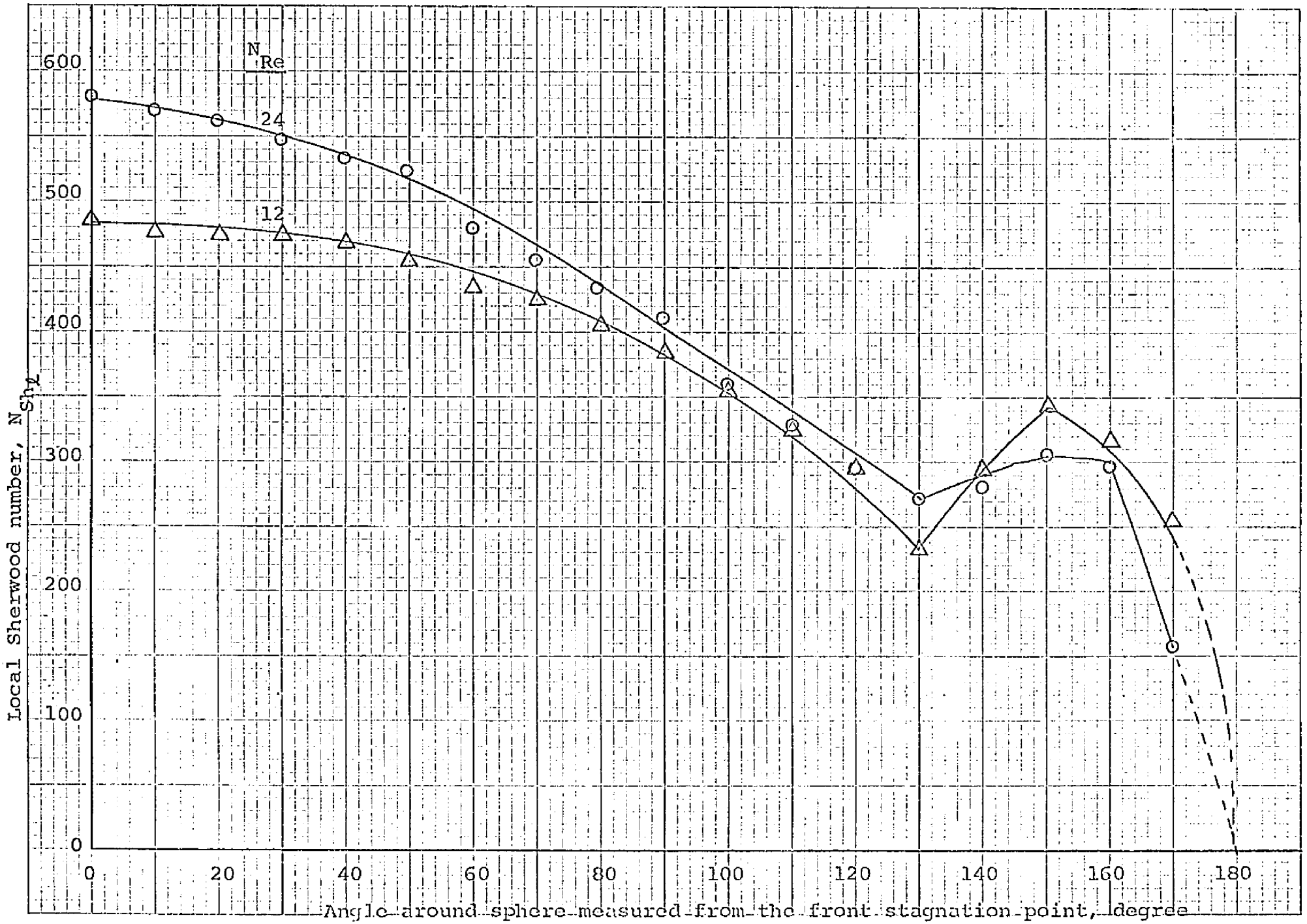

Fig. 61: Local mass transfer rate for series VI, with chemical reaction, $\gamma = 1.52$

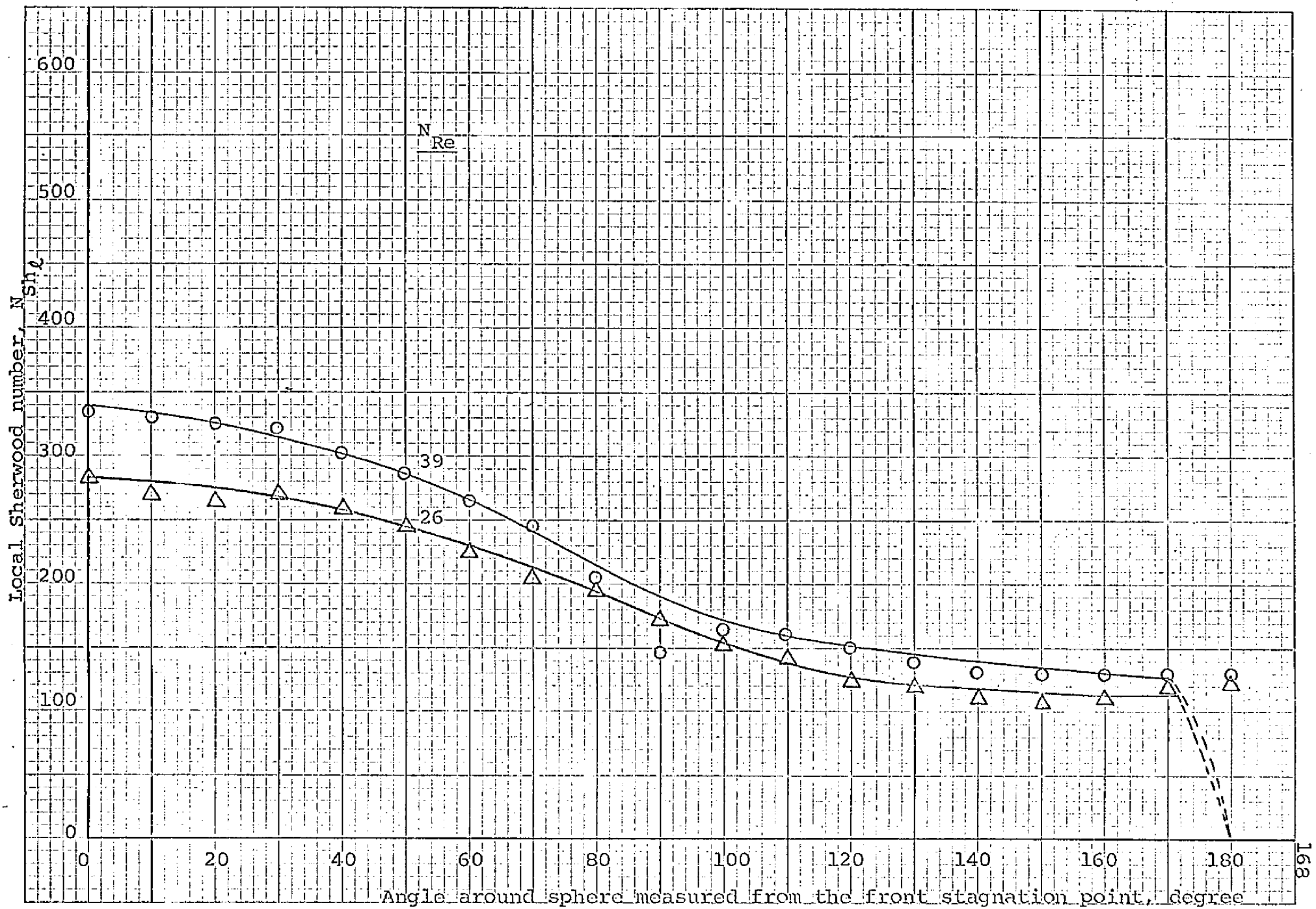

Fig. 62: Overall mass transfer rate for series I, II, and VI, with chemical reaction

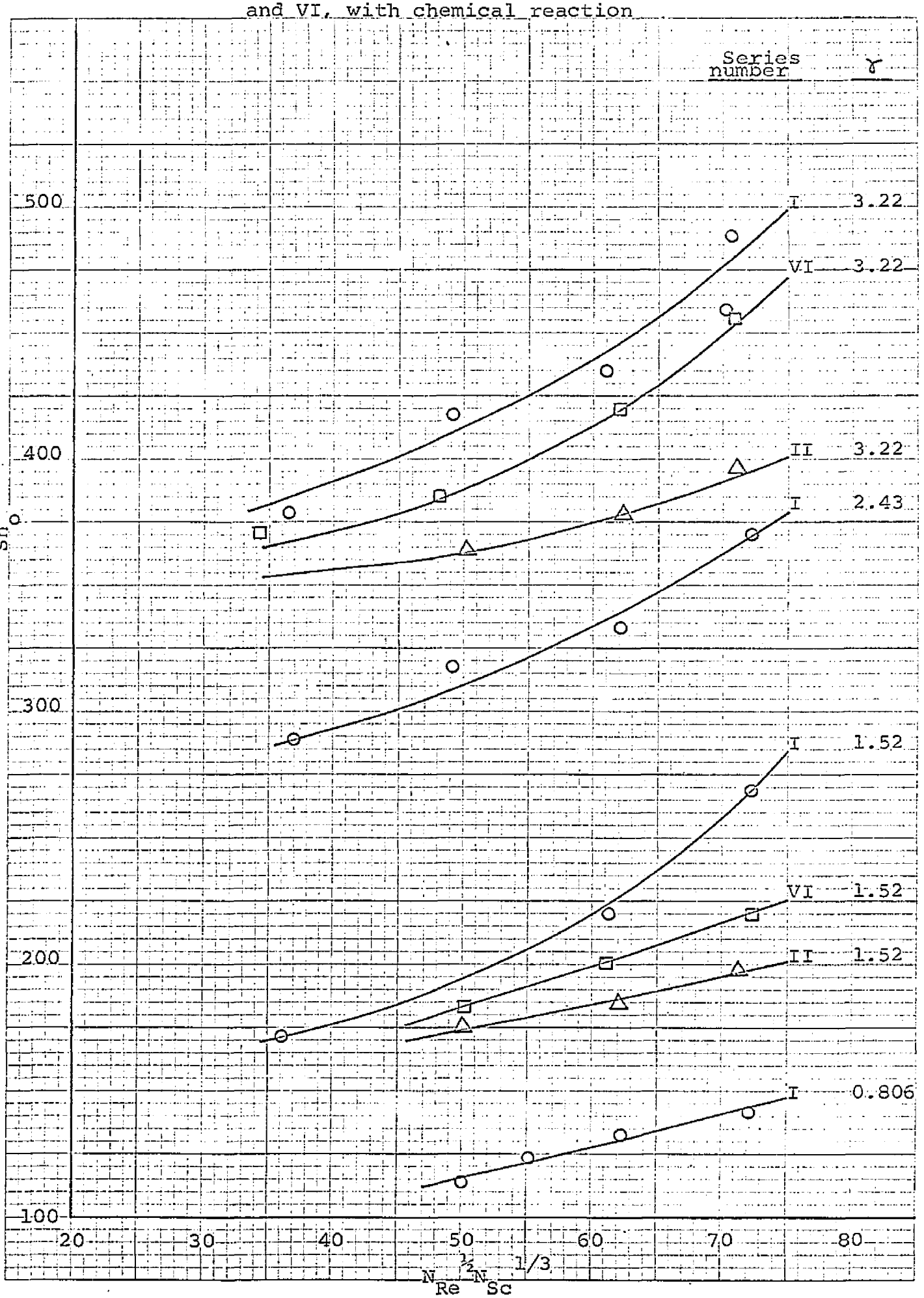

Fig. 63: Effect of concentration ratio, ϕ , on the overall mass transfer rates (series I, II, and VI)

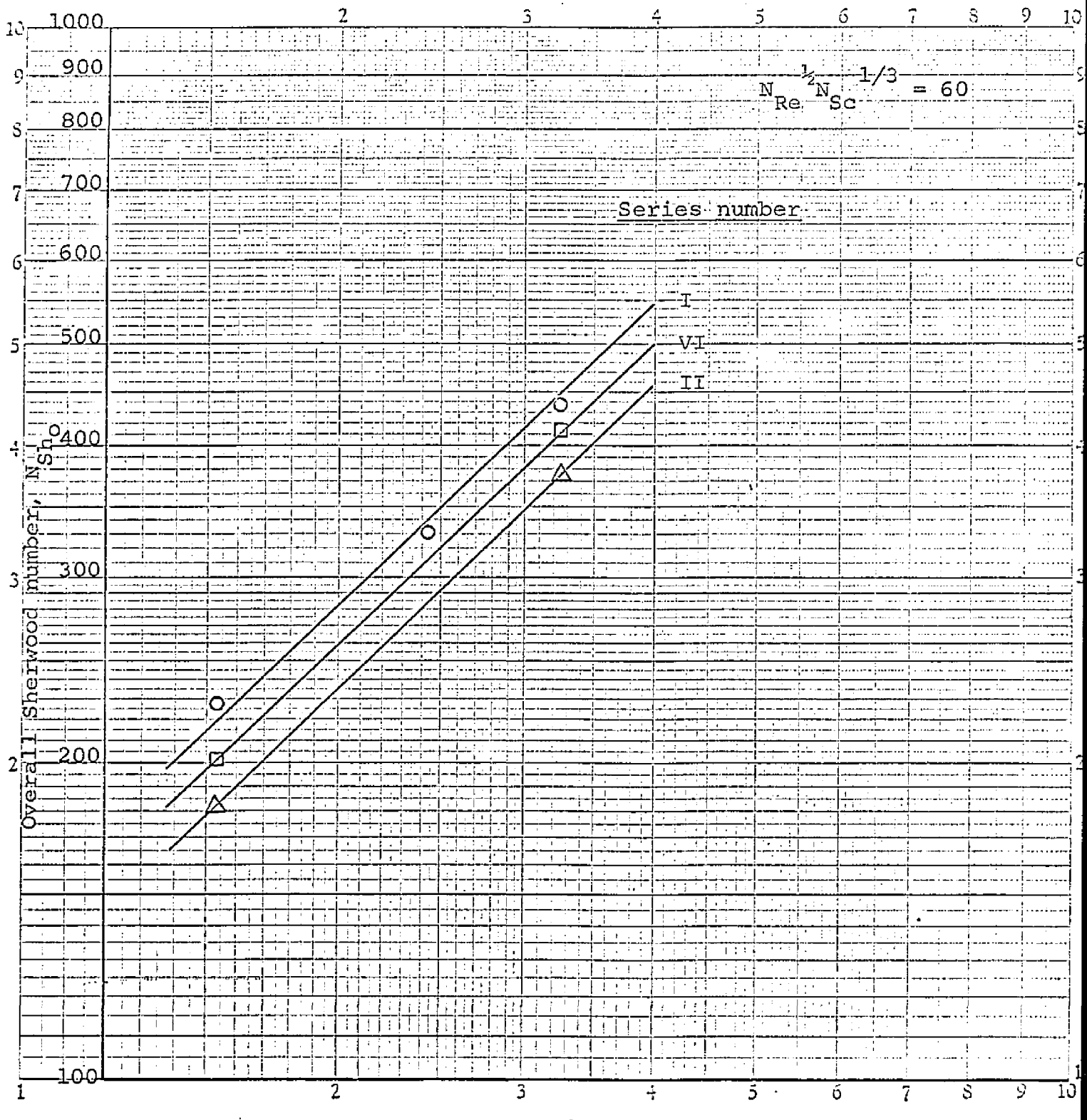

Fig. 64: Effect of particle Reynolds number on the enhancement factor, ϕ

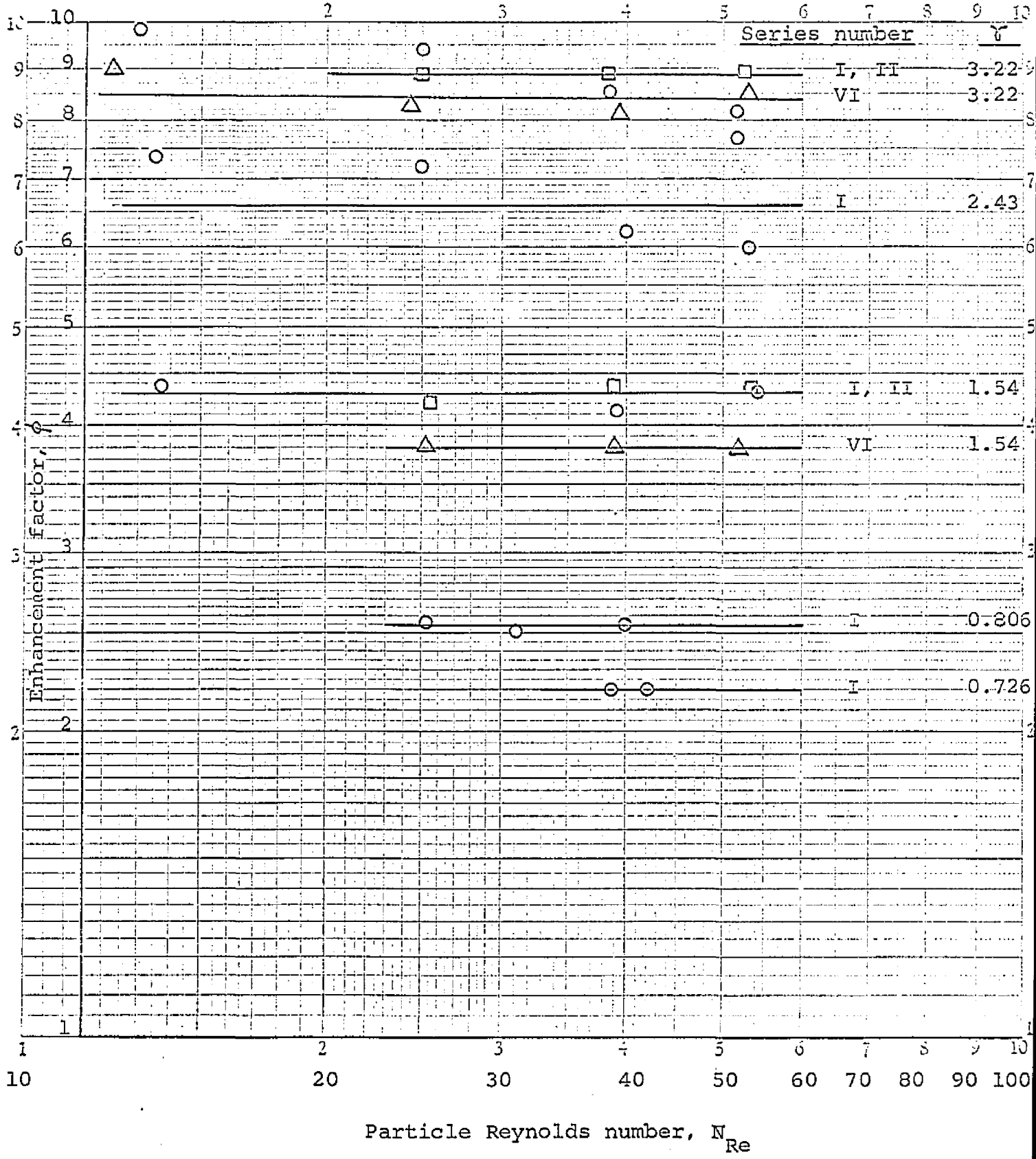

of the particle Reynolds number. This was also predicted in the analytical part of this study. The slight disagreement (10-15%) observed at high value of γ is probably due to experimental error. At these high values of γ (γ = 3.22 or 2.43) the experimental run time is of the order of one hour. Since the start-up and shut-down time are about five minutes each, these short runs could easily result in an experimental error of 10-15%.

A comparison of these experimental results with the predicted relation of enhancement factor ϕ and concentration ratio γ given in the analytical section is shown in Figure 65. The experimental data are in fair agreement with the predicted correlation. The enhancement factor should only be dependent on the flow pattern around the surface of the sphere. The agreements of all the series I, II and VI data verify the prediction.

The Schmidt number ratio α = 3.2 used here assumes that the average Schmidt number of NaOH in water is 300 and that of benzoic acid is 960.

Available experimental data based on simple geometry such as flow over a flat plate or inside a cylinder wall as well as with complicated and unknown hydrodynamic behavior such as flow in an agitated vessel are also shown in Figure 65. The data of these previous investigators also agree very well with the correlation predicted in the analytical analysis. Because of the combination of stagnant fluid and agitated flow over the solid particles, the results from the agitated vessel experiments seem to fall somewhere between the predicted correlation line for flow over a solid sphere and the correlation line predicted using film theory (stagnant fluid).

Fig. 65: Comparison of experimental work and theoretical analysis

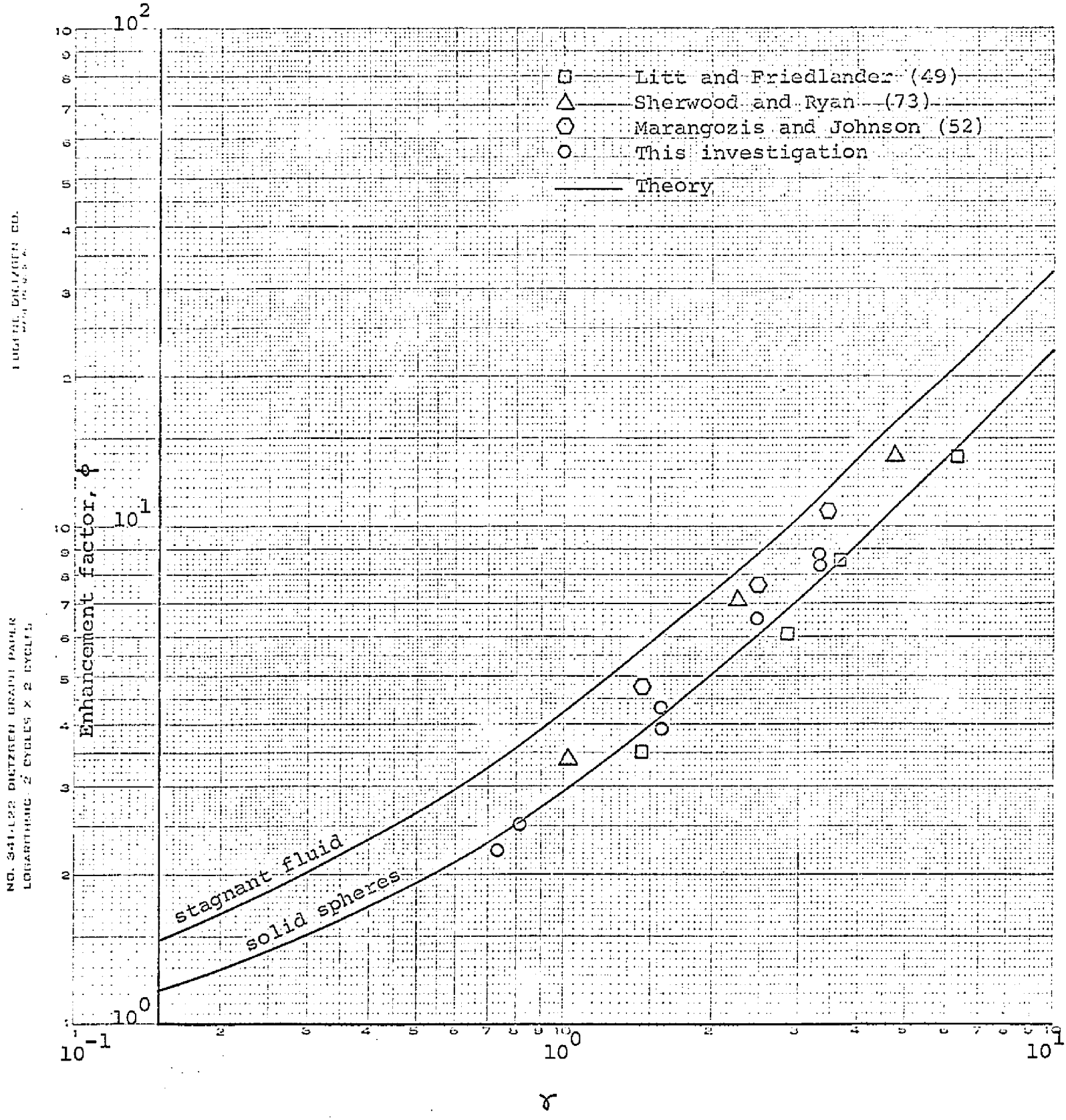

VI. SUMMARY

The effect of homogeneous chemical reactions and the effects of particle-to-particle interaction in a two sphere system on the local and overall mass transfer rates have been studied. Four major objectives have been pursued:

1. The effect of first order homogeneous chemical reaction on the local and overall mass transfer rates around single solid spheres and in multiparticle systems.
2. The effect of particle-to-particle interaction in a two sphere system with and without first order homogeneous chemical reaction on the local and overall mass transfer rates.
3. The effect of rapid, second order, irreversible chemical reaction on the mass transfer rate around solid spheres, liquid drops and gas bubbles.
4. Experimental measurements of local and overall mass transfer rates around single solid spheres and in two sphere systems with or without chemical reactions.

To accomplish the theoretical analyses outlined above, considerable attention has been devoted to the establishment of realistic mathematical models (description of the problem) and the techniques of solving the governing differential equations. In this study the thin boundary layer approximation coupled either with a numerical solution or a perturbation technique was especially emphasized. The experimental work was based on the idea of verifying some of the theoretical analysis.

Numerical solutions for the mass transfer rate around single solid spheres and in multiparticle systems with and without first order homogeneous chemical reaction for creeping flow and boundary layer flow have been obtained. The results agree with the well known fact that the mass transfer rate increases as the reaction rate increases. At very high reaction rate, the mass transfer rate is independent of hydrodynamic behavior. In this first phase of the study, the relative effect of the hydrodynamic terms and the reaction term on the mass transfer rate is emphasized. Generalized parameters, $N_{Pe}^{1/3}/\beta$ for creeping flow, and $N_{Re}^{1/2} N_{Sc}^{1/3}/\beta$ for boundary layer flow have been proposed and utilized as an expression of mass transfer rates. At very low values of $N_{Pe}^{1/3}/\beta$ or $N_{Re}^{1/2}N_{Sc}^{1/3}/\beta$, the mass transfer rate is independent of hydrodynamic behavior (reaction controlled mass transfer) whereas at very large values of $N_{Pe}^{1/3}/\beta$ or $N_{Re}^{1/2}N_{Sc}^{1/3}/\beta$, the mass transfer rate is independent of reaction rates (pure physical mass transfer). With these generalized parameters, the picture of the effect of hydrodynamics and reactions on mass transfer rates is much clearer than before. The results obtained agree very well with previous studies for the two limiting cases of either reaction controlled or pure physical mass transfer.

Numerical solutions of mass transfer rates around a single active sphere in a two sphere system in creeping flow with and without first order homogeneous chemical reaction have also been obtained. In this second phase of the study the effect of particle-to-particle interaction on the system

with and without chemical reaction is especially emphasized. When two spheres are very far apart, the mass transfer rate around the sphere is the same as that for a single sphere. As the two spheres approach each other, the overall mass transfer rate decreases for both cases of the active sphere in front of and behind the inert sphere in the direction of the fluid flow.

For the case of the active sphere placed in front of the inert sphere, the local mass transfer rate around the front stagnation point of the active sphere agrees closely with that of a single sphere. Further away from the front stagnation point, the local transfer rate decreases and is strongly affected by the particle-to-particle interaction and the reaction rate. A minimum local transfer rate appears somewhere around the rear stagnation point depending on the particle-to-particle distance and the reaction rate. At low reaction rates or large particle-to-particle distance, this minimum point is always located at the rear stagnation point, whereas at high reaction rates and small particle-to-particle distance, this minimum point shifts away from the rear stagnation point so that a (second) maximum in local transfer rate occurs at the rear stagnation point.

For the case of the active sphere placed behind the inert sphere, the local mass transfer rate around the rear stagnation point behaves like that of a single sphere. Further away from the rear stagnation point, the local transfer rates are again strongly affected by the particle-to-particle interaction and the reaction rate. When two spheres are very close to each other, there is a minimum local transfer point which appears at the front stagnation point. Therefore, there is an inflection point between the front stagnation point and a maximum

local transfer rate point which is located somewhere between $\theta = 0$ to $\theta = \pi$. When the distance between two spheres or the reaction rate increases, this inflection point shifts to a location which is closer to the front stagnation point. Finally, when two spheres are far apart or the reaction rates are extremely high, this inflection point appears at the front stagnation point. There are no available solutions which can be compared with this phase of the study.

Analytical solutions of mass transfer rates around solid spheres, liquid drops and gas bubbles with second order, irreversible, rapid homogeneous reaction in the continuous phase have also been obtained. In this third phase of the study a general mathematical model using simplified velocity flow patterns has been established for all three cases. For mass transfer from liquid drops, a regular perturbation technique has been applied, and the results show that the mass transfer rates are functions of both the shear stress and velocity on the surface of the liquid drops. The results for solid spheres or gas bubbles are just the limiting cases of either the velocity or shear stress on the surface of the spherical particle set equal to zero. The mass transfer rates are expressed in terms of the enhancement factor. The results show that the enhancement factor for non-separation flow is independent of the hydrodynamic behavior. It is only a function of flow conditions near the surface of the spherical particles, the Schmidt number ratio of the solute to reagent α, and the concentration ratio of the reagent and solute, γ. At high mass transfer rates, the enhancement factor is proportional to the concentration ratio γ and the nth power of the

Schmidt number ratio α. The value of n is a function of shear stress and velocity on the surface of the liquid drops. For mass transfer around gas bubbles, n = ½, and for mass transfer around solid particles n = 2/3. The solution for the mass transfer rate from a dispersed phase into a stagnant fluid have also been obtained. The value n in this case is equal to unity. For the cases of solid spheres and gas bubbles, the results agree with penetration theory and boundary layer theory. However, there is no available solution for comparison with the solution for liquid drops.

The results obtained in this study can be directly applied to any kind of geometry, as long as there is no flow separation on the particle surface.

Experimental measurements of local and overall mass transfer rates around single solid spheres and for two sphere systems have been performed. Benzoic acid spheres and dilute sodium hydroxide solution were used as the chemical system. For the case of no chemical reaction, (pure water as the reagent) the single sphere results agreed with previous studies. The local mass transfer rates were shown to decrease from a maximum at the front stagnation point to a minimum at the flow separation point and then increase to another (second) maximum at the rear stagnation point.

For the case of the active sphere placed behind an inert sphere, the results also agreed with those presented by Peltzman and Pfeffer for two spheres touching, and one diameter apart. The overall mass transfer rates for all of the two sphere experiments were smaller than that for a single sphere except at low Reynolds number where the effect of the particle-to-particle interaction was very weak. These local and overall

mass transfer patterns were found to be similar to those discussed in the theoretical analysis despite the effect of turbulence (in wake region) which was present in the experiments. The local mass transfer rates around the front stagnation point for the case of the active sphere placed in front of the inert sphere and around the rear stagnation point for the case of the active sphere placed behind the inert sphere in the flow direction were found to be similar to that for a single sphere. Particle-to-particle interaction would also shift the maximum and minimum transfer rate locations along the solid sphere depending on the particle Reynolds number and the particle-to-particle distance. This shift of the maximum and minimum points shown also agrees with the theoretical predictions.

For the case of mass transfer with rapid chemical reaction the overall mass transfer rates in terms of the enhancement factor agreed with the predicted values. The linear dependence of the concentration ratio of solute and reagent, δ , on the enhancement factor was also observed. The fact that the enhancement factors are independent of hydrodynamic behavior as predicted in the theoretical analysis was also observed. The local mass transfer profiles are similar to those without chemical reaction. However, the minimum transfer point shifts to a location closer to the rear stagnation point due to the existence of stagnant fluid right behind the flow separation point. Since there are no previous data of this kind available in the literature, no comparison with these results could be made.

This study presents a fundamental investigation of the effects of particle-to-particle interactions and chemical reactions on the local and overall mass transfer rates around spheres. Further verifications of the results presented here

are necessary. More advanced and complicated studies to simulate actual industrial processes such as mass transfer in the polishing of particle surfaces of semi-conductors are required. On the basis of the results of this investigation it is recommended that the following topics should be considered for further study:

1. The effects of higher order reactions on mass transfer rates.
2. Obtaining solutions for the entire Peclet Number range.
3. The effect of particle-to-particle interactions on the flow separation at high Reynolds number.
4. The effect of flow separation on mass transfer rates.
5. The effect of active particles on active particles on mass transfer rates.
6. The effect of charged ions on the mass transfer rate.
7. The effect of second order, rapid chemical reaction on the mass transfer rate for a fluid flow field pattern somewhere between a stagnant fluid and flow over a solid surface.

VII. APPENDICES

Appendix A: Derivation of Diffusion Equations in Bipolar Coordinates

We will briefly introduce bipolar coordinates here first and then give the details of the derivation of the diffusion equation in bipolar coordinates. We take ξ, η, ϕ as bipolar curvilinear coordinates in the meridian plane corresponding to z, ρ, ϕ in cylindrical coordinates. Upon setting

$$z + i\rho = ic \cot \tfrac{1}{2}(\xi + i\eta) \tag{A-1}$$

$c > 0$, we obtain

$$z = c \frac{\sinh \eta}{\cosh \eta - \cos \xi}$$

$$\rho = c \frac{\sin \xi}{\cosh \eta - \cos \xi} \tag{A-2}$$

where

$$0 \leq \xi < \pi \; ; \; -\infty < \eta < \infty \; ; \; 0 \leq \phi < 2\pi$$

The surfaces obtained by rotating the curves η = constant about the axis of z are a family of spheres having $z = 0$ (or $\eta = 0$) for a common radical plane. Two spheres external to each other will be defined by fixing the coordinate and the constant c so that these spheres have any radii and any center to center distance greater than the sum of their radii. It should be noted here that the two spheres of interest here are on the opposite sides of the origin. The inverse transforms of equation (A-2) are obtained by setting

$$R_1^2 = (z-c)^2 + \rho^2 = \frac{2c^2 e^{-\eta}}{\cosh\eta - \cos\xi}$$

$$R_2^2 = (z+c)^2 + \rho^2 = \frac{2c^2 e^{\eta}}{\cosh\eta - \cos\xi} \qquad \text{(A-3)}$$

to give

$$\eta = \ln \frac{R_2}{R_1}$$

$$\cos\xi = \frac{R_1^2 + R_2^2 - 4c^2}{2R_1R_2} \qquad \text{(A-4)}$$

Figures A-1, A-2 and A-3 illustrate these coordinates. For more details of the properties of these coordinates the interested reader is referred to publications by Happel and Brenner (29).

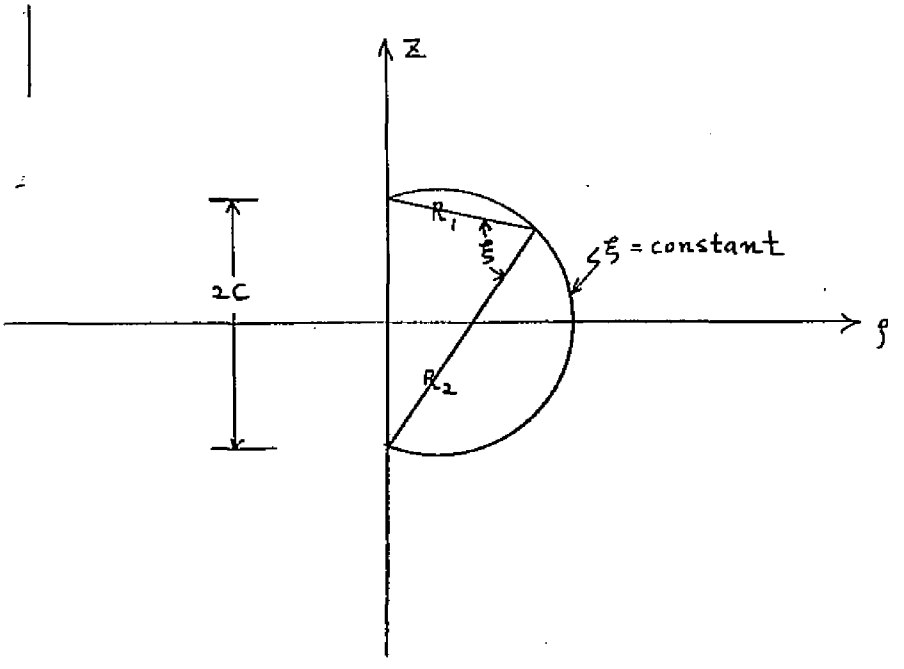

Figure A-1: Bipolar Angle

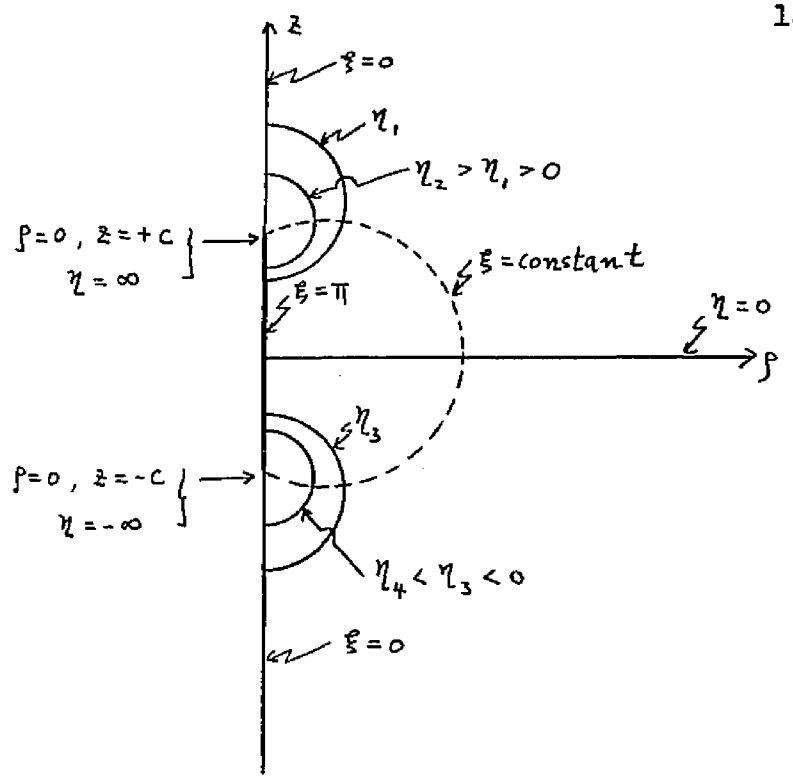

Figure A-2: Bipolar Coordinates in a Meridian Plane

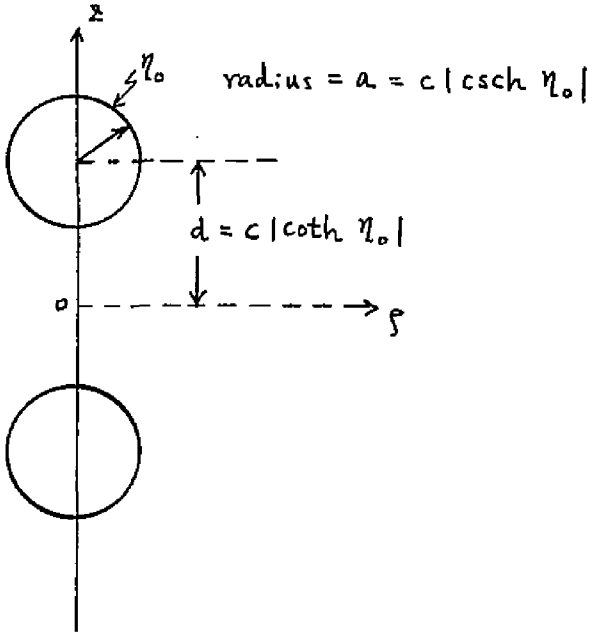

Figure A-3: Coaxial Spheres

To transform the diffusion equation into bipolar coordinates, the Laplacian operator ∇^2 and vector notations ∇ and $\underline{v}$ should be transformed into bipolar coordinates. First, we have assumed that flow is axisymmetric. These notations are given as

$$\nabla^2 = h_1 h_2 i_{\varphi_3} \left[\frac{\partial}{\partial \varphi_1}\left(\frac{h_1}{h_2 h_3} \frac{\partial}{\partial \varphi_1} \right) + \frac{\partial}{\partial \varphi_2}\left(\frac{h_2}{h_3 h_1} \frac{\partial}{\partial \varphi_2} \right) \right] \quad \text{(A-5)}$$

$$\nabla' = \underline{i}_{\varphi_1} h_1 \frac{\partial}{\partial \varphi_1} + \underline{i}_{\varphi_2} h_2 \frac{\partial}{\partial \varphi_2} \quad \text{(A-6)}$$

and

$$\underline{v} = \underline{i}_{\varphi_1} V_{\varphi_1} + \underline{i}_{\varphi_2} V_{\varphi_2} \quad \text{(A-7)}$$

The metric coefficients h_1, h_2 and h_3 are given by Happel and Brenner (29) as

$$h_1 = h_2 = \frac{\cosh \eta - \cos \xi}{c}$$

$$h_3 = \frac{\cosh \eta - \cos \xi}{c \sin \xi} \quad \text{(A-8)}$$

with

$$\varphi_1 = \xi$$

$$\varphi_2 = \eta$$

$$\varphi_3 = \phi$$

Equations (A-5) and (A-8) give

$$\nabla'^2 = \frac{1}{c^2}\left[\frac{(\cosh\eta - \cos\xi)^3}{\sin\xi}\right]\cdot\left[\frac{\partial}{\partial\xi}\left(\frac{\sin\xi}{\cosh\eta-\cos\xi}\frac{\partial}{\partial\xi}\right) + \frac{\partial}{\partial\eta}\left(\frac{\sin\xi}{\cosh\eta-\cos\xi}\frac{\partial}{\partial\eta}\right)\right] \tag{A-9}$$

and equations (A-6) and (A-7) give

$$\underline{V}\cdot\nabla' = \frac{\cosh\eta-\cos\xi}{c}\left(V_\xi\frac{\partial}{\partial\xi} + V_\eta\frac{\partial}{\partial\eta}\right) \tag{A-10}$$

Therefore, equations (A-9), (A-10) and (IV-3) give

$$\frac{(\cosh\eta-\cos\xi)^3}{\sin\xi}\left[\frac{\partial}{\partial\xi}\left(\frac{\sin\xi}{\cosh\eta-\cos\xi}\frac{\partial c}{\partial\xi}\right) + \frac{\partial}{\partial\eta}\left(\frac{\sin\xi}{\cosh\eta-\cos\xi}\frac{\partial c}{\partial\eta}\right)\right] - \frac{1}{2}N_{Pe}\cdot\left(\frac{c}{a}\right)(\cosh\eta-\cos\xi)\left(V_\xi\frac{\partial c}{\partial\xi} + V_\eta\frac{\partial c}{\partial\eta}\right) - \left(\frac{c}{a}\right)^2\beta^2 c = 0 \tag{A-11}$$

This is equation (IV-8).

Appendix B: Order of Magnitude Analysis

The following approximating assumptions are based on boundary layer theory. It is noted (71) that this method was originally devised by L. Prandtl to show that the Navier-Stokes equations could be simplified to yield approximate solutions for many fluid flow problems, especially in aerodynamics. The basic assumption of this theory involves the existence of a boundary layer, a very thin layer near the surface of the particles over which the fluid is flowing. At the edge of this thin boundary layer the velocity is equal to the bulk stream value of the fluid. All the gradients with respect to the normal distance variable must vanish. Inside the boundary layer, the velocities vary from the bulk stream value to that on the surface of the particles. In general, for a problem which involves heat, mass and momentum transport phenomena there will exist thermal, concentration and hydrodynamic boundary layers. For the case of mass transfer, the number of concentration boundary layers depend on the number of species in the systems. The diffusion equation with homogeneous first-order reaction in spherical coordinates is

$$\frac{1}{r^2}\frac{\partial}{\partial r}\left(r^2\frac{\partial C}{\partial r}\right) + \frac{1}{r^2\sin\theta}\frac{\partial}{\partial\theta}\left(\sin\theta\frac{\partial C}{\partial\theta}\right) - \frac{1}{2}N_{Pe}\left(V_r\frac{\partial C}{\partial r} + \frac{V_\theta}{r}\frac{\partial C}{\partial\theta}\right) - \beta^2 C = 0 \qquad \text{(B-1)}$$

Upon setting

$$r = 1 + y \qquad \text{(B-2)}$$

and assuming a thin diffusional layer ($y \ll 1$), equation (B-1) becomes

$$\frac{\partial^2 C}{\partial y^2} + \frac{1}{\sin\theta}\frac{\partial}{\partial\theta}\left(\sin\theta\frac{\partial C}{\partial\theta}\right) - \frac{1}{2}N_{Pe}\left(V_\theta\frac{\partial C}{\partial\theta} + V_y\frac{\partial C}{\partial y}\right) - \beta^2 C = 0 \qquad \text{(B-3)}$$

Using dimensionless variables, each chosen to be of order of magnitude $\mathcal{O}(1)$ defined as

$$
\begin{aligned}
y^* &= \frac{y}{\delta} = \mathcal{O}(1) \\
C &= \mathcal{O}(1) \\
V_\theta^* &= V_\theta \frac{1}{\delta} = \mathcal{O}(1) \\
V_y^* &= V_y \frac{1}{\delta^2} = \mathcal{O}(1)
\end{aligned}
\tag{B-4}
$$

where δ is the dimensionless concentration boundary layer thickness, equation (B-3) becomes

$$
\begin{aligned}
&\frac{1}{\delta^2}\frac{\partial^2 C}{\partial y^{*2}} + \frac{1}{\sin\theta}\frac{\partial}{\partial\theta}\left(\sin\theta\frac{\partial C}{\partial\theta}\right) \\
&\quad -\tfrac{1}{2} N_{Pe}\left(V_y^* \delta \frac{\partial C}{\partial y^*} + V_\theta^* \delta \frac{\partial C}{\partial\theta}\right) - \beta^2 C = 0
\end{aligned}
\tag{B-5}
$$

Therefore, we obtain

$$
\begin{aligned}
&\frac{\partial^2 C}{\partial y^{*2}} + \delta^2 \frac{1}{\sin\theta}\frac{\partial}{\partial\theta}\left(\sin\theta\frac{\partial C}{\partial\theta}\right) \\
&\quad -\tfrac{1}{2} N_{Pe}\,\delta^3\left(V_y^* \frac{\partial C}{\partial y^*} + V_\theta^* \frac{\partial C}{\partial\theta}\right) - \beta^2\delta^2 C = 0
\end{aligned}
\tag{B-6}
$$

since

$$y^* = \frac{y}{\delta} = \mathcal{O}(1)$$

and

$$y \ll 1$$

we say

$$\delta = \mathcal{O}(y) \ll 1$$

and the second term of equation (B-6)

$$\frac{\delta^2}{\sin\theta}\frac{\partial}{\partial\theta}\left(\sin\theta\frac{\partial C}{\partial\theta}\right) = \mathcal{O}(\delta^2) \qquad \text{(B-7)}$$

is negligible. That is, the diffusion term in the angular direction is negligible.

Furthermore, we obtain

$$N_{Pe}\,\delta^3 = \mathcal{O}(1)$$

and

$$\beta^2\delta^2 = \mathcal{O}(1)$$

Therefore,

$$\delta = \mathcal{O}\left(\frac{1}{N_{Pe}}\right)^{1/3} \qquad \text{(B-8)}$$

and

$$\delta = \mathcal{O}\left(\frac{1}{\beta}\right) \qquad \text{(B-9)}$$

Equations (B-4) and (B-5) determine whether the convection term or the reaction term will dominate the mass transfer mechanism depending on the relative magnitude of N_{Pe} and β. Equation (B-4), therefore, becomes

$$\frac{\partial^2 C}{\partial y^{*2}} - \tfrac{1}{2}N_{Pe}\,\delta^3\left(V_\theta^*\frac{\partial C}{\partial\theta} + V_y^*\frac{\partial C}{\partial y^*}\right) - \beta^2\delta^2 C = 0 \qquad \text{(B-10)}$$

and equation (IV-5) is then justified.

Similarly, we can verify equation (IV-8). The diffusion equation with first order homogeneous chemical reaction in bipolar coordinates is given as

$$\frac{(\cosh\eta-\cos\xi)^3}{\sin\xi}\left[\frac{\partial}{\partial\xi}\left(\frac{\sin\xi}{\cosh\eta-\cos\xi}\frac{\partial C}{\partial\xi}\right)+\frac{\partial}{\partial\eta}\left(\frac{\sin\xi}{\cosh\eta-\cos\xi}\frac{\partial C}{\partial\eta}\right)\right] \qquad \text{(B-11)}$$

$$-\tfrac{1}{2}N_{Pe}\left(\frac{C}{a}\right)(\cosh\eta-\cos\xi)\left(V_\xi\frac{\partial C}{\partial\xi}+V_\eta\frac{\partial C}{\partial\eta}\right)-\left(\frac{C}{a}\right)^2\beta^2 C = 0$$

Upon setting

$$\eta = \eta_o + y \quad ; \eta_0 = Y_o$$

and assuming a thin diffusional boundary layer ($y/\eta_0 << 1$), equation (B-11) becomes

$$\frac{(\cosh\eta_o - \cos\xi)^3}{\sin\xi}\left[\frac{\partial}{\partial\xi}\left(\frac{\sin\xi}{\cosh\eta_o-\cos\xi}\frac{\partial c}{\partial\xi}\right) + \frac{\partial}{\partial y}\left(\frac{\sin\xi}{\cosh\eta_o-\cos\xi}\frac{\partial c}{\partial y}\right)\right] \tag{B-12}$$
$$-\frac{1}{2}N_{Pe}\left(\frac{c}{a}\right)(\cosh\eta_o-\cos\xi)\left(V_\xi\frac{\partial c}{\partial\xi} + V_\eta\frac{\partial c}{\partial y}\right) - \left(\frac{c}{a}\right)^2\beta^2 C = 0$$

Using the dimensionless variables, of order of magnitude $\mathcal{O}(1)$ defined as

$$y^* = \frac{y}{\delta} = \mathcal{O}(1)$$
$$c = \mathcal{O}(1)$$
$$V_\xi^* = V_\xi\frac{1}{\delta} = \mathcal{O}(1) \tag{B-13}$$
$$V_y^* = V_y\frac{1}{\delta^2} = \mathcal{O}(1)$$
$$\frac{c}{a} = \mathcal{O}(1)$$

where δ is the dimensionless concentration boundary layer thickness, equation (B-12) becomes

$$\frac{(\cosh\eta_o-\cos\xi)^3}{\sin\xi}\left[\frac{\partial}{\partial\xi}\left(\frac{\sin\xi}{\cosh\eta_o-\cos\xi}\frac{\partial c}{\partial\xi}\right) + \frac{1}{\delta^2}\left(\frac{\sin\xi}{\cosh\eta_o-\cos\xi}\right)\frac{\partial^2 c}{\partial y^{*2}}\right] \tag{B-14}$$
$$-\frac{1}{2}N_{Pe}\left(\frac{c}{a}\right)(\cosh\eta_o-\cos\xi)\left(\delta V_\xi^*\frac{\partial c}{\partial\xi} + \delta V_y^*\frac{\partial c}{\partial y^*}\right)$$
$$-\left(\frac{c}{a}\right)^2\beta^2 C = 0$$

Therefore, we have

$$\frac{(\cosh\eta_o-\cos\xi)^3}{\sin\xi}\left[\delta^2\frac{\partial}{\partial\xi}\left(\frac{\sin\xi}{\cosh\eta_o-\cos\xi}\frac{\partial C}{\partial\xi}\right)+\frac{\sin\xi}{\cosh\eta_o-\cos\xi}\frac{\partial^2 C}{\partial y^{*2}}\right]$$
$$-\frac{1}{2}N_{Pe}\cdot\delta^3\left(\frac{c}{a}\right)(\cosh\eta_o-\cos\xi)\left(V_\xi^*\frac{\partial C}{\partial\xi}+V_y^*\frac{\partial C}{\partial y^*}\right) \qquad \text{(B-15)}$$
$$-\left(\frac{c}{a}\right)^2\delta^2\beta^2 C=0$$

Since

$$\delta^2\frac{\partial}{\partial\xi}\left(\frac{\sin\xi}{\cosh\eta_o-\cos\xi}\cdot\frac{\partial C}{\partial\xi}\right)=O(\delta^2) \qquad \text{(B-16)}$$

this term is negligible compared with the corresponding diffusion term in the y-direction. Furthermore, we note that

$$\delta=O\left(\frac{1}{N_{Pe}}\right)^{1/3} \qquad \text{(B-17)}$$

and

$$\delta=O\left(\frac{1}{\beta}\right) \qquad \text{(B-18)}$$

Note that $c/a = |\sinh\eta_o|$. Therefore, $c/a\longrightarrow 0$ as $\eta_o\longrightarrow 0$. This analysis assumed $c/a = O(1)$, otherwise the results of this analysis should be different. Equations (B-17) and (B-18) determine whether the reaction term or the convection term will dominate the mass transfer rate.

Equation (B-15) then becomes

$$(\cosh\eta_o-\cos\xi)^2\frac{\partial^2 C}{\partial y^{*2}}-\frac{1}{2}N_{Pe}\left(\frac{c}{a}\right)\delta^3(\cosh\eta_o-\cos\xi)\cdot \qquad \text{(B-19)}$$
$$\left(V_\xi^*\frac{\partial C}{\partial\xi}+V_\eta^*\frac{\partial C}{\partial y^*}\right)-\left(\frac{c}{a}\right)^2\delta^2\beta^2 C=0$$

and equation (IV-8) is then justified.

Appendix C: Creeping Flow Around Two Equal Solid Spheres Moving Parallel to Their Line of Centers

Stokes' free stream function (very far from the surface of the particle) for the fluid flowing past a single sphere (or any shape of particle) is given in spherical coordinates as

$$\psi_f = \tfrac{1}{2} r^2 \sin^2\theta \qquad \text{(C-1)}$$

In bipolar coordinates, equation (C-1) becomes

$$\psi_f = \tfrac{1}{2} c^2 \frac{\sin^2\xi}{(\cosh\eta - \cos\xi)^2} \qquad \text{(C-2)}$$

If we superimpose equation (C-2) and the stream function, equation (IV-39), given by Stimson and Jeffrey (77) we obtain the actual stream function to the problem in which the two spheres are fixed and the fluid streams past them with small constant velocity. This equation is

$$\psi = \tfrac{1}{2} c^2 \frac{\sin^2\xi}{(\cosh\eta - \cos\xi)^2} + (\cosh\eta - \cos\xi)^{-3/2} \sum_{n=1} U_n V_n \qquad \text{(C-3)}$$

The velocity expressions in terms of the derivatives of the stream function in orthogonal coordinates are given by equation (IV-42) as

$$V_{q_1} = h_2 h_3 \frac{\partial\psi}{\partial q_2} \quad ; \quad V_{q_2} = -h_3 h_1 \frac{\partial\psi}{\partial q_1} \qquad \text{(C-4)}$$

where the coordinates

$$q_1 = \xi \quad ; \quad q_2 = \eta \qquad \text{(C-5)}$$

and the metric coefficients

$$h_1 = h_2 = \frac{\cosh\eta - \cos\xi}{c}$$
$$h_3 = \frac{\cosh\eta - \cos\xi}{c \sin\xi} \qquad \text{(C-6)}$$

Therefore,

$$V_\xi = \frac{(\cosh\eta - \cos\xi)^2}{c^2 \sin\xi} \frac{\partial\psi}{\partial\eta}$$
$$V_\eta = -\frac{(\cosh\eta - \cos\xi)^2}{c^2 \sin\xi} \frac{\partial\psi}{\partial\xi} \qquad \text{(C-7)}$$

Equations (C-4), (C-5) and (C-6) give

$$V_\xi = -\frac{\sin\xi \sinh\eta}{(\cosh\eta - \cos\xi)} + \frac{\sin\xi}{c^2}\left[-1.5\,(\cosh\eta - \cos\xi)^{-0.5} \cdot \sinh\eta \left\{\sum_{n=1} U_n(\eta) \frac{V_n(\xi)}{\sin^2\xi}\right\}\right. \qquad \text{(C-8)}$$
$$\left. + (\cosh\eta - \cos\xi)^{0.5} \left\{\sum_{n=1} \frac{dU_n(\eta)}{d\eta} \frac{V_n(\xi)}{\sin^2\xi}\right\}\right]$$

$$V_\eta = \frac{1 - \cosh\eta\cos\xi}{(\cosh\eta - \cos\xi)} - \frac{1}{c^2}\left[-1.5\,(\cosh\eta - \cos\xi)^{-0.5} \cdot \sin^2\xi \left\{\sum_{n=1} U_n(\eta) \frac{V_n(\xi)}{\sin^2\xi}\right\}\right. \qquad \text{(C-9)}$$
$$\left. + (\cosh\eta - \cos\xi)^{0.5} \left\{\sum_{n=1} U_n(\eta) \frac{1}{\sin^2\xi} \frac{dV_n(\xi)}{d\xi}\right\}\right]$$

where

$$V_n(\xi) = P_{n-1}(\cos\xi) - P_{n+1}(\cos\xi) \quad ; \; P: \text{Legendre function}$$

$$u_n(\eta) = A_n \cosh(n-1)\eta + C_n \cosh\left(n+\tfrac{3}{2}\right)\eta$$

and

$$\frac{dV_n(\xi)}{d\xi} = \frac{1}{\sin\xi}\left[n\cdot\left\{ P_n(\cos\xi) - \cos\xi\, P_{n-1}(\cos\xi)\right\} \right.$$

$$\left. +(n+2)\left\{ \cos\xi\, P_{n+1}(\cos\xi) - P_{n+2}(\cos\xi)\right\}\right]$$

$$\frac{du_n(\eta)}{d\eta} = A_n\left(n-\tfrac{1}{2}\right)\sinh\left(n-\tfrac{1}{2}\right)\eta + C_n\left(n+\tfrac{3}{2}\right)\sinh\eta$$

Appendix D: Peaceman and Rachford's Method

If we write equation (IV-48) in the special form as

$$
\begin{aligned}
b_1 V_1 + c_1 V_2 &= d_1 \\
a_2 V_1 + b_2 V_2 + c_2 V_3 &= d_2 \\
a_3 V_2 + b_3 V_3 + c_3 V_4 &= d_3 \\
a_4 V_3 + b_4 V_4 + c_4 V_5 &= d_4 \qquad \text{(D-1)} \\
&\cdots \\
&\cdots \\
a_{M-2} V_{M-3} + b_{M-2} V_{M-2} + c_{M-2} V_{M-1} &= d_{M-2} \\
a_{M-1} V_{M-2} + b_{M-1} V_{M-1} &= d_{M-1}
\end{aligned}
$$

where

$$V_j = C_{i+1,j} \qquad ; \; j = 1, 2, 3 \cdots M-1$$

$$a_{j+1} = (\ell_3 + \ell_5)_j$$

$$b_j = (-\ell_2 - \ell_4 - \ell_6)_j$$

$$c_{j-1} = (\ell_1 - \ell_5)_j$$

$$d_1 = -2\,(\ell_3+\ell_5)_{j=1} + C^*_{i,1}\,(\ell_2-\ell_4+\ell_6)_{j=1} + C^*_{i,2}\,(-\ell_1+\ell_5)_{j=1}$$

$$d_j = C^*_{i,j-1}(-\ell_3-\ell_5)_j + C^*_{i,j}\,(\ell_2-\ell_4+\ell_6)_j + C^*_{i,j+1}(-\ell_1+\ell_5)_j \qquad \text{(D-2)}$$

$$d_{M-1} = C^*_{i,M-2}(-\ell_3-\ell_5)_{M-1} + C^*_{i,M-1}(\ell_2-\ell_4+\ell_6)_{M-1}$$

the solution of this set of equations is given by

$$V_{M-1} = \gamma_{M-1}$$

$$V_i = \gamma_i - \frac{c_i V_{i+1}}{\beta_i} \quad ; \; i = M-2, M-3 \cdots 1 \tag{D-3}$$

where

$$\beta_1 = b_1$$

$$\gamma_1 = \frac{d_1}{\beta_1}$$

$$\beta_i = b_i - \frac{a_i c_{i-1}}{\beta_{i-1}} \quad ; \; i = 2, 3 \cdots M-1 \tag{D-4}$$

$$\gamma_i = \frac{d_i - a_i \gamma_{i-1}}{\beta_i} \quad ; \; i = 2, 3 \cdots M-1$$

More details of this method is available in reference (9).

Appendix E: Corresponding Local and Overall Sherwood Numbers in Terms of Bipolar Coordinates

Recall the definition of the local and overall (up to X radians in spherical coordinates) Sherwood number

$$N_{Sh_\ell} = -2 \left.\frac{\partial C}{\partial y}\right|_{y=0} \tag{E-1}$$

$$N_{Sh_o} = -\int_0^X \left.\frac{\partial C}{\partial y}\right|_{y=0} \sin\theta \, d\theta \tag{E-2}$$

Since

$$\left.\frac{\partial C}{\partial y}\right|_{y=0} = \left.\frac{\partial C}{\partial \eta}\right|_{\eta=\gamma_0} \left.\frac{\partial \eta}{\partial y}\right|_{y=0} + \left.\frac{\partial C}{\partial \xi}\right|_{\xi} \left.\frac{\partial \xi}{\partial y}\right|_{y=0} \tag{E-3}$$

where ξ and η are bipolar coordinates, this expression is convenient for transforming $\partial C/\partial y|_{y=0}$ into cylindrical coordinates and then into spherical coordinates and finally into bipolar coordinates.

$$\eta = \ln \frac{R_2}{R_1} \tag{E-4}$$

therefore,

$$\left.\frac{\partial \eta}{\partial y}\right|_{y=0} = \left.\frac{\partial \eta}{\partial r}\right|_{r=1} \tag{E-5}$$

Also

$$\xi = \cos^{-1}\left(\frac{R_1^2 + R_2^2 - 4c^2}{2R_1R_2}\right) \tag{E-6}$$

so that

$$\left.\frac{\partial \xi}{\partial \eta}\right|_{\eta=0} = \left.\frac{\partial \xi}{\partial r}\right|_{r=1} \tag{E-7}$$

For $Y_o > 0$

$$\left.\frac{\partial \eta}{\partial \eta}\right|_{\eta=0} = \frac{1+(d+c)\cos\theta}{(\cos\theta+d+c)^2+\sin^2\theta} - \frac{1+(d-c)\cos\theta}{(\cos\theta+d-c)^2+\sin^2\theta} \tag{E-8}$$

$$\left.\frac{\partial \xi}{\partial \eta}\right|_{\eta=0} = \frac{-1}{\sin\xi}\left[\frac{2(1+d\cos\theta)}{\left\{(\cos\theta+d+c)^2+\sin^2\theta\right\}^{1/2}\left\{(\cos\theta+d-c)^2+\sin^2\theta\right\}^{1/2}}\right. \tag{E-9}$$

$$\left. -\cos\xi\left\{\frac{1+(d+c)\cos\theta}{(\cos\theta+d+c)^2+\sin^2\theta} + \frac{1+(d-c)\cos\theta}{(\cos\theta+d-c)^2+\sin^2\theta}\right\}\right]$$

where

$$\sin\theta = \rho = \frac{c\sin\xi}{\cosh(Y_o) - \cos\xi}$$

$$\cos\theta = z - d = \frac{c\sinh(Y_o)}{\cosh(Y_o) - \cos\xi} - d$$

For $Y_o < 0$, equations (E-3), (E-8) and (E-9) hold if we change d = -d.

Appendix F: Comparisons with Goddard and Acrivos (23) solutions of mass transfer with first-order homogeneous chemical reaction

Goddard and Acrivos treated the problem by considering wedge type flows over a flat plate. The continuity equation which applies to these types of flows is

$$\frac{\partial V_x}{\partial x} + \frac{\partial V_y}{\partial y} = 0 \qquad \text{(F-1)}$$

This equation is different from equation (IV-22), which is the simplified continuity equation derived for the spherical geometry investigated here. Of course, we could apply their techniques using the flow field described in this study. However, as it is noted in the review section, their results were not good for large values of the perturbed parameters. The applicable range of their solution is very small, but their techniques are interesting. Therefore, an approximate comparison of their results with the results obtained here was attempted.

The comparisons are presented in two ways. One involves the differences of the velocity profiles between the two studies. The other is the differences in the mass transfer rate obtained at very fast reaction rate for the two studies. For a very fast reaction, the mass transfer rate is dominated by reaction term (of equation IV-5) and the hydrodynamic behavior is not too important. The latter comparison will give a qualitative idea of the applicable range of the Goddard and Acrivos (23) solution.

i) Comparison of velocity profiles in the problem

The velocity profiles given by Goddard and Acrivos (23) assumed that

$$V_x = 2\psi(x)\, y \qquad \text{(F-2)}$$

V_y is then derived from the continuity equation, equation (F-1) and is given as

$$V_y = -\psi'(x)\, y^2 \qquad \text{(F-3)}$$

For the case of stagnation flow, the velocity profiles were given as

$$V_x = 2b \times y \qquad \text{(F-4)}$$

and

$$V_y = -b\, y^2 \qquad \text{(F-5)}$$

where b is a constant.

The velocity profiles used in this study for the case of first-order homogeneous chemical reaction around single spheres or in multiparticle systems are given in the form of

$$V_x = g(x)\, y \qquad \text{(F-6)}$$

and

$$V_y = -\frac{y^2}{2\sin x}\,\frac{d}{dx}\left[g(x)\sin x\right] \qquad \text{(F-7)}$$

In the region around the front stagnation point, the velocity profiles can be derived from these two equations by letting $x \rightarrow 0$. For the case of flow around a single sphere, the creeping velocity profiles around the front stagnation point are

$$V_x = \frac{3}{2} x y \qquad \text{(F-8)}$$

and

$$V_y = -\frac{3}{2} y^2 \qquad \text{(F-9)}$$

Equations (F-4), (F-5), and (F-5), (F-9) show the difference in the velocity profiles used in the problem. This prevents us from obtaining even a qualitative comparison between the results at slow reaction rates because the convection terms are very important when the reaction rate is very slow.

ii) Comparison of mass transfer rate for fast reaction

Due to the velocity profile differences in the two studies, an exact comparison is impossible. However, as was mentioned previously, a qualitative comparison is possible. To simplify the mathematics involved, we present only the case of flow around a single sphere at low Reynolds number.

In order to make the comparison, we must first compare the notation that was used by Goddard and Acrivos with that in this study. This is most readily

done by comparing equation (4.2) of their paper with equation (IV-53) of this study which are equivalent.

This study

$$\frac{\partial^2 C}{\partial y'^2} - \frac{N_{Pe}}{2\beta^3}\left[g(x)\,y'\frac{\partial C}{\partial x} - \frac{y'^2}{2\sin x}\frac{d}{dx}\left[g(x)\sin x\right]\frac{\partial C}{\partial y'}\right] - C = 0 \qquad \text{(F-10)}$$

Goddard and Acrivos

$$\frac{\partial^2 C}{\partial \omega^2} - \epsilon\left[\beta\omega\frac{\partial C}{\partial \xi} - \frac{1}{2}\beta'\omega^2\frac{\partial C}{\partial \omega}\right] - \theta = 0 \qquad \text{(F-11)}$$

Equivalent Notation

$$y' = \omega$$
$$x = \xi$$
$$c = \theta$$
$$\frac{N_{Pe}}{\beta^3} = \epsilon$$
$$\tfrac{1}{2}g(x) \doteq \beta$$

The results for diffusion with very rapid homogeneous first-order reaction as given by Goddard and Acrivos is

$$-\frac{1}{\sqrt{R}}\left(\frac{\partial\theta}{\partial y}\right)_{y=0} = 1 + \frac{1}{8}\beta' R^{-1/2} - \frac{1}{128}\left(18\beta\beta'' - \beta'^2\right)R^{-1} + O\left(R^{-3/2}\right) \qquad \text{(F-12)}$$

Substituting the notation of this study into equation (F-12) we obtain

$$\frac{-\frac{\partial C}{\partial y}\Big|_{y=0}}{\beta} = 1 + \frac{1}{16}g'(x)\frac{N_{Pe}}{\beta^3} - \frac{1}{512}\left[18\,g''(x) - \left[g(x)\right]^2\right]\left(\frac{N_{Pe}}{\beta^3}\right)^2 + \cdots \qquad \text{(F-13)}$$

For the case of Stokes' flow:

$$g(x) = \frac{3}{2} \sin x$$

$$g'(x) = \frac{3}{2} \cos x$$

$$g''(x) = -\frac{3}{2} \sin x$$

so that equation (F-13) becomes

$$\frac{-\left(\frac{\partial C}{\partial y}\right)_{y=0}}{\beta} = 1 + \frac{3}{32} \cos x \, \frac{N_{Pe}}{\beta^3} + \frac{9}{2048}(1+17\sin^2 x)\left(\frac{N_{Pe}}{\beta^3}\right)^2 + \cdots \quad \text{(F-14)}$$

Since

$$N_{Sh_0} = \int_0^{\pi} -\left(\frac{\partial C}{\partial y}\right)_{y=0} \sin x \, dx \quad \text{(F-15)}$$

we obtain

$$\frac{N_{Sh_0}}{\beta} = 2 + \frac{111}{1024}\left(\frac{N_{Pe}}{\beta^3}\right)^2 + \mathcal{O}\left(\frac{N_{Pe}}{\beta^3}\right)^3$$

or

$$\frac{N_{Sh_0}}{\beta} = 2 + \frac{111}{1024}\left(\frac{N_{Pe}^{1/3}}{\beta}\right)^6 \quad \text{(F-16)}$$

Equation (F-16) has been plotted in Figure 5 for values of the parameter $N_{Pe}^{1/3}/\beta$ between 0.5 and 2.0. As seen by the figure the asymptotic solution deviates from the numerical solution quite rapidly as $N_{Pe}^{1/3}/\beta$ increases.

Appendix G. Corresponding Spherical Bipolar Angles

To obtain a better picture of the bipolar angles, ξ, on the surface of the two spheres system, the bipolar angles were transformed into spherical angles, θ, according to

$$\theta = \cos^{-1}\left(\frac{c \sinh \gamma_o}{\cosh \gamma_o - \cos \xi} - d \right)$$

for $Y_o > 0$ (upper sphere) and

$$\theta = \cos^{-1}\left(\frac{c \sinh \gamma_o}{\cosh \gamma_o - \cos \xi} + d \right)$$

for $Y_o < 0$ (lower sphere). These corresponding values are shown in Tables G-1 and G-2.

TABLE G-1 CORRESPONDING SPHERICAL ANGLES TO BI-POLAR ANGLES ON THE SURFACE OF THE UPPER SPHERE

RADIAN...SPHERICAL ANGLES

BI-THAI..BIPOLAR ANGLES

	YO= 0.1	YO= 0.2	YO= 0.5	YO= 0.8	YO= 1.0	YO= 2.0	YO= 3.0	YO= 4.0	YO= 5.0	YO= 6.0
RADIANS	BI-THAI	BI-THAI	BI-THAI	BI-THAI	BI-THAI	BI-THAI	BI-THAI	BI-THAI	BI-THAI	BI-THAI
0.08727	0.00436	0.00870	0.02139	0.03318	0.04035	0.06648	0.07900	0.08414	0.08612	0.08689
0.17453	0.00874	0.01744	0.04285	0.06646	0.08082	0.13307	0.15805	0.16829	0.17222	0.17370
0.26180	0.01315	0.02624	0.06447	0.09996	0.12153	0.19986	0.23721	0.25248	0.25834	0.26053
0.34907	0.01762	0.03514	0.08632	0.13379	0.16261	0.26698	0.31653	0.33675	0.34449	0.34738
0.43633	0.02215	0.04418	0.10849	0.16807	0.20419	0.33453	0.39607	0.42111	0.43067	0.43425
0.52360	0.02677	0.05340	0.13106	0.20291	0.24639	0.40261	0.47588	0.50557	0.51690	0.52114
0.61086	0.03150	0.06283	0.15414	0.23846	0.28937	0.47133	0.55600	0.59017	0.60313	0.60803
0.69813	0.03636	0.07252	0.17782	0.27484	0.33327	0.54082	0.63650	0.67491	0.68952	0.69496
0.78540	0.04138	0.08252	0.20221	0.31220	0.37825	0.61116	0.71741	0.75983	0.77592	0.78190
0.87266	0.04658	0.09289	0.22743	0.35071	0.42449	0.68249	0.79878	0.84493	0.86239	0.86888
0.95993	0.05200	0.10367	0.25362	0.39054	0.47215	0.75490	0.88067	0.93024	0.94894	0.95588
1.04720	0.05767	0.11496	0.28094	0.43189	0.52146	0.82852	0.96311	1.01576	1.03557	1.04291
1.13446	0.06363	0.12682	0.30956	0.47497	0.57262	0.90346	1.04614	1.10152	1.12229	1.12998
1.22173	0.06993	0.13935	0.33968	0.52004	0.62589	0.97982	1.12979	1.18753	1.20910	1.21708
1.30900	0.07663	0.15266	0.37153	0.56736	0.68152	1.05773	1.21411	1.27378	1.29660	1.30421
1.39626	0.08379	0.16687	0.40538	0.61725	0.73982	1.13728	1.29912	1.36031	1.38301	1.39138
1.48353	0.09149	0.18215	0.44154	0.67007	0.80112	1.21859	1.38484	1.44710	1.47011	1.47859
1.57079	0.09983	0.19868	0.48038	0.72620	0.86577	1.30176	1.47130	1.53417	1.55732	1.56584
1.65806	0.10893	0.21668	0.52235	0.78613	0.93418	1.38683	1.55852	1.62152	1.64463	1.65312
1.74533	0.11894	0.23645	0.56799	0.85037	1.00681	1.47403	1.64649	1.70914	1.73204	1.74044
1.83259	0.13003	0.25833	0.61792	0.91953	1.08413	1.56330	1.73523	1.79705	1.81956	1.82780
1.91986	0.14245	0.28278	0.67296	0.99432	1.16670	1.65473	1.82474	1.88523	1.90717	1.91520
2.00713	0.15652	0.31038	0.73405	1.07554	1.25511	1.74839	1.91501	1.97367	1.99488	2.00263
2.09439	0.17263	0.34189	0.80240	1.16408	1.34998	1.84428	2.00602	2.06238	2.08269	2.09010
2.18166	0.19135	0.37834	0.87951	1.26099	1.45197	1.94243	2.09774	2.15134	2.17058	2.17759
2.26893	0.21346	0.42114	0.96725	1.36740	1.56177	2.04279	2.19017	2.24053	2.25856	2.26513
2.35619	0.24006	0.47226	1.06797	1.48456	1.68001	2.14533	2.28325	2.32995	2.34662	2.35268
2.44346	0.27281	0.53456	1.18462	1.61374	1.80730	2.24996	2.37694	2.41958	2.43476	2.44027
2.53073	0.31428	0.61233	1.32084	1.75624	1.94410	2.35656	2.47120	2.50940	2.52295	2.52788
2.61799	0.36866	0.71221	1.48104	1.91314	2.09068	2.46499	2.56597	2.59938	2.61122	2.61551
2.70526	0.44399	0.84499	1.67025	2.08521	2.24698	2.57506	2.66119	2.68952	2.69953	2.70317
2.79252	0.55218	1.02604	1.89362	2.27258	2.41256	2.68656	2.75680	2.77973	2.78789	2.79085
2.87979	0.72536	1.29599	2.15514	2.47448	2.58651	2.79924	2.85272	2.87014	2.87629	2.87852
2.96706	1.03767	1.70075	2.45541	2.68895	2.76737	2.91284	2.94838	2.96058	2.96471	2.96622
3.05432	1.70510	2.31580	2.78875	2.91276	2.95319	3.02706	3.04519	3.05108	3.05315	3.05393

TABLE G-2CORRESPONDING SPHERICAL ANGLES TO BI-POLAR ANGLES ON THE SURFACE OF THE LOWER SPHERE

RADIAN...SPHERICAL ANGLES

BI-THAI..BIPOLAR ANGLES

	Y0=-0.1	Y0=-0.2	Y0=-0.5	Y0=-0.8	Y0=-1.0	Y0=-2.0	Y0=-3.0	Y0=-4.0	Y0=-5.0	Y0=-6.0
RADIANS	BI-THAI	BI-THAI	BI-THAI	BI-THAI	BI-THAI	BI-THAI	BI-THAI	BI-THAI	BI-THAI	BI-THAI
0.08727	1.70513	2.31583	2.78877	2.91277	2.95319	3.02706	3.04520	3.05108	3.05315	3.05393
0.17453	1.03769	1.70077	2.45542	2.68895	2.76738	2.91204	2.94888	2.96058	2.96471	2.96622
0.26180	0.72537	1.29600	2.15515	2.47449	2.58652	2.79925	2.85272	2.87014	2.87629	2.87852
0.34907	0.55218	1.02895	1.89363	2.27259	2.41257	2.68656	2.75680	2.77978	2.78789	2.79085
0.43633	0.44329	0.84500	1.67026	2.08522	2.24698	2.57506	2.66120	2.68952	2.69953	2.70317
0.52360	0.36866	0.71222	1.48105	1.91315	2.09068	2.46499	2.56598	2.59939	2.61122	2.61552
0.61086	0.31428	0.61233	1.32085	1.75624	1.94411	2.35656	2.47120	2.50940	2.52296	2.52789
0.69813	0.27281	0.53457	1.18462	1.61375	1.80731	2.24996	2.37694	2.41958	2.43476	2.44027
0.78540	0.24006	0.47226	1.06798	1.48456	1.68002	2.14533	2.28325	2.32996	2.34662	2.35269
0.87266	0.21346	0.42114	0.96726	1.36741	1.56177	2.04280	2.19017	2.24054	2.25856	2.26513
0.95993	0.19135	0.37834	0.87952	1.26099	1.45198	1.94243	2.09775	2.15134	2.17058	2.17760
1.04720	0.17263	0.34189	0.80241	1.16408	1.34998	1.84429	2.00602	2.06238	2.08269	2.09010
1.13446	0.15652	0.31038	0.73405	1.07554	1.25511	1.74839	1.91501	1.97367	1.99488	2.00264
1.22173	0.14245	0.28278	0.67296	0.99433	1.16671	1.65474	1.82475	1.88523	1.90717	1.91520
1.30900	0.13003	0.25833	0.61793	0.91954	1.08413	1.56330	1.73524	1.79705	1.81956	1.82781
1.39626	0.11894	0.23645	0.56799	0.85037	1.00681	1.47403	1.64649	1.70915	1.73205	1.74045
1.48353	0.10893	0.21669	0.52235	0.78613	0.93418	1.38688	1.55852	1.62152	1.64463	1.65313
1.57079	0.09983	0.19868	0.48038	0.72621	0.86577	1.30176	1.47131	1.53417	1.55732	1.56584
1.65806	0.09149	0.18215	0.44154	0.67007	0.80112	1.21859	1.38484	1.44710	1.47012	1.47860
1.74533	0.08379	0.16687	0.40538	0.61726	0.73983	1.13728	1.29912	1.36031	1.38301	1.39139
1.83259	0.07663	0.15266	0.37153	0.56737	0.68153	1.05773	1.21411	1.27379	1.29601	1.30422
1.91986	0.06995	0.13935	0.33968	0.52004	0.62589	0.97982	1.12979	1.18753	1.20910	1.21708
2.00713	0.06363	0.12682	0.30957	0.47497	0.57263	0.90346	1.04614	1.10152	1.12229	1.12998
2.09439	0.05767	0.11496	0.28095	0.43189	0.52146	0.82852	0.96311	1.01577	1.03557	1.04291
2.18166	0.05200	0.10368	0.25363	0.39054	0.47216	0.75491	0.88067	0.93024	0.94894	0.95588
2.26893	0.04658	0.09289	0.22743	0.35071	0.42449	0.68249	0.79879	0.84493	0.86239	0.86888
2.35619	0.04138	0.08252	0.20221	0.31220	0.37826	0.61117	0.71741	0.75983	0.77592	0.78190
2.44346	0.03636	0.07252	0.17782	0.27484	0.33328	0.54082	0.63650	0.67491	0.68952	0.69496
2.53073	0.03150	0.06283	0.15414	0.23846	0.28937	0.47134	0.55601	0.59017	0.60318	0.60804
2.61799	0.02677	0.05340	0.13106	0.20292	0.24639	0.40261	0.47588	0.50557	0.51690	0.52113
2.70526	0.02215	0.04418	0.10849	0.16807	0.20419	0.33453	0.39608	0.42111	0.43068	0.43425
2.79252	0.01762	0.03515	0.08632	0.13379	0.16261	0.26698	0.31654	0.33675	0.34449	0.34739
2.87979	0.01316	0.02624	0.06447	0.09996	0.12153	0.19987	0.23721	0.25249	0.25834	0.26054
2.96706	0.00874	0.01744	0.04285	0.06646	0.08082	0.13307	0.15805	0.16829	0.17223	0.17370
3.05432	0.00437	0.00870	0.02139	0.03318	0.04035	0.06648	0.07900	0.08414	0.08612	0.08689

Appendix H. Method of Data Analysis

The data available for each run in this study consisted of run time length, Δt, the weight loss of the test sphere, ΔW, the initial, $\gamma_I(\theta)$, and final, $\gamma_F(\theta)$, radii around the sphere surface as measured from the front stagnation point at each 10 degree location, the volumetric flow rate, G, and the run temperature, T.

From the data of run temperature, it was possible to determine the fluid density, ρ_f, and viscosity, μ_f, the solid density, ρ_s, the equilibrium solubility, c*, the diffusivity, $\mathcal{D}$, and the Schmidt number, N_{Sc}, of the solid (benzoic acid) in the liquid (H_2O) system of this investigation. From the data of the initial and final radii around the sphere surface, the initial and final particle average radius, surface area, volume and surface average radius were computed.

The local and overall mass transfer rates were defined as the local and overall amount of solute (solid) transferred into the liquid per unit time. These were related to the mass transfer driving force (concentration difference), resistance (particle surface area), and mass transfer coefficient and were expressed in terms of the mass flux as

$$N_{a_o} = \frac{\Delta W_o}{\Delta t} = \frac{\Delta V_o \times \rho_s}{\Delta t} = k_o \times A_o \times (C^* - C_o) \qquad \text{(H-1)}$$

$$N_{a_\ell} = \frac{\Delta W_\ell}{\Delta t} = \frac{\Delta V_\ell \times \rho_s}{\Delta t} = k_\ell \times A_\ell \times (C^* - C_o) \qquad \text{(H-2)}$$

where C_o is the bulk stream concentration and is negligible in this investigation.

The mass transfer rates were expressed in terms of the local and overall Sherwood numbers. These were defined as

$$N_{Sh_o} = \frac{K_o \cdot 2 r_{sar}}{\mathcal{D} \rho_f} = \frac{2}{\mathcal{D} \rho_f (C^* - C_o) \Delta t} \frac{\Delta W_o r_{sar}}{A_o} \quad \text{(H-3)}$$

$$N_{Sh_\ell} = \frac{K_\ell \cdot 2 r_a}{\mathcal{D} \cdot \rho_f} = \frac{2}{\mathcal{D} \rho_f (C^* - C_o) \Delta t} \frac{\Delta V_\ell \cdot \rho_s \cdot r_\ell}{A_\ell} \quad \text{(H-4)}$$

To correlate data, the particle Reynolds and Peclet numbers were used. These were defined as

$$N_{Re} = \frac{2 r_{sar} V_c \rho_f}{\mu_f} \quad \text{(H-5)}$$

$$N_{Pe} = N_{Re} N_{Sc} \quad \text{(H-6)}$$

Average values measured before and after the run of the local and overall surface areas, local radii, and surface average radii were used to obtain the particle Reynolds number, Peclet number, and local and overall Sherwood numbers.

The centerline velocity approaching the test sphere was used in the definition of the particle Reynolds number. V_c was defined as

$$V_c = \frac{\int_0^{2\pi} \int_0^{r=0.25''} V_z \, r \, dr \, d\theta}{\int_0^{2\pi} \int_0^{r=0.25''} r \, dr \, d\theta} = \frac{Q}{\pi R^2} \left(2 - \frac{r^2}{R^2}\right) \quad \text{(H-7)}$$

$$V_c = 1.99 \frac{Q}{\pi R^2} \quad \text{(H-8)}$$

where Q is volumetric flow rate and R is the radius of the test section (water tunnel).

Since the radius of the sphere could not be measured at the rear stagnation point (because of the attached rod) the average value of the sphere radius measured at 170° and 190° was taken as the radius at 180°. The average local radii, $r_\ell(\theta)$, the diminution, $\Delta r_\ell(\theta)$ and percentage diminutionm, $\% \Delta V_\ell(\theta)$, as functions of angular position θ were obtained by

$$r_\ell(\theta) = \frac{r_I(\theta) + r_F(\theta)}{2} \qquad \text{(H-9)}$$

$$\Delta r_\ell(\theta) = r_I(\theta) - r_F(\theta) \qquad \text{(H-10)}$$

and

$$\%\Delta r_\ell(\theta) = \frac{\Delta r_\ell(\theta)}{r_I(\theta)} \times 100\,\% \qquad \text{(H-11)}$$

The approximate overall initial and final surface area and volume for the sphere were obtained by integrating the measured radius profile from 0 to 2π using Simpson's rule over a 20 degree section as

$$A = \int_0^{\theta=\pi}\int_0^{\phi=2\pi} r^2 \sin\theta \, d\phi \, d\theta$$

$$= 2\pi \int_0^{\theta=\pi} r^2 \sin\theta \, d\theta \qquad \text{(H-12)}$$

$$= 2\pi \cdot \frac{h}{6}\,\frac{1}{2}\left[2\sum_{k=0}^{17} r_{2k}^2 \left|\sin\theta_{2k}\right| + 4\sum_{k=0}^{17} r_{2k+1}^2 \left|\sin\theta_{2k+1}\right| - r_0^2\left|\sin\theta_0\right| + r_{36}^2\left|\sin\theta_{36}\right|\right]$$

and

$$V = \int_0^{\theta=\pi} \int_0^{\phi=2\pi} \int_0^{r} r^2 \sin\theta \; dr \, d\phi \, d\theta$$

$$= \frac{2}{3}\pi \int_0^{\theta=\pi} r^3 \sin\theta \; d\theta$$

$$= \frac{2}{3}\pi \frac{h}{6} \frac{1}{2} \left[2 \sum_{k=0}^{17} r_{2k}^3 \left|\sin\theta_{2k}\right| + 4 \sum_{k=0}^{17} r_{2k+1}^3 \left|\sin\theta_{2k+1}\right| \right. \qquad \text{(H-13)}$$

$$\left. - r_0^3 \left|\sin\theta_0\right| + r_{36}^3 \left|\sin\theta_{36}\right| \right]$$

where h = 3.14159/9 and k is the index of angle location. The initial and final surface average radius was obtained using

$$r_{sar} = \sqrt{\frac{A}{4\pi}} \qquad \text{(H-14)}$$

These values were then averaged to obtain the average surface average radius to be used in calculating the Reynolds, Peclet and overall Sherwood numbers.

The local initial and final surface area and volume for the location $_i$ were obtained by integrating the measured radii profile from θ_{i-1} to θ_{i+1} using Simpson's rule over its particular 20 degree sector as

$$A_l = \int_{\theta=\theta_{i-1}}^{\theta=\theta_{i+1}} \int_0^{\phi=2\pi} r^2 \sin\theta \; d\phi \; d\theta$$

$$\simeq 2\pi \int_{\theta=\theta_{i-1}}^{\theta=\theta_{i+1}} r^2 \sin\theta \; d\theta \qquad \text{(H-15)}$$

$$= 2\pi \frac{h}{6} \left[r_{\theta_{i-1}}^2 \left|\sin\theta_{i-1}\right| + 4\, r_{\theta_i}^2 \left|\sin\theta_i\right| + r_{\theta_{i+1}}^2 \left|\sin\theta_{i+1}\right| \right]$$

and

$$V_\ell = \int_{\theta=\theta_{i-1}}^{\theta=\theta_{i+1}} \int_0^{\phi=2\pi} \int_0^{r} r^2 \sin\theta \, dr \, d\phi \, d\theta$$

$$= \frac{2\pi}{3} \int_{\theta=\theta_{i-1}}^{\theta=\theta_{i+1}} r^3 \sin\theta \, d\theta \qquad \text{(H-16)}$$

$$= \frac{2\pi}{3} \frac{h}{6} \left[r_{\theta_{i-1}}^3 |\sin\theta_{i-1}| + 4 r_{\theta_i}^3 |\sin\theta_i| + r_{\theta_{i+1}}^3 |\sin\theta_{i+1}| \right]$$

where h = 3.14159/9. The local volume difference which appears in equation (H-3) is the difference between the initial and final values. The density of benzoic acid used in equation (H-4) to compute the local Sherwood numbers was taken as the book value of 1.266 g/cm^3 (62).

In order to check the results and the method of calculation, the density of the solid was computed for each run from the particle weight loss and the total volume change. The computed density was then compared with the particle density measured by using a pycnometer (1.256 gm/cm^3) and the book value (1.266 g/cm^3). The computed densities were all within 15% of the book value. The overall Sherwood numbers were also computed from the local Sherwood numbers using a numerical integration (Simpson's rule) over the surface of the sphere by

$$N_{Sh_{o,INT}} = \int_0^{\pi} \frac{N_{Sh_\ell}}{2} \sin\theta \, d\theta$$

$$= \frac{h}{6} \frac{1}{2} \left[2 \sum_{k=0}^{8} N_{Sh_\ell, \theta_{2k}} \sin(2k\theta) \right. \qquad \text{(H-17)}$$

$$+ 4 \sum_{k=0}^{8} N_{Sh_\ell, \theta_{2k+1}} \sin(2k\theta + \theta)$$

$$\left. - N_{Sh_\ell, \theta_0} |\sin\theta_0| + N_{Sh_\ell, \theta_{18}} |\sin\theta_{18}| \right]$$

and compared with that based on total weight loss. These values were also all within 15% of the value based on weight loss (see table K-1 in Appendix K). The overall Sherwood numbers presented in the correlations and the figures were based on the measured overall weight loss.

Appendix I. Physical Properties of the Chemical Systems

The physical properties of the chemical systems used in the experimental part of this investigation are summarized in the following table. Included are the density and viscosity of water and the equilibrium solubility, diffusivity, and the Schmidt number of benzoic acid in water.

The physical properties of dilute sodium hydroxide solution were assumed the same as that of pure water.

Table I-1: Physical Properties of Benzoic Acid and Water

Temperature °C	C*: Solubility of Benzoic Acid in water, gm. per liter of solution (76)	$\mathcal{D}$: Diffusivity of Benzoic Acid in water, $in.^2$ per hr. x 10^3 (60)	N_{Sc}: Schmidt number of Benzoic Acid in water (60)	μ_f: Viscosity of water, centipose (62)	ρ_f: Density of water, gm/cm^3 (62)
24.0	3.2425	5.00	1030	0.9142	0.9973
24.1	3.2518				0.9973
24.2	3.2611				0.9973
24.3	3.2704				0.9973
24.4	3.2798				0.9972
24.5	3.2892	5.17	1000		0.9972
24.6	3.2986				0.9972
24.7	3.3080				0.9972
24.8	3.3174				0.9971
24.9	3.3269				0.9971
25.0	3.3364	5.25	975	0.8937	0.9971
25.1	3.3459				0.9970
25.2	3.3554				0.9970
25.3	3.3649				0.9970
25.4	3.3745				0.9970
25.5	3.3841	5.31	945		0.9969
25.6	3.3937				0.9969
25.7	3.4033				0.9969
25.8	3.4130				0.9969
25.9	3.4226				0.9968
26.0	3.4323	5.43	920	0.8737	0.9968
26.1	3.4420				0.9968
26.2	3.4518				0.9968
26.3	3.4615				0.9967
26.4	3.4713				0.9967
26.5	3.4811	5.52	890		0.9967

Appendix J. List of Computer Programs

All the programs presented here are written in the MAD language for the IBM 7040 at the City College. The main programs are given first. Subroutines are given at the end of this appendix.

A. Mass transfer with first order homogeneous chemical reactions around single spheres and in multiparticle systems.

Four programs have been written with specified initial stepsize in the radial direction, $\Delta\psi_0$ (as DELY), numbers of steps in the radial and angular directions (as M and N), and stepsize parameter h (see equation IV-46) (as H).

For the case of low Reynolds number flow around single spheres and in multiparticle systems, the Peclet numbers, N_{P_e} (as PE), the reaction rate constants, β (as B) should be specified. For the case of high Reynold number flow around single spheres, the Reynolds number, N_{R_e} (as RE) and the Schmidt number, N_{S_c} (as SC) and reaction rate constant should be specified. Output obtained from these computations consist of the concentration profiles as well as the local and overall Sherwood numbers.

To obtain the results using the generalized parameters, $N_{P_e}{}^{1/3}/\beta$ and $N_{R_e}{}^{\frac{1}{2}}\, N_{S_c}{}^{1/3}/\beta$, values of N_{P_e} and N_{S_c} are not necessary to be specified. The input data were $N_{P_e}{}^{1/3}/\beta$ (as PEB) and $N_{R_e}{}^{1/2}\, N_{S_c}{}^{1/3}/\beta$ (as RESCTS) for low Reynolds number and high Reynolds number flow, respectively. Output obtained from these computation were the local and overall values of N_{sh}/β .

Velocity terms, V_x and V_y, were included as L4(J) and L5(J) in the program. For any other particular velocity profiles,

it is only necessary to change the expressions of L4(J) and L5(J). L4(J) and L5(J) had the standard form of

$$L4(J) = V_x(J).\ L44$$

$$L5(J) = V_y(J).\ L55(J)$$

where L44 and L55(j) are computed in the previous steps of the calculation.

The four programs are listed below.

1. Single spheres and multiparticle systems at low Reynolds number.
2. Single spheres at high Reynold numbers.
3. Use of generalized parameter $N_{P_e}^{1/3}/\beta$ for single spheres and multiparticle systems at low Reynolds number.
4. Use of generalized parameter $N_{R_e}^{1/2} N_{S_c}^{1/3}/\beta$ for single spheres at high Reynolds number.

1. Single spheres and multiparticle systems at low Reynolds number.

```
$COMPILE MAD, IBLDR

. . . .
. . . .      CRANK-NICOLSON METHOD
. . . .      MASS TRANSFER WITH FIRST ORDER HOMOGENEREOUS CHEMICAL
. . . .      REACTIONS
. . . .      SINGLE SPHERES AND MULTIPARTICLE SYSTEMS AT LOW RE
. . . .      N...NUMBER OF STEPS IN ANGULAR DIRECTION
. . . .      M...NUMBER OF STEPS IN RADIAL DIRECTION
. . . .
             INTEGER I,J,K,L,M,NN,N
             DIMENSION C(90),D(90),P(90),Q(90),R(90),V(90),L1(90),
            1 L2(90),L3(90),L55(90),L4(90),L5(90),IP(90),IQ(90),
            2 IR(90),Y(90),SHL(1000)
. . . .
. . . .
             N=90
             DELY=0.00005
             H=1.5
             PE=125.
             M=90
. . . .
             C(1)=1.
             C(M)=0.
             DELX=3.1416/N
             L44=PE/(2.*DELX)
             L4(1)=0.
             L5(1)=0.
             THROUGH ONE, FOR J=2,1,J.G.M
             L1(J)=1./(DELY*DELY*H.P.(2*J-3.)*(H+1.))
             L2(J)=1./(DELY*DELY*H.P.(2*J-3.))
             L3(J)=1./(DELY*DELY*H.P.(2*J-4.)*(H+1.))
             L55(J)=PE      /(4.*DELY*H.P.(J-2)*(H+1.))
             Y(J)=DELY*(H.P.(J-1)-1.)/(H-1.)
ONE          CONTINUE
START        PRINT COMMENT $1$
             READ AND PRINT DATA
             SUM=0.
             THROUGH TWO, FOR I=1,1,I.G.N
             X=DELX*(I-0.5)
             M=30
```

```
                WHENEVER X.G.2.60
                M=M+5
                END OF CONDITIONAL
                WHENEVER X.G.2.7
                M=M+5
                END OF CONDITIONAL
                WHENEVER X.G.2.8
                M=M+5
                END OF CONDITIONAL
                WHENEVER X.G.3.0
                M=M+5
                END OF CONDITIONAL
                WHENEVER X.G.3.05
                M=M+5
                END OF CONDITIONAL
                WHENEVER X.G.3.1
                M=M+5
                END OF CONDITIONAL
                WHENEVER X.G.3.12
                M=M+10
                END OF CONDITIONAL
                WHENEVER X.G.3.13
                M=M+10
                END OF CONDITIONAL
                WHENEVER X.G.3.131
                M=M+10
                END OF CONDITIONAL
                THROUGH TWO1,FOR J=2,1,J.G.M
                L4(J)=1.5*SIN.(X)*Y(J)*L44
                L5(J)=-1.5*COS.(X)*(J).P.2.*L55(J)
TWO1            CONTINUE
. . . .
. . . .
                PRINT RESULTS PE,B,X,SUM
                PRINT COMMENT $ $
                L6=B*B/2.
                WHENEVER I.E.1
                THROUGH BB, FOR J=2,1,J.G.M-1
                IP(J)=2.*(L3(J)+L5(J))
                IQ(J)=-2.*(L2(J)+L6)
                IR(J)=2.*(L1(J)-L5(J))
BB              C(J)=0.
                THROUGH BBB, FOR L=1,1,L.G. 400
                THROUGH BBBB, FOR J=2,1,J.G.M-1
```

```
          C(J)=(C(J-1)*IP(J)+C(J+1)*IR(J))/-IQ(J)
          WHENEVER C(J).L.0.
          THROUGH BB3, FOR K=J,1,K.G.M
BB3       C(K)=0.
          TRANSFER TO BBB
BBBB      END OF CONDITIONAL
BBB       CONTINUE
          X=0.
          VECTOR VALUES OUT=$1,F7.5/S15,10F8.5/S15,10F8.5/S15,
         1 10F8.5* $
          TRANSFER TO FAN
          END OF CONDITIONAL
. . . .
. . . .
          WHENEVER I.E.2
          TRANSFER TO CC1
          OTHERWISE
          TRANSFER TO CC2
          END OF CONDITIONAL
CC1       CONTINUE
          THROUGH SIX, FOR L=1,1,L.G.1000.
CC2       CONTINUE
          X=DELX*(I-1)
          D(2)=-2.*L3(2)-L5(2)-L5(2)+C(2)*(L2(2)-L4(2)+L(6))
         1 +C(3)*(-L1(2)+L5(2))
          THROUGH THREE, FOR J=3,1,J.G.M-1
THREE     D(J)=C(J-1)*(-L3(J)-L5(J))+C(J)*(L2(J)+L6-L4(J))+
         1 C(J+1)*(-L1(J)+L5(J))
          THROUGH FOUR, FOR J=2,1,J.G.M-1
          P(J)=L3(J)+L5(J)
          Q(J)=-L2(J)-L6-L4(J)
FOUR      R(J)=L1(J)-L5(J)
          EXECUTE SOLVE.(2,M-1,P,Q,R,D,V)
          THROUGH FIVE, FOR J=2,1,J.G.M.-1
          C(J)=V(J)
          WHENEVER C(J).L.0.
          THROUGH AA5,FOR K=J,1,K.G.M
AA5       C(K)=0.
          TRANSFER TO AA6
FIVE      END OF CONDITIONAL
AA6       CONTINUE
SIX       CONTINUE
FAN       PRINT FORMAT OUT,X,C(1)...C(30)
          SHL(I)=(1.-C(2))*2./DELY
          SUM=SUM+(1.-C(2))*SIN.(X)*DELX/DELY
```

```
TWO         CONTINUE
            SH=SUM
            PRINT COMMENT $1$
            PRINT RESULTS PE,B,SH
            THROUGH FINAL, FOR I=1,1,I.G.N-1
            SHLOCL=(SHL(I)+SHL(I+1))/2.
            X=DELX*I
FINAL       PRINT RESULTS X,SHLOCL
            TRANSFER TO START
            END OF PROGRAM
```

2. Single spheres at high Reynolds number

```
$COMPILE MAD,IBLDR

. . . .
. . . .     CRANK-NICOLSON METHOD
. . . .     MASS TRANSFER WITH FIRST ORDER HOMOGENEREOUS CHEMICAL
. . . .     REACTIONS
. . . .     SINGLE SPHERES AT HIGH RE
. . . .     N...NUMBER OF STEPS IN ANGULAR DIRECTION
. . . .     M...NUMBER OF STEPS IN RADIAL DIRECTION
. . . .     ANGLE COMPUTED UP TO FLOW SEPARATION POINT, X=1.8850
. . . .
            INTEGER I,J,K,L,M,NN,N
            INTEGER NN3,NN5
            DIMENSION L4(2300,L4DI),L5(2300,L5DI)
            DIMENSION C(30),D(30),P(30),Q(30),R(30),V(30),L1(30),
           1 L2(30),L3(30),L55(30),IP(30),IQ(30),IR(30)
            VECTOR VALUES L4DI=2.1,30
            VECTOR VALUES L5DI=2,1,30
. . . .
. . . .
            N=74
            DELY=0.00005
            H=1.2
            M=30
            SC=1000.
            RE=81.
. . . .
            SUM=0.
            C(1)=1.
            C(M)=0.
            DELX=1.8850/N
            THROUGH ONE,FOR J=2,1,J.G.M
            L1(J)=1./(DELY*DELY*H.P.(2*J-3.)*(H+1.))
            L2(J)=1./(DELY*DELY*H.P.(2*J-3.))
            L3(J)=1./(DELY*DELY*H.P.(2*J-4.)*(H+1.))
            L55(J)=RE*SC/(4.*DELY*H.P.(J-2)*(H+1))
            Y=DELY*(H.P.(J-1)-1.)/(H-1.)
            THROUGH TWO,FOR I=1,1,I.G.N+1
            X=DELX*(I-0.5)
            L44=RE*SC/(2.*DELX)
            WHENEVER X.L.0.20
            L4(I.J)=6.*SQRT.(10.5*RE/120.)*X*Y*L44
```

```
                L5(I,J)=-6.*SQRT.(10.5*RE/120.)*Y.P.2*L55(J)
                OTHERWISE
                INT=SIMPS.(0.,X, 20,F.)
                L4(I,J)=6.*SQRT.(RE/120.*(SIN.(X)).P.12.5/INT)*Y*L44
                L5(I,J)=-1.5*SQRT.(RE/120.)*(14.5*(SIN.(X).P.5.25*
              1 COS.(X)*INT-(SIN.(X).P.15.75)/INT.P.1.5*Y.P.2.*L55(J)
                END OF CONDITIONAL
                L4(I,1)=0
                L5(I,1)=0
TWO             CONTINUE
ONE             CONTINUE
. . . .
START           READ DATA
. . . .
                PRINT COMMENT $1$
                PRINT RESULTS RE,SC,B
. . . .
                SUM=0.
                L6=B*B/2.
                THROUGH BB,FOR J=2,1,J.G.M-1
                IP(J)=2.*(L3(J)+L5(I.J))
                IQ(J)=-2.*(L2(J)+L6)
                IR(J)=2.*(L1(J)-L5(1,J))
BB              C(J)=0
                THROUGH BBB, FOR L=1,1,L.G. 250
                THROUGH BBBB, FOR J=2,1,J.G.M-1
                C(J)=(C(j-1)*IP(J)+C(J=1)*IR(J))/-IQ(J)
                WHENEVER C(J).L.O.
                THROUGH BB3,FOR K=J,1,K.G.M
BB3             C(K)=0.
                TRANSFER TO BBB
BBBB            END OF CONDITIONAL
BBB             CONTINUE
                X=0.
                VECTOR VALUES OUT=$S1,F7.5/S8,11F8.5/S20,10F8.5/S20,
              1 10F8.5*$
                PRINT FORMAT OUT, X,C(0)...C(30)
. . . .
. . . .
. . . .
                THROUGH END, FOR I=2,1,I.G.N+1
                WHENEVER I.E.2
                TRANSFER TO CC1
                OTHERWISE
```

```
                TRANSFER TO CC2
                END OF CONDITIONAL
CC1             CONTINUE
                THROUGH SIX,FOR L=1,1,L.G.300
CC2             CONTINUE
                X=DELX*(I-1)
                D(2)=-2.*L3(2)-L5(I,2)-L5(I   ,2)+C(2)*(L2(2)-L4(I   ,2)
               1 +L6)+C(3)*(-L1(2)+L5(I   ,2))
                THROUGH THREE,FOR J=3,1,J.G.M-1
THREE           D(J)=C(J-1)*(-L3(J)-L5(I   ,J   ))+C(J)*(L2(J)+L6-L4
               1 (I   ,J))+C(J+1)*(-L1(J)+L5(I   ,J   ))
                DUMMY=0
                DUMMY=0
                THROUGH FOUR,FOR J=2,1,J.G.M-1
                P(J)=L3(J)+L5(I,J   )
                Q(J)=-L2(J)-L6-L4(I,J)
FOUR            R(J)=L1(J)-L5(I,J   )
                EXECUTE SOLVE.(2,M-1,P,Q,R,D,V)
                THROUGH FIVE,FOR J=2,1,J.G.M-1
                C(J)=V(J)
                WHENEVER C(J).L.0.
                THROUGH AA5,FOR K=J,1,K.G.M
AA5             C(K)=0.
                TRANSFER TO AA6
FIVE            END OF CONDITIONAL
AA6             CONTINUE
SIX             CONTINUE
                PRINT FORMAT OUT,X,C(0)...C(30)
                FACTOR=(1.-C(2))*2./DELY/(SC.P.0.3333*RE.P.0.5)
                PRINT RESULTS X,FACTOR
                SUM=SUM+(1.-C(2))*SIN.(X)*DELX/DELY
END             CONTINUE
                SH=SUM
                PRINT RESULTS RE,SC,B,SH
                TRANSFER TO START
                END OF PROGRAM
```

3. Use of generalized parameter $N_{Pe}^{1/2}$/ for single spheres and multiparticle systems at low Reynolds number

```
$COMPILE MAD,IBLDR

. . . .    CRANK-NICOLSON METHOD
. . . .    MASS TRANSFER WITH FIRST ORDER HOMOGENEREOUS CHEMICAL
. . . .    REACTIONS
. . . .    SINGLE SPHERES AND MULTIPARTICLE SYSTEMS AT LOW RE
. . . .    USING PE .P.(1/3) /B AS PARAMETER
. . . .    N...NUMBER OF STEPS IN ANGULAR DIRECTION
. . . .    N...NUMBER OF STEPS IN ANGULAR DIRECTION
. . . .    M...NUMBER OF STEPS IN RADIAL DIRECTION
           INTEGER I,J,K,L,M,NN,N
           DIMENSION C(90),D(90),P(90),Q(90),R(90),V(90),L1(90),
         1 L2(90),L3(90),L55(90),L4(90),L5(90),IP(90),IQ(90),
         2 IR(90),Y(90),SHL(1000)
           N=900
           H=1.3
           DELY=0.00005
. . . .    PEB=PE.P.3/B
           M=90
           SUM=0.
           C(1)=1.
           L6=1./2.
           C(M)=0.
           DELX=3.1416/N
           L4(1)=0.
           L5(1)=0.
START      PRINT COMMENT $1$
           READ AND PRINT DATA
           SUM=0.
           A=PEB.P.3.
           L44=A/(2.*DELX)
           THROUGH ONE,FOR J=2,1,J.G.M
           L1(J)=1./(DELY*DELY*H.P.(2*J-3.)*(H+1.))
           L2(J)=1./(DELY*DELY*H.P.(2*J-3))
           L3(J)=1./(DELY*DELY(H.P.(2*J-4.)*(H+1.))
           L55(J)=A/(4.*DELY*H.P.(J-2)*(H+1))
           Y(J)=DELY*(H.P.(J-1)-1.)/(H-1.)
ONE        CONTINUE
           THROUGH TWO,FOR I=1,1,I.G.N
           X=DELX*(I-0.5)
           M=30
```

```
                WHENEVER X.G.2.5
                M=M+10
                END OF CONDITIONAL
                WHENEVER X.G.2.90
                M=M+10
                END OF CONDITIONAL
                WHENEVER X.G.3.05
                M=M+10
                END OF CONDITIONAL
                WHENEVER X.G.3.1
                M=M+10
                END OF CONDITIONAL
                WHENEVER X.G.3.13
                M=M+20
                END OF CONDITIONAL
                THROUGH TW01,FOR J=2,1,J.G.M
                L4(J)=1.5*SIN.(X)*Y(J)*L44
                L5(J)=-1.5*COS.(X)*Y(J).P.2.*L55(J)
TW01            CONTINUE
                PRINT RESULTS PEB,SUM
                WHENEVER I.E.1
                THROUGH BB,FOR J=2,1,J.G.M-1
                IP(J)=2.*(L3(J)+L5(J))
                IQ(J)=-2.*(L2(J)+L6)
                IR(J)=2.*(L1(J)-L5(J))
BB              C(J)=0.
                THROUGH BBB, FOR L=1,1,L.G. 400
                THROUGH BBBB, FOR J=2,1,J.G.M-1
                C(J)=(C(J-1)*IP(J)+C(J+1)*IR(J))/-IQ(J)
                WHENEVER C(J).L.0.
                THROUGH BB3,FOR K=J,1,K.G.M
BB3             C(K)=0.
                TRANSFER TO BBB
                END OF CONDITIONAL
BBB             CONTINUE
                X=0.
                VECTOR VALUES OUT=$S1,F7.5/S15,10F8.5/S15,10F8.5/S15,
               1 10F8.5/S15,10F8.5*$
                TRANSFER TO FAN
BBBB            END OF CONDITIONAL
                WHENEVER I.E.2
                TRANSFER TO CC1
                OTHERWISE
                TRANSFER TO CC2
```

```
            END OF CONDITIONAL
CC1         CONTINUE
            THROUGH SIX,FOR L=1,1,L.G.1000.
CC2         CONTINUE
            X=DELX*(I-1)
            D(2)=-2.*L3(2)-L5(2)-L5(2)+C(2)*(L2(2)-L4(2)+L6)
           1 +C(3)*(-L1(2)+L5(2))
            THROUGH THREE,FOR J=3,1,J.G.M-1
THREE       D(J)=C(J-1)*(-L3(J)-L5(J)+C(J)*(L2(J)+L6-L4(J)+C(J+1)*
           1 (-L1(J)=L5(J))
            THROUGH FOUR, FOR J=2,1,J.G.M-1
            P(J)=L3(J)+L5(J)
            Q(J)=-L2(J)-L6-L4(J)
FOUR        R(J)=L1(J)-L5(J)
            EXECUTE SOLVE.(2,M-1,P,Q,R,D,V)
            THROUGH FIVE, FOR J=2,1,J.G.M-1
            C(J)=V(J)
            WHENEVER C(J),L.0.
            THROUGH AA5,FOR K=J,1,K.G.M
AA5         C(K)=0.
            TRANSFER TO AA6
FIVE        END OF CONDITIONAL
AA6         CONTINUE
SIX         CONTINUE
FAN         CONTINUE
            SHL(I)=(1.-C(2))*2./DELY
            SUM=SUM+(1.-C(2))*SIN.(X)*DELX/DELY
TWO         CONTINUE
            SH=SUM
            PRINT COMMENT $1$
            PRINT RESULTS PEB,SH
            THROUGH FINAL, FOR I=1,1,I.G.N-1
            SHLOCL=(SHL(I)+SHL(I+1))/2.
            X=DELX*I
FINAL       PRINT RESULTS X,SHLOCL
            TRANSFER TO START
            END OF PROGRAM
```

4. Use of generalized parameter $\frac{N_{Re}^{1/2} N_{Sc}^{1/3}}{\beta}$ for single spheres at high Reynolds number

```
$COMPILE MAD,IBLDR

. . . .
. . . .     CRANK-NICOLSON METHOD
. . . .     MASS TRANSFER WITH FIRST ORDER HOMOGENEOUS
. . . .     CHEMICAL
. . . .     REACTIONS
. . . .     SINGLE SPHERES AT HIGH RE
. . . .     USING RE.P.(1/2)*XC.P.(1/3)/B AS PARAMETER
. . . .     N...NUMBER OF STEPS IN ANGULAR DIRECTION
. . . .     N...NUMBER OF STEPS IN ANGULAR DIRECTION
. . . .     M...NUMBER OF STEPS IN RADIAL  DIRECTION
. . . .     ANGLE COMPUTED UP TO FLOW SEPARATION POINT,
. . . .     X=1.8850
. . . .
            INTEGER I,J,K,L,M,NN,N
            DIMENSION L4(2250,L4DI),L5(2250,L5DI)
            DIMENSION C(30),D(30),P(30),Q(30),R(30),V(30),
           1 L1(30),L2(30),L3(30),L55(30),IP(30),IQ(30),INT(90)
            VECTOR VALUES L4DI=2,1,30
            VECTOR VALUES L5DI=2,1,30
. . . .
. . . .
            N=74
            M=30
            DELY=0.00005
            H=1.3
            L6=1./2.
. . . .
            C(1)=1.
            C(M)=0.
            DELX=1.8850/N
            THROUGH ONE,FOR J=2,1,J.G.M.
            L1(J)=1./(DELY*DELY*H.P.(2*J-3.)*(H+1.))
            L2(J)=1./(DELY*DELY*H.P.(2*J-3.))
            L3(J)=1./(DELY*DELY*H.P.(2*J-4.)*(H+1.))
ONE         CONTINUE
            THROUGH TWO,FOR I=1,1,I.G.N.+1
            X=DELX*(I-0.5)
            INT(I)=SIMPS.(0.,X,20,F.)
            L4(I,1)=0
            L5(I,1)=0
```

```
TWO           CONTINUE
START         READ DATA
              PRINT COMMENT $1$
              SUM=0.
              PRINT RESULTS RESCB
. . . .
. . . .       RESCB...RE.P.0.5*SC.P.0.333/B
. . . .
              A=RESCB.P.3.
              L44=A/(2.*DELX)
              THROUGH ONE1,FOR J=2,1,J.G.M
              L55(J)=A/(4.*DELY*H.P.(J-2)*(H+1))
              Y=DELY*(H.P.(J-1)-1.)/(H-1.)
              THROUGH TWO1,FOR I=1,1,I.G.N+1
              X=DELX*(I-0.5)
              WHENEVER X.L.0.20
              L4(I,J)=SQRT.(3.15)*X*Y*L44
              L5(I,J)=-SQRT.(3.15)*Y.P.2.*L55(J)
              OTHERWISE
              L4(I,J)=6.*SQRT.((SIN.(X)).P.12.5/(120.*INT(I)))
             1 *Y*L44
              L5(I.J)=-SQRT.(2.25/120.)*(14.5*(SIN.(X)).P.5.25*
             1 COS.(X)*INT(I)-(SIN.(X)).P.15.75)/INT(I).P.1.5*
             2 Y.P.2.*L55(J)
              END OF CONDITIONAL
TWO1          CONTINUE
ONE1          CONTINUE
              THROUGH BB,FOR J=2,1,J.G.M-1
              IP(J)=2.*(L3(J)+L5(1,J))
              IQ(J)=-2.*(L2(J)+L6)
              IR(J)=2.*(L1(J)-L5(1,J))
BB            C(J)=0.
              THROUGH BBB, FOR L=1,1,L.G. 250
              THROUGH BBBB, FOR J=2,I,J.G.M-1
              C(J)=(C(J-1)*IP(J)+C(J+1)*IR(J))/-IQ(J)
              WHENEVER C(J).L.0.
              THROUGH BB3,FOR K=J,1,K.G.M
BB3           C(K)=0.
              TRANSFER TO BBB
BBBB          END OF CONDITIONAL
BBB           CONTINUE
              X=0.
              VECTOR VALUES OUT=$S1,F7.5/S8,11F8.5/S20,10F8.5/
             1 S20,10F8.5*$
```

```
              PRINT FORMAT OUT,X,C(0)...C(30)
. . . .
. . . .
. . . .
              THROUGH END, FOR I=2,1,I.G.N+1
              WHENEVER I.E.2
              TRANSFER TO CC1
              OTHERWISE
              TRANSFER TO CC2
              END OF CONDITIONAL
CC1           CONTINUE
              THROUGH SIX,FOR L=1,1,L.G.300
CC2           CONTINUE
              X=DELX*(I-1)
              D(2)=-2.*L3(2)-L5(I,2)-L5(I   ,2)+C(2)*(L2(2)-L4
             1 (I   ,2)+L6)+C(3)*(-L1(2)+L5(I   ,2))
              THROUGH THREE,FOR J=3,1,J.G.M-1
THREE         D(J)=C(J-1)*(-3(J)-L5(I   ,J   ))+L6-L4(I   ,J))+
             1 C(J+1)*(-L1(J)+L5(I   ,J))
              DUMMY=0.
              DUMMY=o.
              THROUGH FOUR,FOR J=2,1,J.G.M-1
              P(J)=L3(J)+L5(I,J   )
              Q(J)=-L2(J)-L6-L4(I,J)
FOUR          R(J)=L1(J)-L5(I,J   )
              EXECUTE SOLVE.(2,M-1,P,Q,R,D,V)
              THROUGH FIVE, FOR J=2,1,J.G.M-1
              C(J)=V(J)
              WHENEVER C(J).L.0.
              THROUGH AA5,FOR K=J,1,K.G.M
AA5           C(K)=0.
              TRANSFER TO AA6
FIVE          END OF CONDITIONAL
AA6           CONTINUE
SIX           CONTINUE
              PRINT FORMAT OUT, X,C(0)...C(30)
              SHLOCL=(1.-C(2)*2./DELY
              PRINT RESULTS X,SHLOCL
              SUM=SUM+(1.-C(2))*SIN.(X)*DELX/DELY
END           CONTINUE
              SHALLX=SUM
              SHAVG=SUM*2./1.3090
              PRINT RESULTS RESCB,SHAVG,SHALLX
              TRANSFER TO START
              END OF PROGRAM
```

B. Mass transfer with first order homogeneous chemical reaction in a two spheres system at low Reynolds number

Two programs have been written with specified input data which included the spacing parameter Y_o (as YO), Peclet, number, N_{Pe} (as PE), reaction rate constant, β (as B), constants h_1 (as H1) and h_2 (as H2) (see equations (IV-58) and (IV-61)), step numbers in the angular (as N) and radial (as M) directions, number of terms used for the velocity profiles in the two spheres system (as NN), and number of initial steps in the radial direction (as NNNN). Output obtained from these computation gave the concentration profiles as well as the local and overall Sherwood numbers.

Velocity terms were called from a subroutine. The accuracy of these profiles depends on the value of NN.

The two programs are listed below.

1. The active sphere placed in front of the inert sphere in the direction of flow (YO > 0).
2. The active sphere placed behind the inert sphere in the direction of flow (YO < 0).

1. The active sphere placed in front of the inert sphere in the direction of flow ($Y_o > 0$)

```
$COMPILE MAD, IBLDR

. . . .      1...UPPER SPHERE
. . . .      APPROXIMATED MASS TRANSFER RATES AROUND ONE SPHERE
. . . .      IN TWO SPHERE SYSTEMS AT CREEPING FLOW FOR HIGH
. . . .      PECLET NUMBERS CRANK-NICOLSON METHOD
             INTEGER I,J,K,L,M,NN,N,NNN,NNNN
             DIMENSION DCDX(200),DCDY(200),SX1(200),SHL(200),
            1 C1(100)
             DIMENSION C(100),D(100),P(100),Q(100),R(100),V(100),
            1 L1(100),L2(100),L3(100),A1(100),B1(100),Y(100),
            2 L55(100),VETA(100),VTHAI(100)
             DIMENSION YX(100)
             VECTOR VALUES INPUT=$F10.2,F10.1,F10.1,2F8.5,4I5 *$
             AA=1.
             C(1)=1.
             DCDX(1)=0.
START        READ FORMAT INPUT,Y0,PE,B,H1,H2,N,M,NN,NNNN
             DD=AA*COSH.(Y0)
             CC=DD*(.ABS.(TANH.(Y0)))
             PRINT RESULTS Y0,PE,B,DD
             PRINT RESULTS NN,M,N,NNNN
             PRINT RESULTS H1,H2
             KK=B*B*CC*CC/AA/AA
             SUM=0.
             THROUGH ADD2, FOR I=2,1,I.G. M*2 -1
ADD2         C(J)=0.
             DX=3.14159*(H1-1.)/(H1.P.N-1.)
             DY=(1.570795-0.0349)*(H2-1.)/(H2.P.(M-1)-1.)
             Y(1)=Y0
             THROUGH ONE,FOR J=2,1,J.G.M
             YX(J)=DY*(H2.P.(J-1)-1.)/(H2-1.)
             Y(J)=Y0*COS.(YX(J))
ONE          CONTINUE
             THROUGH ADD1, FOR J=1,1,J.G.M
ADD1         Y(M+J)=-Y(M-J+1)
             NNN=M
             EXECUTE SPHXU1.(Y0,CC,DD,N,H1,DX,SX1)
             M=NNNN
             THROUGH TWO, FOR I=1,1,I.G.N-1
             X=DX*(H1.P.I-1)/(H1-1)
```

```
                DELX=DX*H1.P.(I-1)
                WHENEVER C(M-5).G.0.00001
                M=2*NNN
                END OF CONDITIONAL
                THROUGH TWO1,FOR J=2,1,J.G.M-1
                EXECUTE VELTWO.(NN,ABS.(Y0),CC,Y(J),X,VETA(J),
              1 VTHAI(J))
                A1(J)=(COSH.(Y(J))-COS.(X).P.2
                B1(J)=(COSH.(Y(J))-COS.(X))*(PE/2.*CC/AA*VTHAI(J)/
              1 DELX
                C1(J)=(COSH.(Y(J))-COS.(X))*(PE/2.*CC/AA*VETA(J))/2.
                L1(J)=1./((Y(J+1)-Y(J))*(Y(J=1)-Y(J-1)))
                L2(J)=1./((Y(J+1)-Y(J))*(Y(J  )-Y(J-1)))
                L3(J)=1./((Y(J+1)-Y(J-1))*(Y(J)-Y(J-1)))
                L55(J)=1./ (Y(J+1)-Y(J-1))
TWO1            CONTINUE
                WHENEVER I.E.1
                THROUGH BB,FOR J=2,1,J.G.M-1
                P(J)=2.*(A1(J)*L3(J)+C1(J)*L55(J))
                Q(J)=2.*(-A1(J)*L2(J)-KK/2.)
                R(J)=2.*(A1(J)*L1(J)-C1(J)*L55(J))
BB              CONTINUE
                THROUGH BBB, FOR L=1,1,L.G. 400
                THROUGH BBBB, FOR J=2,I,J.G.M-1
                C(J)=(C(J-1)* P(J)+C(J+1)* R(J))/-Q(J)
                WHENEVER C(J).L.0.
                THROUGH BB3,FOR K=J,1,K.G.M
BB3             C(K)=0.
                TRANSFER TO BBB
BBBB            END OF CONDITIONAL
BBB             CONTINUE
                VECTOR VALUES OUT=$S1,F7.5/S15,10F8.5/S15,10F8.5/S15,
              1 10F8.5/S15,10S15,10F8.5/S15,10F8.5/S15,10F8.5/S15,
              2 10F8.5/S15,10F8.5 *$
                TRANSFER TO FAN
                END OF CONDITIONAL
                THROUGH ADD, FOR J=2,1,J.G.M-1
                P(J)=A1(J)*L3(J)+C1(J)*L55(J)
                Q(J)=-A1(J)*L2(J)-B1(J)-KK/2.
                R(J)=A1(J)*L1(J)-C1(J)*L55(J)
ADD             CONTINUE
                WHENEVER I.E.2
                TRANSFER TO CC1
                OTHERWISE
```

```
                TRANSFER TO CC2
                END OF CONDITIONAL
CC1             CONTINUE
                THROUGH SIX,FOR L=1,1,L.G.1000
CC2             CONTINUE
                D(2)=-2.* P(2)+C(2)*(- Q(2)-2.*B1(2))-C(3)*R(2)
                THROUGH THREE,FOR J=3,1,J.G.M-1
THREE           D(J)=C(J-1)*(-P(J))+C(J)*(-Q (J)-2.*B1(J))-C(J+1)*
               1 R(J)
                EXECUTE SOLVE.(2,M-1,P,Q,R,D,V)
                DCDX(I)=(V(2)-C(2))/DELX
                THROUGH FIVE,FOR J=2,1,J.G.M-1
                WHENEVER V(J).G.1.
                V(J)=1.
                END OF CONDITIONAL
                WHENEVER C(J).G.V(J)
                V(J)=C(J)
                END OF CONDITIONAL
                C(J)=V(J)
                WHENEVER C(J).L.0.
                THROUGH AA5,FOR K=J,1,K.G.M
AA5             C(K)=0.
                TRANSFER TO AA6
FIVE            END OF CONDITIONAL
AA6             CONTINUE
SIX             CONTINUE
FAN             PRINT FORMAT OUT, X,C(1)...C(M)
                DCDY(I)=(C(2)-1.)/(Y(2)-Y(1))
                EXECUTE NSHL.(Y0,AA,CC,X,DCDY(I),DCDX(I),SHL(I))
                SUM=SUM+SHL(I)/2.*SIN.((SX1(I-1)+SX1(I))/2.)*
               1 (SX1(I)-SX1(I-1))
                PRINT RESULTS X,SHL(I),SUM
TWO             CONTINUE
                PRINT COMMENT $1$
                TRANSFER TO START
                END OF PROGRAM
```

2. The active sphere placed behind the inert sphere in the direction of flow ($Y_o < 0$)

```
$COMPILE MAD, IBLDR

. . . .      2...LOWER SPHERE
. . . .      APPROXIMATED MASS TRANSFER RATES AROUND ONE SPHERE
. . . .      IN TWO SPHERE SYSTEMS AT CREEPING FLOW FOR HIGH
. . . .      PECLET NUMBERS CRANK-NICOLSON METHOD
             INTEGER I,J,K,L,M,NN,N,NNN,NNNN
             DIMENSION DCDX(200),DCDY(200),SX2(200),SHL(200),
            1 C1(100)
             DIMENSION C(100),D(100),P(100),Q(100)R(100),V(100),
            1 L1(100),L2(100),L3(100),A1(100),B1(100),Y(100),
            2 L55(100),VETA(100),VTHAI(100)
             DIMENSION YX(100)
             VECTOR VALUES INPUT=$F10.2,F10.1,F10.1,2F8.5,4I5 *$
             AA=1.
             C(1)=1.
             DCDX(1)=0.
START        READ FORMAT INPUT, Y0,PE,B,H1,H2,N,M,NN,NNNN
             DD=AA*COSH.(Y0)
             CC=DD*(.ABS.(TANH.(Y0)))
             PRINT RESULTS Y0,PE,B,DD
             PRINT RESULTS NN,M,N,NNNN
             PRINT RESULTS H1,H2
             KK=B*B*CC*CC/AA/AA
             SUM=0.
             THROUGH ADD2, FOR I=2,1,I.G. M*2 -1
ADD2         C(J)=0.
             DX=3.14159*(H1-1.)/(H1.P.N.-1.)
             DY=(1.570795-0.0349)*(H2-1.)/(H2.P.(M-1)-1.)
             Y(1)=Y0
             THROUGH ONE, FOR J=2,1,J.G.M
             YX(J)=DY*(H2.P.(J-1)-1.)/(H2-1.)
             Y(J)=Y0*COS.(YX(J))
ONE          CONTINUE
             THROUGH ADD1, FOR J=1,1,J.G.M
ADD1         Y(M+J)=-Y(M-J+1)
             M=NNNN
             THROUGH TWO, FOR I=1,1,I.G.N-1
             X=3.14159-DX*(H1.P.I-1.)/(H1-1.)
             DELX=-DX*H1.P.(I-1)
             WHENEVER C(M-5).L.0.00001
```

```
          M=M-1
          END OF CONDITIONAL
          WHENEVER C(M-5).G.0.00001
          M=M+1
          END OF CONDITIONAL
          WHENEVER M.G.2*NNN
          M=2*NNN
          END OF CONDITIONAL
          THROUGH TWO1,FOR J=2,1,J.G.M-1
          EXECUTE VELTWO.(NN,.ABS.(Y0),CC,Y(J),X,VETA(J),
         1 VTHAI(J))
          B1(J)=(COSH.(Y(J))-COS.(X))*(PE/2.*CC/AA*VTHAI(J))/
         1 DELX
          C1(J)=(COSH.(Y(J))-COS.(X))*(PE/2.*CC/AA*VETA(J))/2.
          L1(J)=1./((Y(J+1)-Y(J))*(Y(J+1)-Y(J-1)))
          L2(J)=1./((Y(J+1)-Y(J))*(Y(J  )-Y(J-1)))
          L3(J)=1./((Y(J+1)-Y(J-1))*(Y(J)-Y(J-1)))
          L55(J)=1./ (Y(J+1)-Y(J-1))
TWO1      CONTINUE
          WHENEVER I.E.1
          THROUGH BB,FOR J=2,1,J.G.M-1
          P(J)=2.*(A1(J)*L3(J)+C1(J)*L55(J))
          Q(J)=2.*(-A1(J)*L2(J)-KK/2.)
          R(J)=2.*(A1(J)*L1(J)-C1(J)*L55(J))
BB        CONTINUE
          THROUGH BBB, FOR L=1,1,L.G. 400
          THROUGH BBBB, FOR J=2,1,J.G.M-1
          C(J)=(C(J-1)* P(J)+C(J+1)* R(J))/-Q(J)
          WHENEVER C(J).L.0.
          THROUGH BB3,FOR K=J,1,K.G.M
BB3       C(K)=0.
          TRANSFER TO BBB
BBBB      END OF CONDITIONAL
BBB       CONTINUE
          VECTOR VALUES OUT=$S1,F7.5/S15,10F8.5/S15,10F8.5/S15,
         1 10F8.5/S15,10F8.5/S15,10F8.5/S15,10F8.5/S15,
         2 10F8.5/S15,10F8.5/S15,10F8.5 *$
          TRANSFER TO FAN
          END OF CONDITIONAL
          THROUGH ADD, FOR J=2,1,J.G.M-1
          P(J)=A1(J)*L3(J)+C1(J)*L55(J)
          Q(J)=-A1(J)*L2(J)-B1(J)-KK/2.
          R(J)=A1(J)*L1(J)-C1(J)*L55(J)
```

```
ADD           CONTINUE
              WHENEVER I.E.2
              TRANSFER TO CC1
              OTHERWISE
              TRANSFER TO CC2
              END OF CONDITIONAL
CC1           CONTINUE
              THROUGH SIX, FOR L=1,1,L.G.1000
CC2           CONTINUE
              D(2)=-2.* P(2)+C(2)*(-Q(2)-2.*B1(2))-C(3)*R(2)
              THROUGH THREE, FOR J=3,1,J.G.M-1
THREE         D(J)=C(J-1)*(- P(J))+C(J)*(-Q (J)-2.*B1(J))-C(J+1)
             1 *R(J)
              EXECUTE SOLVE.(2,M-1,P,Q,R,D,V)
              DCDX(I)=(V(2)-C(2))/DELX
              THROUGH FIVE, FOR J=2,1,J.G.M-1
              WHENEVER V(J).G.1.
              V(J)=1.
              END OF CONDITIONAL
              C(J)=V(J)
              WHENEVER C(J),L.0.
              THROUGH AA5,FOR K=J,1,K.G.M
AA5           C(K)=0.
              TRANSFER TO AA6
FIVE          END OF CONDITIONAL
AA6           CONTINUE
SIX           CONTINUE
FAN           PRINT FORMAT OUT, X,C(1)...C(M)
              DCDY(I)=(C(2)-1.)/(Y(2)-Y(1))
              EXECUTE NSH2.(Y0,AA,CC,X,DCDY(I),DCDX(I),SHL(I))
              SUM=SUM+SHL(I)/2.*SIN.((SX2(I-1)+SX2(I))/2.)*
             1 (SX2(I)-SX2(I-1))
              PRINT RESULTS X,SHL(I),SUM
TWO           CONTINUE
              PRINT COMMENT $1$
              TRANSFER TO START
              END OF PROGRAM
```

C. Data Analysis of the experimental work

The program has been written with the following input data required: run number (as RUNNO) run time in hours (as DELT), total weight loss in grams (as DELW), average run temperature in ^{o}C (as TAVGS), diffusivity in in^2/hr (as DIFCO), unit driving force in gm/gm of solution (as CSTAR), Schmidt number, dimensionless, (as SC), fluid density in lb/ft^3 (as RHOFLU) and bulk stream concentration in moles/liters (as CBM). The initial and finial radii profiles must also be read in as data.

The output gives the computed results of the local Sherwood number, the overall Sherwood numbers based on both weight loss and on integration of the local Sherwood number, the calculated density of the solute, the Reynold number, Peclet number, $N_{R_e}^{\frac{1}{2}} N_{S_c}^{1/3}$, $N_{P_e}^{1/3}$ and the concentration ratio .

Program for data analysis; experimental work

```
$COMPILE MAD

          DIMENSION R1(40),R2(40),S1(40),S2(40),C1(40),C2(40),
         1 THETA(40),DR1R2(40),PDR(40),SIMSUM(20),S2MSUM(20),
         2 C1MSUM(20),C2MSUM(20),S1ESUM(20),S2ESUM(20),
         3 CIESUM(20),C2ESUM(20),AREA1L(40),AREA2L(40),
         4 AREALA(40),VOLM1L(40),VOLM2L(40),DVOLML(40)
          DIMENSION SHLVOL(40),SHL(20),R12AVG(40)
          VECTOR VALUES CHEN=$14F5.4/14F5.4/9F5.4/14F5.4/
         1 14F5.4/9F5.4 *$
          VECTOR VALUES WUCHI=$13,F4.1,F5.4,F4.3,F5.1,I4,F6.5,
         1 F6.5,F5.4,F6.2,F6.4 *$
          INTEGER I,RUNNO,SC
          REFER=0.4684
          RHOSOL=1.266*62.43
          MTBA=122.12
          THROUGH ZZZ, FOR I=1,1,I.G.37
ZZZ       THETA(I)=3.14159/18*(I-1)
START     READ FORMAT WUCHI,RUNNO,DELT,DELW,G,TAVGS,SC,DIFCO,
         1 CSTAR,MUFLU,RHOFLU,CBM
          CBMCAO=CBM/CSTAR*MTBA/1000.
          VSUBS = ((1.99*G)/(61.27))
          READ FORMAT CHEN,R1(1)...R1(37),R2(1)...R2(37)
. . . .   LOCAL VALUES
          THROUGH AAA, FOR I=1,1,I.G.37
          R1(I)=R1(I)-REFER
          R2(I)=R2(I)-REFER
          S1(I)=.ABS.(R1(I).P.2*SIN.(THETA(I)))
          S2(I)=.ABS.(R2(I).P.2*SIN.(THETA(I)))
          C1(I)=.ABS.(R1(I).P.3*SIN.(THETA(I)))
          C2(I)=.ABS.(R2(I).P.3*SIN.(THETA(I)))
          DR1R2(I)=R1(I)-R2(I)
          PDR(I)=DR1R2(I)/R1(I)*100.
          R12AVG(I)=(R1(I)+R2(I))/2.
AAA       CONTINUE
. . . .   SECTOR
          H=3.14159/9./2.
. . . .   PARTIAL SUM
          S1MSUM(0)=0.
          S2MSUM(0)=0.
          C2MSUM(0)=0.
          C1MSUM(0)=0.
```

```
      S1ESUM(0)=0.
      S2ESUM(0)=0.
      C1ESUM(0)=0.
      C2ESUM(0)=0.
      THROUGH BBB, FOR I=1,1,I.G.18
      S1MSUM(I)=S1MSUM(I-1)+4*S1(2*I)
      S2MSUM(I)=S2MSUM(I-1)+4*S2(2*I)
      C1MSUM(I)=C1MSUM(I-1)+4*C1(2*I)
      C2MSUM(I)=C2MSUM(I-1)+4*C2(2*I)
      S1ESUM(I)=S1ESUM(I-1)+2*S1(2*I-1)
      S2ESUM(I)=S2ESUM(I-1)+2*S2(2*I-1)
      C1ESUM(I)=C1ESUM(I-1)+2*C1(2*I-1)
      C2ESUM(I)=C2ESUM(I-1)+2*C2(2*I-1)
BBB   CONTINUE
      S1SUM=S1MSUM(18)+S1ESUM(18)-S1(1)+S1(37)
      S2SUM=S2MSUM(18)+S2ESUM(18)-S2(1)+S2(37)
      C1SUM=C1MSUM(18)+C1ESUM(18)-C1(1)+C1(37)
      C2SUM=C2MSUM(18)+C2ESUM(18)-C2(1)+C2(37)
. . . .  TOTAL AREA AND VOLUME
      AREA1T=2.*3.14159*H/3.*S1SUM/2.
      AREA2T=2.*3.14159*H/3.*S2SUM/2.
      VOLM1T=2.*3.14159*H/3.*C1SUM/2./3.
      VOLM2T=2.*3.14159*H/3.*C2SUM/2./3.
      RSAR2=SQRT.(AREA2T /4./3.14159 )
      RSAR1=SQRT.(AREA1T /4./3.14159 )
. . . .  AVERAGE AND DIFFERENCE
      RSAR12=(RSAR1+RSAR2)/2.
      AREATA=(AREA1T+AREA2T)/2.
      DVOLMT=VOLM1T-VOLM2T
      DIMRSA=RSAR1-RSAR2
      DRSARP=DIMRSA/RSAR1*100.
. . . .  LOCAL AREA AND VOLUME
      AREA1L(1)=2.*3.14159*H/3.*(S1(36)+4.*S1(1)+S1(2))
      AREA2L(1)=2.*3.14159*H/3.*(S2(36)+4.*S2(1)+S2(2))
      VOLM1L(1)=2.*3.14159*H/3.*(C1(36)+4.*C1(1)+C1(2))/3.
      VOLM2L(1)=2.*3.14159*H/3.*(C2(36)+4.*C2(1)+C2(2))/3.
      THROUGH CCC, FOR I=2,1,I.G.36
      AREA1L(I)=2.*3.14159*H/3.*(S1(I-1)+4.*S1(I)+S1(I+1))
      AREA2L(I)=2.*3.14159*H/3.*(S2(I-1)+4.*S2(I)+S2(I+1))
      VOLM1L(I)=2.*3.14159*H/3.*(C1(I-1)+4.*C1(I)+C1(I+1))
     1 /3.
      VOLM2L(I)=2.*3.14159*H/3.*(C2(I-1)+4.*C2(I)+C2(I+1))
     1 /3.
```

```
CCC           CONTINUE
. . . .       PARAMETERS...RE,PE,PE.P.(1/3),PE.P.(1/3)*RE.P.(1/6)
              RE1=2.*RSAR1/12.*VSUBS*RHOFLU/MUFLU/0.000672
              RE2=2.*RSAR2/12.*VSUBS*RHOFLU/MUFLU/0.000672
              RE12A=(RE1+RE2)/2.
              PE1=RE1*SC
              PE2=RE2*SC
              PE12A=RE12A*SC
              GAMMA=PE12A.P.(1./3.)
              ALPHA=GAMMA*RE12A.P.(1./6.)
. . . .       AVERAGE AND DIFFERENCE
              THROUGH WAKO, FOR I=1,1,I.G.36
              AREALA(I)=(AREA1L(I)+AREA2L(I))/2.
              DVOLML(I)=VOLM1L(I)-VOLM2L(I)
WAKO          CONTINUE
. . . .       LOCAL SHERWOOD NUMBER
              MF=1728./453.59
              FACTOR=RHOSOL/DIFCO/DELT/RHOFLU/CSTAR
              THROUGH EEE, FOR I=1,1,I.G.36
              SHLVOL(I)=FACTOR*DVOLML(I)*2.*R12AVG(I)/AREALA(I)
EEE           CONTINUE
              SHL(1)=SHLVOL(1)
              THROUGH FFF, FOR I=2,1,I.G.19
              SHL(I)=(SHLVOL(I)+SHLVOL(38-I))/2.
FFF           CONTINUE
. . . .       OVERALL SHERWOOD NUMBER BASED ON WEIGHT LOSS
              SHOMAS=DELW/DELT/DIFCO/RHOFLU/CSTAR/(2.*3.14159*
             1 RSAR12)*MF
. . . .       OVERALL SHERWOOD NUMBER BASED ON VOLUME CHANGE
              SHOVOL=DVOLMT*FACTOR/(2.*RSAR12*3.14159)
. . . .       OVERALL SHERWOOD NUMBER BASED ON LOCAL SHERWOOD
. . . .       NUMBERS
              SUM1=0.
              SUM2=0.
              THROUGH GGG, FOR I=1,1,I.G.9
              SUM1=SUM1+SHL(2*I-1)/2.*SIN.(THETA(2*I-1))
              SUM2=SUM2+SHL(2*I)/2.*SIN.(THETA(2*I))
GGG           CONTINUE
              SHOINT=H/3.*(2.*SUM1+4.*SUM2)
. . . .       CHECK DENSITY
              ROSCAL=DELW/DVOLMT*MF/62.43
              ROSBOK=RHOSOL/62.43
. . . .       PERCENTAGE DIFFERENCE
```

```
      ROSPER=(ROSBOK-ROSCAL)/ROSBOK*100.
      SHODMV=(SHOMAS-SHOVOL)/SHOMAS*100.
      SHODMI=(SHOMAS-SHOINT)/SHOMAS*100.
. . . .  PRINT RESULTS
      PRINT RESULTS RUNNO,RSAR1,RSAR2,ROSCAL,ROSPER,
     1 SHODMV,SHODMI
      PRINT RESULTS SHOMAS,SHOINT,SHOVOL
      PRINT RESULTS RE12A,ALPHA,GAMMA,CBMCAO
      PRINT RESULTS SHL(1)...SHL(19)
      PRINT COMMENT $1$
      TRANSFER TO START
      END OF PROGRAM
```

D. Subroutines

```
$COMPILE MAD,IBLDR

          EXTERNAL FUNCTION (ALPHA,AA,CC,THAI,DCDE,DCDT,SH)
          ENTRY TO NSHL.
          EO=ALPHA
          C=CC
          X=THAI
          Z=C*SINH.(EO)/(COSH.(EO)-COS.(X))
          LO=C*SIN.(X) /(COSH.(EO)-COS.(X))
          D=AA*COSH.(EO)
          A1=1.+(D+C)*(Z-D)
          A2=1.+(D-C)*(Z-D)
          A3=(Z+C).P.2*LO*LO
          A4=(Z-C).P.2+LO*LO
          A5=1.+D*(Z-D)
          DEDY=A1/A3-A2/A4
          DTDY=-1./SIN.(X)*(2.*A5/SQRT.(A3)/SQRT.(A4)-COS.
        1 (X)*(A1/A3+A2/A4))
          DCDY=DCDE*DEDY+DCDT*DTDY
          SH=-2.*DCDY
          RUNCTION RETURN
          END OF FUNCTION

$COMPILE MAD,IBLDR

          EXTERNAL FUNCTION (ALPHA,AA,CC,THAI,DCDE,DCDT,SH)
          ENTRY TO NSH2.
          EO=ALPHA
          C=CC
          X=THAI
          Z=C*SINH.(EO)/(COSH.(EO)-COS.(X))
          LO=C*SIN.(X) /(COSH.(EO)-COS.(X))
          D=AA*COSH.(EO)
          D=-D
          A1=1.+(D+C)*(Z-D)
          A2=1.+(D-C)*(Z-D)
          A3=(Z+C).P.2+LO*LO
          A4=(Z-C).P.2+L)*L)
          A5=1.+D*(Z-D)
          DEDY=A1/A3-A2/A4
          DTDY=-1/SIN.(X)*(2.*A5/SQRT.(A3)/SQRT.(A4)-COS.
        1 (X)*(A1/A3+A2/A4))
          DCDY=DCDE*DEDY+DCDT*DTDY
          SH=-2.*DCDY
          FUNCTION RETURN
          END OF FUNCTION
```

```
$COMPILE MAD,IBLDR

            EXTERNAL FUNCTION (ALPHA,CC,DD,N,H1,DX,SX2)
            ENTRY TO SPHXD2.
            INTEGER I,N
            SX2(0)=0.
            SX2(N)=3.14159
            THROUGH ONE, FOR I=1,1,I.G.N-1
            THAI=DX*(H1.P.I-1.)/(H1-1.)*(-1.)+3.14159
            ZD=DD+CC*SINH.(ALPHA)/(COSH.(ALPHA)-COS.(THAI))
            SX2(I)=ARCCOS.(ZD)
ONE         CONTINUE
            FUNCTION RETURN
            END OF FUNCTION

$COMPILE MAD,IBLDR

            EXTERNAL FUNCTION (N,ALPHA,CC,ETA,THAI,VETA,VTHAI)
            INTEGER I,N
            DIMENSION AN(100),CN(100),WN(100),DW(100)
            ENTRY TO VELTWO.
            UWN=0.
            UDW=0.
            WDU=0.
            X=COS.(THAI)
            Y=SIN.(THAI)
            XX=COSH.(ETA)
            YY=SINH.(ETA)
            Z=XX-X
            Z1=SQRT.(Z)
            Z2=1./Z1
            EXECUTE PANCN.(N,ALPHA,CC,X,Y,AN,CN,WN,DW)
            THROUGH ONE ,FOR I=1,1,I.G.N
            DU=AN(I)*(I-0.5)*SINH.((I-0.5)*ETA)+CN(I)*(I+1.5)
           1*SINH.((I+1.5)*ETA)
            UN=AN(I)*COSH.((I-0.5)*ETA)+CN(I)*COSH.((I+1.5)*ETA)
            UWN=UWN+UN*WN(I)
            WDU=WDU+DU*WN(I)
ONE         UDW=UDW+UN*DW(I)
            VTHAI=Y*YY/Z-Y/CC/CC*(-1.5*Z2*YY*UWN+Z1*WDU)
            VETA=(X*XX-1.)/Z+1./CC/CC*)-1.5*Z2*Y*YUWN+Z1*UDW)
            FUNCTION RETURN
            END OF FUNCTION
```

```
$COMPILE MAD,IBLDR

              EXTERNAL FUNCTION(A,B,N,F.)
              INTEGER I,N
              ENTRY TO SIMPS.
              END=0.0
              MID=0.0
              DH=(B-A)/N
              H=DH/2
              X=A-DH
              THROUGH AAA, FOR I=1,1,I.G.N.
              X=X+DH
              END=END+F.(X)
AAA           MID=MID+F.(X+H)
              SUM=(2.0*END+4.0*MID - F.(A) + F.(B))*H/3.
              FUNCTION RETURN
              END OF FUNCTION

$COMPILE MAD,IBLDR

              EXTERNAL FUNCTION (M,N,A,B,C,D,V)
              INTEGER I,M,N
              DIMENSION A1(100),A2(100)
              ENTRY TO SOLVE.
              A1(M)=B(M)
              A2(M)=D(M)/A1(M)
              THROUGH AAA, FOR I=M+1,1,I.G.N
              A1(I)=B(I)-A(I)*C(I-1)/A(I-1)
AAA           A2(I)=(D(I)-A(I)*A2(I-1))/A1(I)
              V(N)=A2(N)
              THROUGH BBB,FOR I=N-1,-1,I.L.M
BBB           V(I)=A2(I)-C(I)*V(I+1)/A1(I)
              FUNCTION RETURN
              END OF FUNCTION

$COMPILE MAD,IBLDR

              EXTERNAL FUNCTION (X)
              ENTRY TO F.
              FUNCTION RETURN (SIN.(X)).P.9.5
              END OF FUNCTION
```

```
$COMPILE MAD,IBLDR

              EXTERNAL FUNCTION (N,ALPHA,CC,S,Y,AN,CN,VTHAI,DTHAI)
              DIMENSION P(100)
              ENTRY TO PANCN.
              X=S
              INTEGER I,N
              P(0)=1.
              P(1)=X
              WHENEVER X.E.1.
              THROUGH AAA,FOR I=1,1,I.G.N+1
AAA           P(I+1)=1.
              TRANFER TO TWO
              END OF CONDITIONAL
              WHENEVER X.E.-1.
              THROUGH BBB,FOR I=2,1,I.G.N+2
              WHENEVER I*2/2.E.I
              P(I)=1.
              OTHERWISE
              P(I)=-1.
BBB           END OF CONDITIONAL
              TRANSFER TO TWO
              END OF CONDITIONAL
              WHENEVER N.G.1
              THROUGH ONE,FOR I=1,1,I.G.N+1
ONE           P(I+1)=((2.*I+1)*X*P(I)-I*P(I-1))/(I+1)
              END OF CONDITIONAL
TWO           CONTINUE
              THROUGH FOUR,FOR I=1,1,I.G.N
              VTHAI(I)=(P(I-1)-P(I+1))/Y/Y
              DTHAI(I)=(I*(P(I)-X*P(I-I1))+(I+2)*(X*P(I+1)-P(I+2)))
             1 /Y/Y
FOUR          CONTINUE
              THROUGH THREE,FOR I=1,1,I.G.N
              K=CC*CC*I(I+1.)/(SQRT.(2.)*(2.*I-1.)*(2.*I+1.)*(2.*I+3.))
              A1=2.*I+1.
              A2=2.*(1.-EXP.(-A1*ALPHA))
              A3=2.*SINH.(A1*ALPHA)+A1*SINH.(2.*ALPHA)
              AN(I)=-(A1*ALPHA)+A1*SINH.(2.*ALPHA)-1.))/A3
THREE         CN(I)=(A1-2.)*K*(A2+A1*(1.-EXP.(-2.*ALPHA)))/A3
              FUNCTION RETURN
              END OF FUNCTION
```

```
$COMPILE MAD,IBLDR

          EXTERNAL FUNCTION (ALPHA,CC,DD,N,H1,DX,SX1)
          ENTRY TO SPHXU1.
          INTEGER I,N
          SX1(0)=0.
          SX1(N)=3.14159
          THROUGH ONE, FOR I=1,1,I.G.N-1
          THAI=DX*(H1.P.I-1.)/(H.-1.)
          ZD=-DD+CC*SINH.(ALPHA)/COSH.(ALPHA)-COS.(THAI))
          SX1(I)=ARCCOS.(ZD)
ONE       CONTINUE
          FUNCTION RETURN
          END OF FUNCTION
```

Appendix K. List of Experimental Data

The results of experimental work are obtained from a computer program written to process the experiment data. All necessary integrations are performed numerically using Simpson's method. The method of data analysis is presented in detail in Appendix H. The corresponding computer program is also given in Appendix J. All the input data and results are presented here in Tables K-1, K-2, and K-3.

The run numbers indicate the value of the concentration ratio as well as the series number, and are given in general form as IJK. Here I represents the value of the concentration ratio of the reagent to solute, γ, and J represents the series number (see Figure 38) of the run. For a single sphere system, J = 1; for series II, J = 5; series III, J = 6; series IV, J = 7; series V, J = 8; series VI, J = 2; series VII, J = 3; series VIII, J = 4. The value of K is just a sequence number index.

TABLE K-1: Experimental results; comparison of the calculated values of the density of benzoic acid with the book values (1.266 gm/cm) and comparison between the overall Sherwood number based on weight loss and that obtained from an intergration of the local values over the sphere surface

run number	% diminution	calculated density, ρ_s (gm/cm^3)	% difference in density	N_{Sh_o} on weight	N_{Sh_o} integration	% difference in N_{Sh_o}
111	2.824	1.358	-7.263	63.42	59.29	6.512
112	4.838	1.242	1.[illegible]	58.72	60.16	-2.451
113	4.633	1.107	12.530	36.95	42.21	-14.225
114	2.933	1.358	-7.289	53.60	49.54	7.577
115	3.305	1.288	-1.718	48.58	48.25	0.662
116	4.404	1.345	-6.247	40.17	37.87	5.725
117	3.044	1.280	-1.131	44.54	44.04	1.131
121	5.090	1.261	0.360	62.51	62.24	0.432
122	4.355	1.374	-8.508	40.32	37.33	7.416
123	3.055	1.304	-3.005	56.59	54.92	2.943
125	4.064	1.253	0.989	54.06	54.68	-1.150
126	4.844	1.304	-3.038	52.81	51.10	3.236
127	3.839	1.312	-3.602	46.44	44.71	3.732
128	4.142	1.227	3.087	45.35	46.19	-1.858
131	8.243	1.147	9.387	58.30	64.53	-10.675
132	4.596	1.163	8.158	52.57	57.19	-8.792
133	5.142	1.135	10.346	50.46	56.19	-11.356
134	4.766	1.180	6.765	39.66	42.52	-7.232
135	3.973	1.137	10.171	47.82	53.17	-11.193
136	4.677	1.120	11.524	46.51	52.58	-13.047
141	5.338	1.128	10.890	40.90	45.79	-11.963
143	5.045	1.174	7.239	51.10	55.00	-7.617
145	6.123	1.168	7.744	56.67	61.52	-8.558
146	5.873	1.232	2.660	43.70	45.50	-4.123
151	2.907	1.299	-2.597	44.25	43.26	2.238
152	2.863	1.298	-2.550	42.79	42.12	1.566
153	4.859	1.225	3.219	38.30	39.63	-3.458
154	3.321	1.245	1.665	40.30	40.72	-1.065
161	3.884	1.080	14.657	48.21	56.31	-16.801
162	5.029	1.287	-1.627	38.80	37.93	2.243
163	3.425	1.296	-2.363	44.17	42.98	2.681
164	4.466	1.319	-4.176	40.95	39.27	4.106
171	7.029	1.149	9.204	45.36	49.85	-9.894

TABLE K-1, cont'd:

run number	% diminution	calculated density ρ_s (gm/cm)	% difference in density	N_{Sh_o} on weight	N_{Sh_o} integration	% difference in N_{Sh_o}
172	4.099	1.226	3.192	45.22	46.59	-3.013
173	4.876	1.267	-0.043	39.45	39.36	0.243
174	11.560	1.182	6.632	40.24	43.23	-7.432
182	4.301	1.272	-0.438	37.84	37.46	0.994
183	3.379	1.222	3.458	48.59	49.76	-2.405
184	3.530	1.298	-2.538	45.00	43.82	2.621
185	3.567	1.318	-4.096	40.79	38.98	4.417
191	3.467	1.182	6.668	47.66	50.94	-6.900
192	3.620	1.270	-0.330	44.73	44.95	-0.477
193	4.145	1.248	1.397	36.76	37.10	-0.922
194	4.675	1.275	-0.740	45.69	45.32	0.791
212	8.679	1.225	3.216	488.73	504.89	-3.306
213	6.380	1.219	3.681	434.57	451.74	-3.951
214	6.004	1.247	1.508	418.19	424.58	-1.529
215	5.603	1.209	4.482	378.73	395.05	-4.309
216	6.039	1.238	2.198	457.46	469.12	-2.550
311	4.428	1.229	2.930	372.00	382.49	-2.819
312	4.089	1.185	6.434	333.19	356.27	-6.926
313	3.551	1.326	-4.734	317.04	302.36	4.628
314	3.280	1.281	-1.172	289.56	287.57	0.686
411	3.193	1.238	2.178	267.13	272.64	-2.064
412	3.145	1.217	3.837	219.80	229.29	-4.316
413	4.138	1.209	4.538	171.92	180.25	-4.845
511	4.361	1.207	4.682	147.83	155.34	-5.082
512	3.409	1.268	-0.185	148.31	149.48	-0.793
513	3.713	1.190	6.005	149.86	159.62	-6.511
514	3.762	1.251	1.192	145.82	147.82	-1.374
611	3.218	1.190	5.998	136.38	145.63	-6.785
612	3.299	1.226	3.131	130.34	135.35	-3.839
613	3.325	1.201	5.127	113.53	119.86	-5.583
614	3.357	1.184	6.490	118.95	126.84	-6.633
711	3.144	1.227	3.084	114.76	118.70	-3.428
712	3.119	1.250	1.263	116.06	118.57	-2.165
221	6.546	1.248	1.437	369.49	375.80	-1.708
222	6.701	1.213	4.197	456.47	477.55	-4.619
223	5.567	1.214	4.106	419.25	437.19	-4.278
224	4.615	1.211	4.348	383.59	401.30	-4.615
251	5.940	1.273	-0.562	393.92	391.34	0.656
252	5.802	1.202	5.095	377.26	397.59	-5.391
253	4.900	1.196	5.502	362.83	385.83	-6.339

TABLE K-1, cont'd:

run number	% diminution	calculated density, ρ_s (gm/cm)	% difference in density	N_{Sh_o} on weight	N_{Sh_o} integration	% difference in N_{Sh_o}
421	5.369	1.227	3.094	219.05	226.14	-3.238
422	4.915	1.267	-0.056	200.70	202.51	-0.904
423	4.441	1.279	-1.061	181.88	179.78	1.158
451	6.213	1.146	9.487	192.20	213.95	-11.318
452	4.558	1.120	11.544	175.06	198.29	-13.268

Average percentage difference in density = 4.43%

Average percentage difference in N_{Sh_o} = 4.73%

TABLE K-2: Experimental results, overall Sherwood number and enhancement factor

run number	γ	$N_{Pe}^{1/3}$	$N_{Sc}^{1/3} N_{Re}^{1/2}$	N_{Sh_o}	Φ
111	0.000	37.75	73.84	63.42	-
112	0.000	35.11	66.84	58.72	-
113	0.000	20.07	28.62	36.95	-
114	0.000	34.55	64.77	53.60	-
115	0.000	32.42	58.77	48.58	-
116	0.000	25.48	41.46	40.17	-
117	0.000	29.61	51.39	44.54	-
121	0.000	37.10	72.14	62.51	-
122	0.000	22.12	33.20	40.32	-
123	0.000	36.04	69.06	56.59	-
125	0.000	34.05	63.25	54.06	-
126	0.000	32.18	58.26	52.81	-
127	0.000	29.58	51.37	46.44	-
128	0.000	27.29	45.52	45.35	-
131	0.000	37.07	72.04	58.30	-
132	0.000	36.06	69.13	52.57	-
133	0.000	33.71	62.47	50.46	-
134	0.000	21.79	32.48	39.66	-
135	0.000	32.13	58.00	47.82	-
136	0.000	30.12	52.76	46.51	-
141	0.000	23.38	36.08	40.90	-
143	0.000	33.10	60.73	51.10	-
145	0.000	36.81	71.29	56.67	-
146	0.000	29.23	50.32	43.70	-
151	0.000	37.48	72.92	44.25	-
152	0.000	33.67	62.30	42.79	-
153	0.000	23.59	36.54	38.30	-
154	0.000	28.85	49.51	40.30	-
161	0.000	37.14	72.19	48.21	-
162	0.000	23.67	36.73	38.80	-
163	0.000	37.29	72.77	44.17	-
164	0.000	28.99	49.83	40.95	-
171	0.000	37.22	72.69	45.36	-
172	0.000	33.49	61.93	45.22	-
173	0.000	23.61	36.52	39.45	-
174	0.000	28.84	49.44	40.24	-
182	0.000	23.92	37.25	37.84	-
183	0.000	37.28	72.34	48.59	-
184	0.000	33.82	62.62	45.00	-

TABLE K-2, cont'd:

run number	γ	$N_{Pe}^{1/3}$	$N_{Sc}^{1/3} N_{Re}^{1/2}$	N_{Sh_o}	ϕ
185	0.000	29.30	50.40	40.79	-
191	0.000	37.20	72.11	47.66	-
192	0.000	33.92	62.89	44.73	-
193	0.000	23.71	36.75	36.76	-
194	0.000	30.02	52.37	45.69	-
212	3.243	36.54	70.50	488.73	8.12
213	3.224	33.14	60.94	434.57	8.50
214	3.224	28.67	49.05	418.19	9.40
215	3.224	23.49	36.38	378.73	9.80
216	3.224	36.50	70.34	457.46	7.60
311	2.446	37.24	72.37	372.00	6.00
312	2.439	33.67	62.30	333.19	6.26
313	2.432	28.80	49.38	317.04	7.20
314	2.446	23.56	36.40	289.56	7.40
411	1.517	37.21	72.53	267.13	4.30
412	1.526	33.50	61.73	219.80	4.16
413	1.521	23.50	36.33	171.92	4.46
511	0.903	36.88	71.44	147.83	2.43
512	0.903	37.09	72.04	148.31	2.40
513	0.903	37.18	72.30	149.86	2.40
514	0.903	36.56	70.50	145.82	2.40
611	0.806	37.10	72.09	136.38	2.20
612	0.806	33.59	62.09	130.34	2.55
613	0.806	28.93	49.62	113.53	2.55
614	0.806	31.06	55.21	118.95	2.50
711	0.726	33.27	61.20	114.76	2.21
712	0.726	34.17	63.69	116.06	2.19
221	3.243	22.50	34.08	369.49	9.05
222	3.243	36.72	71.04	456.47	8.50
223	3.253	33.63	62.09	419.25	8.00
224	3.243	28.63	48.89	383.59	8.13
251	3.234	36.97	71.70	393.92	8.90
252	3.234	33.65	62.26	377.26	8.90
253	3.234	29.12	50.12	362.83	8.90
421	1.521	37.11	72.09	219.05	3.80
422	1.521	33.37	61.47	200.70	3.80
423	1.521	29.21	50.34	181.88	3.80
451	1.521	36.84	71.30	192.20	4.32
452	1.521	28.91	49.57	175.06	4.30
453	1.521	33.69	62.11	179.22	4.25

TABLE K-3: Experimental data

run #	γ	run temp. C	flow rate, GPM	run time, hr.	weight loss, gm.	$r_{I,sar}$, inches	$r_{F,sar}$, inches	N_{Re}	N_{Sh_o}
111	0.000	25.2	0.403	4.20	0.1204	0.2508	0.2437	56.0	63.42
112	0.000	26.1	0.347	8.00	0.1700	0.2443	0.2325	47.6	58.72
113	0.000	25.3	0.061	9.50	0.1571	0.2499	0.2383	8.4	36.95
114	0.000	25.5	0.312	5.10	0.1235	0.2489	0.2416	43.4	53.60
115	0.000	25.3	0.255	6.00	0.1316	0.2504	0.2421	25.5	48.58
116	0.000	26.5	0.131	9.50	0.1806	0.2500	0.2390	18.6	40.17
117	0.000	25.5	0.196	6.00	0.1210	0.2496	0.2420	27.3	44.54
121	0.000	25.4	0.392	7.00	0.1956	0.2497	0.2370	54.0	62.51
122	0.000	25.4	0.083	10.00	0.1803	0.2489	0.2380	11.4	40.32
123	0.000	25.4	0.350	5.00	0.1298	0.2536	0.2459	49.5	56.59
125	0.000	25.3	0.296	6.50	0.1583	0.2508	0.2406	41.1	54.06
126	0.000	25.4	0.255	8.20	0.1941	0.2501	0.2380	35.3	52.81
127	0.000	25.4	0.197	7.50	0.1571	0.2503	0.2407	27.4	46.44
128	0.000	25.4	0.152	8.00	0.1665	0.2551	0.2446	21.5	45.35
131	0.000	25.4	0.390	11.20	0.2926	0.2544	0.2335	53.9	58.30
132	0.000	25.4	0.352	7.20	0.1730	0.2547	0.2430	49.6	52.57
133	0.000	25.4	0.288	8.20	0.1888	0.2550	0.2419	40.5	50.46
134	0.000	25.4	0.078	10.00	0.1806	0.2540	0.2419	11.0	39.66
135	0.000	25.3	0.250	6.50	0.1394	0.2496	0.2397	34.6	47.82
136	0.000	25.4	0.205	8.00	0.1701	0.2548	0.2429	28.9	46.51
141	0.000	25.4	0.098	10.00	0.1829	0.2501	0.2368	13.5	40.00
143	0.000	25.5	0.276	7.90	0.1813	0.2501	0.2374	38.2	51.10
145	0.000	25.4	0.385	8.50	0.2141	0.2496	0.2343	52.8	56.67
146	0.000	25.3	0.189	11.20	0.2186	0.2510	0.2362	26.0	43.70
151	0.000	25.1	0.389	6.00	0.1194	0.2518	0.2444	54.3	44.25
152	0.000	25.5	0.286	6.00	0.1171	0.2512	0.2440	40.2	42.79
153	0.000	25.5	0.098	11.00	0.1929	0.2547	0.2423	13.8	38.30
154	0.000	25.6	0.183	7.00	0.1287	0.2497	0.2414	25.5	40.30
161	0.000	25.5	0.387	6.00	0.1309	0.2505	0.2408	53.9	48.21
162	0.000	25.5	0.101	11.40	0.1985	0.2499	0.2373	14.0	38.80
163	0.000	25.6	0.388	7.10	0.1458	0.2546	0.2458	55.2	44.17
164	0.000	25.4	0.184	10.10	0.1879	0.2530	0.2417	25.8	40.95
171	0.000	25.7	0.397	12.10	0.2536	0.2541	0.2362	55.5	45.36
172	0.000	25.6	0.288	7.50	0.1539	0.2493	0.2391	40.0	45.22
173	0.000	25.3	0.098	11.00	0.1969	0.2536	0.2413	13.7	39.45
174	0.000	25.4	0.187	23.10	0.4091	0.2543	0.2249	25.4	40.24
182	0.000	25.3	0.103	10.00	0.1699	0.2503	0.2395	14.3	37.84
183	0.000	25.1	0.387	5.90	0.1275	0.2496	0.2412	53.4	48.59
184	0.000	25.3	0.291	7.00	0.1415	0.2494	0.2406	40.3	45.00

TABLE K-3, cont'd:

run #	γ	run temp. C	flow rate, GPM	run time, hr.	weight loss, gm.	$r_{I,sar}$, inches	$r_{F,sar}$, inches	N_{Re}	N_{Sh_o}
185	0.000	25.1	0.187	8.10	0.1476	0.2510	0.2420	25.9	40.79
191	0.000	24.8	0.387	6.00	0.1268	0.2498	0.2411	53.1	47.66
192	0.000	25.3	0.294	7.00	0.1404	0.2490	0.2400	40.6	44.73
193	0.000	25.2	0.101	9.70	0.1593	0.2496	0.2392	13.9	36.76
194	0.000	25.2	0.205	9.00	0.1838	0.2504	0.2387	28.2	45.69
212	3.243	25.4	0.375	1.50	0.3272	0.2540	0.2320	51.6	488.73
213	3.224	25.6	0.281	1.20	0.2348	0.2503	0.2343	38.7	434.57
214	3.224	25.6	0.182	1.20	0.2260	0.2499	0.2349	25.1	418.19
215	3.224	25.6	0.100	1.20	0.2049	0.2496	0.2356	13.8	378.73
216	0.234	25.5	0.373	1.10	0.2243	0.2495	0.2344	51.2	457.46
311	2.446	25.3	0.390	1.00	0.1665	0.2496	0.2386	53.8	372.00
312	2.439	25.5	0.288	1.00	0.1509	0.2509	0.2407	40.2	333.19
313	2.432	25.6	0.183	1.00	0.1439	0.2487	0.2398	25.4	317.04
314	2.446	25.3	0.098	1.00	0.1305	0.2499	0.2417	13.6	289.56
411	1.517	25.6	0.393	1.00	0.1218	0.2493	0.2414	54.8	267.13
412	1.526	25.3	0.282	1.20	0.1188	0.2496	0.2417	39.2	219.80
413	1.521	25.5	0.098	2.00	0.1556	0.2508	0.2404	13.7	171.92
511	0.903	25.5	0.375	2.50	0.1690	0.2537	0.2427	52.8	147.83
512	0.903	25.5	0.384	2.00	0.1347	0.2508	0.2422	53.7	148.31
513	0.903	25.5	0.381	2.10	0.1451	0.2550	0.2455	54.1	149.86
514	0.903	25.5	0.370	2.20	0.1448	0.2497	0.2403	51.4	145.82
611	0.806	25.5	0.378	2.00	0.1260	0.2548	0.2466	53.8	136.38
612	0.806	25.5	0.281	2.20	0.1322	0.2544	0.2460	39.9	130.34
613	0.806	25.5	0.183	2.40	0.1232	0.2496	0.2413	25.5	113.53
614	0.806	25.5	0.226	2.30	0.1240	0.2502	0.2418	31.5	118.95
711	0.726	25.5	0.278	2.30	0.1195	0.2497	0.2418	38.8	114.76
712	0.726	25.5	0.301	2.30	0.1209	0.2497	0.2419	42.0	116.06
221	3.243	25.4	0.088	1.50	0.2463	0.2501	0.2337	12.1	369.49
222	3.243	25.4	0.383	1.20	0.2430	0.2499	0.2331	52.4	456.47
223	3.253	25.2	0.290	1.10	0.2048	0.2499	0.2360	39.6	419.25
224	3.243	25.4	0.179	1.00	0.1725	0.2506	0.2390	24.8	383.59
251	3.234	25.5	0.387	1.30	0.2286	0.2497	0.2349	53.2	393.92
252	3.234	25.5	0.286	1.30	0.2234	0.2546	0.2399	40.1	377.26
253	3.234	25.5	0.188	1.10	0.1792	0.2498	0.2376	26.0	362.83
421	1.521	25.5	0.384	2.10	0.2092	0.2537	0.2400	53.8	219.05
422	1.521	25.5	0.283	2.10	0.1891	0.2497	0.2374	39.1	200.70
423	1.521	25.5	0.186	2.20	0.1832	0.2541	0.2429	26.2	181.88
451	1.521	25.5	0.382	2.50	0.2149	0.2505	0.2350	52.6	192.20
452	1.521	25.5	0.183	2.00	0.1580	0.2507	0.2392	25.4	175.06
453	1.521	25.0	0.286	1.90	0.1534	0.2496	0.2394	39.2	179.22

VIII. LITERATURE CITED

1. Acrivos, A., Chem. Eng. Sci., 13, 57 (1960).
2. Acrivos, A., and Taylor, T.D., Phys. Fluids, 5, 387 (1962).
3. Aksel'rud, G.A., Zh. Fiz. Khim., 27, 1445 (1953).
4. Astarita, G., "Mass Transfer with Chemical Reaction", Elsevier Publishing Co., New York (1967).
5. Baird, M.H.I. and Hamielec, A.E., Can. J. Chem. Eng., 40, 119 (1962).
6. Bowman, C.W., Ward, D.M., Johnson, A.I., and Trass, O., Can. J. Chem. Eng., 39, 9 (1961).
7. Breiman, L., Norman Bridge Laboratory, Calif. Tech., Rept. No. 2F-2 (1952).
8. Brenner, H., Chem. Eng. Sci., 18, 109 (1963).
9. Carnahan, B., Luther, H.A., and Wilkes, J.O., "Applied Numerical Methods," Vol. I and II, John Wiley and Sons, New York (1964).
10. Danckwerts, P.V., and Kennedy, A.M., Chem. Eng. Sci., 8, 201 (1958).
11. Van Dyke, M., "Perturbation Methods in Fluid Mechanics", Academic Press, New York (1964).
12. Fox, L., ed., "The Numerical Solution of Ordinary and Partial Differential Equations", Pergamon Press, London (1962).
13. Frank-Kamenetskii, D.A., "Diffusion and Heat Exchange in Chemical Kinetics", Princeton University Press, Princeton, N.J. (1955).
14. Friedlander, S.K., A.I.Ch.E.Journal, 3, 43 (1957).
15. Friedlander, S.K., A.I.Ch.E.Journal, 7, 347 (1961).
16. Frisch, H.L., J. Chem. Phys., 22, 123 (1954).
17. Froessling, N., Gerlands Beitr. Geophys., 52, 170 (1938).
18. Froessling, N., Lunds Univ. Arsskr. N.F. AVD, 36, #4 (1940).

19. Garner, F.H. and Grafton, R.W., Proc. Roy. Soc., A224, 64 (1954).

20. Garner, F.H. and Hoffman, J.M., A.I.Ch.E. Journal, 6, 579 (1960).

21. Garner, F.H. and Keey, R.B., Chem. Eng. Sci., 9, 119 (1958).

22. Garner, F.H. and Suckling, R.D., A.I.Ch.E. Journal, 4, 114 (1958).

23. Goddard, J.D. and Acrivos, A., Quart. J. Mech. and Appl. Math., 20, 471 (1967).

24. Goldstein, S., ed., "Modern Developments in Fluid Dynamics", Vol. I, Oxford Univ. Press (1938).

25. Grafton, R.W., Chem. Eng. Sci., 18, 457 (1963).

26. Gupta, A.S. and Thodos, G., A.I.Ch.E. Journal, 8, 608 (1962).

27. Gupta, A.S. and Thodos, G., A.I.Ch.E. Journal, 9, 751 (1963).

28. Happel, J., A.I.Ch.E. Journal, 4, 197 (1958).

29. Happel, J. and Brenner, H., "Low Reynolds Number Hydrodynamics", Prentice-Hall, Englewood Cliffs, N.J. (1965).

30. Hatta, S., Technol. Repts. Tohoku Imp. Univ., 8, 1 (1928-29).

31. Hamielec, A.E., Hoffman, T.W., and Ross, L.L., A.I.Ch.E. Journal, 13, 212 (1967).

32. Hamielec, A.E. and Johnson, A.I., Can. J. Chem. Eng., 40, 41 (1962).

33. Hamielec, A.E., Johnson, A.I. and Houghton, W.T., A.I.Ch.E. Journal, 13, 220 (1967).

34. Hamielec, A.E., Storey, S.H., and Whitehead, J.M., Can. J. Chem. Eng., 41, 246 (1963).

35. Houghton, W.T., Ph.D. Thesis, McMaster University, Hamilton, Ontario (1966).

36. Illingworth, C.R., J. Fluid Mech., 7, 442 (1960).

37. Jenson, V.G., Proc. Roy. Soc., A249, 346 (1959).

38. Johnson, A.I. and Akehata, T., Can. J. Chem. Eng., 43, 10 (1965).

39. Johnson, A.I., Hamielec, A.I., and Houghton, W.T., A.I.Ch.E. Journal, 13, 379 (1967).

40. Kawaguti, M., J. Phys. Soc. Japan, 8, 747 (1953).

41. Keey, R.B. and Glen, J.B., Can. J. Chem. Eng., 42, 227 (1964).

42. Kishinevsky, M. Kh., J. Appl. Chem. U.S.S.R. (English translation), 27, 415 (1954).

43. Kitaura, Y. and Tanaka, H., Kagaku Kōgaku (Abridged ed.) 3, 56 (1965).

44. Kronig, R. and Bruijsten, J., Appl. Sci. Res. Sect A, 2, 439 (1951).

45. Lapidus, L., "Digital Computation for Chemical Engineers", McGraw-Hill, New York (1962).

46. Leclair, B.P. and Hamielec, A.E., I & EC Fundamentals, 7, 542 (1968).

47. Levich, V.G., "Physicochemical Hydrodynamics", Prentice-Hall, Englewood Cliffs, N.J. (1962).

48. Linton, M. and Sutherland, K.L., Chem. Eng. Sci., 12, 214, (1960).

49. Litt, M., and Friedlander, S.K., A.I.Ch.E. Journal, 5, 482 (1959).

50. Lochiel, A.C. and Calderbank, P.H., Chem. Eng. Sci., 19, 471 (1964).

51. Marangozis, J. and Johnson, A.I., Can. J. Chem. Eng., 39, 152, (1961).

52. Marangozis, J. and Johnson, A.I., Can. J. Chem. Eng., 40, 231 (1962).

53. McConnachie, J.T.L., and Thodos, G., A.I.Ch.E. Journal, 9, 60, (1963).

54. Meyerink, E.S.C. and Friedlander, S.K., Chem. Eng. Sci., 17, 121 (1962).

55. Nielson, A.E., J. phys. Chem., 65, 46 (1961).

56. Nijsing, R.A.T.O., Hendriksz, R.H. and Kramers, H., Chem. Eng. Sci., 10, 88 (1959).

57. Ogiwara, J., Meteorological Society of Japan, 22,127 (1944).

58. Oseen, C.W., Ark. matematik Astr. Fys. Bd. 6, No. 29 (1910).

59. Peaceman, D.W., Sc. D. Thesis in Chem. Eng., Massachusetts Inst. Technol. (1951).

60. Peltzman, A., Ph.D. Thesis, CUNY, New York, New York (1967).

61. Peltzman, A. and Pfeffer, R., Chem. Eng. Prog. Symposium Series, 63, 49 (1967).

62. Perry, R.H., "Chemical Engineers' Handbook", 4th Ed., McGraw-Hill, New York, (1963).

63. Pfeffer, R., Ind. Eng. Chem. Fundamentals, 3, 380 (1964).

64. Pfeffer, R. and Happel, J., A.I.Ch.E. Journal, 10,605 (1964).

65. Proudman, I. and Pearson, J.R.A., J. Fluid Mech. 2, 237 (1957).

66. Rhodes, J. and Peebles, F.N., A.I.Ch.E. Journal, 11, 481 (1965).

67. Roberts, D, and Danckwerts, P.V., Chem. Eng. Sci., 17, 961 (1962).

68. Rowe, P.N, Claxton, K.T., and Lewis, J.B., Trans. Inst. Chem. Engrs., 43, T14 (1965).

69. Ruckenstein, E., Chem. Eng. Sci., 19, 131 (1964).

70. Rutland, L. and Pfeffer, R., A.I.Ch.E. Journal, 13, 182 (1967).

71. Schliehting, H., "Boundary Layer Theory", McGraw-Hill, New York (1955).

72. Sherwood, T.K. and Pigford, R.L., "Absorption and Extraction", 2nd ed., McGraw-Hill, New York (1952).

73. Sherwood, T.K. and Ryan, J.M. Chem. Eng. Sci., 11, 81 (1959).

74. Sherwood, T.K. and Wei, J.C. Ind. Eng. Chem., 49, 1030 (1957).

75. Steel, L.R. and Geankoplis, C.J. A.I.Ch.E. Journal, 5, 178 (1959).

76. Steinberger, R.L. and Treybal, R.E., A.I.Ch.E. Journal, 6, 227 (1960).

77. Stimson, M. and Jeffrey, G.B., Proc. Roy. Soc. (London), A111, 110 (1926).

78. Stokes, G.G.,Trans. Camb., Phil. Soc., 9, part 2:51 (1851).

79. Taneda, S., Rept. Res. Inst. Appl. Mech. (Japan), 4, 99 (1956).

80. Torobin, L.B., and Gauvin, W.H., Can. J. Chem. Eng., 37, 129 (1959).

81. Vassilatos, G., Trass, O. and Johnson, A.I., Can. J. Chem. Eng. 40. 210 (1962).

82. Ward, D.M., Trass, O., and Johnson, A.I., Can. J. Chem. Eng., 40, 164 (1962).

83. Woo, S.W. and Hamielec, A.E. to be published.

84. Yuge, T., Rept. Inst. High Sp. Mech., Tokoku Univ., 57, 143 (1956).

85. Yuge, T., Trans. A.S.M.E. Series C, 82, 214 (1960).

IX. PRESENTATION AND PUBLICATIONS

There are four papers and one presentation based on the results of this study in various stages of completion. These publications and presentation will be co-authored by the author and Professor Robert Pfeffer

The first paper, entitled "Local and Overall Mass Transfer Rates around Solid Spheres with First Order Homogeneous Chemical Reactions", has been accepted for publication in I/EC Fundamentals.

The second paper, entitled "Mass Transfer Rates around spherical particles with Rapid Homogeneous Chemical Reactions", has been written and will shortly be submitted for publication.

The presentation, entitled "Mass Transfer Rates with First Order Homogeneous Chemical Reaction around Two Spheres", has been scheduled to be presented by the author at the 62nd Annual Meeting of the A.I.Ch.E. in Washington, D.C., during December 1969 and will subsequently be submitted for publication.

The fourth paper which concentrates on the experimental results of this study is in preparation.

X. VITA

Wu-Chi Chen attended Tunghai University, Taichung, Taiwan, and received his Bachelor of Science degree in Chemical Engineering in June 1964.

After one year of service as an officer in the Army of the Republic of China, he came to the United States for graduate study in September 1965.

With the help of a research assistantship sponsored by The City University of New York, he started his graduate study at The City College of The City University of New York. He received his Master of Engineering in Chemical Engineering in February 1967 and continued his studies towards a doctorate degree.

After defending his dissertation, the author plans to remain in the United States and intends to obtain a research position in industry. Eventually he would like to seek an academic position.